MONASH University

Bismuth and gallium phosphinates as antibacterial agents, and additives in Bi-cellulose composites

Megan Elaine Herdman

Bachelor of Biomedical Science, Bachelor of Science (Honours)

A thesis submitted for the degree of Doctor of Philosophy at

Monash University in 2021

School of Chemistry

Table of Contents

Copyright notice vii

Declaration viii

Publications during enrolment ix

Acknowledgements x

Abbreviations xii

Abstract xiv

1 Introduction 3

1.1 Antibacterial resistance 3

1.1.1 Modes of resistance 3

1.1.2 Multi-resistant bacteria 5

1.1.2.1 *Staphylococcus aureus* 6

1.1.2.2 *Enterococci* genus 7

1.1.2.3 *Escherichia coli* 8

1.1.2.4 *Pseudomonas aeruginosa* 8

1.2 Metal antibacterial agents 9

1.2.1 Silver 11

1.2.2 Bismuth 12

1.2.3 Gallium 14

1.3 Objectives 15

2 Bismuth phosphinate complexes 19

2.1 Bismuth phosphinate chemistry 19

2.2 Synthesis 21

2.2.1 Diphenyl bismuth *mono*-phosphinates 22

2.2.2 Phenyl bismuth *bis*-phosphinates 23

2.2.3 Bismuth *tris*-phosphinates 24

2.3 Characterisation 25

2.3.1 X-ray crystallography 29

2.4 Solubility and stability 33

2.4.1 Media stability 36

2.5 Biology 39

2.5.1 Antibacterial activity 40

2.5.2 Mammalian cell viability 42

2.5.3 Selectivity 45

2.6 Conclusions 46

3 Aryl bismuth phosphinate complexes 51

3.1 Structure-activity introduction 51
3.2 Synthesis 53
3.2.1 Diaryl bismuth *mono*-phosphinates 53
3.2.1.1 *Bis*-*p*-methoxyphenyl bismuth *mono*-phosphinates 55
3.2.1.2 *Bis*-*o*-tolyl bismuth *mono*-phosphinates 57
3.3 Characterisation 59
3.3.1 X-ray crystallography 62
3.4 Solubility and stability 67
3.5 Biology 68
3.5.1 Antibacterial activity 68
3.5.2 Mammalian cell viability 70
3.5.3 Selectivity 73
3.6 Conclusions 74
4 Bismuth-cellulose composites 79
4.1 Antibacterial materials 79
4.1.1 Cellulose composites 80
4.2 Composite synthesis 81
4.3 Characterisation 81
4.4 Leaching properties 85
4.5 Biology 86
4.5.1 Antibacterial activity 87
4.5.2 Mammalian cell viability 91
4.6 Conclusions 92
5 Gallium phosphinate complexes 97
5.1 Gallium phosphinate chemistry 97
5.2 Synthesis 98
5.2.1 Diphenyl gallium *mono*-phosphinates 99
5.2.2 Phenyl gallium *bis*-phosphinates 100
5.2.3 Gallium *tris*-phosphinates 101
5.2.4 Gallium cluster 102
5.3 Characterisation 103
5.3.1 X-ray crystallography 107
5.4 Stability 111
5.5 Biology 112
5.5.1 Antibacterial activity 113
5.5.2 Mammalian cell toxicity 116
5.6 Conclusions 117
6 Summary 121

7 Experimental 127
7.1 General 127
7.2 Instrumentation 127
7.3 Biological testing 129
7.3.1 Bacteria preparation 129
7.3.1.1 Zone of inhibition assay 129
7.3.1.2 Minimum inhibitory concentration determination 129
7.3.1.2.1 Visual method 129
7.3.1.2.2 Absorbance method 130
7.3.1.3 Leachate assay 130
7.3.2 Cell culture 130
7.3.2.1 *In vitro* testing towards Cos-7 and human fibroblasts 131
7.3.2.2 Cytotoxicity assay 131
7.4 Reagents and solvents 132
7.5 Schlenk protocol 132
7.6 Precursor synthesis 132
7.6.1 Synthesis of triaryl bismuth 132
7.6.1.1 Triphenyl bismuth [$BiPh_3$] 133
7.6.1.2 *Tris*-(*o*-methoxyphenyl) bismuth [$Bi(o\text{-}MeOPh)_3$] 133
7.6.1.3 *Tris*-(*m*-methoxyphenyl) bismuth [$Bi(m\text{-}MeOPh)_3$] 133
7.6.1.4 *Tris*-(*p*-methoxyphenyl) bismuth [$Bi(p\text{-}MeOPh)_3$] 133
7.6.1.5 *Tris*-(*o*-tolyl) bismuth [$Bi(o\text{-}tol)_3$] 134
7.6.1.6 *Tris*-(*m*-tolyl) bismuth [$Bi(m\text{-}tol)_3$] 134
7.6.1.7 *Tris*-(*p*-tolyl) bismuth [$Bi(p\text{-}tol)_3$] 134
7.6.2 Synthesis of diaryl bismuth chloride 134
7.6.2.1 Diphenyl bismuth chloride [$BiPh_2Cl$] 135
7.6.2.2 *Bis*-(*p*-methoxyphenyl) bismuth chloride [$Bi(p\text{-}MeOPh)_2Cl$] 135
7.6.3 Synthesis of bismuth *tris*-(*tert*-butoxide) [$Bi(O^tBu)_3$][216] 135
7.6.4 Synthesis of triphenyl gallium [$GaPh_3$][195] 135
7.6.5 Synthesis of phosphinato sodium salts 135
7.6.5.1 Phenylphosphinato sodium salt $Na^+O^-(O)P(H)Ph$ 136
7.6.5.2 Diphenylphosphinato sodium salt $Na^+O^-(O)PPh_2$ 136
7.6.5.3 Dimethylphosphinato sodium salt $Na^+O^-(O)PMe_2$ 136
7.6.5.4 *Bis*-(*p*-methoxyphenyl)phosphinato sodium salt $Na^+O^-(O)P(p\text{-}MeOPh)_2$ 136
7.7 Phenyl bismuth phosphinato complexes 137
7.7.1 General procedure 1 (GP1) 137
7.7.1.1 Diphenyl *mono*-phenylphosphinato bismuth $[BiPh_2O(O)P(H)Ph]_\infty$, 2-1 137
7.7.1.2 Diphenyl *mono*-diphenylphosphinato bismuth $[BiPh_2O(O)PPh_2]_\infty$, 2-2 137
7.7.1.3 Diphenyl *mono*-dimethylphosphinato bismuth $[BiPh_2O(O)PMe_2]_\infty$, 2-3 138
7.7.1.4 Diphenyl *mono*-(*bis*-*p*-methoxyphenyl)phosphinato bismuth $[BiPh_2O(O)P(p\text{-}MeOPh)_2]_\infty$, 2-4 139

7.7.1.5 Phenyl *bis*-phenylphosphinato bismuth $[BiPh(O(O)P(H)Ph)_2]_\infty$, 2-5 139
7.7.1.6 Phenyl *bis*-diphenylphosphinato bismuth $[BiPh(O(O)PPh_2)_2]_\infty$, 2-6 139
7.7.1.7 Phenyl *bis*-dimethylphosphinato bismuth $[BiPh(O(O)PMe_2)_2]_\infty$, 2-7 140
7.7.1.8 Phenyl *bis*-(*bis*-*p*-methoxyphenyl)phosphinato bismuth $[BiPh(O(O)P(p\text{-}MeOPh)_2)_2]_\infty$, 2-8 140
7.7.2 General procedure 2 (GP2) 140
7.7.2.1 *Tris*-phenylphosphinato bismuth $[Bi(O(O)P(H)Ph)_3]_\infty$, 2-9 141
7.7.2.2 *Tris*-diphenylphosphinato bismuth $[Bi(O(O)PPh_2)_3]_\infty$, 2-10 141
7.7.2.3 *Tris*-dimethylphosphinato bismuth $[Bi(O(O)PMe_2)_3]_\infty$, 2-11 141
7.7.2.4 *Tris*-(*bis*-*p*-methoxyphenyl)phosphinato bismuth $[Bi(O(O)P(p\text{-}MeOPh)_2)_3]_\infty$, 2-12 141
7.8 Aryl bismuth phosphinato complexes 142
7.8.1 General procedure 3 (GP3) 142
7.8.1.1 *Bis*-*o*-methoxyphenyl *mono*-phenylphosphinato bismuth $[Bi(o\text{-}MeOPh)_2O(O)P(H)Ph]_\infty$, 3-1 142
7.8.1.2 *Bis*-*o*-methoxyphenyl *mono*-diphenylphosphinato bismuth $[Bi(o\text{-}MeOPh)_2O(O)PPh_2]_\infty$, 3-2 142
7.8.1.3 *Bis*-*o*-methoxyphenyl *mono*-(*bis*-*p*-methoxyphenyl)phosphinato bismuth $[Bi(o\text{-}MeOPh)_2O(O)P(p\text{-}MeOPh)_2]_\infty$, 3-3 143
7.8.1.4 *Bis*-*m*-methoxyphenyl *mono*-phenylphosphinato bismuth $[Bi(m\text{-}MeOPh)_2O(O)P(H)Ph]_\infty$, 3-4 143
7.8.1.5 *Bis*-*m*-methoxyphenyl *mono*-diphenylphosphinato bismuth $[Bi(m\text{-}MeOPh)_2O(O)PPh_2]_\infty$, 3-5 144
7.8.1.6 *Bis*-*m*-methoxyphenyl *mono*-(*bis*-*p*-methoxyphenyl)phosphinato bismuth $[Bi(m\text{-}MeOPh)_2O(O)P(p\text{-}MeOPh)_2]_\infty$, 3-6 144
7.8.1.7 *Bis*-*m*-tolyl *mono*-phenylphosphinato bismuth $[Bi(m\text{-}tol)_2O(O)P(H)Ph]_\infty$, 3-13 144
7.8.1.8 *Bis*-*m*-tolyl *mono*-diphenylphosphinato bismuth $[Bi(m\text{-}tol)_2O(O)PPh_2]_\infty$, 3-14 145
7.8.1.9 *Bis*-*m*-tolyl *mono*-(*bis*-*p*-methoxyphenyl)phosphinato bismuth $[Bi(m\text{-}tol)_2O(O)P(p\text{-}MeOPh)_2]_\infty$, 3-15 145
7.8.1.10 *Bis*-*p*-tolyl *mono*-phenylphosphinato bismuth $[Bi(p\text{-}tol)_2O(O)P(H)Ph]_\infty$, 3-16 146
7.8.1.11 *Bis*-*p*-tolyl *mono*-diphenylphosphinato bismuth $[Bi(p\text{-}tol)_2O(O)PPh_2]_\infty$, 3-17 146
7.8.1.12 *Bis*-*p*-tolyl *mono*-(*bis*-*p*-methoxyphenyl)phosphinato bismuth $[Bi(p\text{-}tol)_2O(O)P(p\text{-}MeOPh)_2]_\infty$, 3-18 147
7.9 Bismuth-cellulose composites 147
7.10 Gallium phosphinato complexes 148
7.10.1 General procedure 4 (GP4) 148
7.10.1.1 Diphenyl *mono*-phenylphosphinato gallium $[GaPh_2O(O)P(H)Ph]_2$, 5-1 148
7.10.1.2 Diphenyl *mono*-diphenylphosphinato gallium $[GaPh_2O(O)PPh_2]_2$, 5-2 148
7.10.1.3 Diphenyl *mono*-dimethylphosphinato gallium $[GaPh_2O(O)PMe_2]_2$, 5-3 149
7.10.1.4 Diphenyl *mono*-(*bis*-*p*-methoxyphenyl)phosphinato gallium $[GaPh_2O(O)P(p\text{-}MeOPh)_2]_2$, 5-4 149
7.10.1.4.1 Di-μ_3-oxido tetra-phenyl tetra-(*bis*-*p*-methoxyphenyl)phosphinato tetra-gallium $[Ga_4Ph_4(O(O)P(p\text{-}MeOPh)_2)_4(\mu_3\text{-}O)_2]$ 150
7.10.2 General Procedure 5 (GP5) 150
7.10.2.1 *Tris*-phenylphosphinato gallium $[Ga(O(O)P(H)Ph)_3]_\infty$, 5-9 150
7.10.2.2 *Tris*-diphenylphosphinato gallium $[Ga(O(O)PPh_2)_3]_\infty$, 5-10 151
7.10.2.3 *Tris*-dimethylphosphinato gallium $[Ga(O(O)PMe_2)_3]_\infty$, 5-11 151
7.10.2.4 *Tris*-(*bis*-*p*-methoxyphenyl)phosphinato gallium $[Ga(O(O)P(p\text{-}MeOPh)_2)_3]_\infty$, 5-12 151

7.10.2.5 Octa-μ_3-oxido di-μ-oxido tetra-μ-hydroxido dodeca-phenyl dodeca-gallium DMSO tetrasolvate $[Ga_{12}Ph_{12}(\mu_3\text{-}O)_8(\mu\text{-}O)_2(\mu\text{-}OH)_4].4DMSO$, 5-13 ____ 152

8 References ____ 153

Copyright notice

© Megan Herdman (2021).

I certify that I have made all reasonable efforts to secure copyright permissions for third-party content included in this thesis and have not knowingly added copyright content to my work without the owner's permission.

Declaration

This thesis is an original work of my research and contains no material which has been accepted for the award of any other degree or diploma at any university or equivalent institution and that, to the best of my knowledge and belief, this thesis contains no material previously published or written by another person, except where due reference is made in the text of the thesis.

Megan Herdman

March 2021

Publications during enrolment

Bismuth phosphinates in Bi-nanacellulose composites and their efficacy towards multi-drug resistant bacteria

Werret, M. V.; Herdman, M. E.; Brammananth, R.; Garusinghe, U.; Batchelor, W.; Crellin, P.; Coppel, R. L.; Andrews, P. C. *Chem. Eur. J.* **2018**, *24* (49), 12938-12949.

Impact of structural changes in heteroleptic bismuth phosphinates on their antibacterial activity in Bi-nanocellulose composites

Herdman, M. E.; Werrett, M. V.; Duffin, R. N.; Stephens, L. J.; Brammananth, R.; Coppel, R. L.; Batchelor, W.; Andrews, P. C. *Dalton Trans.* **2020**, *49* (22), 7341–7354.

Acknowledgements

I would like to thank my main supervisor Professor Phil Andrews for being supportive and always having great ideas. I have thoroughly enjoyed your ideas such as antibacterial bismuth slime, which was fun to look into. While you were often busy, you always made the time to address any concerns and help me grow as a chemist.

I wish to thank my co-supervisor A/Prof Warren Batchelor for sharing your vast cellulose knowledge with me, and for helping me to look at things from a different perspective. The opportunity to work in the BioPRIA labs was insightful and very different to a chemistry lab which provided a nice change.

I am so very thankful for my other co-supervisor Dr Melissa Werrett, who has been beyond supportive and encouraging. I really appreciate how approachable you are, helping with any issues and for being great to bounce ideas around with. I always knew a chat with you would give me the motivation to keep going! Even after changing roles, your dedication to helping has been phenomenal. Thank-you Mel!

The Werrett Group members, Maisha Maliha, Sarmi Munuganti and Tania Sultana have been a huge support, for which I am very thankful. Like Mel, you have all been there to chat about the woes of poorly soluble compounds. I have to thank Maisha for working closely with me, especially with the troublesome ICP analyses; it has been fantastic to see your work come together. Sarmi, I am so grateful for all of your insights, stories and support throughout my PhD, notably through our mutual struggles of learning biological assays. I have thoroughly enjoyed many lab chats with Tania and wish you all the best with your exciting chemistry.

I would like to thank Dr Vicki Blair, Dr Sam Orr and Dr Bekka Duffin for all of your help throughout my PhD. You have all shown me what it means to proudly be a woman in chemistry and to get involved in various events. A special thanks to Bekka for the many chemistry, biology and quaker parrot chats over the years.

Thank-you for the support of all the past and present Andrews and Blair Comrades; Dr Yih Ching Ong, Dr Dimuthu Chanaka, Dr Matthew Flynn, Dr Liam Stephens, Jamie Greer, Kirralee Burke, Michael Stevens, Nimrod Eren, Daniel Van Zeil, Shazia Nawaz and Rupinder Kaur. I have thoroughly enjoyed the group dinners and trivia events with you all! A special mention to Yih Ching for our many campus walks, Nimrod for the fun office chats and Dimuthu for the encouraging chats over

the years. Thank-you to Liam for helping with bacterial studies and for taking the time to teach me, and Rajini Brammananth for the initial bacterial studies. I wish Rupinder all the best with your interesting material chemistry.

I have been so lucky to start my PhD at similar times as Kirralee Burke and Michael Stevens; it has been a fantastic journey with you both and I am very grateful for all of your support and assistance with biology and crystallography. I have fond memories of many office chats with Michael about everything from politics to music, and countless discussions with Kirralee about the bismuth and gallium chemistry life, as well as games, whether computer, console or board-based games. Thank-you both for making my PhD journey so memorable.

A huge thank-you to my family and friends for their support, especially my partner Calum for your understanding and patience throughout my PhD, and for keeping the days interesting with your eclectic music tastes throughout the working from home period. I am grateful to my parents, Rhonda and Warren, my sister Kelly, my extended family and Calum's family for being proud of me and for making the effort to understand my project. A special thank-you to Calum and Kelly for listening to my chemistry troubles and offering suggestions, even if you didn't understand it all! I am thankful to my amazing friends Bec, Daniel, Steph, Nick, Marcus, Dylan and Jordyn who have been supportive. Our many board game sessions have been a blast and I am looking forward to more gaming with you all!

Thank-you to Dr Craig Forsyth, you have been fantastic in helping me understand X-ray crystallography and solving some strange structure. I would also like to thank Scott Blundell for all your assistance with MS, ICP and TGA throughout my PhD. A big thanks to Dr Karen Little, Dr Boujemma Moubaraki and Dr Alasdair McKay for always being happy to help. I must acknowledge the use of the Monash X-ray Platform and Monash Analytical Platform, and the Faculty of Science Dean's Scholarship which made it possible for me to conduct this research.

Abbreviations

A. baumannii	*Acinetobacter baumannii*
BHI	Brain heart infusion
BSA	Bovine serum albumin
CO-ADD	Community for Open Antimicrobial Drug Discovery
CPAM	Cationic dimethylaminoethyl methacrylate poly-acrylamide
DCM	Dichloromethane
DMEM	Dulbecco's Modified Eagle Medium
DMSO	Dimethylsulfoxide
DNA	Deoxyribonucleic acid
DSC	Differential scanning calorimetry
E. coli	*Escherichia coli*
E. faecalis	*Enterococcus faecalis*
E. faecium	*Enterococcus faecium*
ESKAPE	*Enterococcus faecium*, *Staphylococcus aureus*, *Klebsiella pneumoniae*, *Acinetobacter baumannii*, *Pseudomonas aeruginosa* and *Enterobacter* species
ESI-MS	Electrospray ionisation mass spectrometry
Et_2O	Diethyl ether
EtOH	Ethanol
FBS	Foetal bovine serum
H. pylori	*Helicobacter pylori*
IC_{50}	Inhibitory concentration 50 %
ICP-MS	Inductively coupled plasma mass spectrometry
ICP-OES	Inductively coupled plasma optical emission spectroscopy
IR	Infrared
K. pneumoniae	*Klebsiella pneumoniae*
LB	Luria-Bertani
LDH	Lactate dehydrogenase
L. major	*Leishmania major*
m	meta
MeOH	Methanol

MFC	Microfibrillated cellulose
MIC	Minimum inhibitory concentration
m.p	Melting point
MRSA	Methicillin-resistant *Staphylococcus aureus*
MS	Mass spectrometry
NMR	Nuclear magnetic resonance
o	ortho
p	para
P. aeruginosa	*Pseudomonas aeruginosa*
PBS	Phosphate buffered saline
ppm	Parts per million
QSAR	Quantitative structure-activity relationship
ROS	Reactive oxygen species
SARS	Severe acute respiratory syndrome
S. aureus	*Staphylococcus aureus*
SEM	Scanning electron microscopy
SF	Solvent free
SI	Selectivity index
TGA	Thermogravimetric analysis
THF	Tetrahydrofuran
tol	tolyl
UV-Vis	Ultraviolet-visible
VRE	Vancomycin-resistant *Enterococcus*
wt%	Weight percentage

Abstract

This study aimed to explore the synthesis, characterisation and stability of heteroleptic and homoleptic bismuth and gallium phosphinato complexes. The produced complexes were assessed for their medicinal relevance as antibacterial agents, specifically towards multi-drug resistant bacteria, as well as their cytotoxicity towards mammalian cell lines.

A series of 12 phenyl bismuth phosphinato complexes were first examined in Chapter 2. The synthesis of the heteroleptic complexes typically utilised $BiPh_3$ in solvent mediated, solvent free or salt metathesis reactions to form complexes $BiPh_2O(O)P(H)Ph]_\infty$ **2-1**, $[BiPh_2O(O)PPh_2]_\infty$ **2-2**, $[BiPh_2O(O)PMe_2]_\infty$ **2-3**, $[BiPh_2O(O)P(p\text{-}MeOPh)_2]_\infty$ **2-4**, $[BiPh(O(O)P(H)Ph)_2]_\infty$ **2-5**, $[BiPh(O(O)PPh_2)_2]_\infty$ **2-6**, $[BiPh(O(O)PMe_2)_2]_\infty$ **2-7** and $[BiPh(O(O)P(p\text{-}MeOPh)_2)_2]_\infty$ **2-8**. The homoleptic bismuth phosphinato complexes were produced through reaction with $Bi(O^tBu)_3$, yielding $[Bi(O(O)P(H)Ph)_3]_\infty$ **2-9**, $[Bi(O(O)PPh_2)_3]_\infty$ **2-10**, $[Bi(O(O)PMe_2)_3]_\infty$ **2-11** and $[Bi(O(O)P(p\text{-}MeOPh)_2)_3]_\infty$ **2-12**. All prepared complexes were characterised by elemental analysis including Bi content by inductively coupled plasma optical emission spectroscopy (ICP-OES), infrared (IR) and nuclear magnetic resonance (^1H, ^{13}C or ^{31}P NMR) spectroscopy. Complexes **2-1** – **2-4** were structurally authenticated by X-ray crystallography which revealed that they are 1D coordination polymers. The DMSO soluble complexes **2-1** – **2-4** proved stable in DMSO for 24 hours, after which $BiPh_3$ and their *bis*-phosphinato analogues **2-5** – **2-8** can be observed to form. Initial solid-state antibacterial studies revealed that the homoleptic complexes are not active, while the heteroleptic complexes show antibacterial activity. Further solution-state assessment of **2-1** – **2-4** showed excellent antibacterial activity towards vancomycin-resistant *Enterococcus* (VRE) and *E. coli*, however the complexes also proved cytotoxic towards Cos-7 and human fibroblast cells. Complex **2-2** has the most lipophilic phosphinato group and exhibited the greatest toxicity towards both bacteria and mammalian cells, hinting at a structure activity relationship.

The series of *mono*-phosphinato bismuth complexes were expanded on in Chapter 3 through changing the bismuth aryl group to methoxyphenyl or tolyl moieties. A further 12 novel complexes were synthesised through the solvent mediated reaction of $BiAr_3$ with one equivalent of phosphinic acid, producing 6 methoxyphenyl complexes $[Bi(o\text{-}MeOPh)_2O(O)P(H)Ph]_\infty$ **3-1**, $[Bi(o\text{-}MeOPh)_2O(O)PPh_2]_\infty$ **3-2**, $[Bi(o\text{-}MeOPh)_2O(O)P(p\text{-}MeOPh)_2]_\infty$ **3-3**, $[Bi(m\text{-}MeOPh)_2O(O)P(H)Ph]_\infty$ **3-4**, $[Bi(m\text{-}MeOPh)_2O(O)PPh_2]_\infty$ **3-5**, $[Bi(m\text{-}MeOPh)_2O(O)P(p\text{-}MeOPh)_2]_\infty$ **3-6**, $[Bi(m\text{-}tol)_2O(O)P(H)Ph]_\infty$ and 6 *bis*-tolyl complexes **3-13**, $[Bi(m\text{-}tol)_2O(O)PPh_2]_\infty$ **3-14**, $[Bi(m\text{-}tol)_2O(O)P(p\text{-}MeOPh)_2]_\infty$ **3-15**, $[Bi(p\text{-}tol)_2O(O)P(H)Ph]_\infty$ **3-16**, $[Bi(p\text{-}tol)_2O(O)PPh_2]_\infty$ **3-17** and $[Bi(p\text{-}tol)_2O(O)P(p\text{-}$

MeOPh)$_2$]$_\infty$ **3-18**. Characterisation included ^{1}H NMR and IR spectroscopy. IR data suggested bridging phosphinato groups which was confirmed by X-ray crystallography as 1D coordination polymers in the solid-state for complexes **3-4**, **3-13** and **3-17**. The bismuth aryl group greatly influences the biological activity of the complexes, allowing for structure activity relationships to be determined. It is apparent that the *o*-methoxyphenyl complexes **3-1** – **3-3** exhibit poor antibacterial activity and minimal cytotoxicity towards Cos-7 cells, while the *m*-methoxyphenyl series display excellent antibacterial activity towards Gram positive bacteria and high levels of selectivity. The *bis*-tolyl series were more similar in their activity, however the *p*-tolyl compounds **3-16** – **3-18** proved to be more selective towards Gram positive bacteria over Cos-7 cells. Poor Gram negative antibacterial activity was observed for all complexes.

The potential use of heteroleptic phenyl bismuth phosphinato complexes as antibacterial additives was examined in Chapter 4, where a series of novel Bi-cellulose composites were produced containing compounds [BiPh$_2$O(O)P(H)Ph]$_\infty$ **2-1**, [BiPh$_2$O(O)PPh$_2$]$_\infty$ **2-2**, [BiPh$_2$O(O)PMe$_2$]$_\infty$ **2-3**, [BiPh$_2$O(O)P(*p*-MeOPh)$_2$]$_\infty$ **2-4**, [BiPh(O(O)P(H)Ph)$_2$]$_\infty$ **2-5**, [BiPh(O(O)PPh$_2$)$_2$]$_\infty$ **2-6**, [BiPh(O(O)PMe$_2$)$_2$]$_\infty$ **2-7**, [BiPh(O(O)P(*p*-MeOPh)$_2$)$_2$]$_\infty$ **2-8** and silver sulfadiazine (**Ag**). Composite characterisation utilised ICP-OES to determine the metal content and scanning electron microscopy (SEM) examined the morphology and dispersion of the Bi complex on the composite surface. The leaching capability of the composites was examined after 24 hour immersion in water, where the phenylphosphinato-containing composites **2-1** and **2-5** proved to have the highest leaching levels. Solid-state zone of inhibition assays showed that the Bi-cellulose composites exhibit antibacterial activity at loadings of 0.20 wt% to 0.37 wt% towards Gram positive bacteria. The leachates were used to determine antibacterial or cytotoxic activity, where only leachates **2-1** and **2-5** were sufficiently concentrated to exert an effect. Bactericidal activity was observed towards *E. coli* at 4.3 and 4.5 μM of **2-1** and **2-5** respectively, as well as bacteriostatic behaviour towards methicillin-resistant *S. aureus* (MRSA) and VRE at the same concentrations.

Chapter 5 pursued the synthesis of heteroleptic diphenyl gallium *mono*-phosphinato complexes from GaPh$_3$, homoleptic gallium *tris*-phosphinato complexes from salt metathesis reaction with GaCl$_3$ and phenyl gallium oxido-hydroxido cluster formation from the hydrolysis of GaPh$_3$. The produced compounds [GaPh$_2$O(O)P(H)Ph]$_2$ **5-1**, [GaPh$_2$O(O)PPh$_2$]$_2$ **5-2**, [GaPh$_2$O(O)PMe$_2$]$_2$ **5-3**, [GaPh$_2$O(O)P(*p*-MeOPh)$_2$]$_2$ **5-4**, [Ga(O(O)P(H)Ph)$_3$]$_\infty$ **5-9**, [Ga(O(O)PPh$_2$)$_3$]$_\infty$ **5-10**, [Ga(O(O)PMe$_2$)$_3$]$_\infty$ **5-11**, [Ga(O(O)P(*p*-MeOPh)$_2$)$_3$]$_\infty$ **5-12** and [Ga$_{12}$Ph$_{12}$(μ_3-O)$_8$(μ-O)$_2$(μ-OH)$_4$].4DMSO **5-13** were characterised by elemental analysis, NMR (^{1}H, ^{13}C or ^{31}P) and IR spectroscopy. Electrospray ionisation mass spectrometry (ESI-MS) was also used in the characterisation of complexes **5-1** and

5-4 which proved the presence of the hydrolysis product making them impure. Compounds **5-2**, **5-3**, **5-13** and the hydrolysis product of **5-4** [$Ga_4Ph_4(O(O)P(p\text{-}MeOPh)_2)_4(\mu_3\text{-}O)_2$] were structurally authenticated by X-ray crystallography. The homoleptic gallium *tris*-phosphinato complexes **5-9** – **5-12** showed antibacterial activity towards *P. aeruginosa* and *A. baumannii* through solid-state assays. Complexes **5-1**, **5-2** and **5-4** exhibited antibacterial activity towards *P. aeruginosa* at 100 μM and saw a reduction in growth of all bacteria as the complex concentration increased, while showing minimal cytotoxicity towards Cos-7 cells. The gallium cluster **5-13** showed poor antibacterial activity and negligible effects on Cos-7 viability, likely due to poor bioavailability of gallium within the cluster.

Chapter 1 Introduction

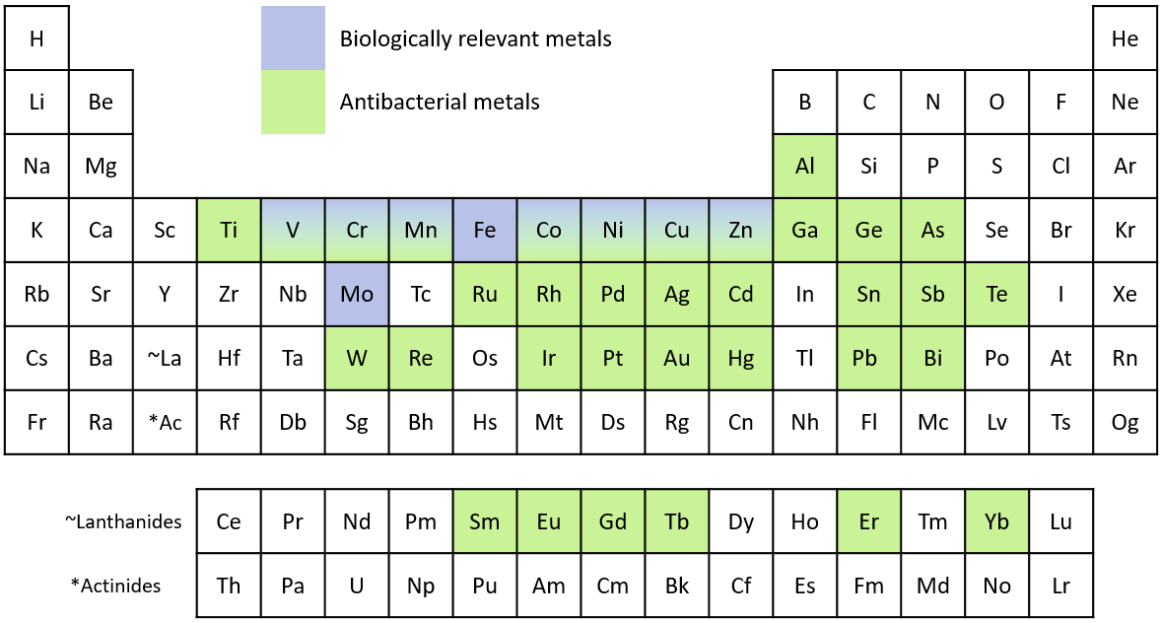

Antibacterial resistance

Metal antibacterial agents

Silver

Bismuth

Gallium

Objectives

1 Introduction

1.1 Antibacterial resistance

Antibacterial resistance is defined as the reduced efficacy of previously effective antibiotics in treating bacterial infections.[1] This resistance can be attributed to the excessive and undiscerning use of antibacterial agents.[2] This is concerning as there has been a reduction in the number of new antibiotics available for treatment (Figure 1-1). Bacteria are capable of developing resistance to new antibiotics shortly after their initial introduction,[3] thus reducing the number of last-line antibiotic treatments. This leads to prolonged illness and potentially death from previously treatable infections.

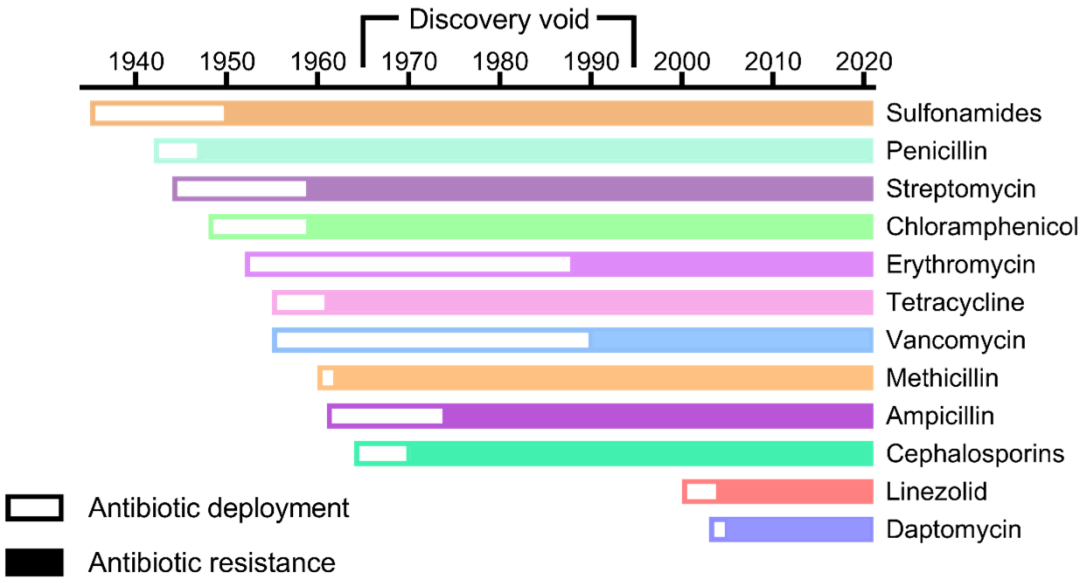

Figure 1-1 Timeline depicting how antibiotic resistance has steadily emerged following the deployment of new antibiotics, while no new antibiotics were produced during the discovery void. (Based on figure by Dantas and Sommer.[3])

1.1.1 Modes of resistance

The mechanism of resistance in bacteria can be separated into four distinct categories, where each renders the antibiotic ineffective through different methods upon exposure as demonstrated in Figure 1-2. One resistance mechanism involves modification of cell wall proteins (Figure 1-2A), resulting in the antibiotic no longer gaining access to the intracellular target.[4] This is seen predominantly in Gram negative bacteria (Figure 1-3), where the outer membrane porin

expression is altered, resulting in hydrophilic antibiotics such as tetracyclines and β-lactams being unable to cross into the periplasmic space.[5] Gram negative bacteria are intrinsically resistant to the antibiotic vancomycin, owing to the glycopeptide being unable to cross the outer membrane.[6]

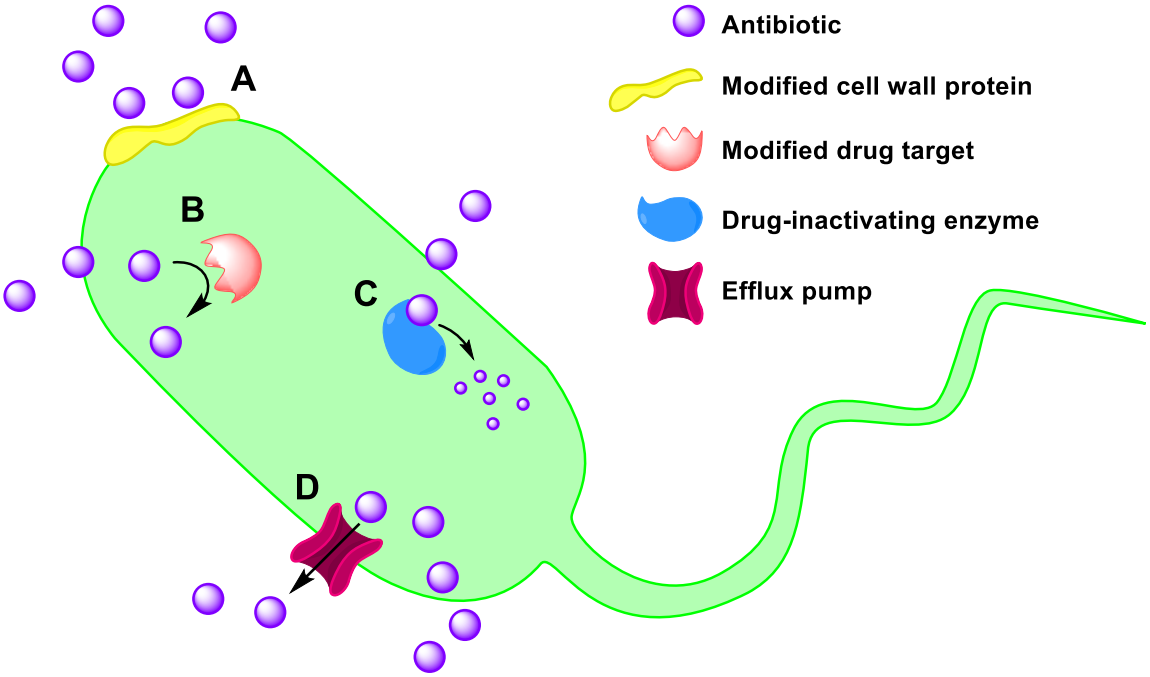

Figure 1-2 Mechanisms of antibiotic resistance observed in bacteria; A) Cell wall protein alteration resulting in loss of permeability towards the antibiotic. B) Modification of proteins that the antibiotic acts upon, inhibiting binding and the antibiotic affect. C) Production of drug-inactivating enzymes that stop the antibiotic from acting on its target. D) Expression of efflux pumps that actively remove antibiotics from the bacteria. (Based on figure by Dantas and Sommer.[3])

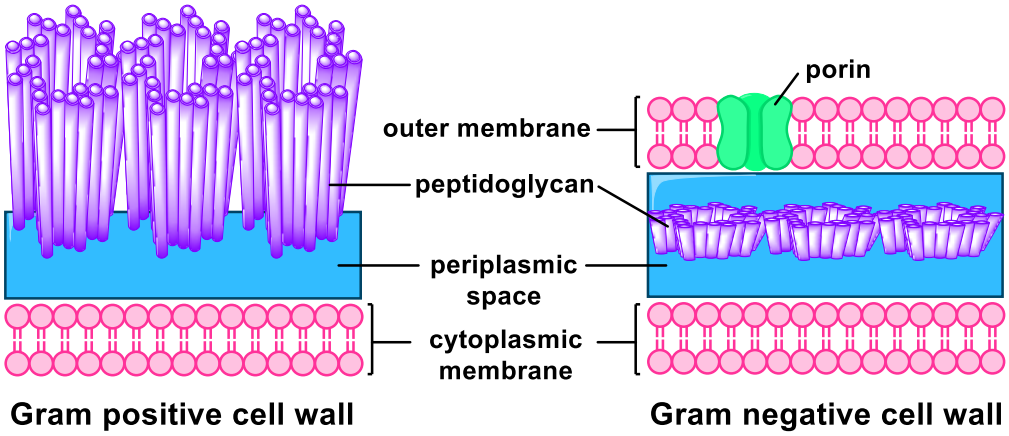

Figure 1-3 Cell wall composition of Gram positive and Gram negative bacteria. Gram positive bacteria have a thick peptidoglycan layer outside the cytoplasmic membrane while Gram negative bacteria have a thin peptidoglycan layer enveloped by an outer membrane.

The second mechanism of antibiotic resistance is through expression of modified target proteins (Figure 1-2B), where the antibiotic cannot bind and exert its effects. An example of this is

resistance to the antibiotic linezolid, where modification of the target ribosomal protein occurs through select gene mutations and enzymatic methylation of the protein, leading to reduced affinity for linezolid binding.[7] This greatly reduces the ability of linezolid to inhibit the initiation of protein synthesis, which would have disrupted growth thus killing the bacteria.[8]

The third mechanism of antibiotic resistance involves bacteria producing enzymes that inhibit the action of antibiotics through chemical alteration (acetylation, phosphorylation) or through destroying part of the molecule (Figure 1-2C). The destruction of β-lactam antibiotics through production of β-lactamases is the main mechanism of resistance to this antibiotic.[9] The β-lactam ring is cleaved through the amide bond by the enzyme as seen in Figure 1-4. The antibiotic is then unable to interact with penicillin-binding protein and exert its effect to stop peptidoglycan cross-linking, a key component in maintaining bacterial cell wall integrity.[10]

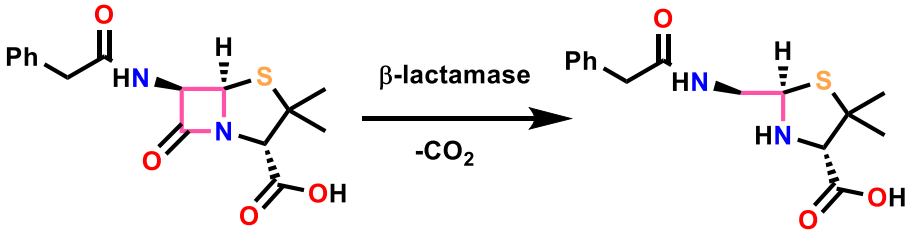

Figure 1-4 Destruction of the penicillin β-lactam ring (shown in pink) via hydrolysis of the amide bond by β-lactamase.

The last mechanism of antibiotic resistance is the expression of efflux pumps, which act to remove antibiotics from the bacteria (Figure 1-2D), and can be substrate specific or have broad specificity to antibiotics.[11] One of the first descriptions of efflux pumps was for removing the antibiotic tetracycline from the cytoplasm of *Escherichia coli* (*E. coli*).[12] This mechanism is used for a wide range of antibiotics, including fluoroquinolones, protein synthesis inhibitors and β-lactams.[4]

1.1.2 Multi-resistant bacteria

The emergence of multi-resistant bacteria is of major concern, where bacteria have developed resistance to more than one type of antibiotic. Resistant genes are acquired through vertical or horizontal gene transmission.[13] Vertical transmission involves the accumulation of genomic mutations, which lead to resistance that is passed on through replication, while horizontal gene transfer involves the swapping of genetic material between bacteria.[14] Resistant genes then allow previously susceptible bacteria to develop antibiotic resistance.

A major concern of multi-resistant bacteria is their prevalence in hospitals and other healthcare environments. Often bacteria are able to form biofilms, which are communities of microorganisms

enclosed in an extracellular polymeric matrix that can adhere to surfaces, including medical devices and implants.[15] Due to the large number of bacteria within the biofilm, multi-resistance to antibiotics is observed, leading to chronic infections.[16] This has led to research into the development of surfaces capable of resisting bacterial growth[17] and development of antibacterial substrates for use in biomedical applications.[18] Further discussion on antibacterial surfaces, coatings and materials are detailed in Chapter 4 (section 4.1).

The World Health Organisation has describe ESKAPE bacteria as a major cause of multi-resistant infections, where ESKAPE species are *Enterococcus faecium* (*E. faecium*), *Staphylococcus aureus* (*S. aureus*), *Klebsiella pneumoniae* (*K. pneumoniae*), *Acinetobacter baumannii* (*A. baumannii*), *Pseudomonas aeruginosa* (*P. aeruginosa*) and *Enterobacter* species.[19] These bacterial species are known for high levels of antibiotic resistance causing extensive morbidity and mortality, suggesting further research is needed to find new effective drugs.[20,21]

1.1.2.1 *Staphylococcus aureus*

One of the more concerning multi-resistant bacteria is methicillin-resistant *S. aureus* (MRSA),[22] as the bacteria are often found on surfaces throughout the community, leading to widespread infection upon contact.[23] In 2019, MRSA caused 18.5 % of *S. aureus* bacteraemia (presence of bacteria in blood) in Australia, with 75.1 % of these infections resulting from community associated MRSA.[24] The population-weighted average percentage of all *S. aureus* infections caused by MRSA in Europe was 15.5 %, showing a decline from 19 % in 2015 compared with an increase in Australia.[24,25]

Methicillin is a β-lactam antibiotic, as shown in Figure 1-5, and the mechanism of resistance in MRSA involves expression of a modified penicillin-binding protein with low affinity to antibiotics with the β-lactam ring moiety.[26] This means that MRSA is resistant to all β-lactam antibiotics, as well as cephalosporins, which have the same β-lactam ring structure (Figure 1-5). MRSA infections are often treated with linezolid or vancomycin, both depicted in Figure 1-5.[27] It has been found that MRSA infections in cancer patients often failed to respond to vancomycin treatment, with a 52 % failure rate,[27] suggesting other antibiotics may be necessary to treat these infections effectively.

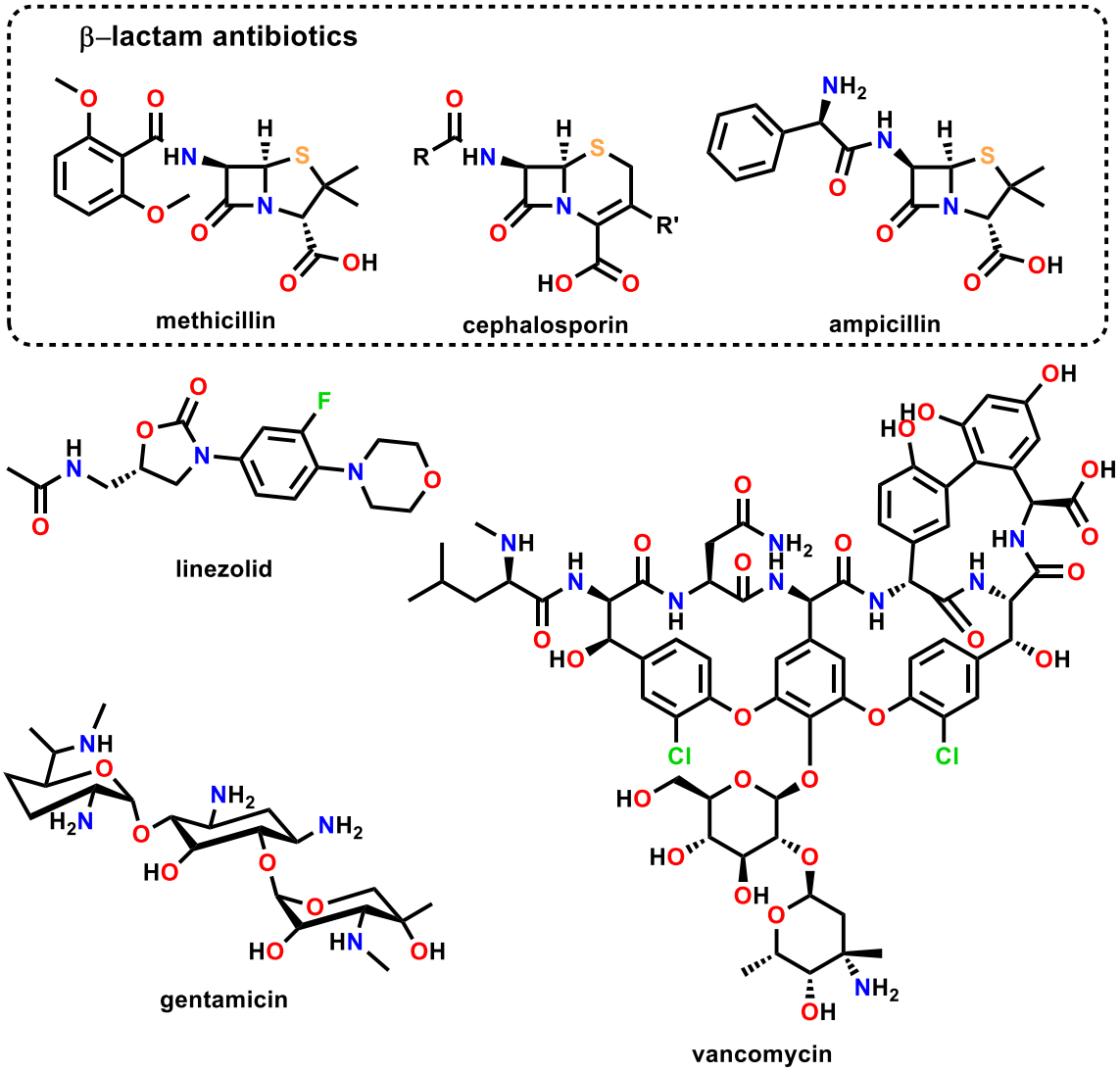

Figure 1-5 General structure of antibiotics including β-lactam including methicillin, cephalosporins and ampicillin, as well as linezolid, gentamicin and vancomycin.

1.1.2.2 *Enterococci* genus

Also of concern is the *Enterococci* genus, specifically *E. faecalis* and *E. faecium*. These bacteria make up close to 1 % of the normal flora found in the large intestine of adults[28] and yet they are commonly the cause of bacteraemia, endocarditis and urinary-tract infections.[29] Australia has a high incidence of vancomycin-resistant *Enterococcus* (VRE), with 41.8 % of all bacteraemia caused by *E. faecium* exhibiting resistance in 2019.[30] Conversely, in Europe, the population-weighted mean percentage of *E. faecium* infections resistant to vancomycin was found to be 18.3 % in 2019.[25] The Australian VRE strain unfortunately also exhibits resistance to ampicillin and high-level gentamicin, with the antibiotic structures shown in Figure 1-5. This is concerning as these antibiotics are the front-line treatment for VRE infections.[31]

Gram positive VRE bacterial infections are often treated with long courses of antibiotics such as linezolid and daptomycin.[32] Daptomycin has a unique mechanism of action, where it binds to the cell membrane and inserts its lipopeptide tail, which then acts as an ion conductor.[33] This causes depolarisation of the membrane and ion efflux, ultimately leading to cell death from DNA, RNA and protein synthesis disruptions.[33,34] It was thought that daptomycin had a low potential for resistance[35] due to its novel mode of action however resistance has been observed in *S. aureus* and *Enterococcus* species.[36]

1.1.2.3 *Escherichia coli*

The Gram negative bacterium *E. coli* was the most commonly reported bacterial species of the eight under surveillance, causing of 44.2 % of invasive infections isolated from blood or cerebrospinal fluid throughout Europe in 2019.[25] Of these *E. coli* isolates, 57.1 % were found to be resistant to at least one class of antibiotics, with the most common antibiotics being aminopenicillins such as ampicillin (Figure 1-5), then fluoroquinolones, cephalosporins and aminoglycosides such as gentamicin (Figure 1-5).[25] Reports of bacteraemia in Australia throughout 2019 also had *E. coli* as one of the main culprits, at 61.8 % of all cases caused by Gram negative bacteria.[37] As similarly reported in Europe, Australia also observed alarmingly high levels of resistance to aminopenicillins at 62.2 % and 26 % of isolates were classed as multi-drug resistant.[37] The recommended treatment for *E. coli* infections is fluoroquinolones such as levofloxacin, as shown in Figure 1-6, however increasing rates of resistance suggest that cephalosporins such as ceftriaxone (Figure 1-6) can lead to better patient outcomes.[38]

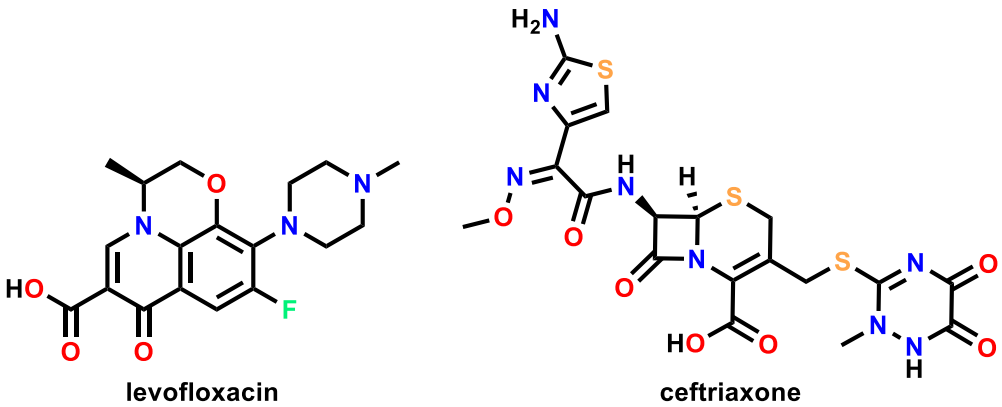

Figure 1-6 Structures of the antibiotics levofloxacin and ceftriaxone.

1.1.2.4 *Pseudomonas aeruginosa*

Infections caused by *P. aeruginosa* are concerning owing to the intrinsic resistance observed towards many early antibiotics including vancomycin, which is due to slow outer membrane porins

with low permeability.[6,20,39] This reduced antibiotic susceptibility further promotes resistance through mutations.[21] In 2019, bacteraemia isolates of *P. aeruginosa* in Australia found that 18.6 % of isolates were resistant to at least one class of antibiotic.[37] This is far less than the 30.8 % of *P. aeruginosa* isolates in Europe that displayed resistance to one or more antibiotic classes.[25] This is of particular concern as *P. aeruginosa* infections are becoming more difficult to treat due to this increased resistance, further prompting research into new alternative antibacterial agents.

1.2 Metal antibacterial agents

Metals and their compounds are being re-examined for their potential as antibacterial agents due to many bacteria displaying multiple resistances to natural and synthetic organic compounds.[40,41] Resistance is less common for metal antibacterial agents compared with organic compounds, due to bacterial metal import systems not being able to discriminate between metal ions that are necessary for bacterial survival and ions that will harm them.[40] Examples of essential metals include manganese, iron, copper and zinc, as shown in Figure 1-7.[42] Antimicrobial metals or metal compounds are also more resistant to decomposition, unlike organic antimicrobial compounds, which can be broken down within the bacteria halting effectiveness. The Community for Open Antimicrobial Drug Discovery (CO-ADD) screened both organic and metal-based compounds for their antimicrobial activity and found that 9.9 % of metal-containing compounds showed activity at concentrations of either 32 µg/mL or 20 µM, compared to only 0.87 % of organic molecules.[43] Figure 1-7 highlights metals which have shown antibacterial activity, including lanthanides such as samarium and europium.[43,44]

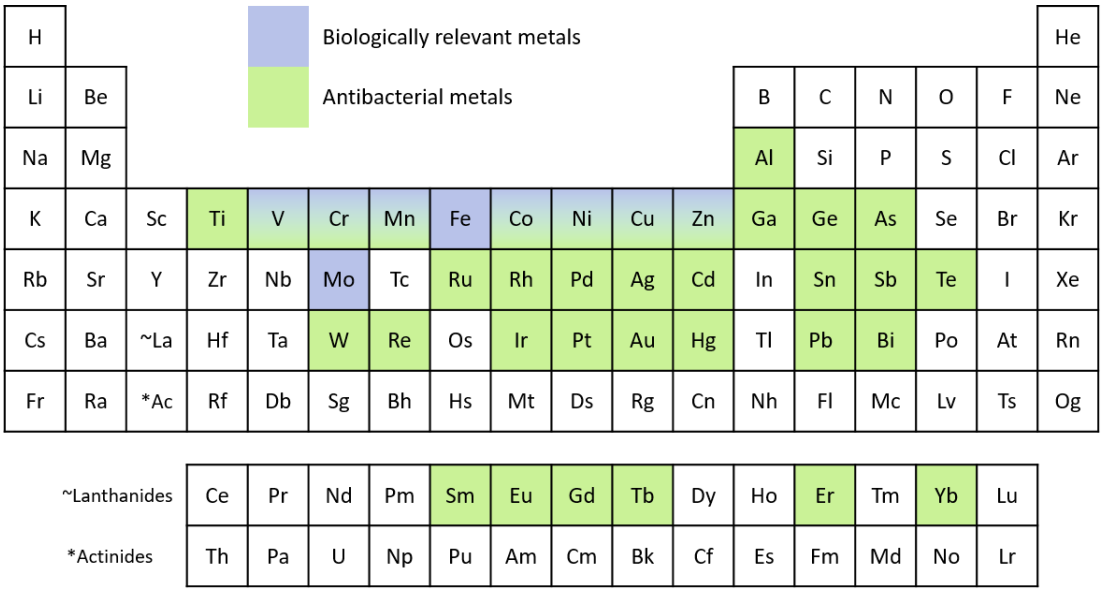

Figure 1-7 Periodic table highlighting biologically relevant metals and metals which have demonstrated antibacterial activity.[42–44]

Metal complexes and nanoparticles can exhibit antimicrobial activity through three main mechanisms, as shown in Figure 1-8. The first mechanism of action is protein dysfunction, observed for many metals including nickel, copper, zinc, silver and lead (Figure 1-8A).[42] Many of these metals act to destroy iron-sulfur clusters in enzymes such as dehydratases, which results in growth inhibition for *E. coli*.[45,46] The release of redox-active iron from the Fe-S clusters can lead to reactive oxygen species (ROS) forming, which in turn cause DNA damage and inhibition of enzymes vital for growth.[42,47] Some transition metals such as vanadium, chromium, nickel and copper can catalyse Fenton chemistry (Figure 1-8B), which ultimately results in the formation of ROS.[48,49]

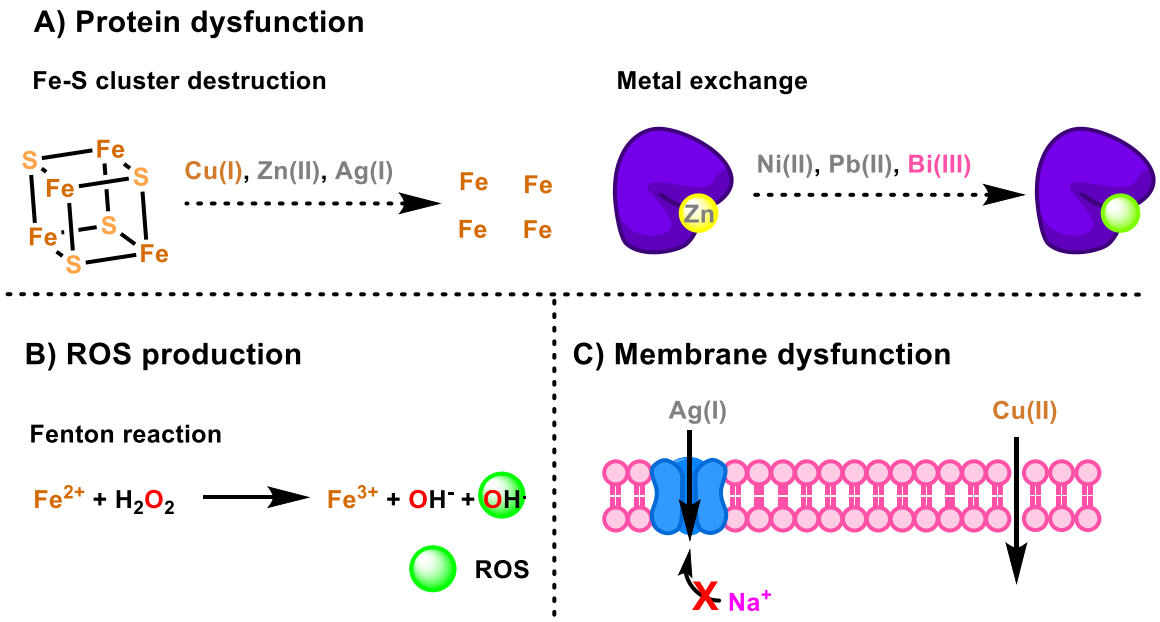

Figure 1-8 Mechanisms of metal antibacterial activity through protein dysfunction (A), production of ROS (B) or impaired membrane function (C).[42,50] (Based on figure by Lemire *et al*.[42])

Further examples of protein dysfunction include metal exchange, where catalytic or structural metals in enzymes are replaced. The enzyme 5-aminolaevulinate dehydratase catalyses the formation of a key precursor in the haem biosynthesis pathway. Lead displaces zinc from the active site of this enzyme, leading to loss of enzyme activity.[51] Bismuth has also been shown to displace zinc in an important chaperone enzyme found within the Gram negative bacteria *Helicobacter pylori* (*H. pylori*), which may lead to cell death.[50] Growth inhibition can be observed in *E. coli* following the displacement of the structural metal zinc by nickel in the enzyme fructose-1,6-biphosphate aldolase.[52] One final example to show zinc is not the only metal to be displaced: silver will substitute copper in Cu,Zn-superoxide dismutase, resulting in greatly reduced enzyme activity in the fungi *Saccharomyces cerevisiae*.[53]

The third mechanism, direct membrane degradation (Figure 1-8C), is observed for copper compounds, which cause oxidation of membrane lipids, ultimately leading to cell death.[54] Silver also acts to compromise the integrity of the cytoplasmic membrane in bacteria through the loss of membrane potential, observed in both *S. aureus* and *E. coli*.[55] These metal-based mechanisms of action have not been extensively studied, however metal antimicrobials are increasingly looked to as bacteria quickly acquire resistance to common antibiotics.

1.2.1 Silver

Silver(I) is the most commonly used antimicrobial metal, with applications in wound dressings and antimicrobial coatings.[56–58] Complexes, such as silver sulfadiazine (Figure 1-9), and silver(0) nanoparticles are employed for their antimicrobial activity.[40] One of the major concerns with the use of silver is the environmental impact, specifically accumulation in aquatic environments. Silver is acutely toxic to freshwater fish due to the interactions of silver ions with enzymes in the gills, disrupting osmoregulation.[59] Another major concern has been raised in regards to silver nanoparticles and their toxicity towards humans.[60] Studies have shown that silver nanoparticles released from wound dressings induce toxicity on human dermal fibroblasts and other skin-derived cells, ultimately leading to inflammation and poor wound healing.[61,62] Further studies have also shown silver nanoparticles can interfere with blood coagulation through intrinsic pathway inhibition, and mice models have also shown decreased platelet aggregation.[63–65] The usage of silver compounds and nanoparticle needs to be re-evaluated given the environmental and human toxicity risks they pose.

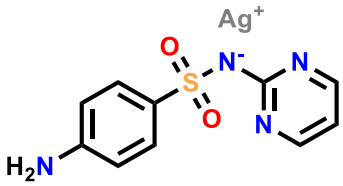

Figure 1-9 Structure of silver sulfadiazine.

Further to toxicity concerns, there have been reports of resistance reported towards silver in bacteria.[56,66] This resistance has been attributed to undiscerning incorporation of silver in consumer products and the lack of policies regarding remediation.[67,68] Silver-resistant Gram negative bacteria express two types of efflux pumps capable of moving silver ions from the cytoplasm to the periplasmic space, then out of the periplasmic space following chaperone protein binding.[69] Gram positive bacteria are less susceptible to the effects of silver,[70] especially silver nanoparticles, due to the interactions of the metal with the negatively-charged peptidoglycan

layer.[71] These resistance concerns with silver usage suggest that other antibacterial compounds should be explored.

1.2.2 Bismuth

Bismuth(III) compounds have been used medicinally to treat skin conditions, gastrointestinal disorders and infections.[72] They display a low toxicity towards humans which has been attributed to their insolubility in neutral aqueous environments.[72,73] A well-known bismuth compound used in medicine is colloidal bismuth subsalicylate (Pepto-bismol), which is used to treat gastrointestinal problems. The proposed mechanism of colloidal bismuth subsalicylate involves the formation of glycoprotein-bismuth complexes within ulcer craters, which act as protective coatings and allow the ulcer to heal.[74]

The Andrews group has previously synthesised bismuth(III) compounds such as bismuth carboxylates, sulfonates, hydroxamates, saccharinates and thiosaccharinates to combat the Gram negative bacteria *H. pylori*, with general compound structures shown in Figure 1-10.[75–80] This bacterium lives in the stomach and can predispose the infected person to peptic ulcers, which can lead to gastritis and gastric cancer.[81] The mechanism of action of bismuth compounds against Gram negative bacteria is dependent upon the iron-uptake system of the bacteria.[82] Iron is essential for the growth of bacteria and bismuth compounds interfere with iron uptake, through binding to proteins such as human lactoferrin, which ultimately leads to inhibition of enzymes essential for bacterial survival.[83] It has been suggested that the antibacterial activity of bismuth compounds can be attributed to their role in iron uptake interference and interactions with thiol-containing bacterial enzymes.[84]

Further antibacterial studies have investigated bismuth thiolates, carboxylates, flavonolates and thiophosphinates as antibacterial agents towards a range of Gram positive and Gram negative bacteria, with complexes shown in Figure 1-10.[85–90] The series of complexes have shown that *tris*-substituted bismuth complexes show far less potential as antibacterial agents when compared to their heteroleptic counter parts. Kotani *et al.* looked at the antimicrobial activity of cyclic organobismuth(III) compounds (Figure 1-10) on Gram positive and Gram negative bacteria through the agar dilution method.[91] The Gram positive bacteria were more susceptible to the bismuth compounds compared to the Gram negative bacteria, which was attributed to the Gram negative bacteria having a lower permeability of its outer membrane.[91] This highlights how bismuth compounds can act directly and indirectly on both Gram positive and negative bacteria to halt bacterial growth, ultimately causing death of the bacteria.

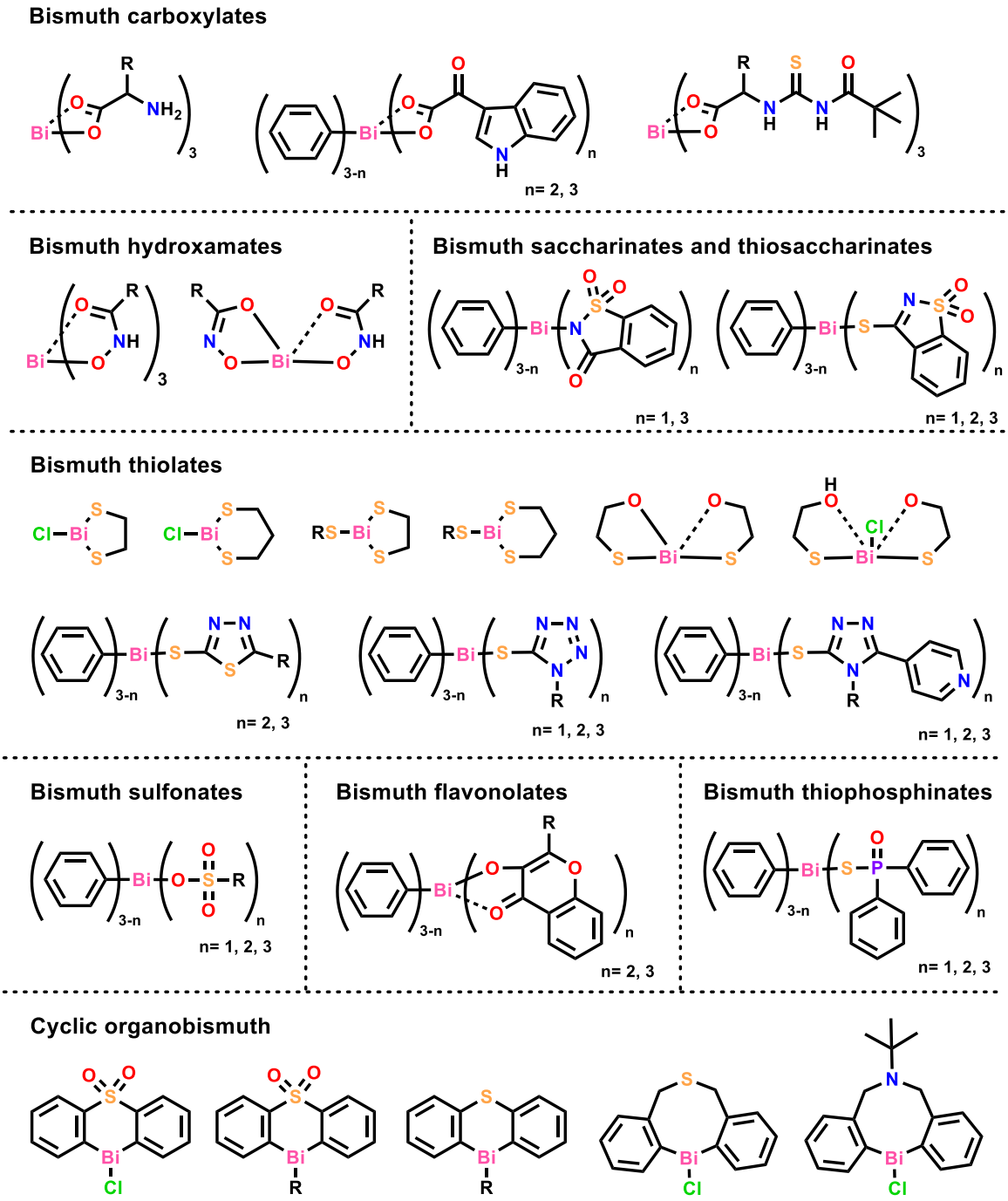

Figure 1-10 General structures of bismuth carboxylates, hydroxamates, saccharinates and thiosaccharinates, thiolates, sulfonates, flavonolates, thiophosphinates and cyclic organobismuth compounds assessed as antibacterial agents to combat Gram positive and Gram negative bacteria, including *H. pylori*.[76–81,86–92]

An investigation of bismuth(III) thiolates against biofilms of MRSA and *P. aeruginosa*, a Gram negative bacteria, has shown that bismuth compounds inhibit the production of exo-polysaccharide.[92–94] This means that bacteria are unable to form the extracellular polymeric matrix which holds the biofilm together. The bismuth thiolates exhibited bactericidal activity towards both Gram positive and negative biofilms. Currently a bismuth thiolate compound (pravibismane)

is in phase 1b/2a clinical trials to treat infected diabetic foot ulcers and pre-clinical trials for serious respiratory infections.[95] Further work on bismuth(III) compounds could enhance this activity towards bacteria and biofilms to suppress the initial colonisation and infection.

1.2.3 Gallium

Gallium(III) compounds have been studied as anticancer, antibacterial and anti-leishmanial agents in recent years.[96–100] Gallium has a two-fold mechanism of action, where it can interact with iron metabolism proteins as well show iron mimicry.[101,102] In bacteria, gallium was found to interfere with nutrient uptake through repression of gene expression involved in essential iron uptake.[103] The ionic radius of gallium(III) and iron(III) are 62 pm and 55 pm respectively, and this similarity means that bacteria and cancer cells cannot easily distinguish between the two metal ions.[96,99] As an iron mimetic, gallium can bind to iron-binding enzymes and proteins such as transferrin, which renders them inactive.[104] This is due to gallium(III) being unable to be reduced under physiological conditions in biological systems, thus resulting in growth inhibition for bacteria and cancer cells.[105,106]

Examples of well researched gallium compounds include gallium nitrate (Ganite™), gallium maltolate, gallium citrate and gallium quinolinolate (KP46), as shown in Figure 1-11.

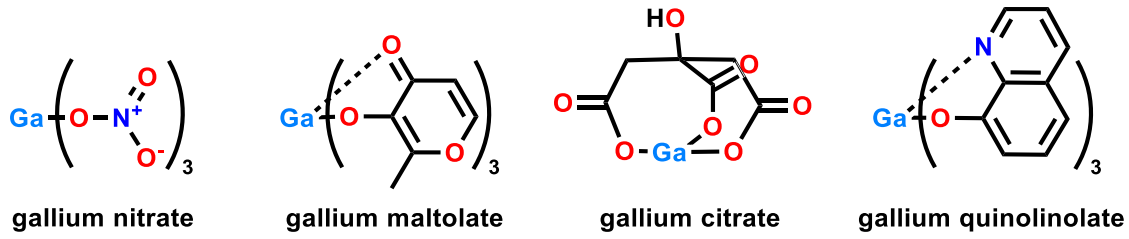

Figure 1-11 Structures of antibacterial or anticancer compounds gallium nitrate, gallium maltolate, gallium citrate and gallium quinolinolate.

Gallium nitrate was approved for the treatment of cancer-associated hypercalcemia, however it is no longer available.[99,106,107] Studies have shown that both gallium nitrate and maltolate are antibacterial towards both Gram positive and Gram negative bacterial strains in broth containing 10 % human serum, with a low iron content to mimic the *in vivo* environmental.[106] Unlike gallium salts such as gallium nitrate, gallium maltolate and citrate are expected to have greater cellular uptake, thus explaining the better bacterial growth inhibition observed.[99,108] Gallium citrate has been shown to localise within malignant cells (as the radioactive ^{67}Ga), as well as exert antibacterial activity towards planktonic *P. aeruginosa* and biofilms.[109,110] Gallium quinolinolate was studied in clinical trials as an anticancer agent, however its hydrolytic stability resulted in poor

gallium release and thus decreased biological activity in comparison to gallium maltolate.[111] It is apparent that gallium compounds can display antibacterial and anticancer activity, however if the compound is too stable, less activity will be observed.

Organogallium complexes have been less extensively studied for their biological potential compared with gallium salts or complexes with organic anions. Alkyl gallium quinolinolato and heterocyclic thiolato complexes have been explored for their anti-leishmanial and anticancer activity respectively. The dimethyl gallium quinolinolate compounds displayed excellent selectivity towards the *Leishmania* parasite over human fibroblasts, however showed no anticancer or antibacterial activity.[100] A series of dimeric or tetrameric dimethyl gallium thiolato complexes were assessed as anticancer agents towards a range of cancer lines, where most compounds inhibited 50 % of growth at concentrations below 30 µM while also showing no effect on the tested human fibroblast cell line at 100 µM.[112] This suggests that organogallium complexes can show good selectivity towards parasites and cancer cells, and further research is needed to investigate their potential as antibacterial agents.

1.3 Objectives

Given the antibacterial activity observed for bismuth and gallium complexes, further research is needed exploring a different ligand system, namely phosphinates. Phosphinic acids (Figure 1-12A) have been used medicinally, most commonly as pseudopeptides due to their non-hydrolysable phosphinate moiety.[113] The phosphinic acid compound shown in Figure 1-12B has been found to inhibit several bacterial enzymes involved in the synthesis of bacterial cell wall structures, such as the peptidoglycan precursor D-alanyl-D-alanine.[114] These enzymes are found in both Gram positive and negative bacteria,[114,115] suggesting phosphinic acids can have broad spectrum activity.

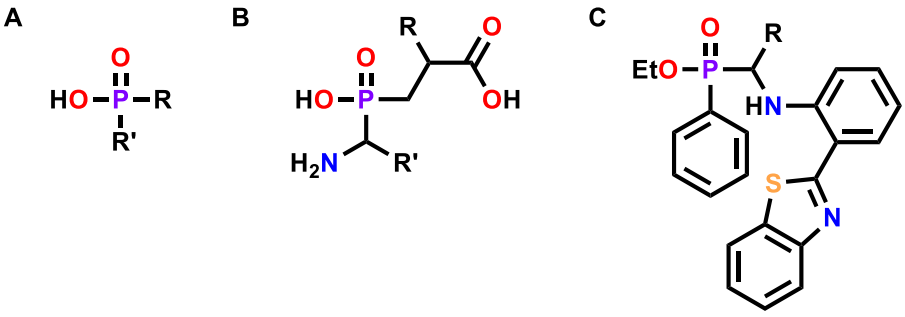

Figure 1-12 General phosphinic acid structure (A) where R and R' are alkyl or aromatic groups, phosphinic acid that disrupts peptidoglycan synthesis (B) and antimicrobial α-aminophosphinato compounds (C).[114,116]

A series of α-aminophosphinato compounds (Figure 1-12C) have also been evaluated for their antimicrobial activity, with bacterial and fungal testing showing antimicrobial activity at a minimum inhibitory concentration of 12.5 μg/mL.[116] This shows that compounds containing the phosphinato moiety have the potential for antimicrobial activity. Previously reported bismuth and gallium phosphinato complexes will be detailed at the beginning of Chapters 2 and 5 respectively.

Simple phosphinic acids will be used for the synthesis of hetero- and homoleptic bismuth(III) (Chapters 2 and 3) and gallium(III) complexes (Chapter 5). The motivation for looking into the series of heteroleptic aryl bismuth phosphinato complexes (Chapters 2 and 3) is to determine potential structure activity relationships through changing phosphinato or aryl moieties. All synthesised metal complexes will be characterised by nuclear magnetic resonance (NMR) spectroscopy (^{1}H, ^{31}P and ^{13}C in either solution- or solid-state), infrared (IR) spectroscopy, melting point, elemental analysis including bismuth content and single X-ray diffraction where possible. Stability in DMSO will be investigated by ^{1}H NMR spectroscopy for all soluble bismuth and gallium phosphinato compounds to determine their suitability for biological assays. Furthermore, solubility analyses will be conducted on all bismuth phosphinato compounds.

The antibacterial activity of the produced bismuth and gallium phosphinato complexes will be assessed towards a range of Gram positive (*S. aureus*, MRSA and VRE) and Gram negative (*E. coli*, *P. aeruginosa* and *A. baumannii*) bacteria. Poorly DMSO soluble compounds will be assessed by solid-state zone of inhibition assays, while DMSO soluble compounds will have their minimum inhibitory concentration (MIC) determined through solution-based assay. The cytotoxicity of the soluble compounds will also be assessed through mammalian cell viability assays using Cos-7 monkey kidney cells and human dermal fibroblast cells, where the concentration to inhibit 50 % cell growth (IC_{50}) value will be determined. The safety of the compounds will be evaluated through comparison of bacterial and mammalian cell toxicities, examining the compounds selectivity towards bacteria. Structure activity relationships will be determined for the heteroleptic bismuth phosphinato complexes.

A series of heteroleptic phenyl bismuth phosphinato complexes will be explored as potential antibacterial additives within a cellulosic matrix, to form Bi-cellulose composites in Chapter 4. The formed composites will be analysed for their bismuth content and scanning electron microscopy (SEM) images to observe the morphology of the surface complexes. Leaching experiments will be conducted, as well as antibacterial and mammalian cell (Cos-7 and human fibroblast) viability studies.

Chapter 2

Bismuth phosphinates

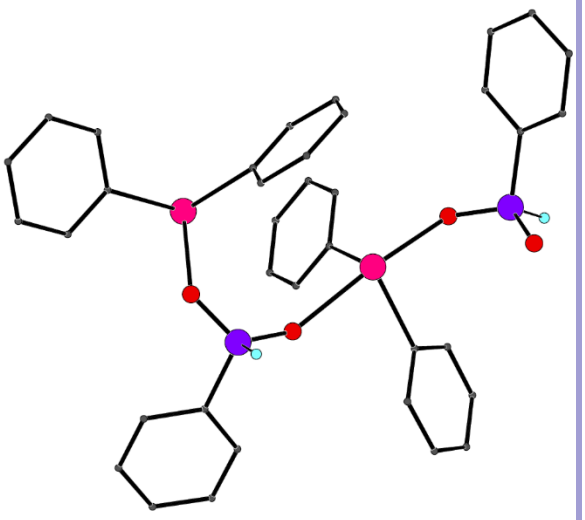

Diphenyl bismuth *mono*-phosphinates

Phenyl bismuth *bis*-phosphinates

Bismuth *tris*-phosphinates

Biology

2 Bismuth phosphinate complexes

2.1 Bismuth phosphinate chemistry

There have been several reports of bismuth(III) phosphinato compounds since 2006,[117] with a predominant focus on structural chemistry and application focus limited to dibismuthane (Bi – Bi bond) formation[118] and catalysis.[119] Scheme 2-1 highlights a number of synthetic routes utilised in the formation of bismuth phosphinato compounds including dearylation or condensation through addition of phosphinic acids, salt metathesis with phosphinate salts or redox-based reactions with phosphine oxides.

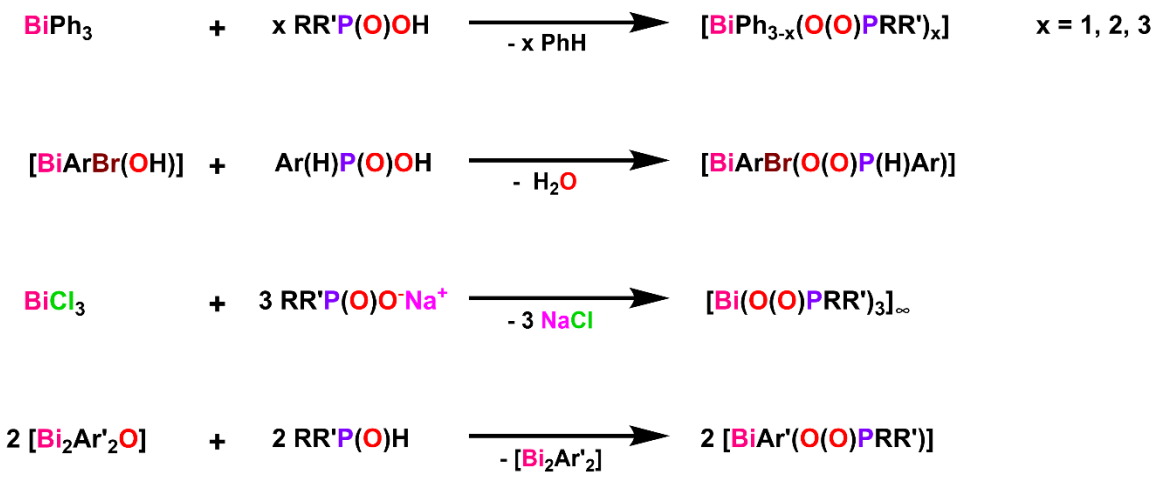

Scheme 2-1 General synthetic routes to form bismuth phosphinate complexes including phenyl cleavage from $BiPh_3$,[119–121] condensation,[122] salt metathesis[117] and redox-based reactions.[118] Ar represents large aromatic moieties.

It has been shown that the steric bulk of both the bismuth substituents and the phosphinato moiety play a large part in determining the final phosphinato bismuth structure. Polymeric structures are reported for the phenyl bismuth complexes with smaller phosphinato groups including 1,1,2,3,3-pentamethyltrimethylenephosphinate (Figure 2-1) and *bis*-(pentafluoroethyl)phosphinate.[119,120] The *tris*-phosphinato bismuth complexes with dimethylphosphinate, diphenylphosphinate and 2-carboxyethyl(phenyl)phosphinate ligands also display polymeric structures due to the bridging binding mode of the phosphinate moiety.[117,123] Sterically bulky phosphinate moieties can lead to reduced bridging on the phosphinate oxygen atoms, as seen for the reaction of $BiPh_3$ with tritylphosphinic acid ($CPh_3(H)P(O)OH$), which produced a tetranuclear cluster as seen in Figure 2-2.[121] Increasing the steric crowding through addition of terphenyl substituents around both the bismuth and phosphinate can produce a

mononuclear complex, stabilised by intramolecular bismuth-arene π-interactions (Figure 2-3).[122] It is evident that many solid-state structures can be accessed through bismuth phosphinato complexes through tuning the bismuth or phosphinato substituents.

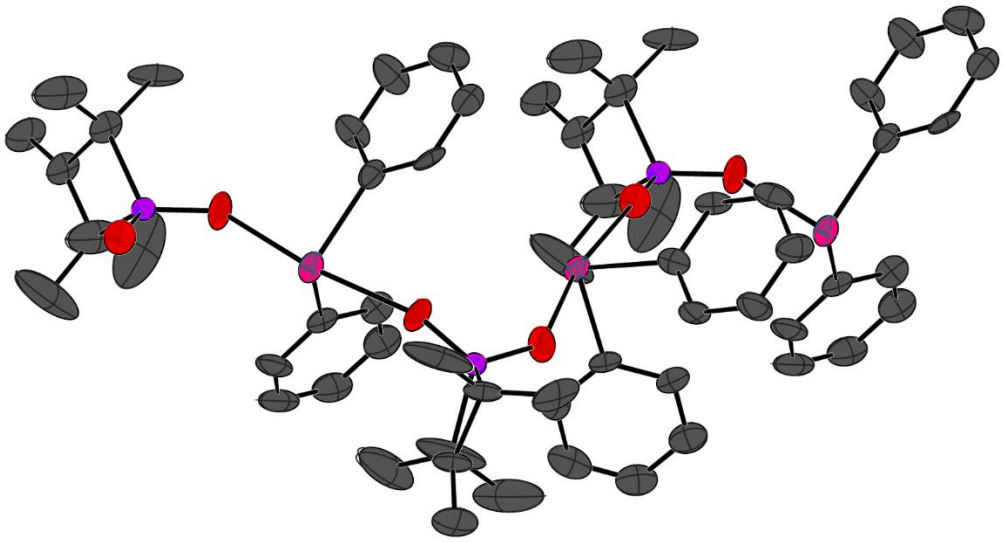

Figure 2-1 Polymeric structure of $[BiPh_2O(O)P(C_2(CH_3)_4CH(CH_3))]_\infty$.[120] Thermal ellipsoids shown at 50 % probability. Hydrogen atoms are omitted for clarity.

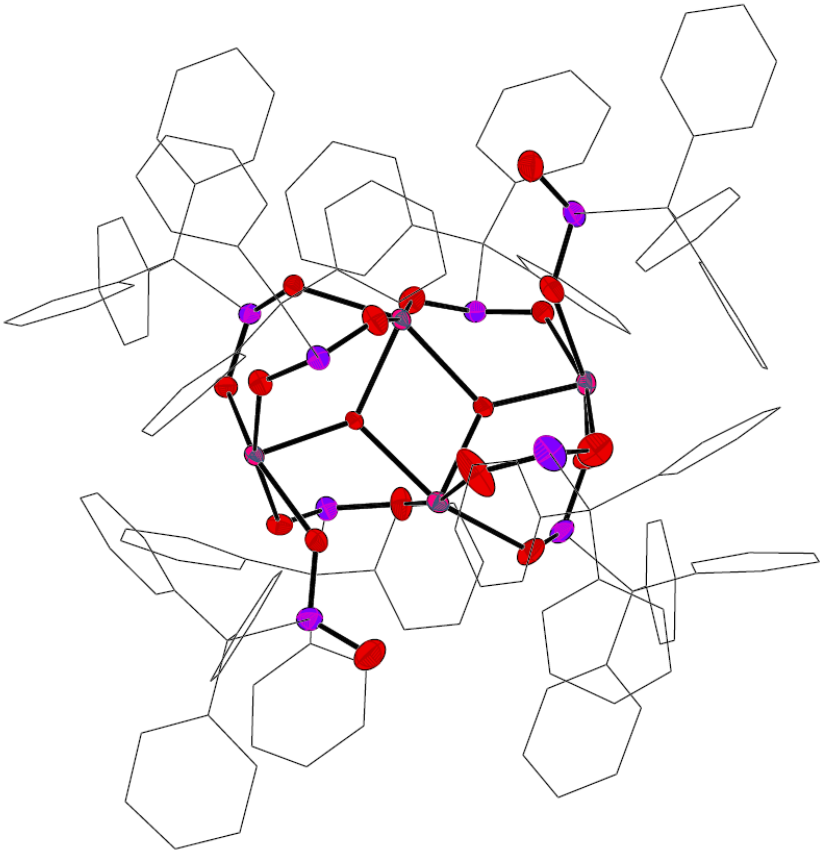

Figure 2-2 Molecular structure of $[Bi_4(\mu_3\text{-}O)_2(O(O)P(H)CPh_3)_8]$.[121] Thermal ellipsoids shown at 50 % probability. Phosphinato substituents shown as wire frame, and hydrogen atoms are omitted for clarity.

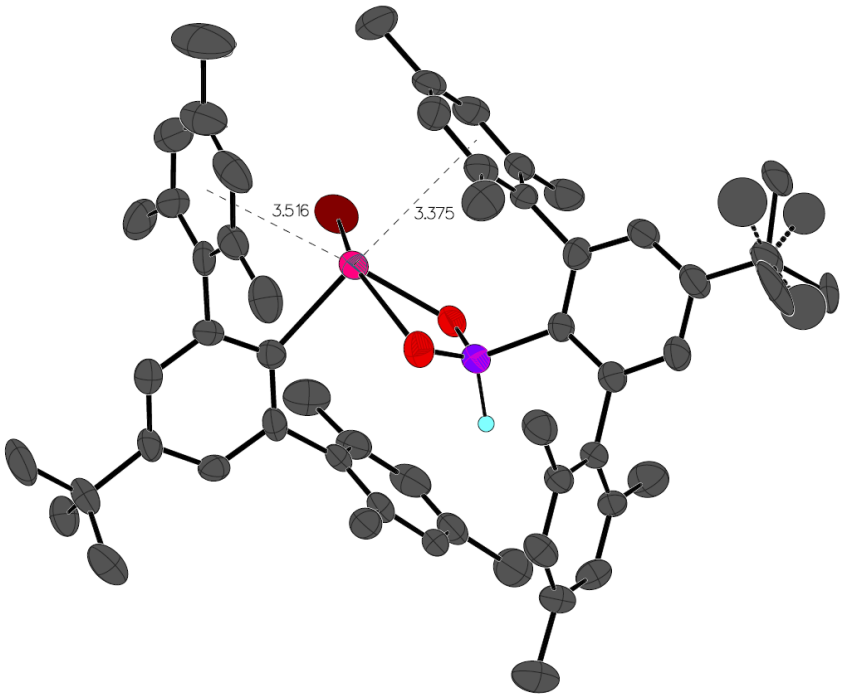

Figure 2-3 Molecular structure of [BiBr((*p*-^{t}Bu)(*o*-mes)$_2$Ph)O(O)P(H)(*p*-^{t}Bu)(*o*-mes)$_2$Ph)].[122] Thermal ellipsoids shown at 50 % probability. Bismuth-arene π distances are in Å. Hydrogen atoms are omitted for clarity. Abbreviations: mes = mesityl.

While bismuth phosphinato complexes solid-state structures are well documented, there are less reports of their solution stability. The sterically congested terphenyl bismuth phosphinato complex was shown to be stable in solution due to intramolecular stabilisation.[122] An NCN chelated organobismuth *bis*-phenylphosphinate complex proved to be unstable in solution, resulting in the formation of elemental bismuth and oxidation of the phosphinate group.[124] It is important to further investigate solution-state stability of bismuth phosphinato compounds to better understand their behaviour.

It is interesting that many ligand classes have been investigated for their potential as antibacterial agents upon complexation to bismuth, however there have not been any reports of bismuth phosphinato compounds. This chapter aims to address the shortcomings in reported solution-state stability of phenyl bismuth phosphinate complexes and begin assessing their potential for use as antibacterial agents.

2.2 Synthesis

Four phosphinic acids were chosen as starting materials: phenylphosphinic acid (Ph(H)P(=O)OH), diphenylphosphinic acid (Ph$_2$P(=O)OH), dimethylphosphinic acid (Me$_2$P(=O)OH) and *bis*-(*p*-methoxyphenyl)phosphinic acid ((*p*-MeOPh)$_2$P(=O)OH), which are displayed in Figure 2-4. Key features considered when choosing the phosphinic acids were increasing steric bulk from methyl

to phenyl moieties, and altering hydrophilicity through introduction of *para*-methoxyphenyl groups. The series of bismuth phosphinato complexes consist of eight heteroleptic complexes of the type $[BiPh_2O(O)PRR']_\infty$ or $[BiPh(O(O)PRR')_2]_\infty$ and four homoleptic complexes of the type $[Bi(O(O)PRR')_3]_\infty$.

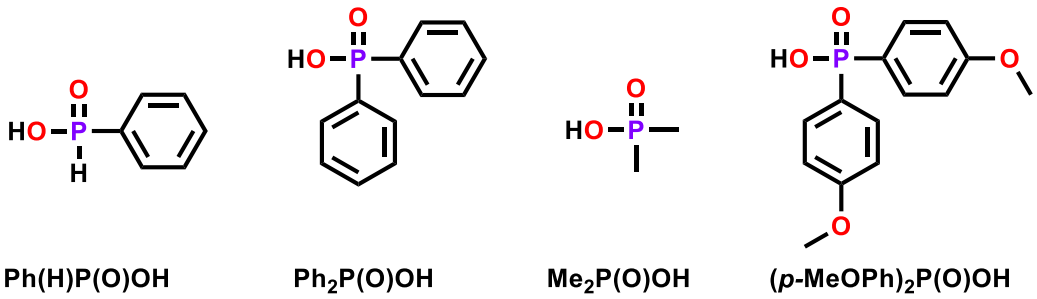

Figure 2-4 Phosphinic acids used for synthesis of bismuth phosphinato complexes.

2.2.1 Diphenyl bismuth *mono*-phosphinates

The diphenyl *mono*-phosphinato bismuth complexes were formed through the equimolar reaction of $BiPh_3$ and phosphinic acid in ethanol at room temperature, as seen in Scheme 2-2. The formed precipitate is washed with hot ethanol and diethyl ether to isolate the diphenyl *mono*-phosphinato bismuth complexes $[BiPh_2O(O)P(H)Ph]_\infty$ **2-1**, $[BiPh_2O(O)PPh_2]_\infty$ **2-2** and $[BiPh_2O(O)P(p\text{-}MeOPh)_2]_\infty$ **2-4** as white powders in yields of 70, 40 and 27 % respectively. Further optimisation of the synthetic route found that heating of the reaction to 50 °C lead to greater yields for complexes **2-2** and **2-4**, 90 % and 86 % respectively. Similar results have been reported, where a room temperature reaction in tetrahydrofuran (THF) produced a diphenyl bismuth *mono*-phosphinato complex in 40 % yield,[120] while a reaction in dichloromethane (DCM) at reflux afforded the *mono*-phosphinato complex in 78 % yield.[119]

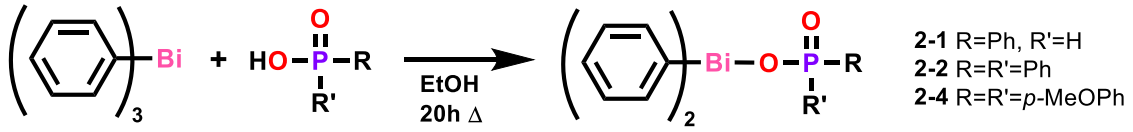

Scheme 2-2 Synthetic route to form diphenyl bismuth *mono*-phosphinato complexes **2-1**, **2-2** and **2-4**.

Synthesis of the *mono*-dimethylphosphinato complex $[BiPh_2O(O)PMe_2]_\infty$ **2-3** proved difficult using the $BiPh_3$ route, with very poor yields and mixtures being obtained. Attempts to form the complex using dimethylsulfoxide (DMSO) as a solvent and using higher temperatures (130 °C) also proved ineffective. An alternative salt metathesis route was employed to form complex **2-3** using $BiPh_2Cl$ and the sodium salt of dimethylphosphinic acid (Scheme 2-3). $BiPh_2Cl$ was synthesised through a redistribution reaction between two equivalents of $BiPh_3$ and one equivalent of $BiCl_3$ and stored

in a dry box in the absence of air and moisture. The sodium salt of dimethylphosphinic acid was produced through the reaction of sodium hydroxide and dimethylphosphinic acid in methanol and was isolated, by removal of methanol, prior to use. The sodium phosphinate was dried *in vacuo* before addition of dry methanol. $BiPh_2Cl$ was added to the sodium phosphinate via solid addition to prevent redistribution in solution. A precipitate was formed immediately upon addition of $BiPh_2Cl$, which was filtered and washed with hot methanol and water to isolate complex **2-3** as a cream coloured powder in a 42 % yield.

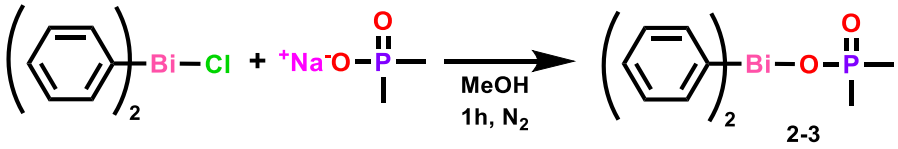

Scheme 2-3 Salt metathesis route to form diphenyl *mono*-dimethylphosphinato bismuth complex **2-3**.

2.2.2 Phenyl bismuth *bis*-phosphinates

The heteroleptic phenyl *bis*-phosphinato bismuth complexes were formed similarly to the *mono*-phosphinato complexes, reacting $BiPh_3$ with two equivalents of phosphinic acid as seen in Scheme 2-4. The reaction was conducted at reflux using ethanol for complexes $[BiPh(O(O)P(H)Ph)_2]_\infty$ **2-5** and $[BiPh(O(O)PPh_2)_2]_\infty$ **2-6** and DMSO for complex $[BiPh(O(O)PMe_2)_2]_\infty$ **2-7**. The *bis*-substituted complex was collected by filtration and washed with hot ethanol and diethyl ether to remove any unreacted reagents producing yields in the range of 72 to 93 %. Similar methods have been reported to produce the phenyl bismuth *bis*-phosphinato compounds by refluxing in methanol or THF for 24 hours, affording yields of 68 to 90 % and 36 % respectively.[119,120]

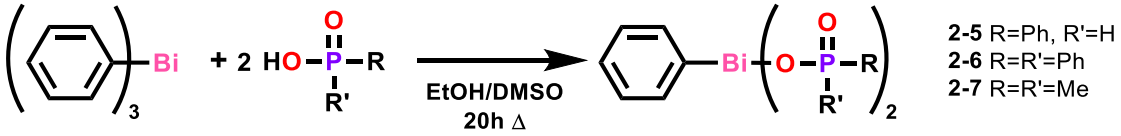

Scheme 2-4 Synthetic route to form phenyl *bis*-phosphinato bismuth complexes **2-5**, **2-6** and **2-7**.

The reaction of $BiPh_3$ and two equivalents of *bis*-(*p*-methoxyphenyl)phosphinic acid in ethanol did not produce complex $[BiPh(O(O)P(p\text{-}MeOPh)_2)_2]_\infty$ **2-8** as expected, but produced complex $[BiPh_2O(O)P(p\text{-}MeOPh)_2]_\infty$ **2-4**. It was thought that increasing the reaction temperature using DMSO as the solvent at reflux might produce **2-8**, however this lead to the *tris*-phosphinato bismuth complex $[Bi(O(O)P(p\text{-}MeOPh)_2)_3]_\infty$ **2-12** forming. As these phosphinic acids have relatively low pK_a values (1.53 to 3.08),[125] they would be suitable for solvent free (SF) reactions by promoting proton exchange with the $BiPh_3$. The relatively low melting point of $BiPh_3$ at 81 °C further promotes the SF reaction and supports its suitability. The thermochemical profile of the 1:2 $BiPh_3$ to *bis*-(*p*-

methoxyphenyl)phosphinic acid reaction was determined through differential scanning calorimetry (DSC) as seen in Figure 2-5, showing an endotherm at 80.9 °C followed by an exotherm at 109 °C. The endotherm is consistent with the melting of $BiPh_3$[126] and the exotherm suggests the formation of complex **2-8**. Conducting the SF reaction using a Kugelrohr oven at 110 °C for 4 hours produced a white solid, which was washed with hot ethanol and diethyl ether to afford **2-8** in a 72 % yield. Discussion for the characterisation of each reaction product is detailed in Section 2.3.

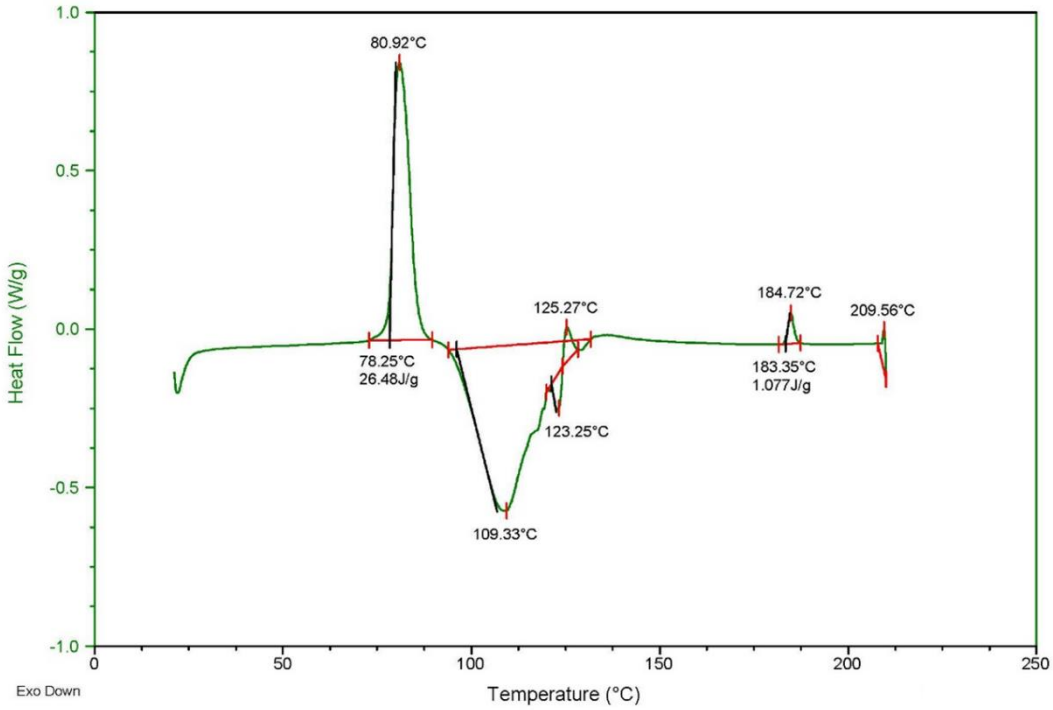

Figure 2-5 DSC trace of 1:2 mixture of $BiPh_3$ and *bis*-(*p*-methoxyphenyl)phosphinic acid from 30 to 210 °C.

2.2.3 Bismuth *tris*-phosphinates

Literature preparations of bismuth *tris*-phosphinato compounds include reactions with bismuth powder or $BiPh_3$ and the phosphinic acid at temperatures exceeding 100 °C overnight or use of $BiCl_3$ and sodium phosphinate salts.[117,119,121] Synthesis of bismuth *tris*- thiolates and sulfonates typically use $Bi(O^tBu)_3$ owing to the simple acid-base reaction producing high yields and ease of product isolation.[77,86] The homoleptic *tris*-phosphinato bismuth complexes $[Bi(O(O)P(H)Ph)_3]_\infty$ **2-9**, $[Bi(O(O)PPh_2)_3]_\infty$ **2-10**, $[Bi(O(O)PMe_2)_3]_\infty$ **2-11** and $[Bi(O(O)P(p\text{-}MeOPh)_2)_3]_\infty$ **2-12** were synthesised through reaction of $Bi(O^tBu)_3$ with three equivalents of the respective phosphinic acid, as depicted in Scheme 2-5. The reaction was conducted under Schlenk conditions at -78 °C due to the high reactivity of $Bi(O^tBu)_3$. Upon warming to room temperature, the resulting precipitate was isolated by filtration and washed with hot ethanol and diethyl ether to afford the complexes in yields ranging from 53 to 92 %.

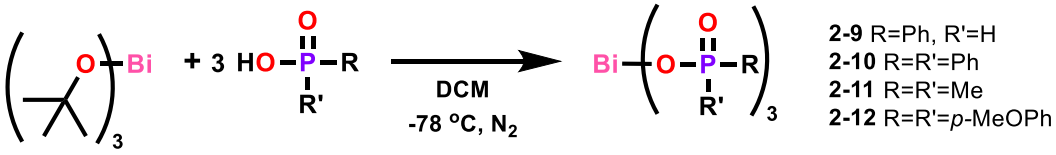

Scheme 2-5 Synthetic route to form *tris*-phosphinato bismuth complexes **2-9** – **2-12** through reaction with $Bi(O^tBu)_3$ and their respective phosphinic acids.

2.3 Characterisation

The *mono*-phosphinato complexes $[BiPh_2O(O)P(H)Ph]_\infty$ **2-1**, $[BiPh_2O(O)PPh_2]_\infty$ **2-2**, $[BiPh_2O(O)PMe_2]_\infty$ **2-3** and $[BiPh_2O(O)P(p\text{-}MeOPh)_2]_\infty$ **2-4** display solubility is DMSO, while the *bis*- and *tris*-substituted complexes are poorly soluble in most solvents, with the exception of $[Bi(O(O)PMe_2)_3]_\infty$ **2-11** which is soluble in water, DMSO and chloroform. The soluble complexes were analysed by solution-state ^1H and ^{31}P nuclear magnetic resonance (NMR) spectroscopy while the insoluble complexes were characterised by solid-state ^{13}C and ^{31}P NMR.

The ^1H NMR spectra of complexes **2-1** – **2-4** and **2-11** show an upfield shift of the phosphinato protons upon deprotonation and coordination to bismuth due to the delocalised nature of the PO_2 moiety when compared to their respective phosphinic acids. The key feature of the *mono*-phosphinato complex spectra is the appearance of the *ortho*- *meta*- and *para*-protons of the bismuth-phenyl, which show downfield shifts when compared to $BiPh_3$, depicted in Figure 2-6.

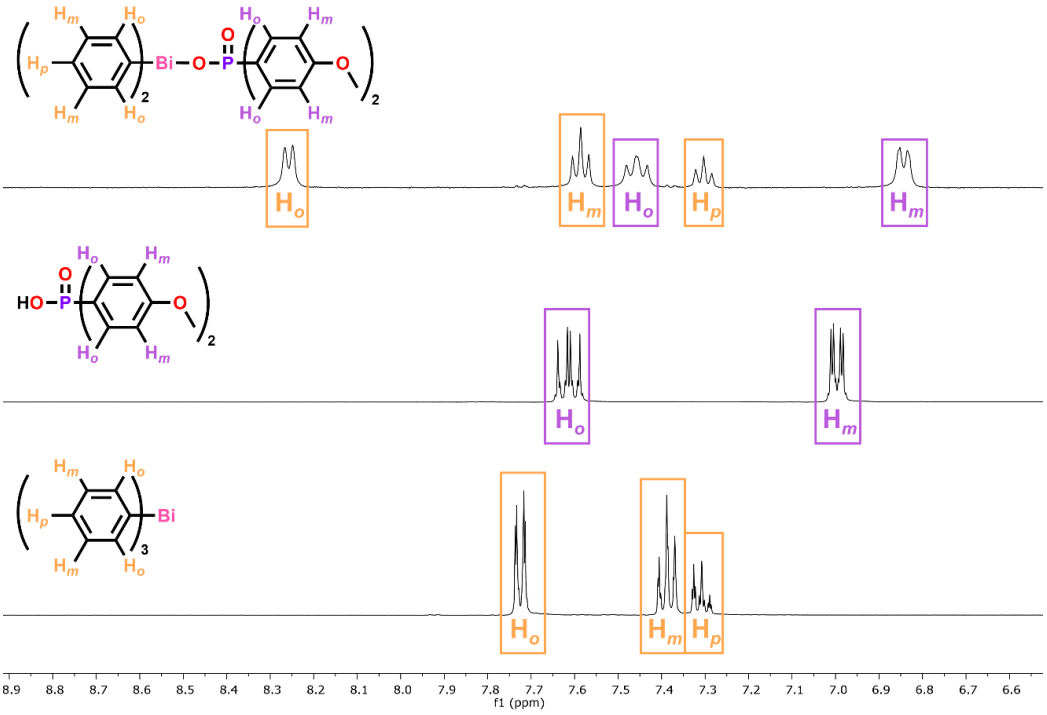

Figure 2-6 ^1H NMR of complex $[BiPh_2O(O)P(p\text{-}MeOPh)_2]_\infty$ **2-4** (top), *bis*-(*p*-methoxyphenyl)phosphinic acid (middle) and $BiPh_3$ (bottom) in d_6-DMSO.

The bismuth phosphinato complexes solid- and solution-state ^{31}P NMR spectra show that the deprotonation of the phosphinic acids lead to a high field shift for the complexes phosphinato group, which is also observed in previously reported bismuth phosphinato compounds.[117] This is illustrated by diphenylphosphinic acid which has ^{31}P signals at 23.5 ppm (d_6-DMSO) and 27.7 ppm (solid) whereas the *mono*-, *bis*- and *tris*-phosphinato complexes have signals at 20.4 ppm (**2-2**, d_6-DMSO), 20.5 ppm (**2-6**) and 24.2 ppm (**2-10**) respectively, as depicted in Table 2-1.

Table 2-1 ^{31}P NMR signals obtained in solution- (‡/*) or solid-state and Δ*v* determined as the difference between asymmetric and symmetric PO_2 stretching bands in IR spectra for complexes **2-1** – **2-12** and their respective phosphinic acids.

Compound		^{31}P (ppm)	Δ*v* (cm^{-1})	Compound		^{31}P (ppm)	Δ*v* (cm^{-1})
$[BiPh_2O(O)P(H)Ph]_\infty$	**2-1**	13.6‡	130 107	$[BiPh_2O(O)PMe_2]_\infty$	**2-3**	39.0‡	113 103
$[BiPh(O(O)P(H)Ph)_2]_\infty$	**2-5**	13.6	103 74	$[BiPh(O(O)PMe_2)_2]_\infty$	**2-7**	46.3	130 131
$[Bi(O(O)P(H)Ph)_3]_\infty$	**2-9**	17.3	82	$[Bi(O(O)PMe_2)_3]_\infty$	**2-11**	47.7*	67
Ph(H)P(O)OH		16.7‡ 18.5	164	$Me_2P(O)OH$		45.5‡ 57.1	180
$[BiPh_2O(O)PPh_2]_\infty$	**2-2**	20.4‡	114 110	$[BiPh_2O(O)P(p\text{-}MeOPh)_2]_\infty$	**2-4**	21.4‡	105 94
$[BiPh(O(O)PPh_2)_2]_\infty$	**2-6**	20.5	116 105	$[BiPh(O(O)P(p\text{-}MeOPh)_2)_2]_\infty$	**2-8**	24.6	105 91
$[Bi(O(O)PPh_2)_3]_\infty$	**2-10**	24.2	93 81	$[Bi(O(O)P(p\text{-}MeOPh)_2)_3]_\infty$	**2-12**	23.8	104
$Ph_2P(O)OH$		23.5‡ 27.7	168	$(p\text{-}MeOPh)_2P(O)OH$		24.2‡ 25.2	177

‡ NMR in d_6-DMSO, * NMR in $CDCl_3$

Infrared (IR) spectroscopy provides valuable insights into the binding mode of the phosphinato moiety through the appearance of strong asymmetric and symmetric PO_2 stretching bands.[127] The difference between the asymmetric and symmetric stretching bands (Δ*v*) is indicative of the phosphinato binding, where a small Δ*v* compared with the phosphinic acid suggests symmetrical binding in a chelating or bridging fashion. Dimethylphosphinic acid has a Δ*v* of 180 cm^{-1} and the corresponding bismuth complexes have Δ*v* of 113 and 103 cm^{-1} **2-3**, 131 and 130 cm^{-1} **2-7** and 67 cm^{-1} **2-11**, suggesting symmetric bridging phosphinato groups. Two asymmetric and symmetric

PO_2 stretching bands were observed for most of the complexes (**2-1** – **2-8** and **2-10**), which may be due to a delocalised coordination mode that is not completely symmetrical. This has been reported for an analogous antimony complex of **2-2** ($[SbPh_2(O(O)PPh_2)]_\infty$), where Δ*v* was 123 and 107 cm^{-1} and x-ray crystallography confirmed a symmetric bridging binding mode.[128] Complexes **2-1** – **2-12** all show the absence of broad P-OH bands typically observed around 1600 cm^{-1} and above 2000 cm^{-1} in their respective phosphinic acids. The Δ*v* for all complexes and their respective phosphinic acids are detailed in Table 2-1.

Melting point and decomposition data for complexes **2-1** – **2-12** were obtained using DSC and thermogravimetric analysis (TGA). The *mono*-phosphinato bismuth complexes decomposition points were 158 °C ($[BiPh_2O(O)P(H)Ph]_\infty$ **2-1**), 207 °C ($[BiPh_2O(O)PPh_2]_\infty$ **2-2**), 190 °C ($[BiPh_2O(O)PMe_2]_\infty$ **2-3**) and 221 °C ($[BiPh_2O(O)P(p\text{-}MeOPh)_2]_\infty$ **2-4**) and coincided with a mass loss on the gravimetric plot. The initial mass loss was in the range of 27 to 36 % which was attributed to the loss of two phenyl rings from the bismuth. Temperatures beyond 280 °C saw further decomposition of the complexes, as seen in Figure 2-7.

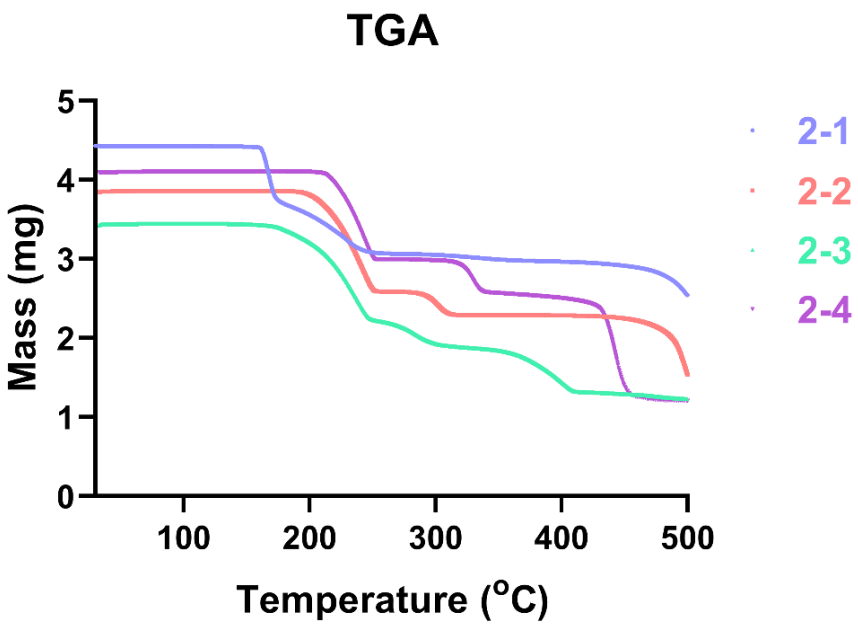

Figure 2-7 TGA trace showing mass loss of *mono*-phosphinato complexes **2-1** – **2-4** from 30 to 500 °C.

Thermogravimetric analysis was employed to determine the products from the 1:2 $BiPh_3$ to *bis*-(*p*-methoxyphenyl)phosphinic acid reactions in ethanol, DMSO or via SF methods (Figure 2-8). The mass loss at each decomposition point is correlated to a structural change, where it is expected the phenyl groups will come off the bismuth first. This is observed for the ethanol (**2-4**) and SF (**2-8**) reaction conditions, where a mass loss of 27 % and 13 % occurs respectively. The further

decomposition of the complexes beyond 400 °C is likely due to the breakdown of the phosphinato ligand, where it is expected bismuth phosphate would be the final decomposition product.[123]

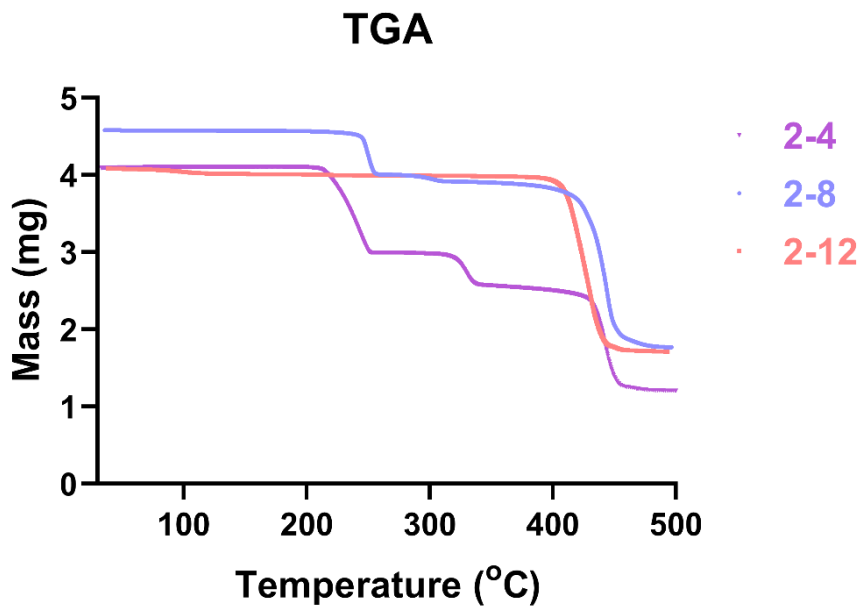

Figure 2-8 TGA trace from 30 to 500 °C of complexes synthesised through 1:2 $BiPh_3$ to *bis*-(*p*-methoxyphenyl)phosphinic acid using different reaction conditions: ethanol reflux (**2-4**), SF (**2-8**) and DMSO reflux (**2-12**).

Decomposition and melting point analysis of phenyl *bis*-phosphinato bismuth complexes also saw the decomposition points with the initial mass loss corresponding to the loss of a phenyl group from the bismuth. The *bis*-substituted compounds had higher melting points in comparison to the *mono*-phosphinato compounds with the same phosphinato groups: 197 °C ($[BiPh(O(O)P(H)Ph)_2]_\infty$ **2-5**), 330 °C ($[BiPh(O(O)PPh_2)_2]_\infty$ **2-6**), 300 °C ($[BiPh(O(O)PMe_2)_2]_\infty$ **2-7**) and 250 °C ($[BiPh(O(O)P(p\text{-}MeOPh)_2)_2]_\infty$ **2-8**).

The *tris*-phosphinato bismuth complexes show good thermal stability up to temperatures of 330 °C, with the exception of complex $[Bi(O(O)P(H)Ph)_3]_\infty$ **2-9** which decomposes at 170 °C. Interestingly, the melting points of the complexes do not correspond with their decomposition points for complexes **2-9**, $[Bi(O(O)PPh_2)_3]_\infty$ **2-10** and $[Bi(O(O)P(p\text{-}MeOPh)_2)_3]_\infty$ **2-12**, as seen for their corresponding *mono*- and *bis*-phosphinato bismuth complexes. Both the *tris*-diphenylphosphinato (**2-10**) and *tris*-dimethylphosphinato ($[Bi(O(O)PMe_2)_3]_\infty$ **2-11**) complexes have greater melting points than their *mono*- and *bis*-substituted counterparts at 340 and 420 °C respectively, which is significantly higher than the previously reported 237 °C (**2-10**) and 71 to 73 °C (**2-11**).[117] It is unknown why the melting points are substantially different, however the spectroscopic data is in agreement with formation of complexes **2-10** and **2-11**. The *tris*-

phenylphosphinato complex **2-9** has a melting point of 130 °C, which is significantly lower than the *bis*-phenylphosphinato complex **2-5** melting point of 197 °C. Similarly, the *bis*-(*p*-methoxyphenyl)phosphinato-containing complex **2-12** has a lower melting point of 230 °C when compared with 250 °C for the *bis*-substituted complex **2-8**.

Further characterisation included elemental analysis for carbon and hydrogen values of the bulk sample, as well as bismuth content analysis through use of inductively-coupled plasma optical emission spectroscopy (ICP-OES). The bismuth analysis was necessary for complexes containing the diphenylphosphinato group (**2-2**, **2-6** and **2-10**) and the *bis*-(*p*-methoxyphenyl)phosphinato group (**2-4**, **2-8** and **2-12**) due to their very similar carbon and hydrogen contents, as seen in Table 2-2. Complexes with the phenylphosphinato and dimethylphosphinato ligands had sufficiently different carbon and hydrogen values between their complexes, where the carbon, hydrogen and bismuth content are described in Chapter 7 (Experimental section 7.7). The elemental analysis results support the formation of all desired complexes **2-1** – **2-12**.

Table 2-2 Calculated and experimental elemental analysis and ICP-OES bismuth content analysis on complexes containing diphenylphosphinato **2-2**, **2-6** and **2-10** and *bis*-(*p*-methoxyphenyl)phosphinato **2-4**, **2-6** and **2-12**.

Compound		Calculated			Experimental		
		C (%)	H (%)	Bi (%)	C (%)	H (%)	Bi (%)
$[BiPh_2O(O)PPh_2]_\infty$	**2-2**	49.67	3.47	36.01	49.73	3.38	36.4
$[BiPh(O(O)PPh_2)_2]_\infty$	**2-6**	50.01	3.50	29.0	49.72	3.45	30.4
$[Bi(O(O)PPh_2)_3]_\infty$	**2-10**	50.25	3.51	24.3	50.26	3.56	23.5
$[BiPh_2O(O)P(p\text{-}MeOPh)_2]_\infty$	**2-4**	48.76	3.78	32.6	48.75	3.69	31.1
$[BiPh(O(O)P(p\text{-}MeOPh)_2)_2]_\infty$	**2-8**	48.58	3.96	24.9	48.82	3.82	23.8
$[Bi(O(O)P(p\text{-}MeOPh)_2)_3]_\infty$	**2-12**	48.47	4.07	20.1	48.53	4.09	19.6

2.3.1 X-ray crystallography

The DMSO solubility of the diphenyl bismuth *mono*-phosphinato complexes allowed for the isolation of crystals suitable for single-crystal X-ray diffraction. Complexes $[BiPh_2O(O)P(H)Ph]_\infty$ **2-1**, $[BiPh_2O(O)PPh_2]_\infty$ **2-2**, $[BiPh_2O(O)PMe_2]_\infty$ **2-3** and $[BiPh_2O(O)P(p\text{-}MeOPh)_2]_\infty$ **2-4** were heated in DMSO and the hot solutions filtered before being left to stand for several days, after which colourless crystals could be observed. The *mono*-phosphinato complexes form 1D coordination polymers, with bismuth centres connected by bridging phosphinato groups as similarly reported

in both transition metal (Cr(III),[129] Mn(II)[130] and Cu(II)[131]) and group 15 complexes (Sb(III)[128] and Bi(III)[119–121,123]).

The 1D polymeric chains for complexes **2-1** – **2-3** have a distorted square pyramidal geometry around the five-coordinate bismuth centre which bridge two phosphinato oxygen atoms with almost linear O(1)–Bi(1)–O(2) bond angles of 161.63(13)° for **2-1**, 170.9(2)° for **2-2** and 163.68(18)° for **2-3**. Figures 2-9 to 2-11 depict the isostructural diphenyl bismuth *mono*-phosphinato coordination polymers **2-1** – **2-3**, with selected bond lengths and angles detailed in Table 2-3. It can be observed that each bismuth atom interacts with an adjacent bismuth-bound phenyl group, with a Bi-arene$_{centroid}$ distance of 3.743 Å for **2-1**, 3.437 Å for **2-2** and 3.654 Å for **2-3**, which are typical of bismuth-arene π-interactions.[132] Reports of diphenyl bismuth or antimony phosphinato complexes have shown similar coordination modes of the phosphinato moiety however there was no mention of metal-arene π-interactions as seen for complexes **2-1** – **2-3**.[120,128] It can be noted that the P-O bond lengths are similar (Table 2-3) due to the strong interactions of both phosphinato oxygen atoms with bismuth which indicates a delocalised coordination mode.[133]

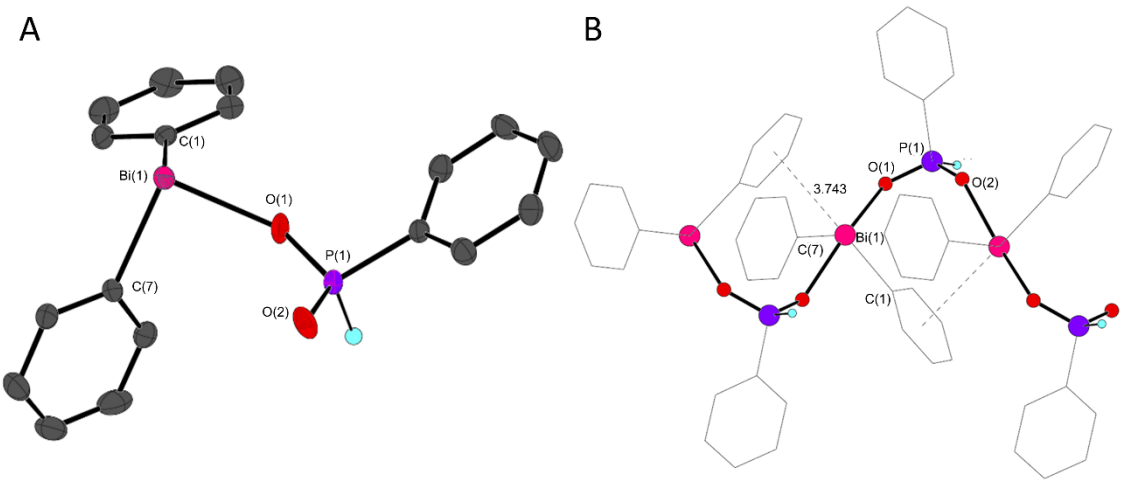

Figure 2-9 Molecular (A) and polymeric (B) structure of $[BiPh_2O(O)P(H)Ph]_\infty$, **2-1**. Thermal ellipsoids shown at 50 % probability in molecular structure. Bismuth-arene π distances are in Å. Hydrogen atoms on phenyl rings are omitted for clarity.

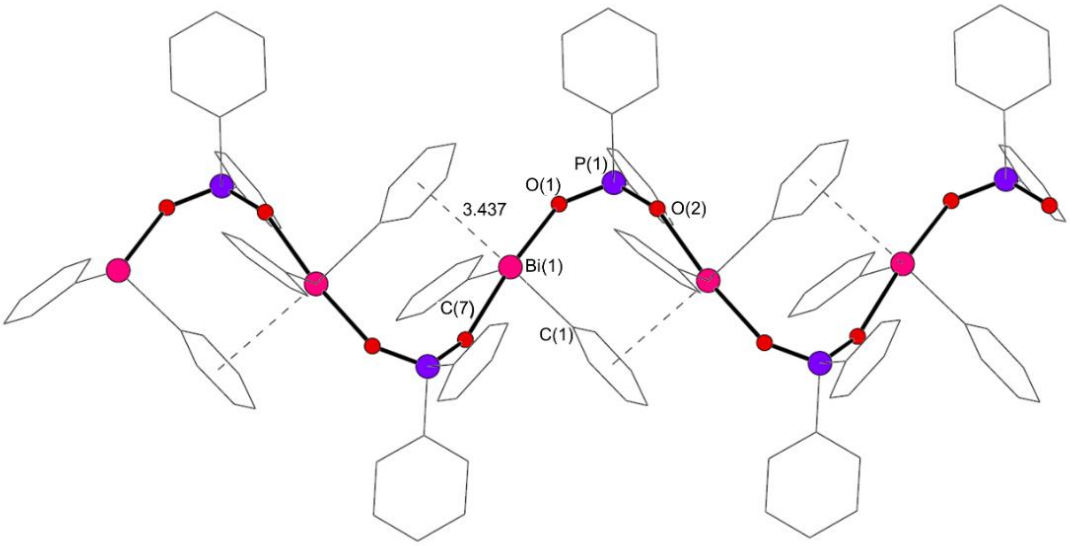

Figure 2-10 Polymeric structure of $[BiPh_2O(O)PPh_2]_\infty$, **2-2**. Bismuth-arene π distances are in Å. Hydrogen atoms are omitted for clarity.

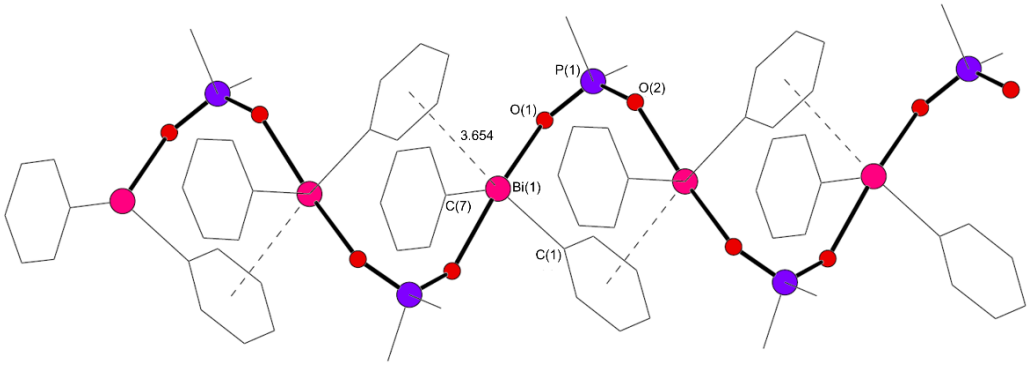

Figure 2-11 Polymeric structure of $[BiPh_2O(O)PMe_2]_\infty$, **2-3**. Bismuth-arene π distances are in Å. Hydrogen atoms are omitted for clarity.

Table 2-3 Selected bond lengths and bond angles for complexes **2-1** – **2-4**.

Bond lengths (Å)	**2-1**	**2-2**	**2-3**	**2-4**
Bi(1) – C(1)	2.251(5)	2.243(8)	2.267(6)	2.248(4)
Bi(1) – C(7)	2.246(5)	2.255(9)	2.267(6)	2.250(4)
Bi(1) – O(1)	2.354(3)	2.342(5)	2.350(4)	2.344(3)
Bi(1) – O(2)*	2.328(3)	2.324(6)	2.331(4)	2.368(3)
P(1) – O(1)	1.496(3)	1.504(6)	1.499(5)	1.518(3)
P(1) – O(2)	1.505(3)	1.501(6)	1.515(4)	1.508(3)
Bond angles (°)				
C(1) – Bi(1) – C(7)	94.33(17)	93.4(3)	93.8(2)	91.37(14)
C(1) – Bi(1) – O(1)	81.80(14)	88.5(3)	85.01(19)	84.49(13)
C(1) – Bi(1) – O(2)*	87.13(15)	86.3(3)	82.96(19)	83.74(13)
C(7) – Bi(1) – O(1)	84.51(14)	83.9(3)	83.51(18)	88.18(13)
C(7) – Bi(1) – O(2)*	81.75(14)	89.0(3)	86.34(18)	87.04(13)
O(1) – Bi(1) – O(2)*	161.63(13)	170.9(2)	163.68(18)	167.19(10)
O(1) – P(1) – O(2)	118.2(2)	117.8(3)	116.3(3)	115.70(17)

*Symmetry transformations used to generate equivalent atoms: **2-1** (-x + 1/2, y + 1/2, -z + 1/2), **2-2** (x + 1/2, -y + 3/2, -z + 1), **2-3** (x – 1/2, -y + 1/2, -z + 1), **2-4** (-x + 3/2, y – 1/2, -z + 1/2).

Complex **2-4** adopts a distorted disphenoidal conformation around the four-coordinate bismuth centre, bridged by two *bis*-(*p*-methoxyphenyl)phosphinato moieties to form the 1D coordination polymer chain, as seen in Figure 2-12, with select bond lengths and angles in Table 2-3. There is strong evidence of a sterically active lone pair due to the C–Bi–O and C–Bi–C bond angles averaging 86.97° while the O–Bi–O bond angle is 167.19(10)°. The difference in conformation compared with complexes **2-1** – **2-3** can be attributed to the alignment of bismuth-phenyl and phosphinato-methoxyphenyl groups through π-π interactions. The methoxy moiety in the *para* position causes a dipole-induced dipole interaction between the aromatics rings, resulting in an offset face-to-face π-π interaction.[134] The aromatic C-H – centroid distance is 3.654 Å which is typical of interplanar π-π interactions.[134] It is apparent that the addition of the methoxy group is necessary to induce π-π interactions as the unsubstituted diphenylphosphinato group does not show any. Unlike complexes **2-1** – **2-3**, there are no interactions between the bismuth atoms and adjacent bismuth-phenyl moieties for complex **2-4**, as similarly reported for diphenyl bismuth *mono*-diphenylthiophosphinato and *mono*-mesitylsulfonato complexes.[75,90]

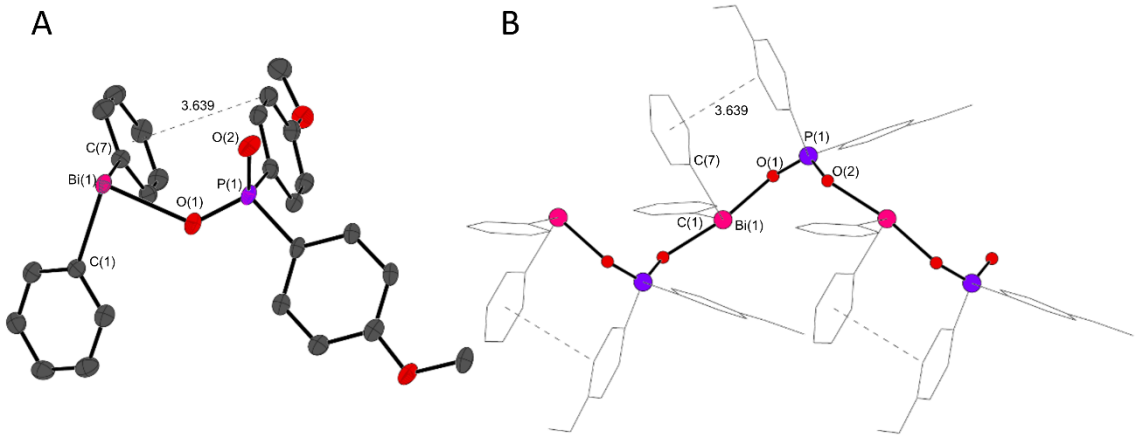

Figure 2-12 Molecular (A) and polymeric (B) structure of $[BiPh_2O(O)P(p\text{-}MeOPh)_2]_\infty$, **2-4**. Thermal ellipsoids shown at 50 % probability in molecular structure. Aromatic C-H – centroid distances are in Å. Hydrogen atoms are omitted for clarity.

Many attempts to grow and isolate crystals of the phenyl bismuth *bis*-phosphinato and *tris*-phosphinato complexes were unsuccessful. There have been reports of phenyl bismuth *bis*-phosphinato crystal structures which contain four bridging phosphinato moieties in a square plane, with the phenyl group and sterically active lone pair giving a distorted square pyramidal geometry.[119,120] It is apparent the phosphinato moiety effects the overall structure, with formation of a tetranuclear macrocycle with the sterically hindered 1,1,2,3,3-pentamethyltrimethylenephosphinate and a continuous chain with *bis*(pentafluoroethyl)phosphinate. Similarly, a phenyl bismuth *bis*-diphenylthiophosphinato complex adopts the continuous polymeric chain conformation, with Bi-S covalent and Bi-O dative bonds.[90] It is most likely that the *bis*-phosphinato complexes $[BiPh(O(O)P(H)Ph)_2]_\infty$ **2-5**, $[BiPh(O(O)PPh_2)_2]_\infty$ **2-6**, $[BiPh(O(O)PMe_2)_2]_\infty$ **2-7** and $[BiPh(O(O)P(p\text{-}MeOPh)_2)_2]_\infty$ **2-8** would adopt a continuous chain structure, owing to their poor solubility. This is further supported by the IR data that the phosphinato group is binding in a chelating or bridging fashion, as seen for the *mono*-phosphinato complexes **2-1** – **2-4**.

2.4 Solubility and stability

The bismuth phosphinato complexes **2-1** – **2-12** display relatively poor solubility in most solvents, likely due to their polymeric solid-state structures. It is important to understand the solubility and stability of the complexes in aqueous solution to determine their suitability for use as antibacterial agents. The water solubility of complexes were determined through dispersion of the solid complex in water for 24 hours at 25 °C. The suspension was filtered through 0.2 µm syringe filters and the filtrate diluted with nitric acid. ICP-OES and inductively coupled plasma mass

spectrometry (ICP-MS) were used to analyse the filtrates of complexes **2-1** – **2-12**, determining the bismuth content of the water and thus the amount of complex solubilised (Table 2-4).

Table 2-4 Water solubility and clogP values of complexes **2-1** – **2-12** as determined by ICP-OES (**2-1** – **2-3**, **2-5** – **2-12**) or ICP-MS (**2-4**). clogP values were calculated using ChemDraw Professional 17.0. Complexes are listed in order of greatest to lowest water solubility.

Compound		Water solubility (ppm(wt/wt))	clogP value*
$[Bi(O(O)PMe_2)_3]_\infty$	**2-11**	4023	-3.874
$[BiPh(O(O)PMe_2)_2]_\infty$	**2-7**	2043	-0.481
$[BiPh_2O(O)PMe_2]_\infty$	**2-3**	469	2.912
$[Bi(O(O)P(H)Ph)_3]_\infty$	**2-9**	348	0.223
$[BiPh(O(O)P(H)Ph)_2]_\infty$	**2-5**	147	1.941
$[BiPh_2O(O)P(H)Ph]_\infty$	**2-1**	42.7	3.659
$[Bi(O(O)P(p\text{-}MeOPh)_2)_3]_\infty$	**2-12**	3.90	6.514
$[Bi(O(O)PPh_2)_3]_\infty$	**2-10**	2.79	7.000
$[BiPh_2O(O)PPh_2]_\infty$	**2-2**	1.58	5.918
$[BiPh(O(O)PPh_2)_2]_\infty$	**2-6**	0.39	6.459
$[BiPh(O(O)P(p\text{-}MeOPh)_2)_2]_\infty$	**2-8**	0.31	6.135
$[BiPh_2O(O)P(p\text{-}MeOPh)_2]_\infty$	**2-4**	0.11	5.756

* The clogP values are likely higher than stated as the complexes exist in polymeric form, however the relative order is expected to remain unchanged.

It is immediately apparent that the dimethylphosphinato complexes (**2-3**, **2-7** and **2-11**) display the greatest water solubility, followed by the complexes containing phenylphosphinato groups (**2-1**, **2-5** and **2-9**). It can be noted that the calculated clogP values for these complexes are lower than those for the diphenylphosphinato and *bis*-(*p*-methoxyphenyl)phosphinato compounds, which is in agreement with the determined solubility results.

A general trend can be observed where the homoleptic bismuth *tris*-phosphinato complexes demonstrate greater water solubility than their heteroleptic counterparts, in which the *bis*-phosphinato complexes display greater solubility than the *mono*-phosphinato complexes. The solid-state structure of the *mono*-phosphinato complexes may provide insights into their lower solubility, where the 1D coordination polymer with bismuth-arene interactions (**2-1** – **2-3**) or π-π interactions (**2-4**) may result in a more hydrophobic compound.

It is important to note that the solubility results were determined based on bismuth content within the water, where the complex may not be intact. Previous studies on bismuth sulfonate complexes have shown their ability to rearrange in solution,[75] and bismuth complexes derived from amino acids rapidly hydrolyse in solution to form bismuth oxido-clusters.[78] To analyse the species solubilised in the water, aliquots of the filtered suspension were evaporated to obtain a residue. The residue was analysed by ^{1}H NMR spectroscopy in d_6-DMSO, where it could be observed that $[BiPh(O(O)PMe_2)_2]_\infty$ **2-7** had rearranged giving aromatic signals consistent with the presence of $BiPh_3$ and $[BiPh_2O(O)PMe_2]_\infty$ **2-3**, as depicted in Figure 2-13. Comparison of the integration of aromatic and methyl signals also suggest formation of the *tris*-dimethylphosphinato complex $[Bi(O(O)PMe_2)_3]_\infty$ **2-11**. It can be noted that signals associated with phosphinic acids were not observed for any of the complexes upon analysis of their water solubilised residues, suggesting hydrolysis does not occur.

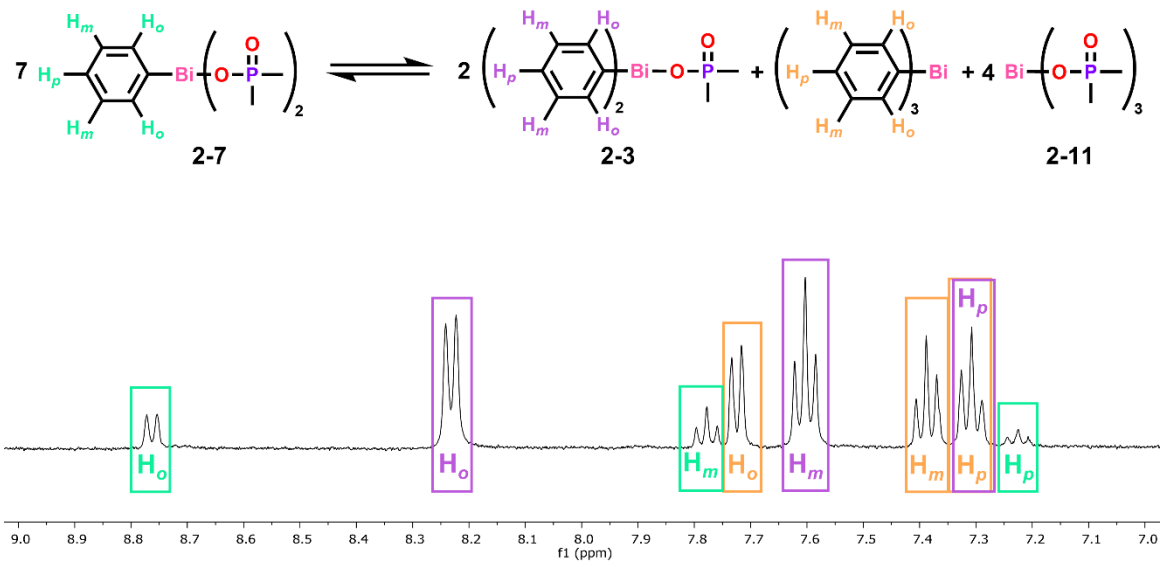

Figure 2-13 ^{1}H NMR spectrum of the solid recovered from water following solubilisation of complex **2-7** in d_6-DMSO, highlighting the rearrangement in solution to form complex **2-3** and $BiPh_3$ (methyl signals are not shown but suggest the formation of complex **2-11**).

It is difficult to comment on the water stability of the remaining *bis*- and *tris*-phosphinato complexes due to poor solubility of their residues in d_6-DMSO. The rearrangement observed for the *bis*-dimethylphosphinato complex suggests that some rearrangement can be expected for the other heteroleptic bismuth complexes. This is further supported by ^{1}H NMR analysis of the *mono*-phosphinato complex residues, which show multiple signals in the aromatic region consistent with formation of $BiPh_3$. It must be noted that not all of the residue could be solubilised, which may be the poorly soluble *bis*- and *tris*-phosphinato complexes.

Further solution-state stability studies were conducted on the *mono*-phosphinato complexes $[BiPh_2O(O)P(H)Ph]_\infty$ **2-1**, $[BiPh_2O(O)PPh_2]_\infty$ **2-2**, $[BiPh_2O(O)PMe_2]_\infty$ **2-3** and $[BiPh_2O(O)P(p\text{-}MeOPh)_2]_\infty$ **2-4** in d_6-DMSO, where it was found that the complex was stable at room temperature for 24 hours before rearrangement was observed. The observed redistribution saw the formation of $BiPh_3$, which has been previously described for diphenyl bismuth *mono*-sulfonato complexes.[75] The *mono*-sulfonato complex rearrangement also saw the formation of the phenyl bismuth *bis*-sulfonato complex by ^{1}H NMR. Herein, an internal standard of ferrocene was used to determine if the *bis*-phosphinato complex was also forming as part of the redistribution. A solid can be observed precipitating in the NMR tube and the *mono*-phosphinato ^{1}H NMR signals decrease more rapidly than the increase of $BiPh_3$ associated signals, indicating that the poorly soluble *bis*-phosphinato complex is formed, as seen in Table 2-5.

Table 2-5 ^{1}H NMR relative integrations of *ortho*-phenyl protons with the initial integration and integration following 5 days in solution for complexes **2-1** – **2-4**. Integration is relative to the ferrocene standard set to integration of 1.00.

Compound		Time (days)	*o*-Ph integration ($[BiPh_2O(O)PRR']_\infty$)	*o*-Ph integration ($BiPh_3$)
$[BiPh_2O(O)P(H)Ph]_\infty$	**2-1**	t = 0	1.95	-
		t = 5	1.05	0.23
$[BiPh_2O(O)PPh_2]_\infty$	**2-2**	t = 0	2.04	-
		t = 5	0.85	0.10
$[BiPh_2O(O)PMe_2]_\infty$	**2-3**	t = 0	1.62	-
		t = 5	0.70	0.10
$[BiPh_2O(O)P(p\text{-}MeOPh)_2]_\infty$	**2-4**	t = 0	3.12	-
		t = 5	0.36	0.11

2.4.1 Media stability

The stability of complexes **2-1** – **2-4** in DMSO for up to 24 hours allows for solution-based biological assays to be performed. Triaryl bismuth(V) *bis*-carboxylato compounds have proved to be unstable in cell culture media with implications of glucose involved in the decomposition process,[135,136] so it is important to assess the stability of bismuth(III) complexes. The stability of the *mono*-phosphinato complex $[BiPh_2O(O)P(H)Ph]_\infty$ **2-1** was assessed in Dulbecco's Modified Eagle Medium (DMEM), as well as in the presence of common media components such as disodium phosphate, glucose and the amino acid cysteine to gain insight into their behaviour in

cell culture media. Cysteine is not the most abundant amino acid found in culture media, however the thiophilic nature of bismuth prompted its exploration.

The stability of complex **2-1** in DMEM was examined over 48 hours by UV-Vis spectroscopy. Studies with phenyl bismuth(III) *bis*-flavonolate complexes have shown that the serum proteins help to maintain the compounds in solution through the addition of foetal bovine serum (FBS) to culture media.[89] This prompted two studies with DMEM alone and DMEM containing 10 % FBS, as shown in Figure 2-14. It is immediately obvious that the absorption band of **2-1** at 290 nm in DMEM decreases over time, which coincides with the formation of precipitate in the cuvette. The spectrum of **2-1** in DMEM with FBS is not well resolved, despite the baseline correction which may be indicative of the complex binding to serum proteins as no precipitate was observed. FBS is known to contain bovine serum albumin (BSA) which possess both Zn(II) and Cu(II) binding sites.[137] It is likely that complex **2-1** interacts with BSA, as bismuth has been reported to displace Zn(II) within binding sites in proteins, such as those found in *H. pylori* and SARS coronavirus.[50,138,139] While it is difficult to comment on the overall stability of complex **2-1**, it is apparent that the addition of FBS to the culture media is necessary to maintain the complex in solution.

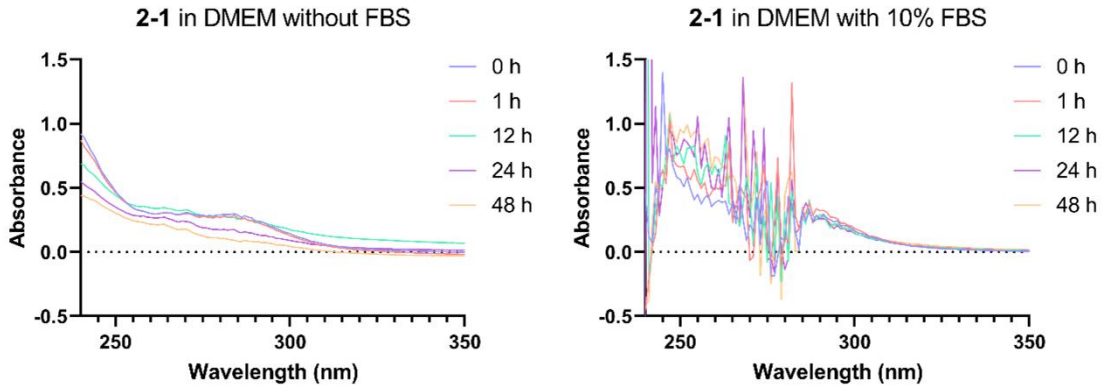

Figure 2-14 Absorption spectra of $[BiPh_2O(O)P(H)Ph]_\infty$ **2-1** at 100 µM in plain DMEM and in DMEM with 10 % FBS over 48 hours.

^{1}H NMR spectroscopic studies were conducted in d_6-DMSO to determine if complex **2-1** reacted with or rearranged in the presence of media components. The studies with glucose found that no rearrangement occurred, with the ^{1}H NMR spectra of the complex unchanged after 24 hours. It was found that complex **2-1** does interact with sodium phosphate, with the appearance of benzene evident after 7 hours. Despite the appearance of benzene, the signals associated with **2-1** remained unchanged and it could be observed that a solid precipitated out of solution. There is no evidence of phenylphosphinic acid forming, suggesting ligand exchange does not occur. It is

most likely that the sodium phosphate facilitates the protolysis of a phenyl group due to the high water content of DMSO, forming phenyl bismuth phenylphosphinato hydroxide (Scheme 2-6).

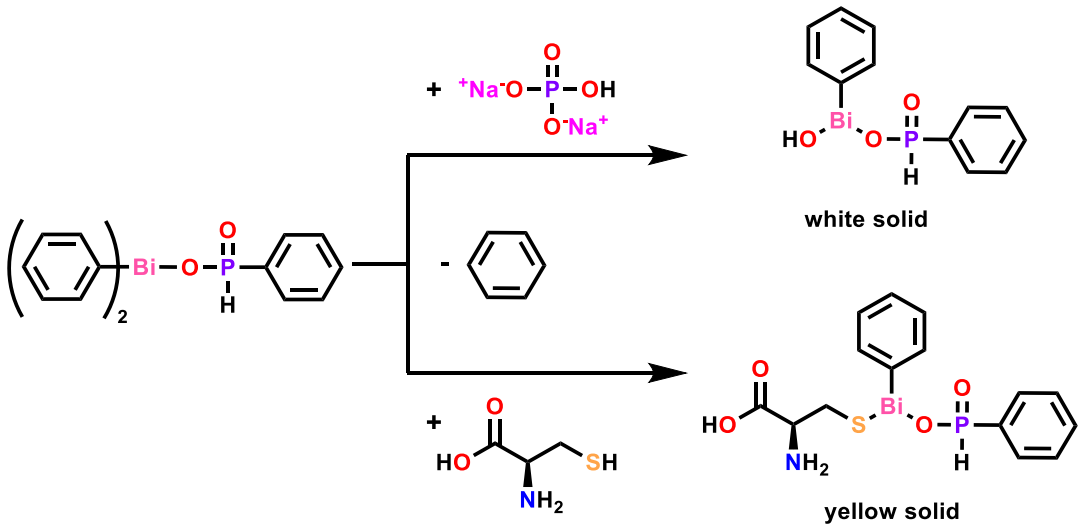

Scheme 2-6 Proposed product formation for complex $[BiPh_2O(O)P(H)Ph]_\infty$ **2-1** reacting with disodium phosphate or L-cysteine in DMSO, leading to the elimination of benzene.

Complex **2-1** was found to interact with cysteine, as benzene could be identified in the ^{1}H NMR spectrum and multiple aromatic bismuth-phenyl signals could be observed including $BiPh_3$. The cysteinyl proton signals at 2.76 and 2.88 ppm are noticeably absent upon addition to complex **2-1**, with new signals appearing at 3.71 and 3.87 ppm. A yellow solid precipitated from the d_6-DMSO solution which was found to be poorly soluble in most common solvents and would decompose to form a black solid if it remained in DMSO. The black solid formation is suggestive of bismuth sulfide, implying the cysteine is bound to bismuth in the yellow solid. TGA was performed on the yellow solid which saw a mass loss of 14.7 %, consistent with the loss of a phenyl ring from the proposed product in Scheme 2-6.

Further analysis examined the interaction of complex **2-1** with glutathione, a cysteine-containing tripeptide found in relatively high concentrations within mammalian cells and has been shown to be involved in heavy metal detoxification.[140] The poor DMSO solubility of glutathione prompted the ^{1}H NMR study to be conducted in a solvent mixture of 15:85 d_6-DMSO to D_2O. Addition of complex **2-1** to the solvent mixture produced an opaque solution which required heating to solubilise the complex. Addition of complex **2-1** to three equivalents of glutathione (in the d_6-DMSO/D_2O solution) however resulted in immediate solubilisation. ^{1}H NMR analysis showed a shift in aromatic bismuth-phenyl signals and the appearance of phenylphosphinic acid. There were also obvious shifts of cysteinyl CH_2 protons which signified complexation with bismuth, as shown in Figure 2-15. Upfield shifts can also be observed for other glutathione proton signals, suggesting

possible chelation of the amide oxygen to bismuth. Phenyl bismuth *bis*-flavonolato complexes have been shown to react with glutathione to form phenyl bismuth *bis*-glutathione complexes, where the glutathione replaces the flavonolate ligand.[89] It is apparent that a similar fate occurs for the *mono*-phosphinato bismuth complex with formation of the diphenyl bismuth glutathione complex.

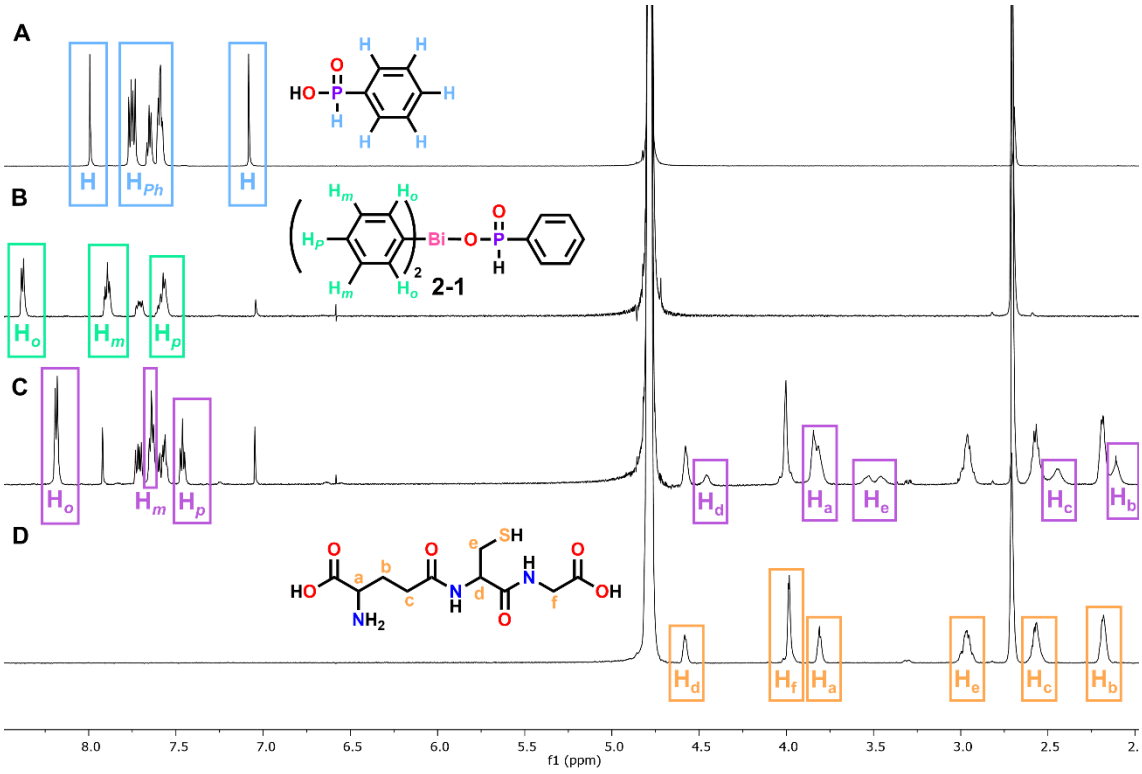

Figure 2-15 ^{1}H NMR spectrum of phenylphosphinic acid (A), complex $[BiPh_2O(O)P(H)Ph]_\infty$ **2-1** (B), complex **2-1** with 3 equivalents of glutathione (C) and glutathione (D) in 85:15 D_2O to d_6-DMSO. The signals highlighted in purple (spectrum C) show significant shifts in bismuth-phenyl and glutathione signals, as well as the formation of phenylphosphinic acid.

2.5 Biology

The heteroleptic and homoleptic bismuth complexes $[BiPh_2O(O)P(H)Ph]_\infty$ **2-1**, $[BiPh_2O(O)PPh_2]_\infty$ **2-2**, $[BiPh_2O(O)PMe_2]_\infty$ **2-3**, $[BiPh_2O(O)P(p\text{-}MeOPh)_2]_\infty$ **2-4**, $[BiPh(O(O)P(H)Ph)_2]_\infty$ **2-5**, $[BiPh(O(O)PPh_2)_2]_\infty$ **2-6**, $[BiPh(O(O)PMe_2)_2]_\infty$ **2-7**, $[BiPh(O(O)P(p\text{-}MeOPh)_2)_2]_\infty$ **2-8**, $[Bi(O(O)P(H)Ph)_3]_\infty$ **2-9**, $[Bi(O(O)PPh_2)_3]_\infty$ **2-10**, $[Bi(O(O)PMe_2)_3]_\infty$ **2-11** and $[Bi(O(O)P(p\text{-}MeOPh)_2)_3]_\infty$ **2-12** were assessed for their biological activity towards bacteria. The bacterial assays using the complexes in the solid-state were conducted with three Gram positive (*Staphylococcus aureus* (*S. aureus*), methicillin-resistant *S. aureus* (MRSA) and vancomycin-resistant *Enterococcus* (VRE)) and one Gram negative bacterial strain (*Escherichia coli* (*E. coli*)). The DMSO soluble *mono*-phosphinato complexes **2-1** – **2-4** were also assessed in solution-based assays using two Gram

positive (MRSA and VRE) and two Gram negative (*E. coli* and *Pseudomonas aeruginosa* (*P. aeruginosa*)) bacterial strains. Mammalian cell assays require soluble complexes, so the *mono*-phosphinato complexes were assessed towards Cos-7 monkey kidney cells and human fibroblast cell lines to examine the effects on the cell viability. The phosphinic acids were also assessed for their activity towards bacterial and mammalian cells, while $BiPh_3$ has been previously shown to exhibit minimal Gram negative antibacterial and cytotoxic activity.[88,135] $BiPh_3$ has been reported to exhibit minimum inhibitory concentration (MIC) values of 28.4 and 14.2 µM towards MRSA and VRE respectively, proving antibacterial activity towards Gram positive bacteria.[88,89]

2.5.1 Antibacterial activity

The initial bacterial assays utilised the solid complexes by placing them onto a pre-spread lawn of bacteria and measuring any zones of inhibition following overnight incubation at 37 °C. It is expected that the bacteria will not grow around the solid complexes that are antibacterial due to diffusion into the agar, producing zones of inhibition. The measured zones are displayed in Figure 2-16, though it should be noted that the amount of solid was not consistent between assays. This solid-based zone of inhibition assay provides qualitative results and is employed to determine bacteria that are susceptible to the bismuth phosphinato complexes.

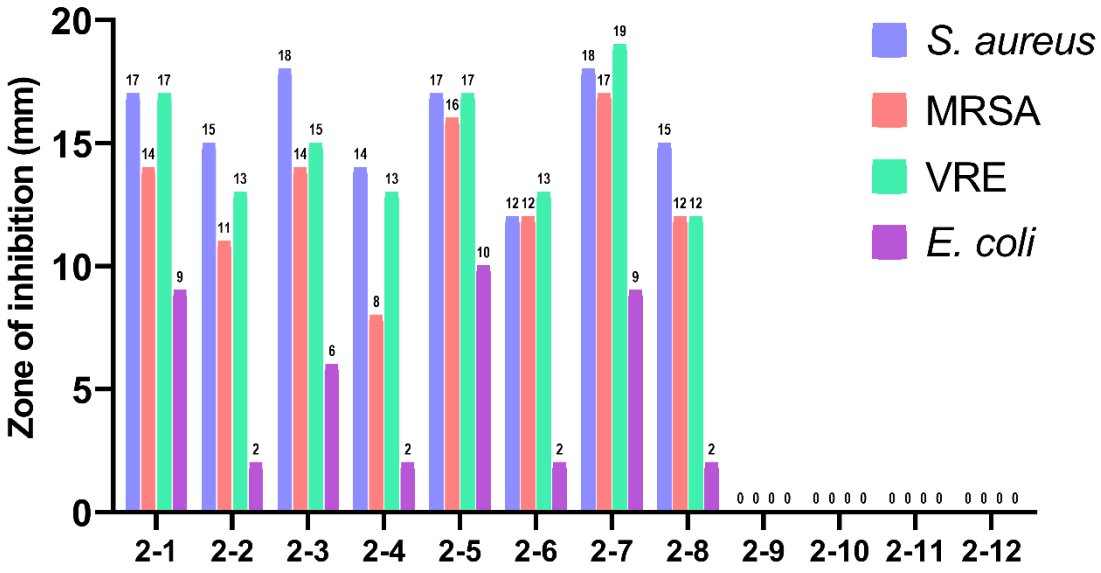

Figure 2-16 Zones of inhibition measured after incubation at 37 °C of *S. aureus*, MRSA, VRE and *E. coli* with complexes **2-1** – **2-12** overnight.

It is immediately apparent that the heteroleptic phosphinato complexes **2-1** – **2-8** displayed antibacterial activity while the homoleptic complexes **2-9** – **2-12** were not active. The zone of inhibition assay relies upon the complex diffusing into the agar, so complexes with poor aqueous solubility may not show as large of a zone compared with more soluble compounds. The *tris*-phosphinato complexes displayed the greater water solubility compared to their *mono*- and *bis*-phosphinato analogues, suggesting this was not a factor in their lack of antibacterial activity. Previous work by Andrews *et al.* with bismuth thiolato complexes have shown similar results, where heteroleptic complexes displayed far greater antibacterial activity compared to their *tris*-thiolato counterparts.[86,88]

The zone of inhibition assay suggests that the Gram positive bacteria *S. aureus*, MRSA and VRE are more susceptible to the bismuth phosphinato complexes than the Gram negative bacterium *E. coli*, however confirmation is required from solution-based assays. This trend has been previously reported for cyclic organobismuth complexes, where it was suggested the outer membrane of the Gram negative bacteria is less permeable to bismuth compounds.[91] Furthermore, it can be noted that the phenylphosphinato complexes **2-1** and **2-5** and the dimethylphosphinato complexes **2-3** and **2-7** display greater zones of inhibition than the diphenylphosphinato- and *bis*-(*p*-methoxyphenyl)phosphinato-containing complexes (**2-2**, **2-4**, **2-6** and **2-8**). This is likely due to greater diffusion into the agar owing to their greater water solubility.

Solution-state bacterial assays were conducted to determine the MIC of the bismuth compounds. Given the *mono*-phosphinato complexes are stable in DMSO for up to 24 hours, DMSO solutions of complexes **2-1** – **2-4** were freshly prepared at 1 mM and diluted down to give concentrations ranging from 0.315 to 10 µM in bacterial broth. Overnight bacterial cultures of two Gram positive strains (MRSA and VRE) and two Gram negative strains (*E. coli* and *P. aeruginosa*) were added to the broth and incubated overnight at 37°C. Visual inspection of the bacterial vials then determined the MIC as the lowest concentration where bacteria did not grow, shown in Table 2-6.

Table 2-6 Minimum inhibitory concentration (MIC) of complexes **2-1** – **2-4** and their respective phosphinic acids towards MRSA, VRE, *E. coli* and *P. aeruginosa* after overnight incubation at 37 °C.

Compound		MIC (μM)			
		MRSA	VRE	*E. coli*	*P. aeruginosa*
$[BiPh_2O(O)P(H)Ph]_\infty$	**2-1**	4.1	1.25	2.5	5.0
$[BiPh_2O(O)PPh_2]_\infty$	**2-2**	2.5	0.63	1.25	2.5
$[BiPh_2O(O)PMe_2]_\infty$	**2-3**	5.0	1.25	2.5	5.0
$[BiPh_2O(O)P(p\text{-}MeOPh)_2]_\infty$	**2-4**	5.0	1.25	5.0	7.5
Ph(H)P(O)OH		>100	>100	>100	>100
$Ph_2P(O)OH$		>100	>100	>100	>100
$Me_2P(O)OH$		>100	>100	>100	>100
$(p\text{-}MeOPh)_2P(O)OH$		>100	>100	>100	>100

It is apparent that the phosphinato moieties influence the MIC values, where the more lipophilic diphenylphosphinato complex **2-2** consistently displays lower MIC values compared with the other *mono*-phosphinato complexes. The zone of inhibition assay implied that MRSA would be more susceptible than *E. coli*, however the availability of the complex in solution shows the converse. This suggests that the different agar for Gram positive and Gram negative bacteria may influence the diffusion of the complex and thus the size of the zones of inhibition, which reaffirms the qualitative nature of the zone of inhibition assay using solid compounds. VRE displayed a greater susceptibility to the *mono*-phosphinato complexes than MRSA, which is in agreement with the zone of inhibition assay. Comparison of MIC values with diphenyl bismuth thiolato and phenyl bismuth *bis*-flavonolato complexes show similarly low concentrations required to stop the growth of MRSA, *E. coli* and *P. aeruginosa*, while higher concentrations were required to combat VRE (2.7 to 12.5 μM).[88,89]

2.5.2 Mammalian cell viability

It is important to determine whether the *mono*-phosphinato bismuth complexes cause cytotoxicity towards mammalian cells if they are to be used as antibacterial agents. This was assessed through the CellTiter-Blue viability assay which involves metabolically-active cells converting the blue resazurin dye to a pink resorufin end product that can be quantitatively measured by fluorescence.[141] The determined cell viability is compared to a control of cells without compound added which is treated as 100 % viable. Cos-7 and human fibroblast cells were assessed towards complexes **2-1** – **2-4** and their respective phosphinic acids. The compounds were

solubilised in DMSO where the maximum DMSO concentration (1 %) was also included as a control with an average viability of 90 % across both Cos-7 and human fibroblasts cells. The phosphinic acids proved non-toxic, with viability not reduced in both cell lines at the highest tested concentration of 100 µM, as seen in Figure 2-17.

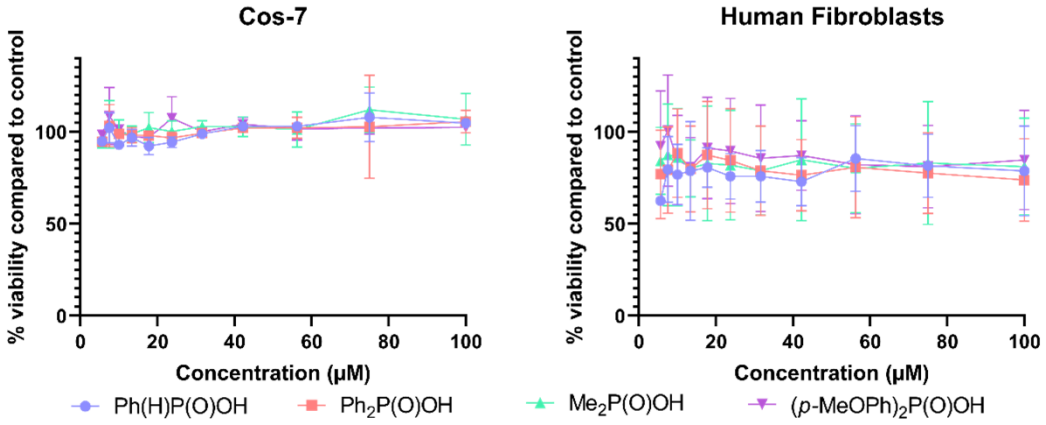

Figure 2-17 Cos-7 and human fibroblast cell viability following 24 hour incubation at 37 °C with phenylphosphinic acid, diphenylphosphinic acid, dimethylphosphinic acid and *bis*-(*p*-methoxyphenyl)phosphinic acid. The IC_{50} for all is >100 µM.

The results, as seen in Figure 2-18, suggest that human fibroblast cells are more susceptible to the bismuth complexes, with the concentration to inhibit 50 % of cell viability (IC_{50}) much lower for fibroblasts (1.16 to 1.91 µM) compared to Cos-7 cells (3.26 to 4.69 µM).

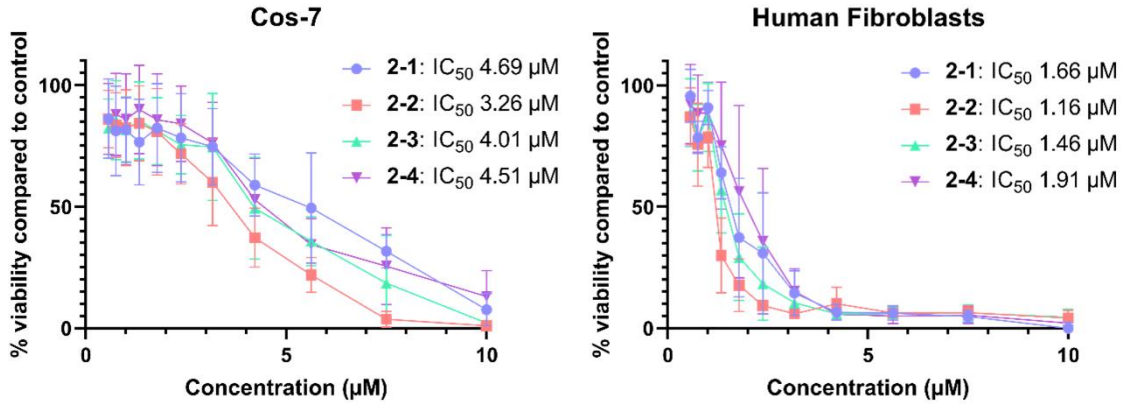

Figure 2-18 Cos-7 and human fibroblast cell viability following 24 hour incubation at 37 °C with complexes **2-1** – **2-4**.

Complex **2-2** exhibits the lowest IC_{50} values and thus greatest toxicity towards mammalian cells, which is in agreement with the bacterial MIC values. This suggests that the more lipophilic complexes exert greater toxicity towards both mammalian and bacterial cells. This phenomenon has been previously described by Thomas *et al.*, where it was shown that bismuth compounds

that have undergone methylation processes show greater lipophilicity and thus increased membrane permeability, resulting in greater toxicity.[142] Bismuth compounds are widely accepted as 'non-toxic' due to their inherent insolubility in biological systems,[73] however numerous reports have described carboxylato and thiolato bismuth compounds showing toxicity towards mammalian cells, where the ligand is proposed to moderate the toxic effects of bismuth.[80,88,143] It is expected that the *mono*-phosphinato bismuth complexes will display higher toxicity due to their greater lipophilicity when compared with the *bis*-phosphinato compounds. This trend has been seen for phenyl bismuth *mono*- and *bis*-thiolato complexes, where the *mono*-thiolato compounds proved more toxic with a lower Cos-7 IC_{50} values (2.23 to 5.51 μM) compared to the *bis*-thiolato compounds (4.61 to 7.34 μM).[88] Similarly, diphenyl bismuth *mono*-diphenylthiophosphinato complexes have shown greater cytotoxicity towards Cos-7 cells (IC_{50} 10 μM) than their phenyl bismuth *bis*-diphenylthiophosphinato counterpart (IC_{50} 21 μM).[90] While the phenyl bismuth *bis*-phosphinato complexes cannot be assayed in the same way as complexes **2-1** – **2-4**, their relative toxicities will be discussed through material incorporation and leaching studies in Chapter 4 (section 4.5).

Following cell viability assays, complex $[BiPh_2O(O)P(H)Ph]_\infty$ **2-1** was examined using a cytotoxicity assay to further probe the cause of the reduced viability observed. The CytoTox-ONE™ assay measures the extracellular presence of lactate dehydrogenase (LDH), an enzyme that is found within cells and is released due to impaired membrane integrity. Similar to the CellTiter-Blue assay, CytoTox-ONE™ is a colorimetric assay that depends upon the conversion of resazurin to resorufin which is facilitated by LDH, however the presence of resorufin is now indicative of cytotoxicity.[144] Cytotoxicity is determined relative to a lysed cell control which is treated with a lysis solution to represent maximum LDH release, as seen in Figure 2-19. Further controls included 1 % DMSO, $BiPh_3$ (100 μM) and phenylphosphinic acid (100 μM). Complex **2-1** has an IC_{50} of 4.69 μM for Cos-7 cells, so three concentrations of 2, 4 and 8 μM **2-1** were assessed in the cytotoxicity assay. At 8 μM of **2-1**, 60 % cytotoxicity was observed compared to only 16 % cytotoxicity at 2 μM, which is comparable with the 100 μM $BiPh_3$ control. It can be observed that an increase in concentration of complex **2-1** corresponded with increased cytotoxicity of Cos-7 cells, suggesting a dose-dependent relationship. The Cos-7 cytotoxicity results correspond with the obtained viability results, where at 8 μM of complex **2-1**, 60% cytotoxicity and approximately 30 % viability is observed, suggesting the non-viable cells have incurred membrane damage. It is apparent that the *mono*-phosphinato bismuth complex causes reduced membrane integrity in the cells, either through direct or indirect membrane disruption. Further studies are needed to determine the cellular target of the complexes leading to cytotoxicity.

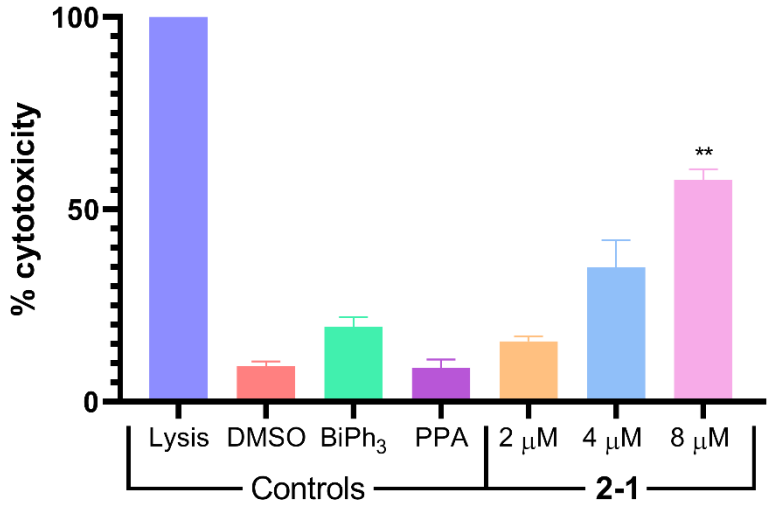

Figure 2-19 Cos-7 cytotoxicity following 24 hour incubation at 37 °C with complex $[BiPh_2O(O)P(H)Ph]_\infty$ **2-1** at 2, 4 and 8 µM, controls of phenylphosphinic acid (PPA) and $BiPh_3$ at 100 µM, 1 % DMSO control and lysis control of 0.18 % Triton® X-100 solution. ** $P < 0.01$ (analysis of variance Dunn's).

2.5.3 Selectivity

It is important to examine the selectivity of the *mono*-phosphinato complexes to determine their potential as antibacterial agents. The selectivity index (SI) is a ration that measures the difference in the concentration to exert the desired effect on bacteria and the concentration that causes toxicity in mammalian cells. Herein, the higher the SI, the theoretically more effective and safe a compound is. This is calculated using Cos-7 IC_{50} and bacterial MIC data, with the results shown in Table 2-7. An ideal SI for compounds is a minimum two-fold difference, as anything below this requires further safety testing measures.[145]

Table 2-7 Selectivity indices of complexes **2-1** – **2-4**.

Compound		**Selectivity index***			
		MRSA	VRE	*E. coli*	*P. aeruginosa*
$[BiPh_2O(O)P(H)Ph]_\infty$	**2-1**	1.1	3.8	1.9	0.9
$[BiPh_2O(O)PPh_2]_\infty$	**2-2**	1.3	5.2	2.6	1.3
$[BiPh_2O(O)PMe_2]_\infty$	**2-3**	0.8	3.2	1.6	0.8
$[BiPh_2O(O)P(p\text{-}MeOPh)_2]_\infty$	**2-4**	0.9	3.6	0.9	0.6

* Selectivity index (SI) = IC_{50}/MIC.

The results demonstrate that most of the *mono*-phosphinato bismuth complexes are non-selectively toxic towards bacteria with the exception of VRE, with the SI ranging from 3.2 to 5.2. Complex **2-2** displayed the best selectivity towards all the tested bacteria, however the poor

selectivity towards MRSA and *P. aeruginosa* suggest this complex is not suitable as a therapeutic antibacterial agent. It has been demonstrated that heteroleptic bismuth thiolato complexes cause membrane destruction in bacterial cells.[88] It was suggested that similarities within bacterial and mammalian cell membranes may lead to comparable membrane damage in Cos-7 cells. It may be concluded that the diphenyl bismuth *mono*-phosphinato complexes act in a similar manner to impair the membrane integrity in Cos-7 cells, resulting in non-selective toxicity.

2.6 Conclusions

A series of novel heteroleptic phenyl phosphinato bismuth complexes were synthesised through solvent mediated or solvent free reactions of phosphinic acids with $BiPh_3$, or salt metathesis of the sodium dimethylphosphinate salt with $BiPh_2Cl$, to afford diphenyl *mono*-phosphinato bismuth complexes **2-1** – **2-4** with general formula $[BiPh_2O(O)PRR']_\infty$ and phenyl *bis*-phosphinato bismuth complexes **2-5** – **2-8** with general formula $[BiPh(O(O)PRR')_2]_\infty$. The homoleptic phosphinato complexes were produced through reaction of phosphinic acids with $[Bi(O^tBu)_3]$ resulting in complexes **2-9** – **2-12** of the general $[Bi(O(O)PRR')_3]_\infty$. All complexes were isolated as solids and displayed poor solubility in most common solvents. Characterisation of the phosphinato bismuth compounds included IR, ^{31}P NMR, TGA, elemental and ICP-OES for bismuth content analysis. The *mono*-phosphinato complexes **2-1** – **2-4** were structurally authenticated by X-ray crystallography, which confirmed the formation of 1D coordination polymers as had previously been described for this type of complex.

The solubility of the synthesised bismuth complexes were determined to be very poor in water, with the general trend that the *tris*-phosphinato complexes displayed greater solubility than the *mono*- and *bis*-phosphinato complexes. The phenylphosphinato- and dimethylphosphinato-containing complexes showed greater water solubility compared with the diphenylphosphinato and *bis*-(*p*-methoxyphenyl)phosphinato compounds, owing to their greater hydrophilicity in line with the calculated clogP values. The heteroleptic phenyl bismuth *bis*-phosphinato complex **2-7** was found to rearrange in aqueous solution with evidence of $BiPh_3$, **2-3** and **2-11** formation. The DMSO soluble *mono*-phosphinato complexes were also shown to redistribute after 24 hours in DMSO to produce $BiPh_3$ and their *bis*-substituted counterparts.

Reports of previous bismuth phosphinato complexes had not examined their biological activity, therefore the synthesised complexes were assessed for their activity towards both Gram positive and Gram negative bacteria. Solid-state antibacterial assays showed the heteroleptic complexes **2-1** – **2-8** displayed antibacterial activity while the homoleptic complexes **2-9** – **2-12** proved

inactive. Solution-based assays with the *mono*-phosphinato complexes **2-1** – **2-4** showed low micro-molar activity, with the diphenylphosphinato complex **2-2** consistently displaying the lowest MIC values of 0.63 µM towards VRE, 1.25 µM towards *E. coli* and 2.5 µM towards both MRSA and *P. aeruginosa*. Given the promising antibacterial studies, the activity of complexes **2-1** – **2-4** were assessed towards mammalian cell lines (Cos-7 and human fibroblasts), where they proved to be cytotoxic at low micro-molar concentrations. Further examination through use of a membrane integrity assay indicated that complex **2-1** causes disruptions in the membrane of Cos-7 cells, resulting in cytotoxicity.

It is apparent that the *mono*-phosphinato complexes **2-1** – **2-4** display potent antibacterial activity, but are also cytotoxic towards mammalian cells. Examination of their selectivity index suggests that the compounds are non-selectively toxic, which is likely due to their interaction with both mammalian and bacterial cell membranes. While the *mono*-phosphinato complexes display poor selectivity in terms of use as a therapeutic, there is potential for incorporation of the heteroleptic complexes within materials to produce antibacterial materials, as discussed in Chapter 4.

Chapter 3

Aryl bismuth phosphinates

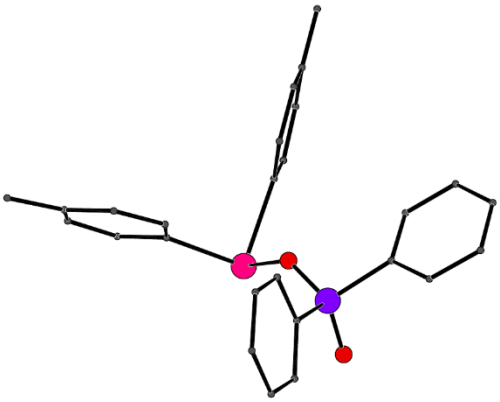

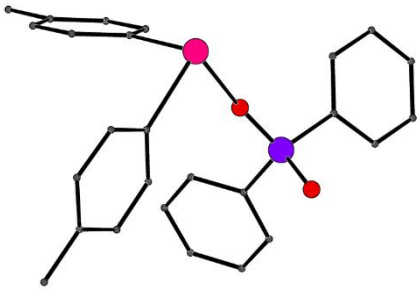

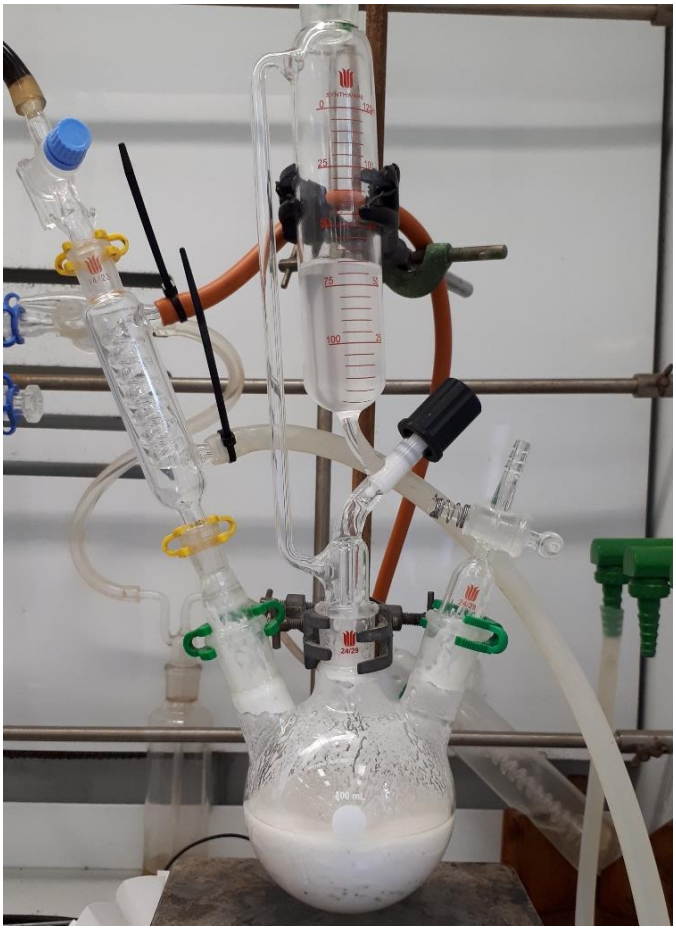

Methoxyphenyl bismuth phosphinates

Tolyl bismuth phosphinates

Biology

3 Aryl bismuth phosphinate complexes

3.1 Structure-activity introduction

In medicinal chemistry, structure-activity relationships are determined by making small structural changes to molecules and examining the effect on biological performance. While this is common practice for drug discovery, typically for organic molecules, it can also be applied to organometallic compounds. Organometallic complexes offer many potential sites for structural modification due to the different coordination modes of metals, with further changes possible in ligands and even counter ions.

A study on bismuth dithiocarbamate complexes employed quantitative structure-activity relationships (QSAR) to gain insight into their antibacterial activity.[146] QSARs incorporates computational techniques and can be used to predict the biological activity of designed molecules based on the activity of known compounds.[147] Two main trends were determined through the QSAR studies; an increase in the bismuth compounds' molecular weight will increase antibacterial activity and if the complexes are more likely to undergo nucleophilic attack and subsequently bind covalently to biological receptors, they will possess greater antibacterial activity.[146]

Investigations into the antifungal activity of organobismuth complexes highlighted a number of potential modification sites for change in the bismuth-bound aryl or halogen groups, or the alkyl aryl ketone ligand,[148] as shown in Figure 3-1. It was determined that antifungal activity was dependent on the bismuth-bound aryl group (Ar), and that heavier halogen atoms (X) lead to increased activity. Furthermore, changes to the alkyl aryl ketone ligands such as lengthening the alkyl chain (R') or introducing an aryl substituent (R) lead to reduced antifungal activity due to steric crowding around the bismuth atom. These findings reflect the importance of exploring an organometallic system to gain insights into structure-activity relationships for further optimisation.

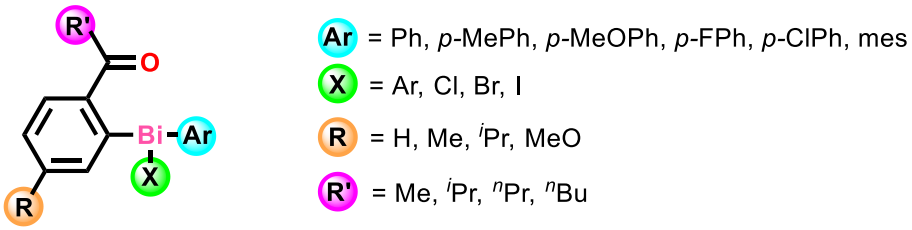

Figure 3-1 Structural changes investigated in an organobismuth complex including bismuth-bound aryl or halogen groups, alkyl or aryl groups of the alkyl aryl ketone ligand.[148]

Another example of structure-activity relationships can be gleaned from anti-leishmanial studies with pentavalent triaryl antimony and bismuth dicarboxylato complexes, which have demonstrated that different aryl groups produce diverse cytotoxicity and selectivity results.[135,136,149–151] Table 3-1 highlights the human fibroblast cell viability and selectivity towards the *Leishmania major* (*L. major*) parasite for triaryl antimony (S)-mandelate and triaryl bismuth *bis*-(*o*-ethoxyphenyl)carboxylato complexes.

Table 3-1 Human fibroblast viability (IC_{50}) and selectivity index (SI) towards *L. major* promastigotes of triaryl antimony (S)-mandelate and triaryl bismuth *bis*-(*o*-ethoxyphenyl)carboxylato complexes, where L = OC(O)C(OH)HPh and L' = OC(O)(*o*-EtOPh).[135,136,149–151] Abbreviations: tol = tolyl and mes = mesityl.

Compound	IC_{50} (µM)	SI*	Compound	IC_{50} (µM)	SI*
$[SbPh_3L_2]$	72.8	5.0	$[BiPh_3L'_2]$	3.84	1.6
$[Sb(o\text{-tol})_3L_2]$	19.3	1.3	$[Bi(o\text{-tol})_3L'_2]$	17.1	18.4
$[Sb(m\text{-tol})_3L_2]$	21.8	4.8	$[Bi(m\text{-tol})_3L'_2]$	11.6	13.0
$[Sb(p\text{-tol})_3L_2]$	16.1	6.1	$[Bi(p\text{-tol})_3L'_2]$	7.82	4.4
$[Sb(mes)_3L_2]$	6.04	28.8			
$[Sb(o\text{-MeOPh})_3L_2]$	≥100	-			
$[Sb(p\text{-}^t\text{BuPh})_3L_2]$	2.90	5.0			

* SI = IC_{50} (human fibroblasts)/IC_{50} (*L. major* promastigote).

It is evident that the substitution of the bismuth phenyl group with a tolyl group improves both human fibroblast cell viability and promastigote selectivity. Interestingly, the mammalian cell viability drastically decreases for the antimony compounds when the phenyl moiety is exchanged for a tolyl, mesityl or *tert*-butylphenyl group. Only the antimony *tris*-*o*-methoxyphenyl complex proved less toxic to human fibroblast cells, however it also proved ineffective at 100 µM towards promastigotes. Despite increased toxicity, greater selectivity was observed for the antimony *p*-tolyl and mesityl derivatives. These studies have shown the value in varying the metal-bound aryl substituent for better selectivity.

The vastly different selectivity observed from simple structural changes prompted the investigation into different bismuth aryl groups for the *mono*-phosphinato bismuth complexes. This chapter aims to examine the bacterial activity and mammalian cell toxicity of diaryl bismuth *mono*-phosphinato complexes and furthermore, determine any structure-activity relationships with comparison to the diphenyl *mono*-phosphinato bismuth complexes.

3.2 Synthesis

Two series of aryl bismuth compounds were chosen for this study: *ortho*-, *meta*- and *para*-methoxyphenyl bismuth series and *ortho*-, *meta*- and *para*-tolyl bismuth series. The two series were chosen for their differences in potential hydrophilic (methoxyphenyl) or hydrophobic (tolyl) interactions. Due to the DMSO solubility of the diphenyl *mono*-phosphinato bismuth complexes, allowing for quantitative biological studies, the targeted series of aryl bismuth phosphinato complexes are of the type $[BiAr_2O(O)PRR']_\infty$, consisting of 18 complexes as summarised in Figure 3-2.

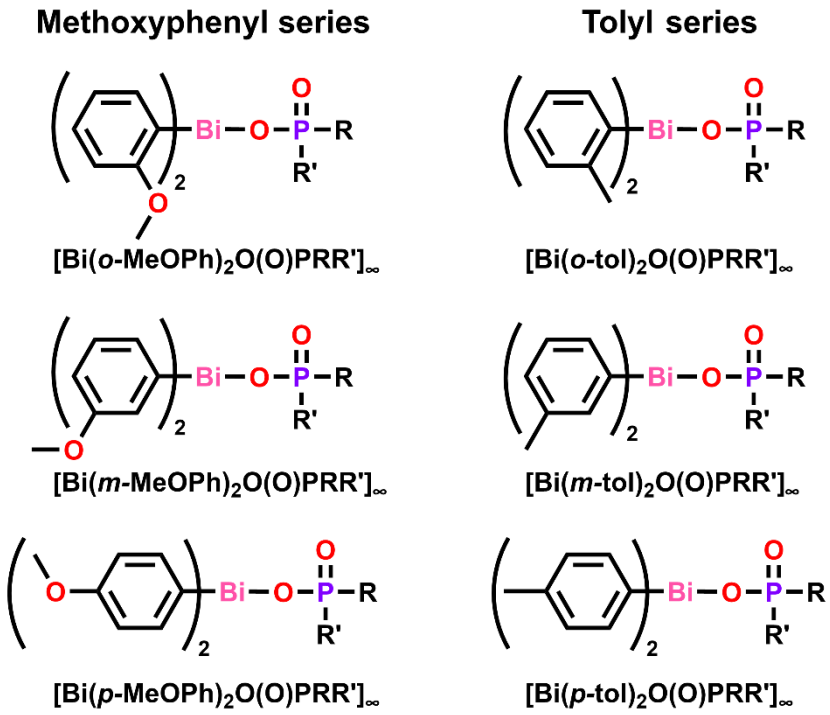

Figure 3-2 Summary of diaryl bismuth phosphinato complexes in the methoxyphenyl and tolyl series.

3.2.1 Diaryl bismuth *mono*-phosphinates

Following the successful equimolar reaction of $BiPh_3$ and phosphinic acid to form the *mono*-phosphinato bismuth complexes, the same synthetic route was trialled for both the methoxyphenyl and tolyl series with phenylphosphinic acid, diphenylphosphinic acid and *bis*-(*p*-methoxyphenyl)phosphinic acid. The successful reactions are shown in Scheme 3-1, where the *o*- and *m*-methoxyphenyl and *m*- and *p*-tolyl bismuth reactions resulted in formation of a precipitate. It is important to heat both Bi(*m*-tol)$_3$ and Bi(*p*-tol)$_3$ in ethanol prior to phosphinic acid addition, due to their poor solubility in room temperature ethanol. Isolation of the precipitate was followed by washing with hot ethanol, acetone and diethyl ether to give the desired diaryl *mono*-phosphinato bismuth complexes: $[Bi(o\text{-}MeOPh)_2O(O)P(H)Ph]_\infty$ **3-1**, $[Bi(o\text{-}MeOPh)_2O(O)PPh_2]_\infty$ **3-2**,

[Bi(*o*-MeOPh)$_2$O(O)P(*p*-MeOPh)$_2$]$_\infty$ **3-3**, [Bi(*m*-MeOPh)$_2$O(O)P(H)Ph]$_\infty$ **3-4**, [Bi(*m*-MeOPh)$_2$O(O)PPh$_2$]$_\infty$ **3-5**, [Bi(*m*-MeOPh)$_2$O(O)P(*p*-MeOPh)$_2$]$_\infty$ **3-6**, [Bi(*m*-tol)$_2$O(O)P(H)Ph]$_\infty$ **3-13**, [Bi(*m*-tol)$_2$O(O)PPh$_2$]$_\infty$ **3-14**, [Bi(*m*-tol)$_2$O(O)P(*p*-MeOPh)$_2$]$_\infty$ **3-15**, [Bi(*p*-tol)$_2$O(O)P(H)Ph]$_\infty$ **3-16**, [Bi(*p*-Tol)$_2$O(O)PPh$_2$]$_\infty$ **3-17** and [Bi(*p*-tol)$_2$O(O)P(*p*-MeOPh)$_2$]$_\infty$ **3-18**.

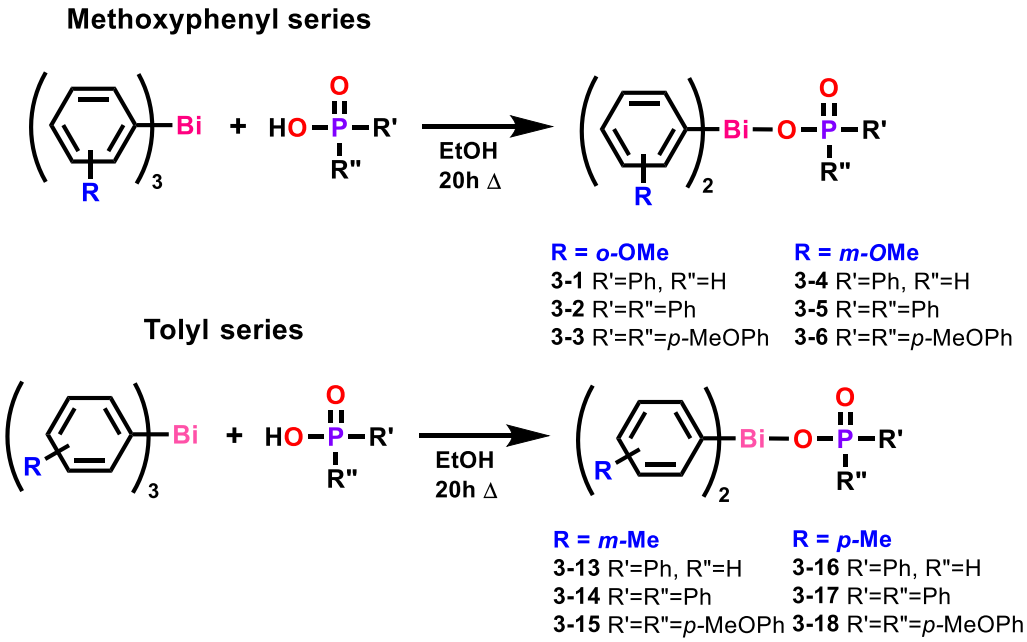

Scheme 3-1 Synthetic route to form *bis*-methoxyphenyl and *bis*-tolyl bismuth *mono*-phosphinato complexes **3-1** – **3-6** and **3-13** – **3-18** respectively.

Reactions with phenylphosphinic acid were conducted at room temperature, while diphenylphosphinic acid and *bis*-(*p*-methoxyphenyl)phosphinic acid reactions were carried out at 50 to 55 °C. The initial yields for all reactions were relatively poor, with the exception of the heated *o*-methoxyphenyl and *m*-tolyl reactions, as seen in Table 3-2. The reactions were not further optimised and while it is expected that higher temperatures could produce greater yields, it is also likely that higher temperatures will push the reaction to the aryl bismuth *bis*-phosphinato product.

Table 3-2 Percentage yields for methoxyphenyl series (**3-1** – **3-6**) and tolyl series (**3-13** – **3-18**) bismuth complexes of the type [BiAr$_2$O(O)PRR']$_\infty$.

Compound	**Yield (%)**			
	o-MeOPh	*m*-MeOPh	*m*-tol	*p*-tol
[BiAr$_2$O(O)P(H)Ph]$_\infty$	27	33	54	31
[BiAr$_2$O(O)PPh$_2$]$_\infty$	76	43	93	51
[BiAr$_2$O(O)P(*p*-MeOPh)$_2$]$_\infty$	63	33	77	57

The method outlined in Scheme 3-1 did not result in the formation of the *p*-methoxyphenyl or *o*-tolyl bismuth analogues [Bi(*p*-MeOPh)$_2$O(O)P(H)Ph]$_\infty$ **3-7**, [Bi(*p*-MeOPh)$_2$O(O)PPh$_2$]$_\infty$ **3-8**, [Bi(*p*-MeOPh)$_2$O(O)P(*p*-MeOPh)$_2$]$_\infty$ **3-9**, [Bi(*o*-tol)$_2$O(O)P(H)Ph]$_\infty$ **3-10**, [Bi(*o*-tol)$_2$O(O)PPh$_2$]$_\infty$ **3-11** and [Bi(*o*-tol)$_2$O(O)P(*p*-MeOPh)$_2$]$_\infty$ **3-12**. Further attempts to isolate the *bis*-*p*-methoxyphenyl and *bis*-*o*-tolyl bismuth products involved changing the solvent to DMSO and heating at reflux overnight, with the hope that increased temperatures would allow for the *mono*-phosphinato complex to form. A very small amount of precipitate was isolated following the reaction, however the poor yields (<10 %) lead to alternative synthetic routes to be examined (sections 3.2.1.1 and 3.2.1.2).

3.2.1.1 *Bis*-*p*-methoxyphenyl bismuth *mono*-phosphinates

DSC was used to understand the viability of solvent free (SF) reactions to form the *bis*-*p*-methoxyphenyl bismuth *mono*-phosphinato complexes. DSC analysis was conducted on an equimolar mixture of triaryl bismuth and phosphinic acid to determine the temperature at which a reaction may occur. Bi(*p*-MeOPh)$_3$ has a greater melting point than BiPh$_3$ (81 °C) at 190 °C, so the required SF reaction temperatures are expected to be greater. Figure 3-3 depicts the thermochemical profile for the Bi(*p*-MeOPh)$_3$ reaction with diphenylphosphinic acid, typical for SF reactions of Bi(*p*-MeOPh)$_3$.

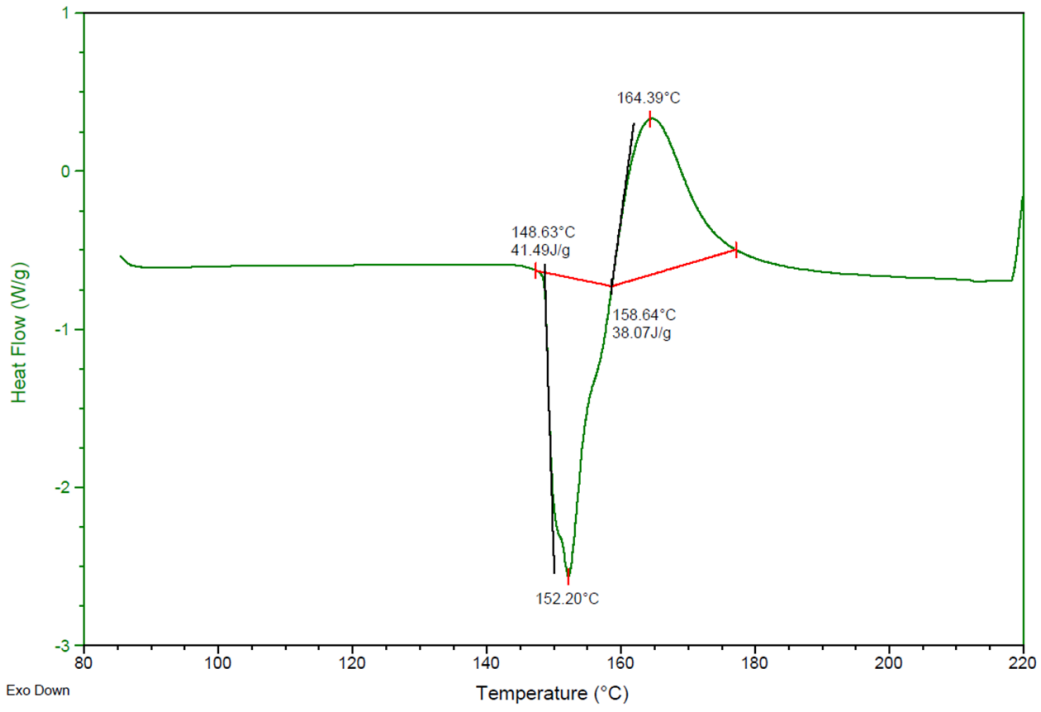

Figure 3-3 DSC trace of 1:1 mixture of Bi(*p*-MeOPh)$_3$ and diphenylphosphinic acid from 85 to 220 °C.

It is interesting to note that the *p*-methoxyphenyl reactions show an exotherm prior to an endotherm, whereas most typical SF reactions show an endothermic melt followed by the

exothermic reaction. While the profile was atypical, the SF reactions were trialled and proved unsuccessful in forming the *bis*-*p*-methoxyphenyl bismuth *mono*-phosphinato complexes [Bi(*p*-MeOPh)$_2$O(O)P(H)Ph]$_\infty$ **3-7**, [Bi(*p*-MeOPh)$_2$O(O)PPh$_2$]$_\infty$ **3-8** and [Bi(*p*-MeOPh)$_2$O(O)P(*p*-MeOPh)$_2$]$_\infty$ **3-9**. Starting material was all that could be isolated following attempted reactions, which may be due to insufficient temperatures to promote the reaction.

Following unsuccessful solvent mediated and solvent free methods starting with Bi(*p*-MeOPh)$_3$, an alternative salt metathesis route was investigated. The synthetic route utilised Bi(*p*-MeOPh)$_2$Cl and the sodium salt of the respective phosphinic acids to produce complexes **3-7** – **3-9** (Scheme 3-2).

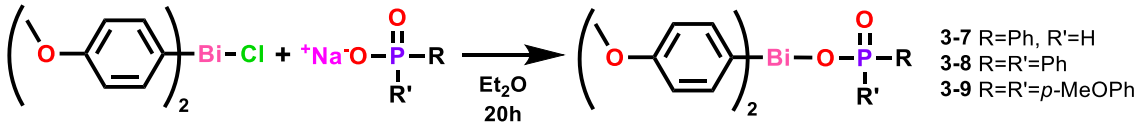

Scheme 3-2 Salt metathesis route to form *bis*-*p*-methoxyphenyl *mono*-phosphinato bismuth complexes **3-7** – **3-9**.

Bi(*p*-MeOPh)$_2$Cl was formed through the redistribution reaction of two equivalents of Bi(*p*-MeOPh)$_3$ and one equivalent of BiCl$_3$ in dry diethyl ether, producing a yellow solid that was stored in a dry box. Previous reports of Bi(*p*-MeOPh)$_2$Cl highlighted poor stability in solvents such as THF and chloroform, where rearrangement will rapidly occur to produce Bi(*p*-MeOPh)$_3$ and Bi(*p*-MeOPh)Cl$_2$.[152] Initial reactions using dry methanol as the solvent proved ineffective due to the rearrangement reaction, and heterogeneous reactions in DCM were also unsuccessful. Diethyl ether was selected as the reaction solvent to mitigate the rearrangement, despite both the bismuth and sodium phosphinato salts displaying poor solubility in it. Bi(*p*-MeOPh)$_2$Cl was suspended in diethyl ether and dry sodium phosphinato salt was added via solid addition to produce a yellow suspension, as seen in Figure 3-4. The suspension changed from yellow to white upon prolonged stirring for up to several days, and was isolated by filtration followed by hot methanol and water washing to produce complexes **3-8** and **3-9** in crude yields of 42 and 36 % respectively. The low yields are due to rearrangement occurring, as Bi(*p*-MeOPh)$_3$ can be observed to form based on ^{1}H NMR analysis, discussed in section 3.3. The phenyl phosphinato complex **3-7** proved much more difficult to isolate due to the rearrangement forming Bi(*p*-MeOPh)$_3$ and the *p*-methoxyphenyl bismuth *bis*-phenylphosphinato complex, as discussed in section 3.3. The long reaction times of overnight for complex **3-8** and three days for **3-7** and **3-9** greatly contributed to increased rearrangement producing Bi(*p*-MeOPh)$_3$ and the *bis*-phosphinato bismuth product. The difficulties in synthesis and purifications lead to complexes **3-7** – **3-9** not being further explored.

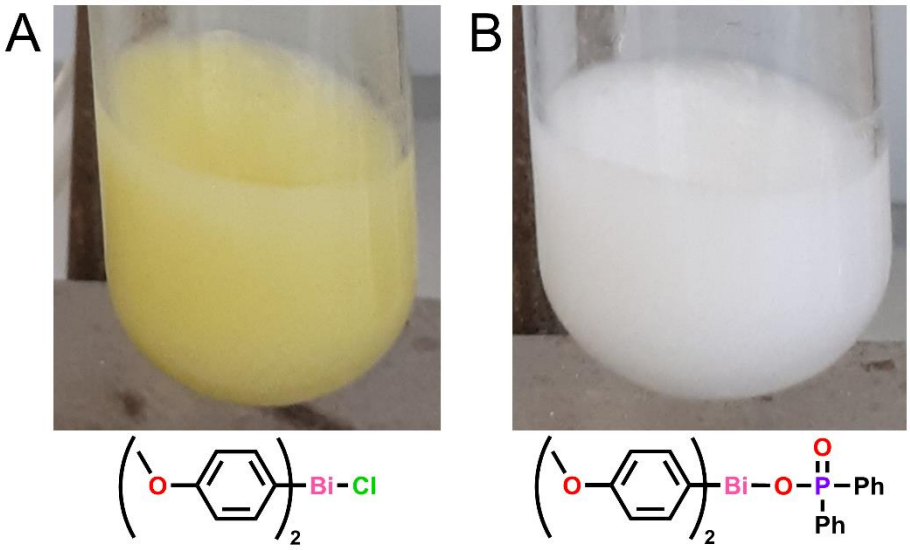

Figure 3-4 Salt metathesis reaction showing colour change from Bi(*p*-MeOPh)$_2$Cl (A) to complex **3-8** [Bi(*p*-MeOPh)$_2$O(O)PPh$_2$]$_\infty$ (B) after stirring with $Na^+O^-(O)PPh_2$ overnight in diethyl ether.

3.2.1.2 *Bis-o*-tolyl bismuth *mono*-phosphinates

DSC and TGA were used to investigate SF reactions to form the *bis-o*-tolyl bismuth *mono*-phosphinato complexes [Bi(*o*-tol)$_2$O(O)P(H)Ph]$_\infty$ **3-10**, [Bi(*o*-tol)$_2$O(O)PPh$_2$]$_\infty$ **3-11** and [Bi(*o*-tol)$_2$O(O)P(*p*-MeOPh)$_2$]$_\infty$ **3-12**. Figure 3-5 depicts a typical thermochemical profile for the Bi(*o*-tol)$_3$ reaction with the phosphinic acids investigated. DSC analysis showed reaction exotherms at 86 °C for phenylphosphinic acid, 130 °C for diphenylphosphinic acid and 136 °C for *bis*-(*p*-methoxyphenyl)phosphinic acid. TGA was utilised to determine the mass loss occurring at the exothermic temperatures for the Bi(*o*-tol)$_3$ reactions, showing only one tolyl group is lost for complexes **3-11** and **3-12**, supporting the use of SF synthesis. The phenylphosphinic acid reaction formed the *bis*-phosphinato bismuth product through the SF method, as confirmed by TGA and ^{1}H NMR. SF reactions were conducted for compounds **3-11** and **3-12** in a Kugelrohr oven for 2 hours with occasional mixing at the exotherm temperatures. The isolated solids were found to be really poorly soluble which suggested it was unlikely to be the desired complexes, so the SF method was no longer pursued.

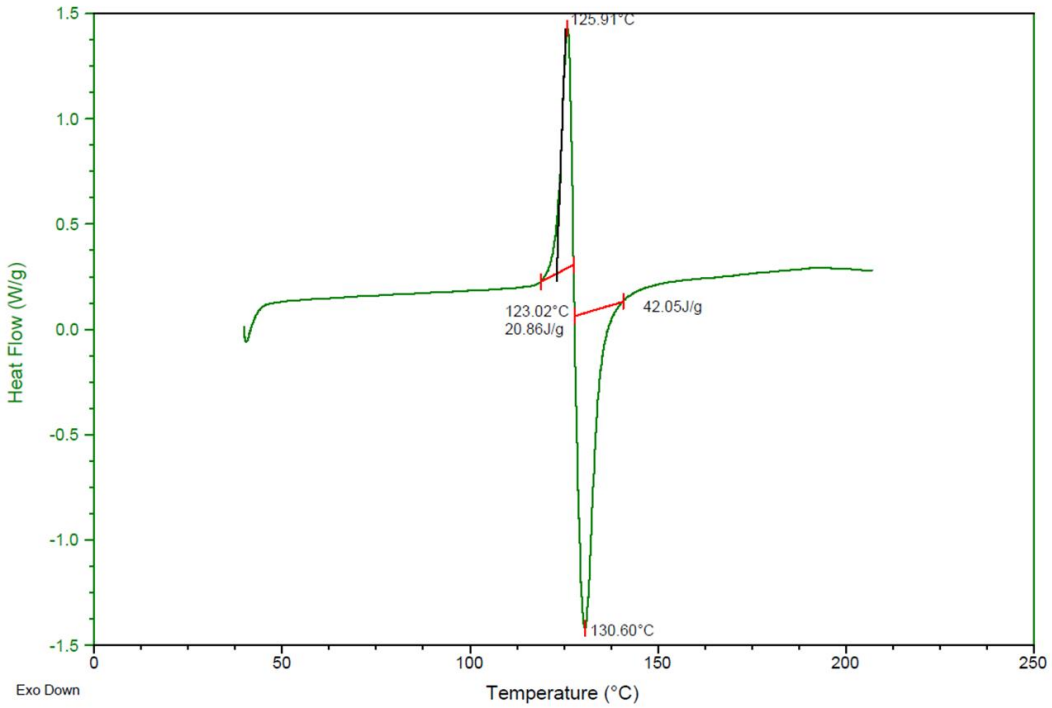

Figure 3-5 DSC trace of 1:1 mixture of Bi(*o*-tol)$_3$ and diphenylphosphinic acid from 40 to 210 °C.

An alternative salt metathesis route was trialled through *in situ* preparation of Bi(*o*-tol)$_2$Cl and addition of the sodium phosphinato salts, as per Scheme 3-3. The Bi(*o*-tol)$_2$Cl salt is soluble in diethyl ether, however the sodium phosphinato salts are not, so the salts were solubilised in dry methanol before addition. Upon addition, a white precipitate immediately formed and the suspension was allowed to stir for a further two hours before isolation of the solid, which was washed with hot water, acetone and ethanol. The phenylphosphinato complex **3-10** was isolated in very poor yields (<5 %). Only the sodium phosphinato salt and Bi(*o*-tol)$_3$ were isolated from the diphenylphosphinato and *bis*-(*p*-methoyphenyl)phosphinato reactions. A similar method using only diethyl ether as the solvent and stirring the heterogeneous reaction for longer time periods was investigated, but again proved unyielding. Due to the poor yields and synthetic difficulties, the *bis*-*o*-tolyl bismuth *mono*-phosphinato complexes **3-10** – **3-12** were no longer pursued.

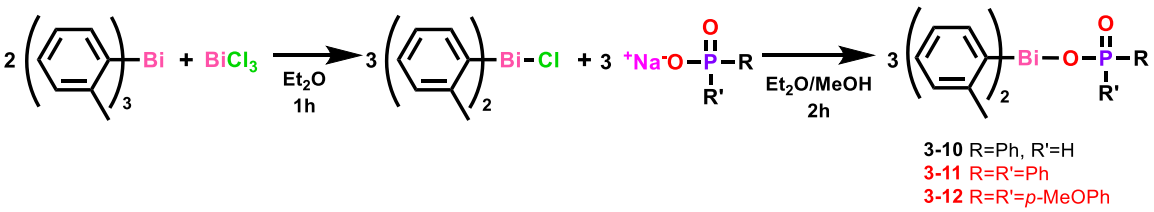

Scheme 3-3 Salt metathesis route trialled to form *bis*-*o*-tolyl bismuth *mono*-phosphinato complexes **3-10** – **3-12**, however only complex **3-10** proved successful.

Of the 18 targeted diaryl bismuth *mono*-phosphinato complexes, 12 were able to be isolated cleanly in reasonable yields. The six *bis*-methoxyphenyl and six *bis*-tolyl bismuth *mono*-phosphinato complexes (**3-1** – **3-6** and **3-13** – **3-18**) are detailed in the remaining sections of this chapter.

3.3 Characterisation

The diaryl *mono*-phosphinato bismuth complexes [Bi(*o*-MeOPh)$_2$O(O)P(H)Ph]$_\infty$ **3-1**, [Bi(*o*-MeOPh)$_2$O(O)PPh$_2$]$_\infty$ **3-2**, [Bi(*o*-MeOPh)$_2$O(O)P(*p*-MeOPh)$_2$]$_\infty$ **3-3**, [Bi(*m*-MeOPh)$_2$O(O)P(H)Ph]$_\infty$ **3-4**, [Bi(*m*-MeOPh)$_2$O(O)PPh$_2$]$_\infty$ **3-5**, [Bi(*m*-MeOPh)$_2$O(O)P(*p*-MeOPh)$_2$]$_\infty$ **3-6**, [Bi(*m*-tol)$_2$O(O)P(H)Ph]$_\infty$ **3-13**, [Bi(*m*-tol)$_2$O(O)PPh$_2$]$_\infty$ **3-14**, [Bi(*m*-tol)$_2$O(O)P(*p*-MeOPh)$_2$]$_\infty$ **3-15**, [Bi(*p*-tol)$_2$O(O)P(H)Ph]$_\infty$ **3-16**, [Bi(*p*-tol)$_2$O(O)PPh$_2$]$_\infty$ **3-17** and [Bi(*p*-tol)$_2$O(O)P(*p*-MeOPh)$_2$]$_\infty$ **3-18** display solubility in hot DMSO and very poor solubility in most other common solvents, as similarly observed for the diphenyl bismuth *mono*-phosphinato analogues. Solution-state characterisation was conducted by ^{1}H NMR spectroscopy, and solid-state analysis included IR spectroscopy, TGA, melting point and elemental analysis including ICP-OES for bismuth content.

Complexes **3-1** – **3-6** and **3-13** – **3-18** show an upfield shift of the phosphinato protons in the ^{1}H NMR spectra upon binding to bismuth, due to the delocalisation of electrons in the PO_2 group compared with the phosphinic acid. Figures 3-6 and 3-7 highlight this, as well as the downfield shift observed for bismuth-aryl protons upon coordination of the phosphinato moiety. This is observed for all diaryl complexes (**3-1** – **3-6** and **3-13** – **3-18**), as well as the diphenyl bismuth *mono*-phosphinato analogues.

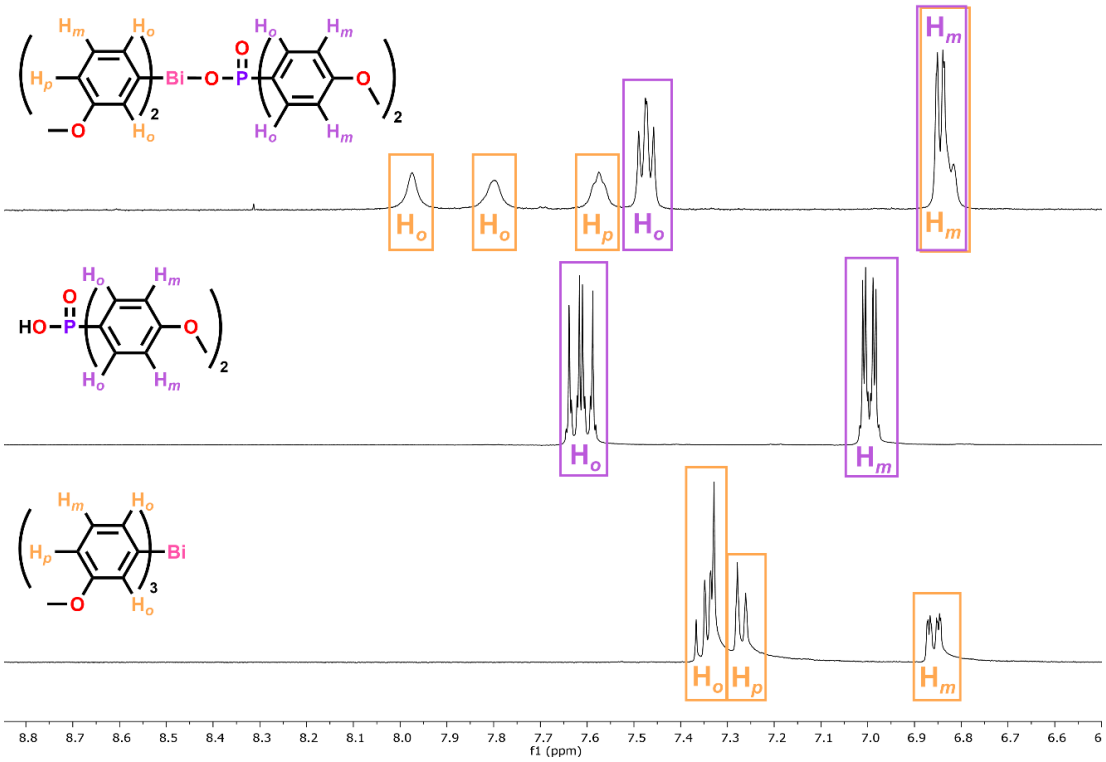

Figure 3-6 ^{1}H NMR of complex **3-6** (top), *bis*-(*p*-methoxyphenyl)phosphinic acid (middle) and Bi(*m*-MeOPh)$_3$ (bottom) in d$_6$-DMSO.

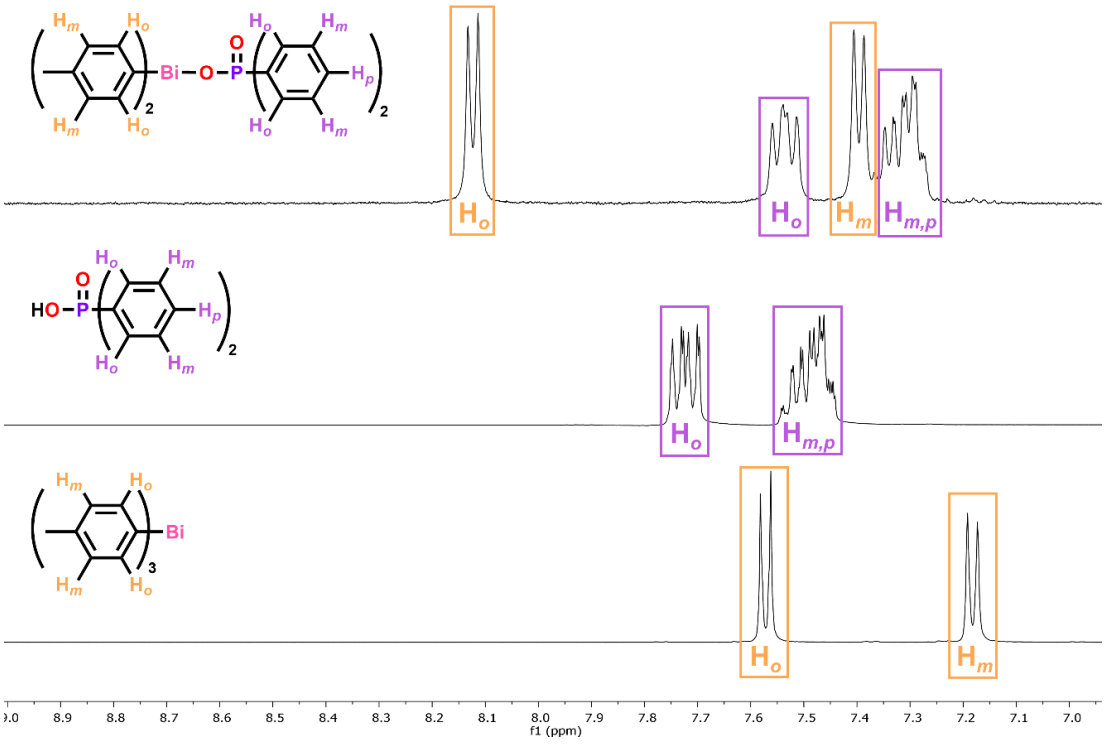

Figure 3-7 ^{1}H NMR of complex **3-17** (top), diphenylphosphinic acid (middle) and Bi(*p*-tol)$_3$ (bottom) in d$_6$-DMSO.

Complex **3-7** shows a similar upfield shift of phosphinato protons, however multiple bismuth-aryl protons can be observed. Figure 3-8 depicts the aromatic region of the ^{1}H NMR spectrum showing the *mono*-phosphinato complex **3-7**, the *bis*-phenylphosphinato complex and Bi(*p*-MeOPh)$_3$. Both *p*-methoxyphenyl bismuth phosphinato complexes display poor solubility in most solvents except DMSO, resulting in great difficulties separating the compounds, thus no further characterisation was conducted for complex **3-7**.

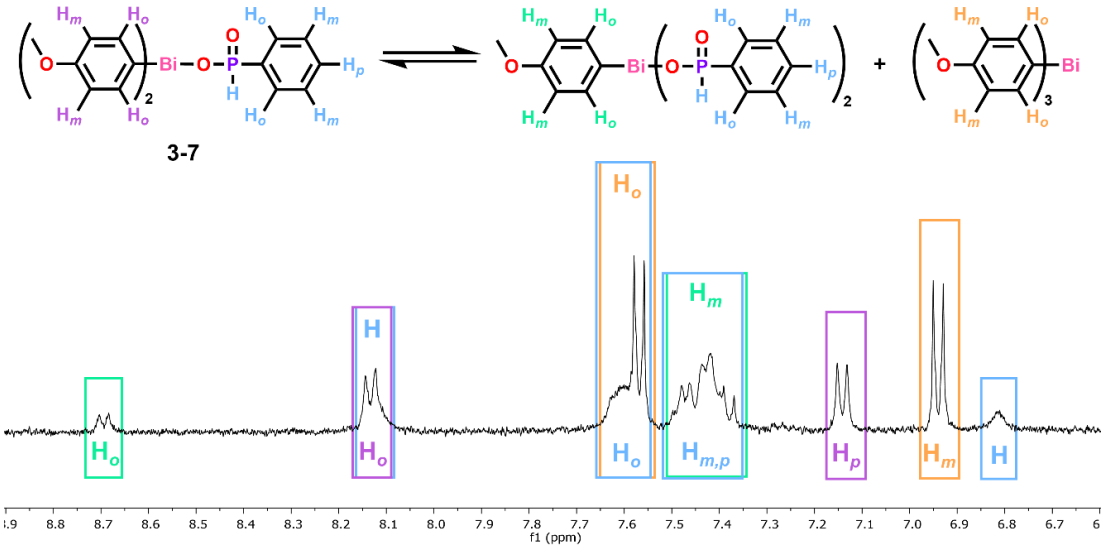

Figure 3-8 ^{1}H NMR of complex **3-7** showing impurities of [Bi(*p*-MeOPh)(O(O)P(H)Ph)$_2$] and Bi(*p*-MeOPh)$_3$ in d_6-DMSO.

Solid-state results including IR spectroscopy, TGA and melting point analysis are depicted in Table 3-3. The differences between the phosphinato asymmetric and symmetric PO_2 stretching bands ($\Delta\nu$) can provide insights into the binding mode of the phosphinato moiety. The determined $\Delta\nu$ for complexes **3-1** – **3-6** and **3-13** – **3-18** are very similar to the diphenyl bismuth phosphinato complexes, suggesting a symmetric chelating or bridging binding mode. The poor solubility of the compounds indicates possible coordination polymers, which is consistent with bridging phosphinato groups.

Melting point analysis of complexes **3-1** – **3-6** and **3-13** – **3-18** shows the phenylphosphinato-containing complexes consistently melt at lower temperatures compared to the diphenylphosphinato- and *bis*-(*p*-methoxyphenyl)phosphinato-containing complexes. Elemental analysis and bismuth content analysis by ICP-OES of complexes **3-1** – **3-6** and **3-13** – **3-18** were consistent with the expected values for compounds of the type [BiAr$_2$O(O)PRR']$_\infty$, as detailed in Chapter 7 (Experimental section 7.8). While neither analysis was able to differentiate between monomeric and polymeric structures, IR spectroscopy suggested the complexes adopt polymeric structures which was confirmed by X-ray crystallography.

Table 3-3 Solid-state analyses including Δ*v* determined as the difference between asymmetric and symmetric PO_2 stretching bands in IR spectra for complexes **3-1** – **3-6** and **3-13** – **3-18** and TGA and melting point analysis.

Compound		Δ*v* (cm^{-1})	Melting point (°C)	Decomposition point (°C)
[Bi(*o*-MeOPh)$_2$O(O)P(H)Ph]$_\infty$	**3-1**	94, 105	149	149
[Bi(*o*-MeOPh)$_2$O(O)PPh$_2$]$_\infty$	**3-2**	110, 111	177	177
[Bi(*o*-MeOPh)$_2$O(O)P(*p*-MeOPh)$_2$]$_\infty$	**3-3**	107, 112	186	186
[Bi(*m*-MeOPh)$_2$O(O)P(H)Ph]$_\infty$	**3-4**	91, 98	127	163
[Bi(*m*-MeOPh)$_2$O(O)PPh$_2$]$_\infty$	**3-5**	111, 130	161	161
[Bi(*m*-MeOPh)$_2$O(O)P(*p*-MeOPh)$_2$]$_\infty$	**3-6**	92, 110	151	190
[Bi(*m*-tol)$_2$O(O)P(H)Ph]$_\infty$	**3-13**	90, 100	139	145
[Bi(*m*-tol)$_2$O(O)PPh$_2$]$_\infty$	**3-14**	75, 98	152	170
[Bi(*m*-tol)$_2$O(O)P(*p*-MeOPh)$_2$]$_\infty$	**3-15**	98, 99	239	239
[Bi(*p*-tol)$_2$O(O)P(H)Ph]$_\infty$	**3-16**	108, 130	156	156
[Bi(*p*-tol)$_2$O(O)PPh$_2$]$_\infty$	**3-17**	88, 93	219	219
[Bi(*p*-tol)$_2$O(O)P(*p*-MeOPh)$_2$]$_\infty$	**3-18**	101, 108	188	188

3.3.1 X-ray crystallography

The solid-state structure of diphenyl bismuth *mono*-phosphinato complexes has been well established, where the complexes form 1D coordination polymers with phosphinato groups bridging bismuth centres. Given the similarities between the diphenyl and diaryl bismuth *mono*-phosphinato complexes, it is expected that they will possess a similar polymeric structure. Crystals were isolated from ethanol during the synthesis of [Bi(*m*-tol)$_2$O(O)P(H)Ph]$_\infty$ **3-13**, or through dissolution of complexes [Bi(*m*-MeOPh)$_2$O(O)P(H)Ph]$_\infty$ **3-4** and [Bi(*p*-tol)$_2$O(O)PPh$_2$]$_\infty$ **3-17** in hot DMSO and analysed by single-crystal X-ray diffraction.

Complexes **3-4** and **3-13** are both diaryl bismuth phenylphosphinato complexes with a *meta*-substituted aryl group, allowing for comparison between solid-state structures for the *m*-methoxyphenyl (**3-4**) and *m*-tolyl (**3-13**) functionalities. Both complexes form 1D coordination polymers with bridging phosphinato ligands (Figures 3-9 and 3-10), however only complex **3-4** shows bismuth-arene π-interactions with adjacent bismuth-bound methoxyphenyl moieties, with a Bi-arene$_{centroid}$ distance of 3.849 Å. Complex **3-4** adopts a distorted square pyramidal geometry around the five-coordinate bismuth centre, with evidence of a sterically active lone pair based on bond angles around the bismuth centre including C(8)–Bi(1)–arene$_{centroid}$ angle of 166.28 °, with

bond angles as detailed in Table 3-4. Interestingly, complex **3-13** does not show the typical bismuth-arene π-interactions, instead adopted a distorted disphenoidal confirmation around the four-coordinate bismuth centre.

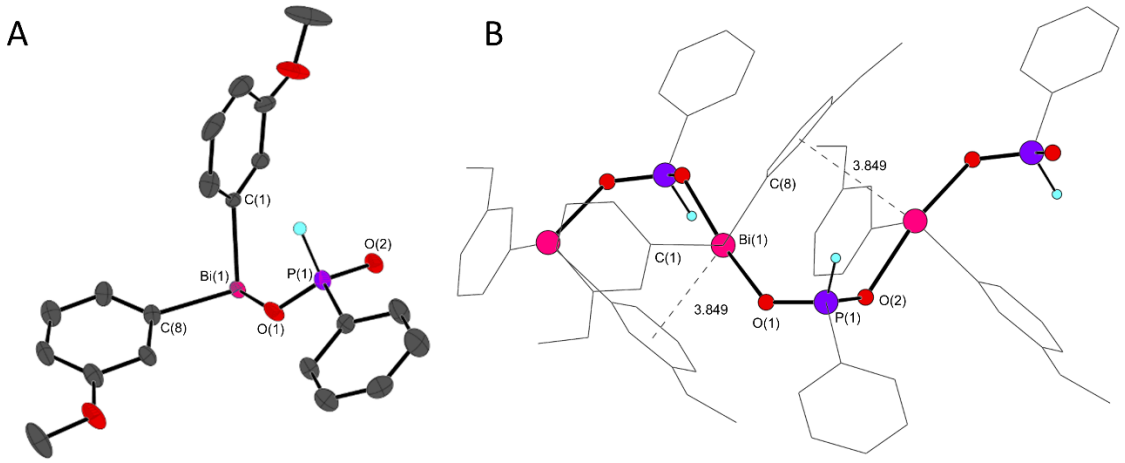

Figure 3-9 Molecular (A) and polymeric (B) structure of [Bi(*m*-MeOPh)$_2$O(O)P(H)Ph]$_\infty$, **3-4**. Thermal ellipsoids shown at 50 % probability in molecular structure. Bismuth-arene π distances are in Å. Hydrogen atoms on aromatic groups are omitted for clarity.

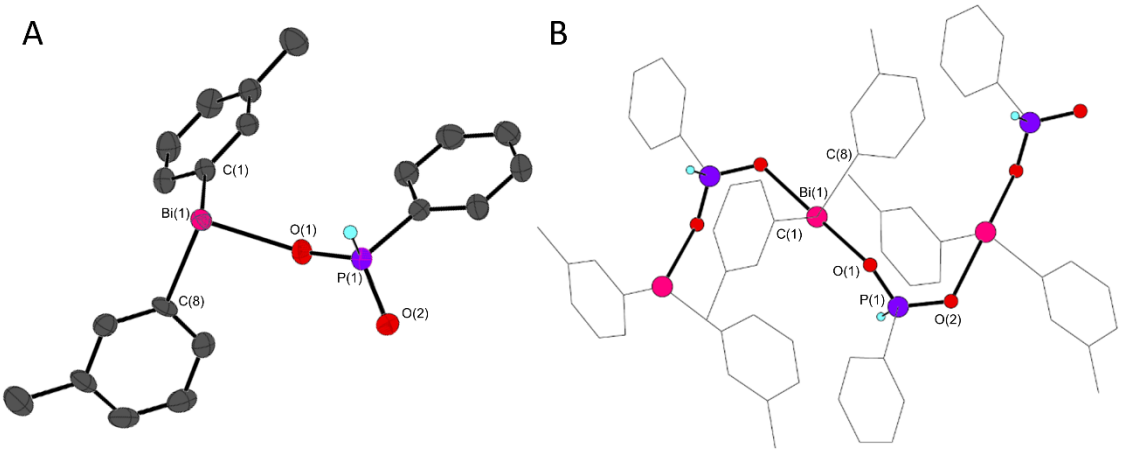

Figure 3-10 Molecular (A) and polymeric (B) structure of [Bi(*m*-tol)$_2$O(O)P(H)Ph]$_\infty$, **3-13**. Thermal ellipsoids shown at 50 % probability in molecular structure. Hydrogen atoms on aromatic groups are omitted for clarity.

Table 3-4 Selected bond lengths and angles for complexes **3-4**, **3-13** and **3-17** (A and B).

Bond lengths (Å)	**3-4**	**3-13**	**3-17** (A)	**Bond lengths (Å)**	**3-17** (B)
Bi(1) – C(1)	2.245(5)	2.224(7)	2.272(8)	Bi(2) – C(27)	2.249(10)
Bi(1) – C(8)	2.241(6)	2.240(6)	2.254(9)	Bi(2) – C(23)	2.262(9)
Bi(1) – O(1)	2.377(4)	2.382(5)	2.379(6)	Bi(2) – O(3)	2.355(6)
Bi(1) – O(2)*	2.375(4)	2.373(5)	2.329(6)	Bi(2) – O(4)*	2.361(6)
P(1) – O(1)	1.512(4)	1.508(5)	1.492(7)	P(2) – O(3)	1.516(7)
P(1) – O(2)	1.510(4)	1.517(5)	1.511(6)	P(2) – O(4)	1.502(6)
Bond angles (°)				**Bond angles (°)**	
C(1) – Bi(1) – C(8)	95.4(2)	95.5(2)	90.8(3)	C(27) – Bi(2) – C(34)	93.2(3)
C(1) – Bi(1) – O(1)	87.28(18)	83.5(2)	84.4(3)	C(27) – Bi(2) – O(3)	85.8(3)
C(1) – Bi(1) – O(2)*	87.53(18)	86.4(2)	89.0(3)	C(27) – Bi(2) – O(4)*	87.8(3)
C(8) – Bi(1) – O(1)	84.78(19)	88.9(2)	90.2(3)	C(34) – Bi(2) – O(3)	86.4(3)
C(8) – Bi(1) – O(2)*	84.23(19)	86.9(2)	85.5(3)	C(34) – Bi(2) – O(4)*	88.0(3)
O(1) – Bi(1) – O(2)*	167.34(16)	168.60(17)	172.1(2)	O(3) – Bi(2) – O(4)*	171.2(2)
O(1) – P(1) – O(2)	117.6(2)	116.7(3)	118.9(4)	O(3) – P(2) – O(4)	117.4(4)

*Symmetry transformations used to generate equivalent atoms: **3-4** (-x + 1, y + 1/2, -z + 2), **3-13** (-x + 1, y + 1/2, -z + 1), **3-17** (A) (-x + 1, y + 1/2, -z + 2), **3-17** (B) (-x, y + 1/2, -z + 1).

Complex **3-17** forms a 1D coordination polymer with distorted square pyramidal geometry around the five-coordinate bismuth centre with evidence of sterically active lone pair. Figures 3-11 and 3-12 depict the monomeric and polymeric structures of the *bis-p*-tolyl bismuth *mono*-diphenylphosphinato complex **3-17**. It is interesting to note that the asymmetric unit contains two independent molecules that show differences in bond lengths and angles, as detailed in Table 3-4. This was similarly observed for the diphenyl bismuth *mono*-(1,1,2,3,3-pentamethyltrimethylene)phosphinato complex (Chapter 2, Figure 2-1), however was not discussed.[120] Complex **3-17** shows interactions of bismuth atoms and adjacent bismuth-bound tolyl groups, with Bi-arene$_{centroid}$ distances of 3.429 Å (**3-17** (A)) and 3.509 Å (**3-17** (B)), as similarly observed in the diphenyl bismuth *mono*-phosphinato complexes **2-1** – **2-3**.

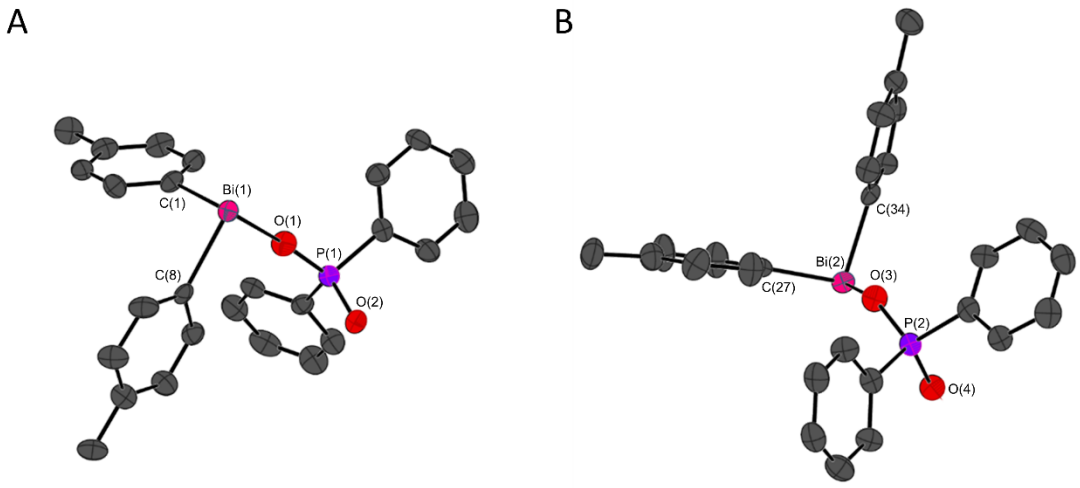

Figure 3-11 Molecular structure of [Bi(*p*-tol)$_2$O(O)PPh$_2$]$_\infty$, **3-17** showing the asymmetric unit containing two structurally independent units denoted **3-17** (A) and **3-17** (B). Thermal ellipsoids shown at 50 % probability. Hydrogen atoms are omitted for clarity.

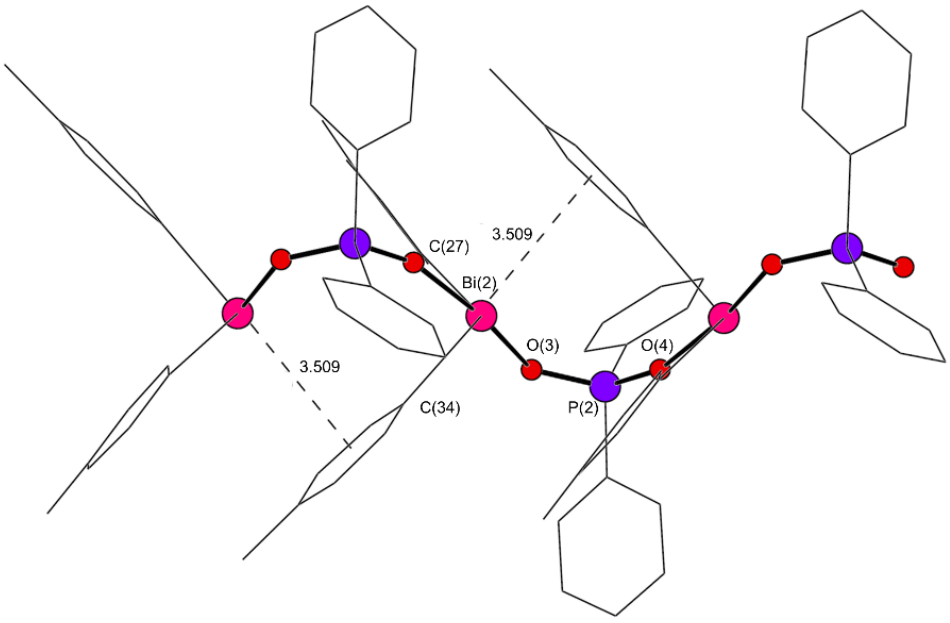

Figure 3-12 Polymeric structure of [Bi(*p*-tol)$_2$O(O)PPh$_2$]$_\infty$, **3-17** (B). Bismuth-arene π distances are in Å. Hydrogen atoms omitted for clarity.

Small needle-shaped crystals of complex [Bi(*m*-tol)$_2$O(O)P(*p*-MeOPh)$_2$]$_\infty$ **3-15** were also isolated from DMSO and analysed by single-crystal X-ray crystallography. The obtained structure revealed that both the diaryl bismuth *mono*-phosphinato complex **3-15** and the aryl bismuth *bis*-phosphinato complex had co-crystallised to give the twinned structure showing both complexes in the asymmetric unit, as shown in Figure 3-13. Processing of the twinned data was unsuccessful so the bond lengths and angles cannot be commented on, however valuable insights into the connectivity of the *bis*-phosphinato complex can be gained. Figure 3-14 depicts the polymeric structures, where it can be noted that complex **3-15** adopts a distorted square pyramidal

geometry around the bismuth centre and the *bis*-phosphinato complex adopts a square pyramidal geometry around the bismuth atom. The *m*-tolyl bismuth *bis*-(*bis*-*p*-methoxyphenyl)phosphinato complex shows each bismuth atom bound to one tolyl and four phosphinato moieties, forming a $Bi_2O_4P_2$ puckered ring. Similar connectivity has been reported for the phenyl bismuth *bis*-(*bis*-pentafluoroethyl)phosphinato and phenyl bismuth *bis*-diphenylthiophosphinato complexes.[90,119]

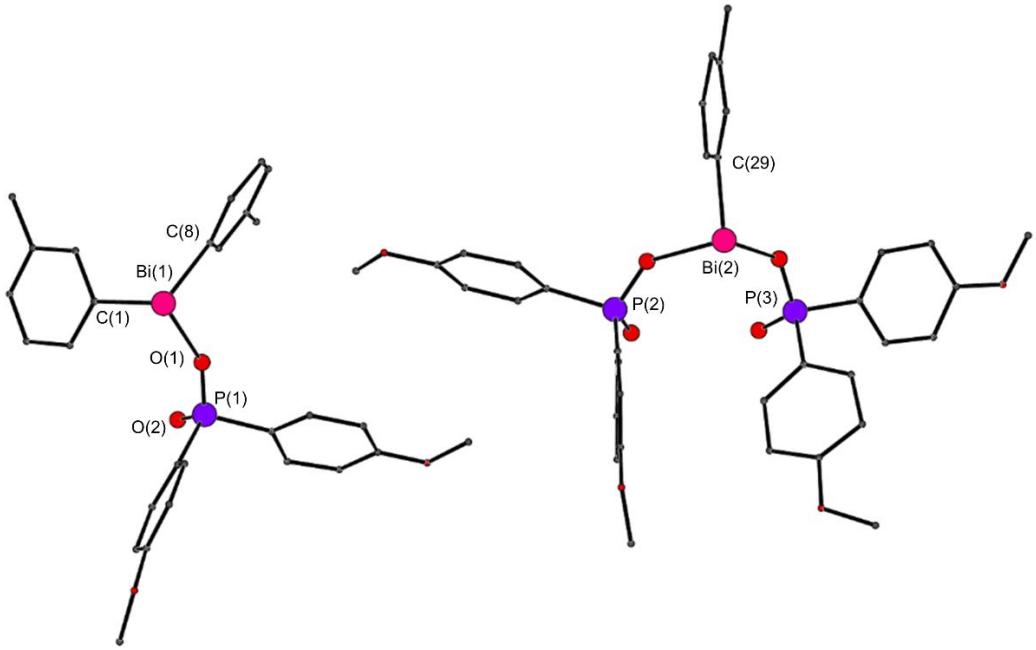

Figure 3-13 Molecular structure of both $[Bi(m\text{-tol})_2O(O)P(p\text{-MeOPh})_2]_\infty$ **3-15** and $[Bi(m\text{-tol})(O(O)P(p\text{-MeOPh})_2]_2]_\infty$ in the asymmetric unit showing connectivity. Hydrogen atoms omitted for clarity.

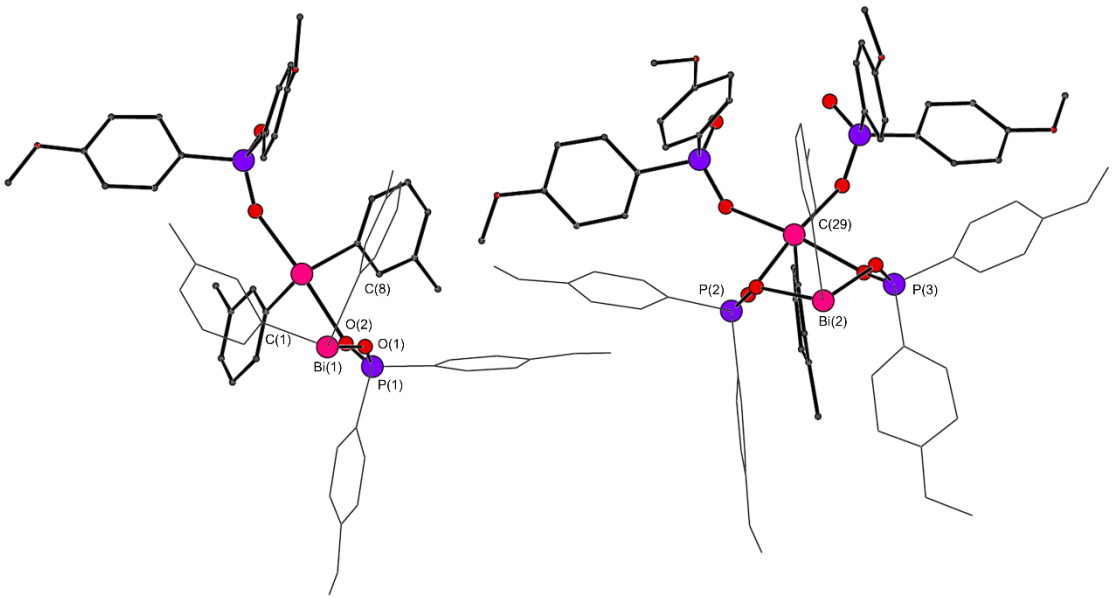

Figure 3-14 Polymeric structure of both $[Bi(m\text{-tol})_2O(O)P(p\text{-MeOPh})_2]_\infty$ **3-15** and $[Bi(m\text{-tol})(O(O)P(p\text{-MeOPh})_2]_2]_\infty$. The labelled wire frame monomers are closest, with the thicker edged monomers behind. Hydrogen atoms omitted for clarity.

3.4 Solubility and stability

The water solubility of the diaryl bismuth phosphinato complexes **3-1** – **3-6** and **3-13** – **3-18** were analysed to understand the role of the different aryl moieties. Solubility analysis was conducted by dispersing the compounds in water at 25 °C for 24 hours, followed by filtration using 0.2 µm syringe filters. The filtrates were analysed by ICP-OES to determine the bismuth content, and thus determine the amount of complex solubilised based on the solubilised bismuth, as shown in Figure 3-15.

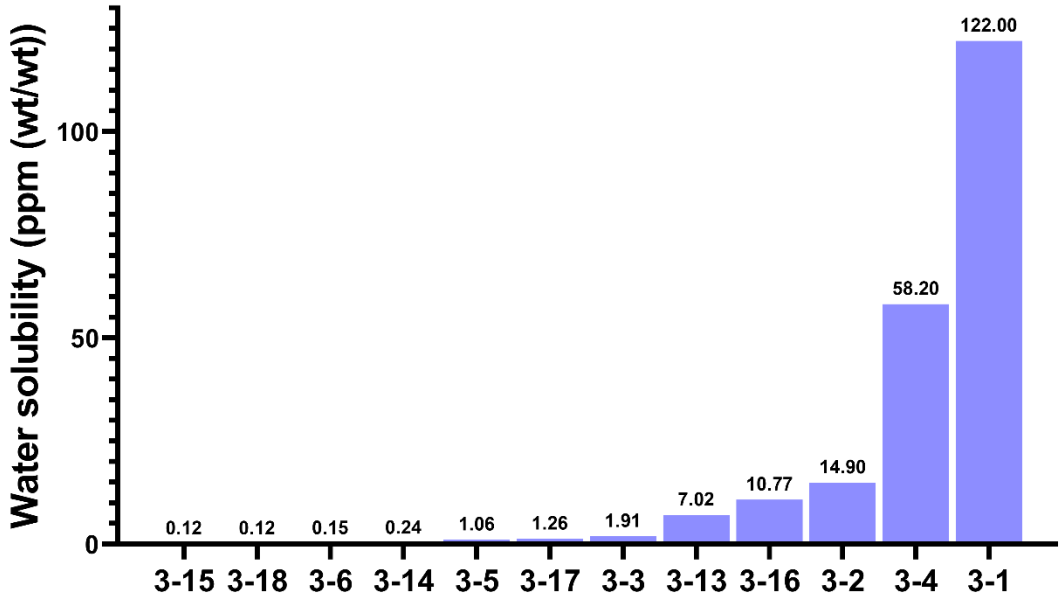

Figure 3-15 Water solubility of complexes **3-1** – **3-6** and **3-13** – **3-18** as determined by ICP-OES, in order of increasing solubility.

The water solubility results show two main trends; the phenylphosphinato-containing complexes display the greatest water solubility in this series and that the *bis*-methoxyphenyl bismuth complexes **3-1** – **3-6** show superior water solubility when compared with the *bis*-tolyl bismuth complexes **3-13** – **3-18**. The first trend has previously been noted for the phenyl bismuth phenylphosphinato complexes (**2-1**, **2-5**, **2-9**) when compared with the diphenylphosphinato and *bis*-(*p*-methoxyphenyl)phosphinato complexes, with only the dimethylphosphinato compounds displaying greater water solubility.

The methoxyphenyl series (**3-1** – **3-6**) was expected to show greater water solubility owing to the greater hydrophilicity in comparison with the tolyl series (**3-13** – **3-18**). It is interesting to note that the position of the methoxy group greatly influences the solubility, with the *bis*-*o*-methoxyphenyl bismuth complexes **3-1** – **3-3** showing much greater solubility when compared with the *bis*-*m*-

methoxyphenyl complexes **3-4** – **3-6**. It is apparent that the *meta*-substituted diaryl complexes display lower water solubility compared with both the *o*-methoxyphenyl and *p*-tolyl complexes.

Stability studies of the complexes in solution were conducted by ^{1}H NMR in the solution-state in d_6-DMSO, where complexes **3-1** – **3-6** and **3-13** – **3-18** proved stable at room temperature for 24 hours before rearrangement was observed. As similarly noted for the diphenyl bismuth *mono*-phosphinato complexes, the diaryl compounds saw the formation of the triaryl bismuth species in solution after 24 hours. There is no evidence of the phosphinic acids forming, indicating the aryl bismuth *bis*-phosphinato complex also forms as part of the redistribution reaction. Although not seen by NMR due to low solubility, this is evidenced through the co-crystallisation of complex **3-15** and its *bis*-phosphinato analogue. Interestingly, all attempts to crystallise complexes **3-1** – **3-3** from DMSO only produced crystals of Bi(*o*-MeOPh)$_3$, suggesting the redistribution will continue to form the triaryl bismuth and aryl bismuth *bis*-phosphinato compounds.

3.5 Biology

The diaryl bismuth *mono*-phosphinato complexes **3-1** – **3-6** and **3-13** – **3-18** were assessed for their antibacterial activity towards the Gram positive bacteria methicillin-resistant *S. aureus* (MRSA) and vancomycin-resistant *Enterococcus* (VRE), and the Gram negative bacteria *E. coli* and *P. aeruginosa*, and their MIC determined. The triaryl bismuth compounds used for synthesis were also assessed for their antibacterial potential, while the phosphinic acids are known to be inactive, as detailed in Chapter 2 (section 2.5). Mammalian cell assays were conducted using Cos-7 monkey kidney cells to determine if the complexes **3-1** – **3-6**, **3-13** – **3-18** or their triaryl bismuth analogues effect cell viability, and thus examine the selectivity of the complexes towards bacteria.

3.5.1 Antibacterial activity

The MIC of the bismuth complexes **3-1** – **3-6** and **3-13** – **3-18** were determined through solution-based assays. The complexes and their respective triaryl bismuth compounds were solubilised in DMSO at concentrations of 4 mM for **3-1** – **3-3**, 2 mM for **3-4** – **3-6** and **3-13** – **3-15**, 1 mM for **3-16** – **3-18** and 10 mM for $BiAr_3$, then diluted to 1:100 in bacterial broth giving a maximum DMSO concentration of 1 %. Several 1:2 serial dilutions were performed before the addition of overnight bacterial cultures to the broth and incubation overnight at 37 °C. The assays were conducted in 96 well plates to allow absorbance readings at 600 nm, where broth only was treated as the negative control and the positive bacterial control was regarded as 100 % growth, containing no added compound. The results are shown in Table 3-5, where the MIC was determined as the lowest concentration to inhibit ≥80 % growth, as similarly defined by CO-ADD.[43]

Table 3-5 Minimum inhibitory concentration of complexes **3-1** – **3-6**, **3-13** – **3-18** and their triaryl bismuth analogues ($BiAr_3$) to inhibit ≥80 % growth of MRSA, VRE, *E. coli* and *P. aeruginosa*, as measured by absorbance at 600 nm following overnight incubation at 37 °C.

Compound		**MIC (μM)**			
		MRSA	VRE	*E. coli*	*P. aeruginosa*
[Bi(*o*-MeOPh)$_2$O(O)P(H)Ph]$_\infty$	**3-1**	>40	>40	>40	>40
[Bi(*o*-MeOPh)$_2$O(O)PPh$_2$]$_\infty$	**3-2**	40	40	20	40
[Bi(*o*-MeOPh)$_2$O(O)P(*p*-MeOPh)$_2$]$_\infty$	**3-3**	>40	>40	>40	>40
[Bi(*m*-MeOPh)$_2$O(O)P(H)Ph]$_\infty$	**3-4**	1.25	1.25	10	20
[Bi(*m*-MeOPh)$_2$O(O)PPh$_2$]$_\infty$	**3-5**	0.63	1.25	10	20
[Bi(*m*-MeOPh)$_2$O(O)P(*p*-MeOPh)$_2$]$_\infty$	**3-6**	0.63	1.25	10	20
[Bi(*m*-tol)$_2$O(O)P(H)Ph]$_\infty$	**3-13**	10	10	10	20
[Bi(*m*-tol)$_2$O(O)PPh$_2$]$_\infty$	**3-14**	5.0	5.0	10	20
[Bi(*m*-tol)$_2$O(O)P(*p*-MeOPh)$_2$]$_\infty$	**3-15**	10	10	10	20
[Bi(*p*-tol)$_2$O(O)P(H)Ph]$_\infty$	**3-16**	5.0	5.0	10	10
[Bi(*p*-tol)$_2$O(O)PPh$_2$]$_\infty$	**3-17**	2.5	2.5	10	10
[Bi(*p*-tol)$_2$O(O)P(*p*-MeOPh)$_2$]$_\infty$	**3-18**	5.0	5.0	10	10
Bi(*o*-MeOPh)$_3$		>100	>100	>100	>100
Bi(*m*-MeOPh)$_3$		>100	>100	>100	>100
Bi(*m*-tol)$_3$		>100	>100	>100	>100
Bi(*p*-tol)$_3$		>50	>50	>50	>50

Two main trends are immediately apparent from the MIC results; the diaryl bismuth *mono*-phosphinato complexes are most active towards Gram positive bacteria over Gram negative, and the triaryl bismuth compounds do not show any antibacterial activity at the concentrations examined. While the former trend has been previously described for various heteroleptic bismuth compounds including thiolato, flavonolato and cyclic organobismuth complexes,[86,88,89,91,153,154] the latter is surprising, given the activity of $BiPh_3$ towards MRSA at 28.4 μM and VRE at 14.2 μM.[88,89]

It is evident that the bismuth aryl group has a profound influence on antibacterial activity, with the *bis*-*o*-methoxyphenyl bismuth complexes **3-1** – **3-3** displaying much higher MIC values in comparison with the *bis*-*m*-methoxyphenyl analogues **3-4** – **3-6**. This is interesting as the *o*-methoxyphenyl bismuth complexes show greater water solubility than the *m*-methoxyphenyl analogues. This suggests better aqueous solubility in compounds leads to poorer antibacterial activity, which is due to more lipophilic compounds displaying greater membrane permeability

and thus exerting greater toxicity.[142] The position of the methyl substituent on the bismuth tolyl group also has an effect on antibacterial activity, with the *para*-substituted complexes **3-16** – **3-18** showing lower MIC values towards MRSA, VRE and *P. aeruginosa* compared with the *bis*-*m*-tolyl complexes **3-13** – **3-15**. The phosphinato group also has an effect on antibacterial activity, with the diphenylphosphinato-containing complexes typically displaying lower MIC values than the phenylphosphinato and *bis*-(*p*-methoxyphenyl)phosphinato complexes, as similarly noted for the diphenyl bismuth complexes in Chapter 2 (section 2.5.1).

Overall, the MIC of the complexes towards Gram negative bacteria are much higher for the diaryl bismuth *mono*-phosphinato complexes than the diphenyl bismuth *mono*-phosphinato complexes **2-1** – **2-4** (1.25 to 7.5 µM). This may be due to the outer membrane having a lower permeability to the bulkier aromatic moieties on the bismuth centre. It is interesting to note that complexes **3-4** – **3-6** show greater antibacterial activity towards MRSA, with lower MIC values of 0.63 to 1.25 µM compared to their diphenyl bismuth analogues (2.5 to 5.0 µM) (Chapter 2, section 2.5.1).

3.5.2 Mammalian cell viability

The complexes **3-1** – **3-6**, **3-13** – **3-18** and their respective $BiAr_3$ compounds were assessed for their cytotoxicity towards Cos-7 cells through use of the CellTiter-Blue viability assay. Cos-7 cells are seeded and adhered to 96 well plates before the addition of the bismuth compounds solubilised in DMSO such that the maximum DMSO concentration is 1 % (2 % for **3-1** – **3-3**). After overnight incubation at 37 °C, the CellTiter-Blue dye (resazurin) is added to the cells and incubated for a further 4 hours to allow the metabolically-active cells to convert the blue dye to the pink product resorufin, which is measured by fluorescence. A positive control of cells without added compound is included and treated as 100 % viable. The triaryl bismuth compounds proved non-toxic, with Cos-7 viability minimally reduced (>80 %) at the highest tested concentrations of 50 or 100 µM, as seen in Figure 3-16.

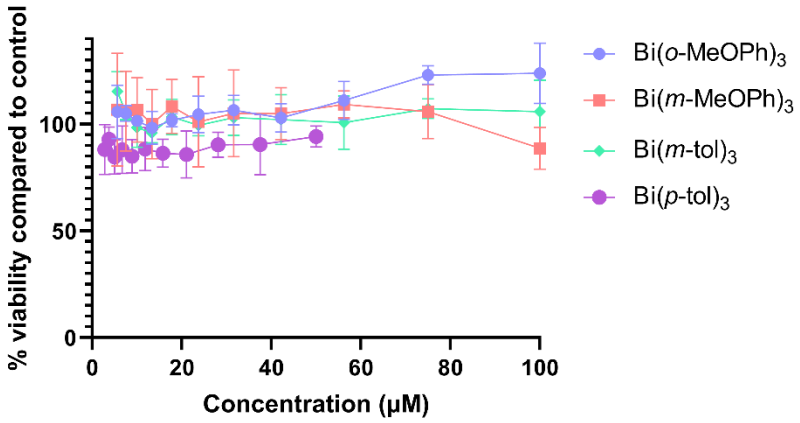

Figure 3-16 Cos-7 viability following 24 hour incubation at 37 °C with Bi(*o*-MeOPh)$_3$, Bi(*m*-MeOPh)$_3$, Bi(*m*-tol)$_3$ and Bi(*p*-tol)$_3$.

Figure 3-17 displays the Cos-7 viability results and the determined IC_{50} values for complexes [Bi(*o*-MeOPh)$_2$O(O)P(H)Ph]$_\infty$ **3-1**, [Bi(*o*-MeOPh)$_2$O(O)PPh$_2$]$_\infty$ **3-2**, [Bi(*o*-MeOPh)$_2$O(O)P(*p*-MeOPh)$_2$]$_\infty$ **3-3**, [Bi(*m*-MeOPh)$_2$O(O)P(H)Ph]$_\infty$ **3-4**, [Bi(*m*-MeOPh)$_2$O(O)PPh$_2$]$_\infty$ **3-5**, [Bi(*m*-MeOPh)$_2$O(O)P(*p*-MeOPh)$_2$]$_\infty$ **3-6**, [Bi(*m*-tol)$_2$O(O)P(H)Ph]$_\infty$ **3-13**, [Bi(*m*-tol)$_2$O(O)PPh$_2$]$_\infty$ **3-14**, [Bi(*m*-tol)$_2$O(O)P(*p*-MeOPh)$_2$]$_\infty$ **3-15**, [Bi(*p*-tol)$_2$O(O)P(H)Ph]$_\infty$ **3-16**, [Bi(*p*-tol)$_2$O(O)PPh$_2$]$_\infty$ **3-17** and [Bi(*p*-tol)$_2$O(O)P(*p*-MeOPh)$_2$]$_\infty$ **3-18**. It is apparent that the bismuth aryl moieties have an impact on the toxicity of the diaryl bismuth *mono*-phosphinato complexes, as similarly observed in antibacterial activity results. Complexes containing the *o*-methoxyphenyl bismuth aryl group are the least toxic, with both **3-1** and **3-3** proving non-toxic at the highest tested concentration of 80 µM. The diphenylphosphinato complex **3-2** has an IC_{50} of 38 µM which is far greater than the diphenyl bismuth diphenylphosphinato analogue (**2-2**) IC_{50} of 3.26 µM. It must be noted that the DMSO concentration was 2 % at the maximum concentration tested, as the DMSO-complex solutions could be made up at 4 mM at most. Cos-7 controls containing 2 % DMSO had an average viability of 90 %, suggesting the toxicity observed for **3-2** was not due to the increased DMSO content.

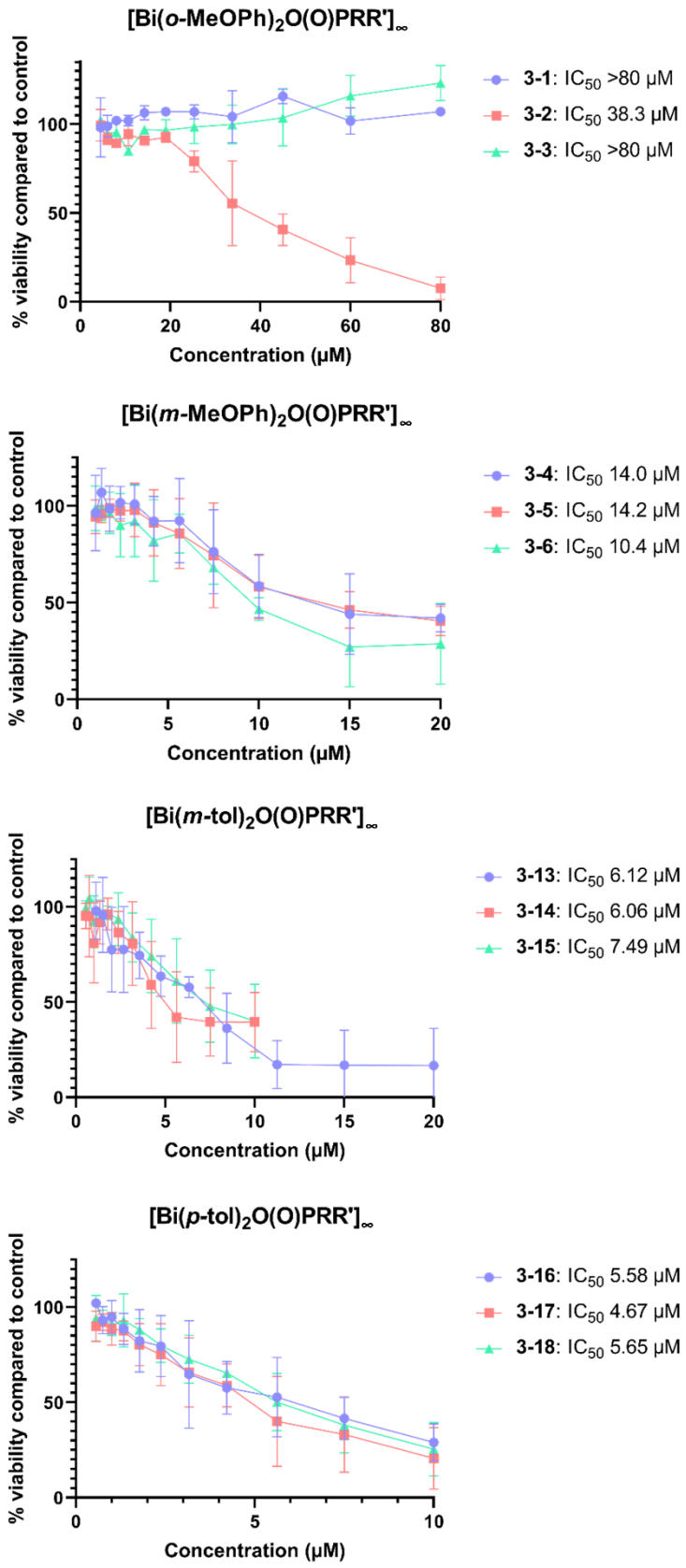

Figure 3-17 Cos-7 viability following 24 hour incubation at 37 °C with complexes **3-1** – **3-6** and **3-13** – **3-18**.

Complexes **3-4** – **3-6** and **3-13** – **3-18** had a greater effect on Cos-7 viability, with IC_{50} values ranging from 4.67 to 14.2 µM. A general trend can be observed where the *m*-methoxyphenyl aryl groups show greater viability than the *m*-tolyl group, which typically shows less toxicity towards Cos-7 cells than the *p*-tolyl bismuth complexes. All complexes with the exception of **3-13** and **3-16** are less toxic to Cos-7 than their diphenyl bismuth *mono*-phosphinato analogues. It is interesting that the diphenylphosphinato-containing complexes do not have the lowest IC_{50} values within the different diaryl bismuth series, proving they are not as toxic despite being highly active towards bacteria. It is expected that more lipophilic complexes would exert a greater toxicity on both bacterial and mammalian cells based on observations from the diphenyl bismuth phosphinato series (Chapter 2, section 2.5). Table 3-6 details the calculated clogP values of complexes **3-1** – **3-6** and **3-13** – **3-18**, where it can be noted that the diaryl *mono*-diphenylphosphinato bismuth compounds are expected to display the lowest hydrophilicity. It is noteworthy that both *bis*-tolyl bismuth *mono*-diphenylphosphinato complexes (**3-14** and **3-17**) show the greatest cytotoxicity, suggesting that clogP values are a good predictor of relative cytotoxicity based on lipophilicity, as similarly noted in a study where greater lipophilicity correlated with an increased likelihood of toxicity.[155]

Table 3-6 clogP values for complexes **3-1** – **3-6** and **3-13** – **3-18**, determined using ChemDraw Professional 17.0.

Compound		clogP value
$[Bi(MeOPh)_2O(O)P(H)Ph]_\infty$	**3-1**, **3-4**	3.497
$[Bi(MeOPh)_2O(O)PPh_2]_\infty$	**3-2**, **3-5**	5.756
$[Bi(MeOPh)_2O(O)P(p\text{-}MeOPh)_2]_\infty$	**3-3**, **3-6**	5.414
$[Bi(tol)_2O(O)P(H)Ph]_\infty$	**3-13**, **3-16**	4.657
$[Bi(tol)_2O(O)PPh_2]_\infty$	**3-14**, **3-17**	6.916
$[Bi(tol)_2O(O)P(p\text{-}MeOPh)_2]_\infty$	**3-15**, **3-18**	6.574

3.5.3 Selectivity

It is important to examine the selectivity of potential antibacterial agents, where the SI will demonstrate the relative difference in concentration between stopping bacterial growth and exerting toxicity on mammalian cells. The SI of complexes **3-1** – **3-6** and **3-13** – **3-18** are shown in Table 3-7, where the values were calculated using Cos-7 IC_{50} and bacterial MIC data.

Table 3-7 Selectivity indices of complexes **3-1** – **3-6** and **3-13** – **3-18**.

Compound		Selectivity index*			
		MRSA	VRE	*E. coli*	*P. aeruginosa*
[Bi(*o*-MeOPh)$_2$O(O)P(H)Ph]$_\infty$	**3-1**	-	-	-	-
[Bi(*o*-MeOPh)$_2$O(O)PPh$_2$]$_\infty$	**3-2**	1.0	1.0	1.9	1.0
[Bi(*o*-MeOPh)$_2$O(O)P(*p*-MeOPh)$_2$]$_\infty$	**3-3**	-	-	-	-
[Bi(*m*-MeOPh)$_2$O(O)P(H)Ph]$_\infty$	**3-4**	11.2	11.2	1.4	0.7
[Bi(*m*-MeOPh)$_2$O(O)PPh$_2$]$_\infty$	**3-5**	22.6	11.3	1.4	0.7
[Bi(*m*-MeOPh)$_2$O(O)P(*p*-MeOPh)$_2$]$_\infty$	**3-6**	16.7	8.3	1.0	0.5
[Bi(*m*-tol)$_2$O(O)P(H)Ph]$_\infty$	**3-13**	0.6	0.6	0.6	0.3
[Bi(*m*-tol)$_2$O(O)PPh$_2$]$_\infty$	**3-14**	1.2	1.2	0.6	0.3
[Bi(*m*-tol)$_2$O(O)P(*p*-MeOPh)$_2$]$_\infty$	**3-15**	0.8	0.8	0.8	0.4
[Bi(*p*-tol)$_2$O(O)P(H)Ph]$_\infty$	**3-16**	1.1	1.1	0.6	0.6
[Bi(*p*-tol)$_2$O(O)PPh$_2$]$_\infty$	**3-17**	1.9	1.9	0.5	0.5
[Bi(*p*-tol)$_2$O(O)P(*p*-MeOPh)$_2$]$_\infty$	**3-18**	1.1	1.1	0.6	0.6

* SI = IC_{50}/MIC.

The determined SIs suggest that the diaryl bismuth *mono*-phosphinato complexes are non-selectively toxic, exhibiting little differentiation between bacterial and mammalian cells. The only exception is the *bis*-*m*-methoxyphenyl complexes **3-4** – **3-6**, which show good selectivity towards the Gram positive bacteria MRSA and VRE. It can be noted that selectivity differs between Gram positive and Gram negative bacteria, where the Gram positive bacteria are generally more susceptible to the compounds, thus leading to better a SI. While complexes **3-4** – **3-6** show poor Gram negative bacteria selectivity, there is potential for investigations into their use as therapeutic antibacterial agents targeting Gram positive bacteria with further optimisation.

3.6 Conclusions

A series of novel diaryl *mono*-phosphinato bismuth complexes were synthesised through solvent mediated reactions of $BiAr_3$ with phosphinic acids to afford complexes **3-1** – **3-6** with the general formula [Bi(MeOPh)$_2$O(O)PRR']$_\infty$ and complexes **3-13** – **3-18** with the general formula [Bi(tol)$_2$O(O)PRR']$_\infty$. Attempts to synthesise complexes **3-7** – **3-9** ([Bi(*p*-MeOPh)$_2$O(O)PRR']$_\infty$) and **3-10** – **3-12** ([Bi(*o*-tol)$_2$O(O)PRR']$_\infty$) trialled solvent mediated, solvent free and salt metathesis reactions, however poor yields, compound rearrangement and impurities lead to the complexes no longer being pursued.

Complexes **3-1** – **3-6** and **3-13** – **3-18** were isolated as solids and characterised by ^{1}H NMR, IR, TGA, elemental analysis and ICP-OES for bismuth content. Complexes **3-4**, **3-13** and **3-17** were structurally authenticated by X-ray crystallography and confirmed the presence of bridging phosphinato moieties as indicated by the IR spectra, showing the formation of 1D coordination polymers. Complex **3-15** was also studied through single-crystal X-ray diffraction, where it became apparent that rearrangement occurs in DMSO with the twinned crystal showing both the diaryl bismuth *mono*-phosphinato complex **3-15** and the aryl bismuth *bis*-phosphinato analogue in the unit cell. Further studies into the DMSO stability showed the *mono*-phosphinato complexes are stable for 24 hours before rearrangement is observed.

The antibacterial activity of complexes **3-1** – **3-6** and **3-13** – **3-18** were determined towards Gram positive and Gram negative bacteria. The bismuth aryl groups greatly influenced the observed antibacterial activity, with the *bis*-*o*-methoxyphenyl compounds displaying high MIC values while the *bis*-*m*-methoxyphenyl produced the lowest MIC values. The complexes required high concentrations to stop the growth of Gram negative bacteria, with growth inhibition proving more difficult towards *P. aeruginosa* compared with *E. coli*. The viability of Cos-7 cells was also determined in the presence of complexes **3-1** – **3-6** and **3-13** – **3-18**, where the *bis*-tolyl bismuth complexes proved more cytotoxic than the *bis*-methoxyphenyl series. The potent antibacterial activity of complexes **3-4** – **3-6** can be an indicator for high mammalian cell toxicity, however the Cos-7 viabilities were relatively high, with an IC_{50} range of 9.54 to 15.2 µM.

It is apparent that the bismuth aryl group greatly influences antibacterial and cytotoxic activity of the *mono*-phosphinato complexes. While the majority of the tested complexes proved to be non-selectively toxic, insights were gained into the effect of position of functional group (OMe, Me). The *o*-methoxyphenyl series had poor biological activity while the *m*-methoxyphenyl series displayed good selectivity. The high selectivity of the *bis*-*m*-methoxyphenyl bismuth *mono*-phosphinato complexes towards Gram positive bacteria illustrates their potential as antibacterial agents.

Chapter 4

Bismuth-cellulose composites

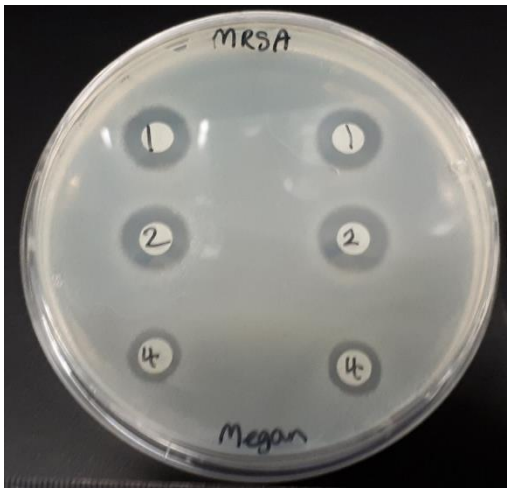

Bismuth *mono*-phosphinates

Bismuth *bis*-phosphinates

Leaching studies

Biology

4 Bismuth-cellulose composites

4.1 Antibacterial materials

Hospitals and healthcare facilities face many challenges due to ever present bacteria and their increasing antibiotic resistance. As such, it is important to prevent the spread of bacteria and thus infections, through use of antibacterial materials in problem areas such as high-contact surfaces, packaging, wound dressings and coated medical devices.[156,157] The materials may be inherently antibacterial, in the case of copper surfaces,[158] or have an active antimicrobial agent incorporated through physical or chemical means. An example of physical incorporation includes using curcumin to dye and impart antibacterial activity to wool and cotton. Both studies showed the dyed fibres showed antibacterial activity, however the activity was reduced following laundering and exposure to light.[159,160]

Examples of chemically bound antibacterial functionalities include carbohydrate-based surfaces which were produced by the Engel group, where lipophilic and polycationic moieties have been incorporated onto the carbohydrate units.[161] The active compounds have also been incorporated into glass, polystyrene and protein-based surfaces,[162,163] where they disrupt the bacterial cell membrane.[164] The advantage of chemically binding the active agent to the surface is that there is very little degradation in the antibacterial activity over time and unlike physical incorporation, the surface is still active after washing.[161]

Metal-polymer composites cover a broad range of polymers, from petroleum-based polymers such as polyethylene to biopolymers like cellulose, which contain metals or metal-based compounds physically or chemically incorporated. Studies have emerged looking at the use of metal nanoparticles as agents to kill or stop the growth of bacteria on surfaces.[165] These metal nanoparticles can exist within polymeric surface coatings and retain their antimicrobial activity, which is highly applicable in many problem environments such as hospitals.[166] The main problem associated with the use of metal nanoparticles, such as silver nanoparticles, is the toxicity they present,[167] so alternative compounds are required.

Silver is one of the most commonly used metals in antimicrobial biomedical applications. Silver nanoparticles can be applied in polymeric surface coatings or directly added onto surfaces to reduce bacterial adhesion and growth.[168] Silver has also been incorporated into wound dressings such as cotton gauze,[169] to aid in wound healing and to prevent infection. While this may assist

with healing, it has been shown that silver ions can exert toxic effects on human skin fibroblasts due to an increased production of reactive oxygen species which induces oxidative stress upon the skin cells.[170] This suggests that silver may hinder wound healing more than assist it, so other antimicrobial compounds should be examined.

4.1.1 Cellulose composites

Nanocellulose such as microfibrillated cellulose (MFC) is cellulose that has been broken down into microfibrils or bundles of microfibrils. MFC containing inorganic materials have been studied owing to the advantageous properties such as high hydrophilicity, high strength, large specific surface area and low thermal expansion coefficient.[171,172] A wide variety of potential applications for nanocellulose-inorganic material composites include catalysis, sensors, optical and electronic materials and antibacterial and biomedical materials.[173] MFC has been found to have antimicrobial properties when used in packaging,[174] and as wound dressings, where Liyaskina *et al.* saturated cellulose with an antibiotic and reported high antibacterial activity of the resulting biocomposite against *S. aureus.*[175] Silver has been incorporated into nanocellulose with direct silver sulfadiazine addition[176] and the *in situ* synthesis of silver nanoparticles investigated.[177] Both incorporation methods produced composites suitable for wound dressings that exhibit antibacterial activity.

The potential use of bismuth phosphinato-cellulose composites in active packaging materials have been studied with the phenyl bismuth *bis*-diphenylphosphinato complex $[BiPh(O(O)PPh_2)_2]_\infty$ **2-6**.[178] The composite material was produced through mechanical incorporation of complex **2-6** within the cellulosic matrix and the suspension sprayed onto stainless steel plates. The produced sheets proved effective at inhibiting bacterial and fungal growth and possessed acceptable water vapour permeability for use in packaging.

This chapter aims to expand on the previous bismuth phosphinato-cellulose composite through incorporation of complexes $[BiPh_2O(O)P(H)Ph]_\infty$ **2-1**, $[BiPh_2O(O)PPh_2]_\infty$ **2-2**, $[BiPh_2O(O)PMe_2]_\infty$ **2-3**, $[BiPh_2O(O)P(p\text{-}MeOPh)_2]_\infty$ **2-4**, $[BiPh(O(O)P(H)Ph)_2]_\infty$ **2-5**, $[BiPh(O(O)PPh_2)_2]_\infty$ **2-6**, $[BiPh(O(O)PMe_2)_2]_\infty$ **2-7** and $[BiPh(O(O)P(p\text{-}MeOPh)_2)_2]_\infty$ **2-8** with MFC, to better understand the interaction of the different complexes within the cellulosic matrix. The antibacterial activity of the produced Bi-composites will be determined, and evaluation into their safety as antibacterial additives examined, with potential applications as antibacterial surface coatings or packaging.

4.2 Composite synthesis

MFC composites are typically formed through combining an MFC suspension with the additive suspended in water. The solid bismuth phosphinate complexes (**2-1** – **2-8**) are highly hydrophobic and will aggregate on the surface of the water. To combat this, the complexes were dispersed in a 20 % *iso*-propanol solution and stirred until added to the MFC suspension. Inorganic additives in cellulose composites have greater retention when combined with cationic polyacrylamide (CPAM),[179,180] so a 1 % CPAM solution (in water) was also added to give a loading of 1 mg per gram of dry cellulose. The MFC-Bi-CPAM suspension was poured through a British handsheet maker onto filter paper, then the suspension was agitated and drained to form a thin cellulose sheet. Once filtered, the Bi-cellulose sheet is separated from the filter paper and dried at 105 °C. Figure 4-1 depicts the produced Bi-cellulose composite, which has a consistent diameter of 15.9 cm and a final cellulose mass of approximately 1.2 g. The mass of complex used is based on weight percentage (wt%) loading using the final mass as 1.2 g. The same method was carried out using silver sulfadiazine (**Ag**) to produce silver-cellulose sheets for comparative studies.

Figure 4-1 Bi-cellulose composite sheets.

4.3 Characterisation

Characterisation of the Bi-cellulose composites used two approaches; analysing the total bismuth content and examining the surface of the composite. Total bismuth phosphinato complex content was determined through use of inductively coupled plasma optical emission spectroscopy (ICP-OES), based on the average bismuth content from at least three sections of the Bi-composite sheet. Scanning electron microscopy (SEM) was used to examine the dispersion and morphology of the complexes on the surface of the composite sheet.

Analysis of the total bismuth or silver content in the composite sheets was carried out using ICP-OES. Ten hole punched discs were taken from three separate sections of the cellulose sheets and the organic material was removed by ashing samples at 600 °C. The remaining residue was dissolved in concentrated nitric acid, then diluted for analysis by ICP-OES. The determined metal loading, shown in Table 4-1, is consistently lower than the targeted loading. This is due to losses in the sheet making process, where it was observed that traces of the complex and cellulose remained in the British handsheet maker. It is also expected that complexes with higher water solubility such as **2-1**, **2-3**, **2-5** and **2-7** would produce composite sheets with lower actual loadings due to complex solubilisation. It is interesting to note that of the more hydrophobic complexes (**2-2**, **2-4**, **2-6** and **2-8**), the composites containing the phenyl bismuth *bis*-phosphinato complexes showed the greatest retention within the cellulose sheet.

Table 4-1 Targeted and determined bismuth complex loadings for bismuth-cellulose sheets and silver sulfadiazine loadings for silver-cellulose sheets. Actual loadings were determined in triplicate by ICP-OES and final values are averages with the standard deviation. The percentage of compound retained in the sheet based on the targeted loading is also detailed for each composite.

Compound		Targeted loading (wt%)	Actual loading (wt%)	% Retained
$[BiPh_2O(O)P(H)Ph]_\infty$	**2-1**	0.75	0.30 ± 0.01	40
		4.90	3.17 ± 0.10	65
$[BiPh_2O(O)PPh_2]_\infty$	**2-2**	0.51	0.31 ± 0.01	61
		4.88	2.51 ± 0.31	51
$[BiPh_2O(O)PMe_2]_\infty$	**2-3**	0.30	0.16 ± 0.04	53
		5.21	2.45 ± 0.06	47
$[BiPh_2O(O)P(p\text{-}MeOPh)_2]_\infty$	**2-4**	0.49	0.20 ± 0.01	41
		4.94	1.43 ± 0.06	30
$[BiPh(O(O)P(H)Ph)_2]_\infty$	**2-5**	0.50	0.21 ± 0.01	42
		5.67	2.92 ± 0.06	51
$[BiPh(O(O)PPh_2)_2]_\infty$	**2-6**	0.49	0.34 ± 0.00	69
		6.24	5.32 ± 0.22	85
$[BiPh(O(O)PMe_2)_2]_\infty$	**2-7**	0.50	0.18 ± 0.01	36
		5.09	1.12 ± 0.07	22
$[BiPh(O(O)P(p\text{-}MeOPh)_2)_2]_\infty$	**2-8**	0.49	0.37 ± 0.06	76
		6.42	5.27 ± 0.52	82
Silver sulfadiazine	**Ag**	0.55	0.43 ± 0.04	78
		5.12	3.35 ± 0.88	65

The morphology and dispersion of the bismuth phosphinato complexes **2-1** – **2-4** and **2-6** on the surface of the cellulose sheets was observed by SEM. It can be observed that complex **2-6** has long, thin needles entangled in the cellulose fibres, whereas the *mono*-phosphinato complexes **2-1** – **2-4** are more atypical in shape, as seen in Figure 4-2. There is a large distribution of particulate sizes within the composite sheets, ranging from 2 to 20 µm for complexes **2-1** – **2-4** and 1 – 30 µm for **2-6**. Backscattered election images clearly indicate the presence of the bismuth phosphinato complexes, due to the strong (bright) signal from the high atomic number of bismuth compared with carbon and oxygen in cellulose. The complex particulates are closely arranged as shown in Figure 4-3, suggesting the dispersion of the complexes on the cellulose surface is not uniform. This is likely due to the hydrophobicity of the complexes, leading to aggregation. While a better dispersion agent could assist with a more uniform distribution of the complexes in the cellulose sheet, it is apparent that the composite contains the bismuth phosphinato complex.

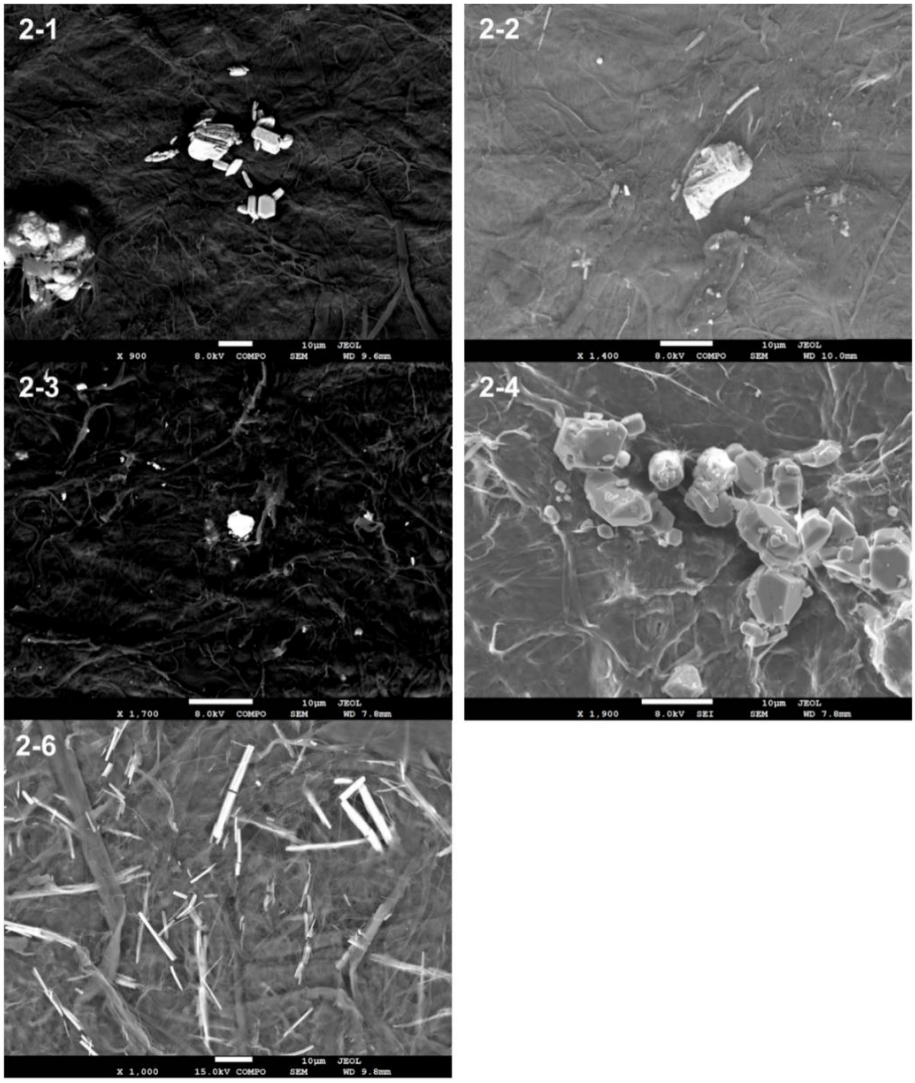

Figure 4-2 Backscattered electron images of Bi-cellulose composites containing higher-loadings of complexes **2-1** – **2-4** and **2-6**. Scale bars are 10 µm.

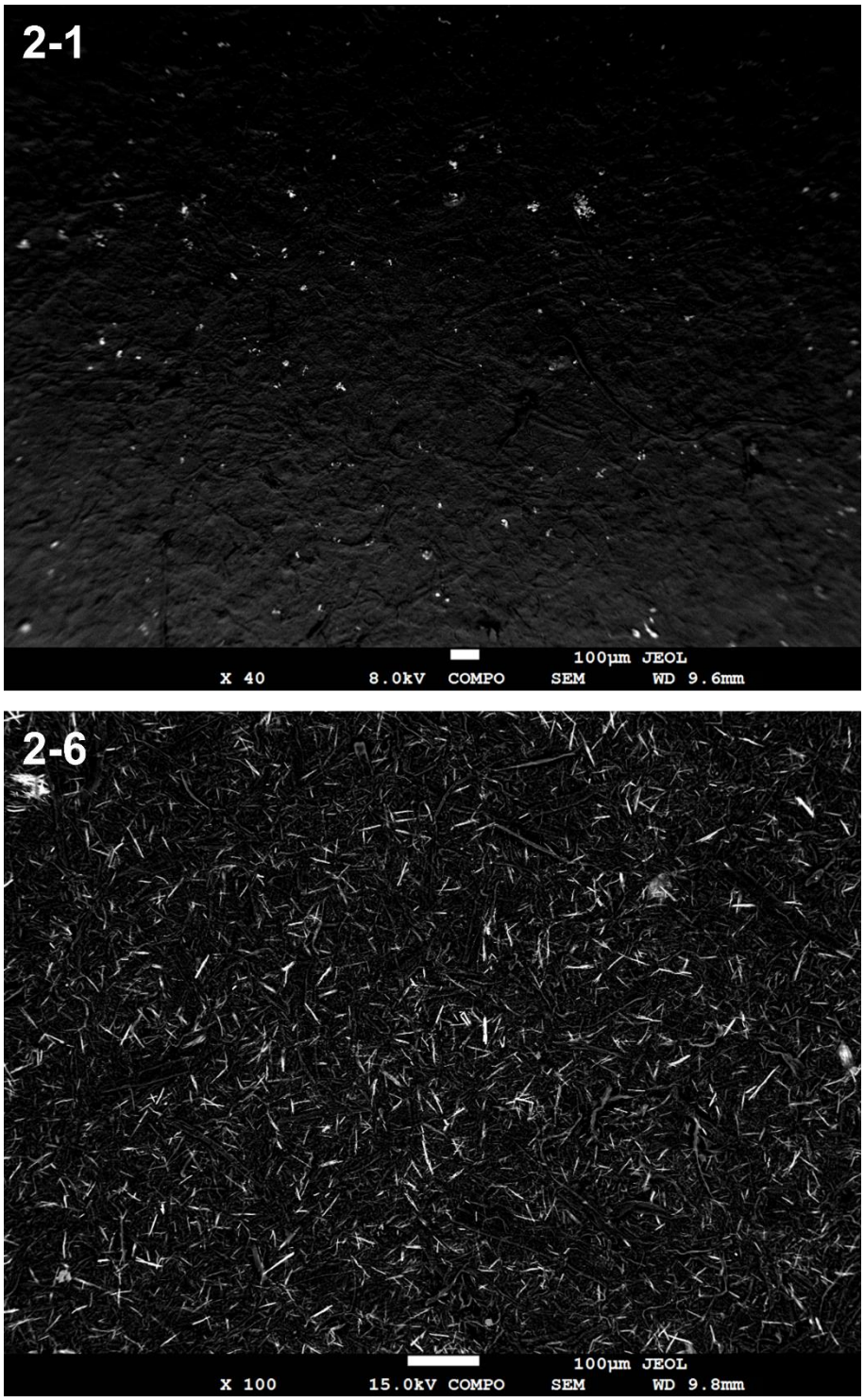

Figure 4-3 Backscattered electron images of Bi-cellulose composites containing 3.17 wt% **2-1** and 5.32 wt% **2-6**. Scale bars are 100 µm.

4.4 Leaching properties

It is a well-known phenomenon that antibacterial additives will leach from their host material to give rise to the antibacterial activity, therefore the leaching properties of the bismuth and silver cellulose composites were examined. The higher-loading composites were assessed by placing uniform rectangles (1 cm x 2 cm) into water at 25 °C for 24 hours. The composites were removed and the water which is referred to as the leachate, was analysed by ICP-MS for Bi and Ag content (M_L). The composites were ashed at 600 °C, then diluted with nitric acid for ICP-OES analysis to determine the remaining metal content (M_F). The initial metal content of the individual cellulose composite (M_I) samples can be determined from the final paper and leachate metal concentrations, allowing for the % metal leached to be calculated, as seen in Equation 4-1 and Table 4-2.

$$M_I = M_L + M_F$$

$$\%M_L = \frac{M_L}{M_I} \times 100$$

M_I is the initial metal mass in the composite
M_L is the metal content leached into the water
M_F is the final metal mass in the composite after leaching

Equation 4-1 Equation showing how the initial metal content in the composite (M_I) is determined and how the percentage metal leached into the water ($\%M_L$) is calculated.

Table 4-2 Leaching studies of composites containing complexes **2-1** – **2-8** and **Ag** showing the percentage of metal that leaches from the metal-cellulose composites in water as determined by ICP-MS. Initial metal in the composite (M_I) is determined by addition of final metal in paper (M_F) and metal leached into water (M_L). Values are the mean ± SD from three experiments.

Compound		M_I (µg)	M_L (µg)	% M_L
$[BiPh_2O(O)P(H)Ph]_\infty$	**2-1**	195 ± 5	29 ± 6	15 ± 3
$[BiPh_2O(O)PPh_2]_\infty$	**2-2**	135 ± 5	5 ± 0.7	4 ± 0.3
$[BiPh_2O(O)PMe_2]_\infty$	**2-3**	135 ± 9	9 ± 0.4	6 ± 0.7
$[BiPh_2O(O)P(p\text{-}MeOPh)_2]_\infty$	**2-4**	54 ± 2	1 ± 0.3	2 ± 0.6
$[BiPh(O(O)P(H)Ph)_2]_\infty$	**2-5**	143 ± 4	32 ± 5	24 ± 1
$[BiPh(O(O)PPh_2)_2]_\infty$	**2-6**	244 ± 10	7 ± 2	3 ± 0.3
$[BiPh(O(O)PMe_2)_2]_\infty$	**2-7**	21 ± 20	0.9 ± 0.2	8 ± 8
$[BiPh(O(O)P(p\text{-}MeOPh)_2)_2]_\infty$	**2-8**	210 ± 2	5 ± 1	3 ± 0.5
Silver sulfadiazine	**Ag**	210 ± 36	9 ± 0.6	4 ± 0.6

It is evident that the phosphinato moiety influences the level of leaching of the complex from the Bi-cellulose composite, with both of the phenylphosphinato-containing complexes **2-1** and **2-5** showing the highest levels of leaching at 15 and 24 % respectively. The poorly water soluble diphenylphosphinato and *bis*-(*p*-methoxyphenyl)phosphinato complexes (**2-2**, **2-4**, **2-6** and **2-8**) display much lower leaching levels between 2 and 4 %. Interestingly, the dimethylphosphinato complexes **2-3** and **2-7** have the greatest water solubility (as determined in Chapter 2, section 2.4), however the leaching levels are less than the phenylphosphinato bismuth composites. This low-level leaching for the more water soluble complexes may be due to complexes **2-3** and **2-7** interacting with the cellulose. It is likely that the less bulky methyl groups on the phosphinato moiety allow for greater hydrogen bonding interactions with cellulose when compared with the bulky phenyl groups of the other bismuth phosphinato complexes.

Silver sulfadiazine has water solubility of 72.7 ppm, which is between complexes **2-1** and **2-5** at 42.7 and 147 ppm respectively. The leaching levels observed were closer to complex **2-2**, which has a water solubility of 1.58 ppm. This suggests that water solubility is not the only factor to influence compound leaching from the composites. It is likely the low leaching levels are due to silver sulfadiazine interacting with the cellulosic matrix as a result of several possible hydrogen bonding sites, as highlighted in Figure 4-4.

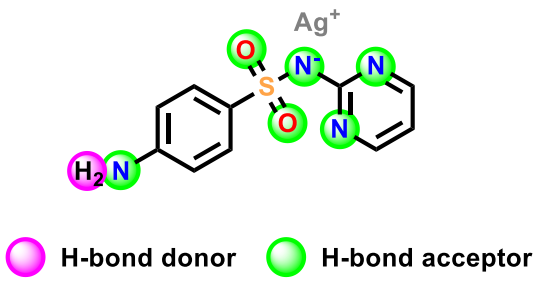

Figure 4-4 Silver sulfadiazine **Ag** highlighting hydrogen bond acceptor and donor sites.

4.5 Biology

Previous studies on antimicrobial materials such as silver-coated catheters and cotton gauzes have evaluated cytotoxicity through incubation of the material leachates, in media and phosphate buffered saline (PBS) respectively, with cells.[169,181] This suggests that the use of leachates is a viable method for determining cell viability. One study also examined the effects of solvent on the leaching of silver from silver-coated cotton gauze, where water, PBS and media were examined and found to have minimal differences on the silver release.[169] This prompted the use of leachates obtained from water to be used for both mammalian cell and bacterial assays for consistency.

The composites were assessed for their antibacterial activity in the solid-state through disc diffusion assay towards both Gram positive (*S. aureus*, methicillin-resistant *S. aureus* (MRSA) and vancomycin-resistant *Enterococcus* (VRE)) and Gram negative (*E. coli*) bacterial strains. Further bacterial assays were also conducted using the leachate solutions with a known bismuth or silver concentration. The solution-based assays using the leachates were conducted with the Gram positive MRSA and VRE, and Gram negative *E. coli* and *P. aeruginosa*. Mammalian cell assays were conducted using the leachate solutions towards Cos-7 and human fibroblast cell lines to examine the effect on cell viability. As the *bis*-phosphinato complexes $[BiPh(O(O)P(H)Ph)_2]_\infty$ **2-5**, $[BiPh(O(O)PPh_2)_2]_\infty$ **2-6**, $[BiPh(O(O)PMe_2)_2]_\infty$ **2-7** and $[BiPh(O(O)P(p\text{-}MeOPh)_2)_2]_\infty$ **2-8** display poor DMSO solubility, their mammalian cell cytotoxicity was not determined in Chapter 2, however the potential to examine the effects of their composite leachate on mammalian cells can provide valuable insights into structure-activity relationships.

4.5.1 Antibacterial activity

Disc diffusion assays were conducted on the low-loading Bi-cellulose composites using 5 mm discs of the composite placed onto a pre-spread lawn of bacteria and incubated overnight at 37 °C. The zones of inhibition are due to the diffusion of the complexes into the agar and the observed size of the zones are detailed in Figure 4-5. Interestingly, the higher leaching composites containing **2-1** and **2-5** do not have the largest zones. This may be due to the lower antibacterial activity seen for complex **2-1** when compared with **2-2** in the solution-state, as well as the lower loading of 0.21 wt% **2-5** compared with the other *bis*-phosphinato complexes at 0.34 wt% **2-6** and 0.37 wt% **2-8**. Both of the dimethylphosphinato complexes (**2-3** and **2-7**) do not show any zones of inhibition, suggesting 0.16 to 0.18 wt% complex loading is too low to exert antibacterial activity.

The **Ag**-containing composite had the highest metal loading, but showed smaller zones for all Gram positive bacteria in comparison with the Bi-composites. It can be noted that only the **Ag** composite produced zones for the Gram negative *E. coli*. This may be due to poor diffusion of the bismuth complexes into the LB agar as suggested in Chapter 2, or that the bismuth concentration is not sufficient to stop bacterial growth.

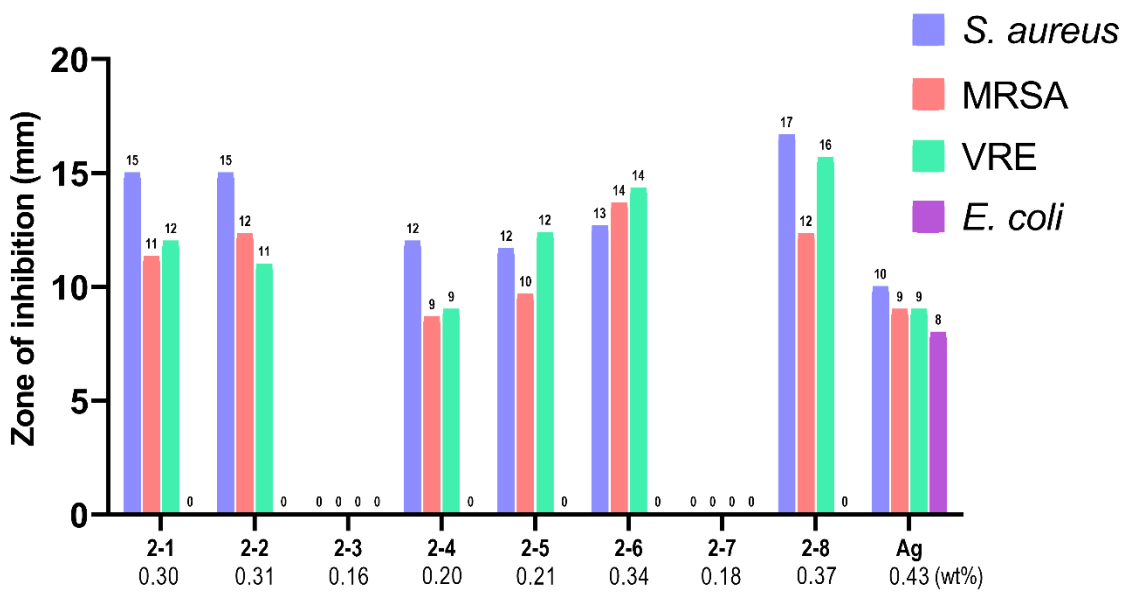

Figure 4-5 Zones of inhibition measured after incubation at 37 °C of *S. aureus*, MRSA, VRE and *E. coli* with low-loading Bi- and Ag-cellulose composites (percentage weight loadings shown). Zones of inhibition are measured as the diameter including the disc diameter of 5 mm. Readings of 0 mm indicate no clearing around the 5 mm composite disc.

The phenyl bismuth *mono*-phosphinato (**2-1** – **2-4**) series and *bis*-phosphinato (**2-5** – **2-8**) complexes were assessed for antibacterial activity through leachate assays to understand any differences between the series and differences in activity with different phosphinato moieties. Solution-based bacterial assays were conducted by adding the bismuth- or silver-containing water leachates to bacterial broth at a 1:3 ratio and incubating overnight at 37 °C. The concentration of complexes **2-1** – **2-8** and **Ag** in the water leachate was determined by ICP-MS and adjusted for the broth dilution. Following incubation, the bacterial broth is diluted in sterile PBS and spread onto agar plates to count the colony forming units in triplicate. The individual experiments were conducted in triplicate using fresh leachate samples, which meant that concentrations differed between experiments. The highest leachate concentrations tested towards MRSA, VRE, *E. coli* and *P. aeruginosa* are shown in Figure 4-6.

Given the high level of leaching from the composites containing phenylphosphinato bismuth complexes **2-1** and **2-5**, it is not surprising that they displayed potent antibacterial activity towards MRSA, VRE and *E. coli* at 4.3 and 4.5 µM respectively. Both leachates were bacteriostatic towards the Gram positive bacteria, and bactericidal towards *E. coli*. Neither complex halted the growth of *P. aeruginosa*, which is not unexpected, as many reports have demonstrated that bismuth complexes are less active towards Gram negative bacteria.[91,153]

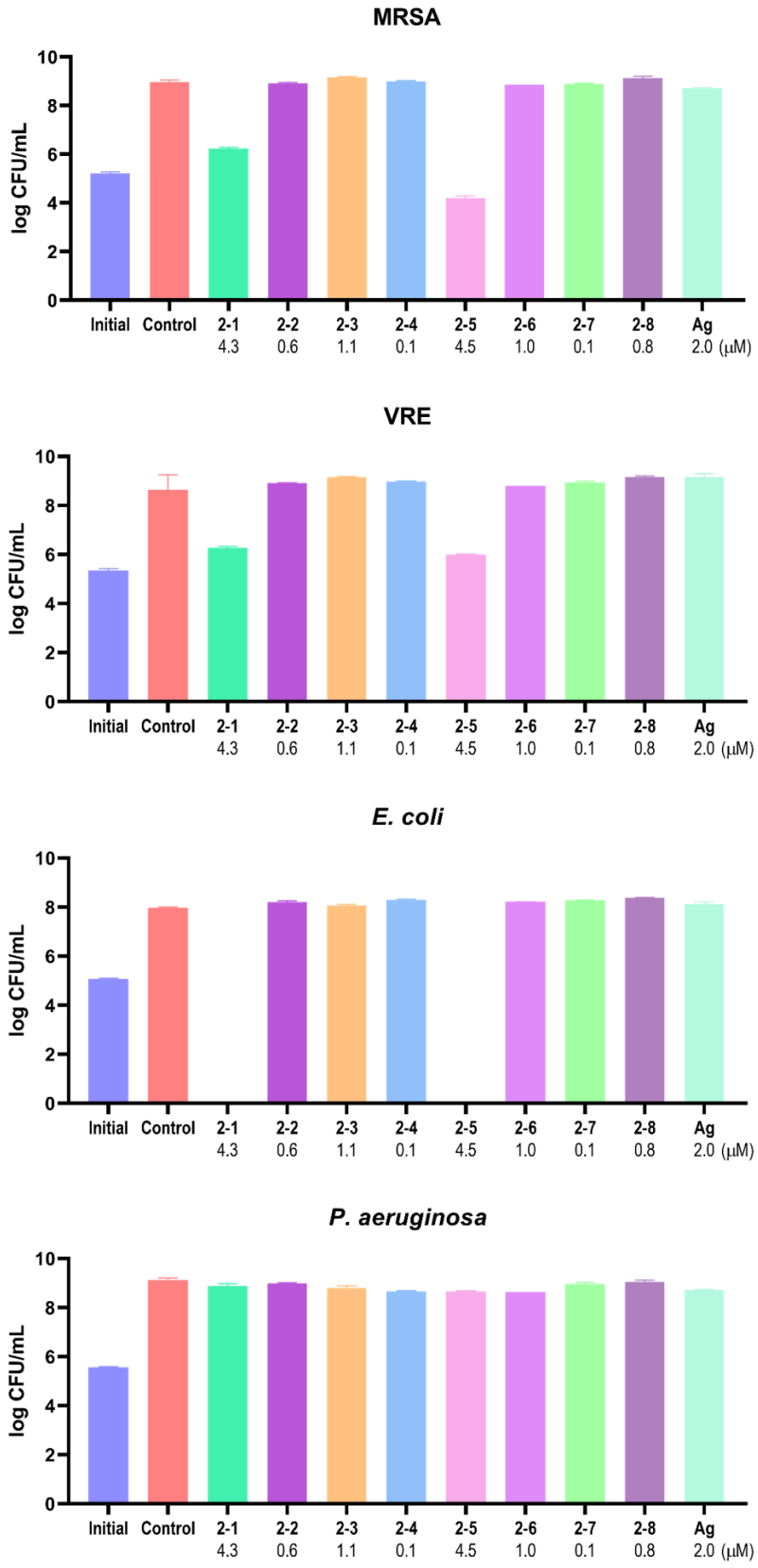

Figure 4-6 Logarithmic colony forming units per mL (CFU/mL) following 20 hour incubation of composite leachates (concentrations shown) and a control of water with MRSA, VRE, *E. coli* or *P. aeruginosa* in broth.

Composite leachates containing complexes **2-2** – **2-4** and **2-6** – **2-8** had concentrations in the range of 0.1 to 1.1 µM and were all insufficient to stop bacterial growth, with similar CFU values to the water control. It is interesting to note that complex **2-2** has a determined MIC value of 0.63 µM towards VRE (DMSO as vehicle solvent), however the leachate at 0.6 µM (in water) was unable to stop the growth of VRE. This difference may be due to lower complex dissolution in water compared with DMSO, which may impact the size of the polymeric compound and thus the bioavailability. Previous reports of bismuth complexes of α-amino acids also found that lower antibacterial activity was observed when solubilised in water compared with DMSO, which was likely due to increased hydrolysis in water.[78] The silver sulfadiazine **Ag**-containing leachate was also ineffective at halting bacterial growth at a concentration of 2 µM.

The phenylphosphinato bismuth composite leachates **2-1** and **2-5** were bactericidal towards *E. coli* at the highest tested concentration, however at the lowest concentration of 2.8 and 3.2 µM respectively, both were bacteriostatic. The highest concentration was bacteriostatic towards MRSA but the lowest concentrations did not stop growth, so further leachate samples were assessed for a better concentration distribution. Figure 4-7 depicts the CFU of both leachates **2-1** and **2-5** towards MRSA and *E. coli*.

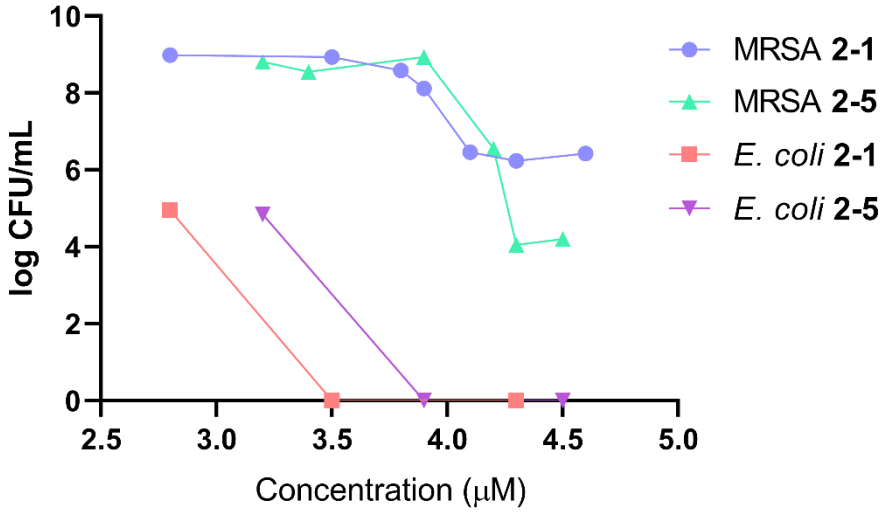

Figure 4-7 Logarithmic colony forming units per mL (CFU/mL) following 20 hour incubation at 37 °C of composite leachates containing $[BiPh_2O(O)P(H)Ph]_\infty$ **2-1** and $[BiPh(O(O)P(H)Ph)_2]_\infty$ **2-5** with MRSA or *E. coli* broth. Initial bacterial concentration at 10^6 CFU/mL.

At first it appears that leachate **2-1** is more active towards MRSA than **2-5**, with a faster reduction in growth observed from 3.9 µM. However, once the concentration is above 4.3 µM, leachate **2-5** shows a further decrease in bacterial growth, suggesting bactericidal behaviour. It is expected that concentrations of leachate **2-5** higher than 4.5 µM would result in a further decrease in growth

until, like *E. coli*, no growth is observed. It is difficult to deduce any structure-activity relationships between the *mono*- and *bis*-phosphinato bismuth complexes, although the phenyl bismuth *bis*-phenylphosphinato complex **2-5** has shown bactericidal activity towards both *E. coli* and MRSA. It is apparent that both **2-1** and **2-5** are potent antibacterial agents and show promising activity within the cellulosic matrix.

4.5.2 Mammalian cell viability

It has been shown that complexes **2-1** – **2-4** reduce the viability of Cos-7 and human fibroblast cells, so it is important to determine if the amount of compound leaching from the Bi-cellulose composites will also have an effect. Mammalian cell viability was determined by the CellTiter-Blue viability assay, where cells grown without additives were treated as 100 % viable. The leachates were added to the adherent cells in a ratio of 1:3 leachate to media and incubated for 20 hours prior to CellTiter-Blue addition. The cells were incubated for a further 4 hours and the results measured by fluorescence. Three independent experiments were conducted using freshly prepared leachates, and the highest concentration results are shown in Figure 4-8. The water leachate concentrations of **2-1** – **2-8** and **Ag** were determined by ICP-MS and the assay concentrations adjusted for the media dilution. The water control used deionised water added to the media in the same manner as the leachate samples, to determine if this may have an effect on cell viability. It is apparent that addition of water at 25 % of the total volume does not drastically reduce the viability of either Cos-7 or human fibroblast cells, with obtained viabilities of 95 and 103 % respectively.

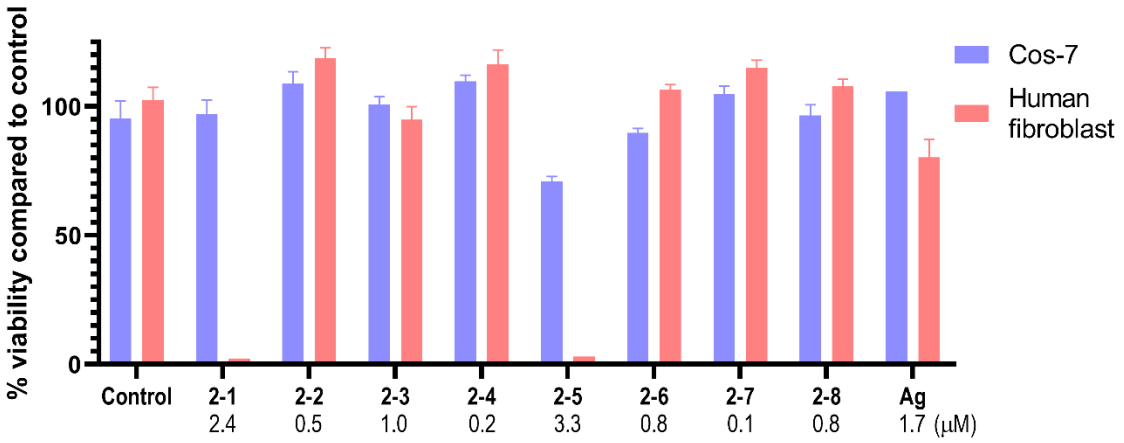

Figure 4-8 Viability of Cos-7 and human fibroblast cells following 24 hour incubation at 37 °C with leachates **2-1** – **2-8** and **Ag** (concentrations shown) added to media. A control of cells without compound addition was treated as 100 % viable and a water control was included.

It is immediately obvious that the leachates containing the phenylphosphinato bismuth complexes **2-1** and **2-5** greatly reduced the viability of human fibroblast cells at 2.4 and 3.3 µM respectively. It can also be noted that leachate containing 3.3 µM **2-5** reduced the Cos-7 viability to 70 %. This suggests that the *bis*-phenylphosphinato complex **2-5** may have a similar toxicity profile to the *mono*-phenylphosphinato complex **2-1**, which has a determined IC_{50} value of 4.69 µM towards Cos-7. The concentrations assessed towards mammalian cells are lower than those used in bacterial assays, which suggests that the higher concentrations required to exert a bacteriostatic or bactericidal effect will have a greater cytotoxic effect on mammalian cells.

The viability of Cos-7 exposed to leachates with compound concentrations of 1 µM or less were non-toxic, where the viability was approximately 100 %. It can be noted that human fibroblast cells exposed to leachates containing **2-2**, **2-4** and **2-6** – **2-8** all had viabilities greater than 100 %, which suggests that the cells continued to grow upon exposure to the leachates. While this is promising for potential uses such as wound dressings, these low concentrations are not sufficient to stop bacterial growth. This suggests that potential uses such as antibacterial surfaces, allowing direct contact with the composite surface, would be viable.

It is interesting that the silver sulfadiazine **Ag**-containing leachate reduced the viability of human fibroblast cells to 80 % at a low concentration of 1.7 µM. It has been previously reported that silver sulfadiazine displays toxicity towards human fibroblast cells at higher concentrations.[182] This is important to note as it is used in commercial topical treatments to prevent infections of wounds and burns,[183] however the results suggest that human fibroblast cells are affected at concentrations lower than what is needed to stop bacterial growth.

4.6 Conclusions

A series of novel phenyl bismuth phosphinato containing cellulose composites were produced through compound dispersion in MFC fibres prior to the sheet making process. The produced Bi-cellulose sheets were characterised by SEM to examine the morphology and dispersion of the compounds, and by ICP-OES for bismuth content analysis. Two different bismuth phosphinato loadings were produced; low loading composites in the range of 0.16 to 0.37 wt% and high loading composites between 1.12 to 5.32 wt% loading of complexes $[BiPh_2O(O)P(H)Ph]_\infty$ **2-1**, $[BiPh_2O(O)PPh_2]_\infty$ **2-2**, $[BiPh_2O(O)PMe_2]_\infty$ **2-3**, $[BiPh_2O(O)P(p\text{-}MeOPh)_2]_\infty$ **2-4**, $[BiPh(O(O)P(H)Ph)_2]_\infty$ **2-5**, $[BiPh(O(O)PPh_2)_2]_\infty$ **2-6**, $[BiPh(O(O)PMe_2)_2]_\infty$ **2-7** and $[BiPh(O(O)P(p\text{-}MeOPh)_2)_2]_\infty$ **2-8**. Silver sulfadiazine **Ag** composites were produced at loadings of 0.43 and 3.35 wt% **Ag** for comparative purposes.

The leaching properties of the high loading composites were assessed and it was determined that the water solubility does not have a great influence on the amount of complex leached. Composites containing phenylphosphinato complexes **2-1** and **2-5** had the highest levels of leaching at 15 and 24 % respectively, while the most water soluble complexes containing the dimethylphosphinato group **2-3** and **2-7** displayed lower leaching levels at 6 and 8 %.

Disc diffusion assays were conducted on the low-loading papers to examine their effect on *S. aureus*, MRSA, VRE and *E. coli*. Zones of inhibition were present at complex loadings between 0.20 to 0.37 wt%, however both dimethylphosphinato loaded composites did not show any activity at lower loadings of 0.16 to 0.18 wt%. The bismuth phosphinato composites **2-1** – **2-8** did not show any zones for *E. coli*, however the 0.43 wt% **Ag** composite did, suggesting a higher bismuth loading may be needed to combat Gram negative bacteria.

The aqueous leachates were assessed for their antibacterial activity towards MRSA, VRE, *E. coli* and *P. aeruginosa*, and only the most concentrated leachates showed any activity. Leachates **2-1** and **2-5** were bacteriostatic towards MRSA and VRE at 4.3 and 4.5 µM respectively, and surprisingly bactericidal to *E. coli* despite the poor activity from the disc diffusion assay. The potent activity of the leachates from composites containing **2-1** and **2-5** towards *E. coli* is further proof that disc diffusion assays are dependent on the ability of the active compound to diffuse through the agar and should be used in conjunction with solution-based assays.

Mammalian cell viability studies were conducted with the aqueous leachates to determine their toxicity towards Cos-7 and human fibroblast cells, with the results. Similar to the bacterial results, only the phenylphosphinato leachates **2-1** and **2-5** had a concentration great enough to exert an effect on human fibroblast cells, significantly reducing the viability to 2 %. Leachate **2-5** also reduced Cos-7 to a 70 % cell viability at a concentration of 3.3 µM. Interestingly, the silver sulfadiazine leachate **Ag** also exerted an effect on human fibroblast cells at 1.7 µM, with a cell viability of 80 %.

It is apparent that the different phosphinato moiety has an effect on how the complex interacts within the cellulosic matrix and in turn, how they interact with bacterial and mammalian cells. While the apparent non-selective toxicity of the phenyl bismuth *mono*- and *bis*-phenylphosphinato composites is a concern, their high leaching rates are evidence for their potential use in antibacterial surfaces.

Chapter 5

Gallium phosphinates

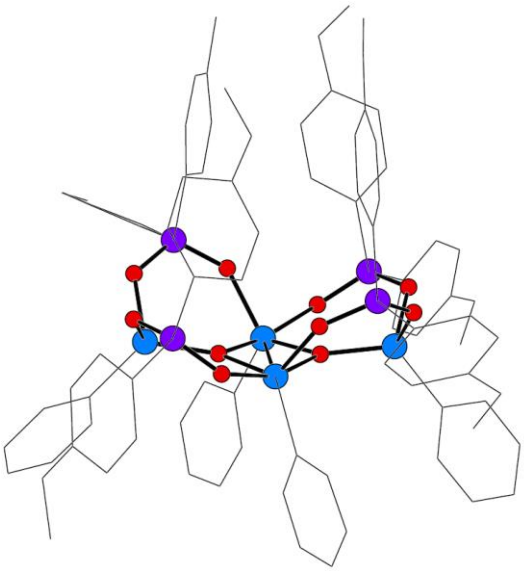

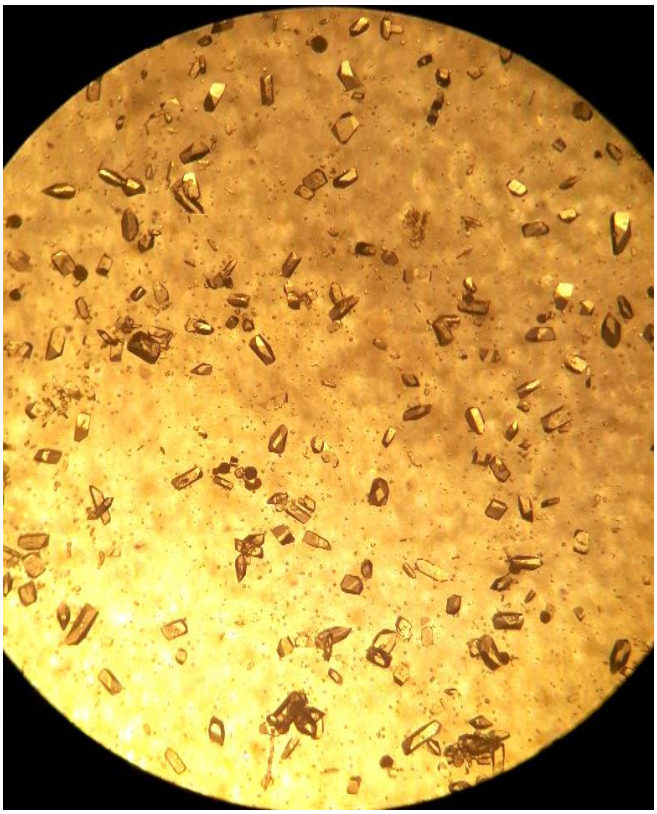

Diphenyl gallium *mono*-phosphinates

Gallium *tris*-phosphinates

Biology

5 Gallium phosphinate complexes

5.1 Gallium phosphinate chemistry

The structural chemistry of gallium(III) phosphinato compounds was first reported by Coates and Mukherjee in 1964 with reactions of $GaMe_3$ with dimethylphosphinic acid and diphenylphosphinic acid.[184] This study highlighted that the phosphinato groups form three-atom bridges in the dimethyl gallium complexes, suggesting an eight-membered ring structure, as shown in Figure 5-1. Additional studies reacting $GaMe_3$ or $GaEt_3$ with dimethylphosphinic acid or difluorophosphinic acid also supported an eight-membered ring structure of the complexes.[185–187] This proposed structure was confirmed by X-ray crystallography in 1990,[188] and further dialkyl gallium *mono*-phosphinato complexes have all shown similar dimeric structures, including diethyl gallium and *bis-tert*-butyl gallium diphenylphosphinates.[189,190] Cryoscopic measurements in benzene also suggest that the dimeric structure is retained in the solution-state.[184]

Figure 5-1 General dimeric eight-membered ring structure of dialkyl gallium *mono*-phosphinato complexes and proposed *tris*-phosphinato gallium binding.[191]

Tris-phosphinato gallium complexes have been synthesised through reaction of $GaCl_3$ with methyl methylphenylphosphinate,[191] or with dimethylphosphinic acid and triethylamine,[192] as summarised in Scheme 5-1.

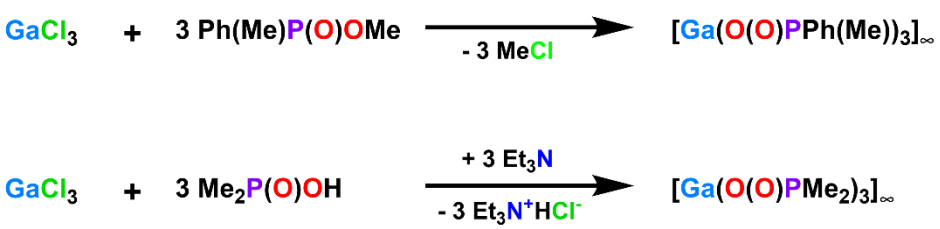

Scheme 5-1 Synthetic routes to form gallium *tris*-phosphinato complexes from reaction with $GaCl_3$ with methyl methylphenylphosphinate and dimethylphosphinic acid with triethylamine.[191,192]

Both studies suggest the gallium *tris*-phosphinato complexes form polymers with bridging phosphinato groups, with the proposed binding mode shown in Figure 5-1. It is interesting that attempts to isolate a *tris*-phosphinato complex through reaction with $GaMe_3$ were unsuccessful, where only the dimethyl gallium *mono*-phosphinato complex could be recovered.[188] It can be noted that while the gallium *tris*-dimethylphosphinato complex is poorly water soluble, suspension in water will result in the hydrated complex $[Ga(O(O)PMe_2)_3].H_2O$, suggesting the complex is stable to hydrolysis.[192]

It is apparent that the reaction of trialkyl gallium with phosphinic acids form discrete dimers of dialkyl gallium *mono*-phosphinato complexes, however this has not been expanded to examine reactions with triaryl gallium. The solution-state stability of the dialkyl gallium *mono*-phosphinato complexes has not been studied beyond the presence of the dimeric structure in benzene. There have been no reports of *bis*-phosphinato gallium compounds to date and there is limited solubility and stability data for *tris*-phosphinato gallium complexes.

It is important to investigate the solution-state stability of gallium phosphinato complexes to better understand their potential applications and in particular, their use as antibacterial agents. As detailed in the introduction, organogallium compounds have been assessed for their anticancer properties, however research is lacking into their use as antibacterial agents with a predominant focus on gallium(III) salts. This chapter aims to expand on the library of reported *mono*- and *tris*-phosphinato gallium complexes, characterise the novel *bis*-phosphinato gallium complexes and evaluate the potential of gallium phosphinato complexes and a phenyl gallium oxido cluster as antibacterial agents.

5.2 Synthesis

The triaryl gallium source chosen was $GaPh_3$, which is synthesised through transmetalation of $HgPh_2$ and gallium metal, as shown in Scheme 5-2.

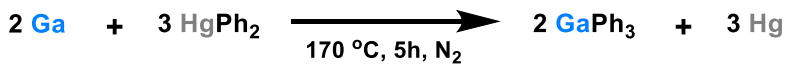

Scheme 5-2 Synthetic route to form $GaPh_3$ through transmetalation of $HgPh_2$ and gallium metal.

While most trialkyl gallium compounds can be synthesised through simple metathesis of $GaCl_3$ with Grignard reagents, it has been found that the reaction of $GaCl_3$ with PhMgBr forms the metallate species $[Mg_3Br_3Cl_2(O(Et)_2)_6][GaPh_2Br_2]$ or $[MgBr(THF)_5][GaPh_3Br]$, depending on the solvent used.[193] This leads to the use of $HgPh_2$ as the phenyl source, which was first detailed in 1940, with a reaction time of 50 hours,[194] and was subsequently modified to reduce the time to 5

hours with increased reaction temperatures.[195] The produced $GaPh_3$ is moisture sensitive, decomposing to $GaPh_2OH$ if not handled under inert conditions. Due to the potential toxicity hazards of mercury, ICP-MS was conducted on the isolated $GaPh_3$ prior to complex synthesis, to determine if any mercury was present, with the results showing negligible (<0.02 %) amounts.

The phosphinic acids chosen to react with $GaPh_3$ were the same as chosen to react with $BiPh_3$ in Chapter 2. Both diphenylphosphinic acid and dimethylphosphinic acid have been studied for their reactivity with trialkyl gallium sources, so this will provide a good comparison with $GaPh_3$. Phenylphosphinic acid and *bis*-(*p*-methoxyphenyl)phosphinic acid will also allow for reactivity comparison with the synthesised bismuth phosphinato complexes. The targeted series of gallium phosphinato complexes consists of eight heteroleptic complexes of the type $[GaPh_2O(O)PRR']_2$ or $[GaPh(O(O)PRR')_2]$ and four homoleptic complexes of the type $[Ga(O(O)PRR')_3]_\infty$.

5.2.1 Diphenyl gallium *mono*-phosphinates

The ease of synthesis of dialkyl gallium *mono*-phosphinato complexes prompted the similar reaction to be investigated with $GaPh_3$. The synthetic route employed the equimolar reaction of $GaPh_3$ and phosphinic acid in THF or toluene, as shown in Scheme 5-3. It must be noted that while $GaPh_3$ was soluble in the selected solvent, the phosphinic acids were not soluble so the $GaPh_3$ solution was added to the phosphinic acid suspension. Upon $GaPh_3$ addition, immediate dissolution of the phosphinic acid was observed producing a colourless solution. The solvent was removed *in vacuo* to produce the desired diphenyl gallium *mono*-phosphinato complexes $[GaPh_2O(O)P(H)Ph]_2$ **5-1**, $[GaPh_2O(O)PPh_2]_2$ **5-2**, $[GaPh_2O(O)PMe_2]_2$ **5-3** and $[GaPh_2O(O)P(p\text{-}MeOPh)_2]_2$ **5-4** in yields ranging from 55 to 79 %, as shown in Table 5-1. It must be noted that **5-1** and **5-4** could not be isolated 100 % pure (by elemental analysis), with small amounts of hydrolysis products continually observed. The characterisation is discussed in further detail in section 5.3.

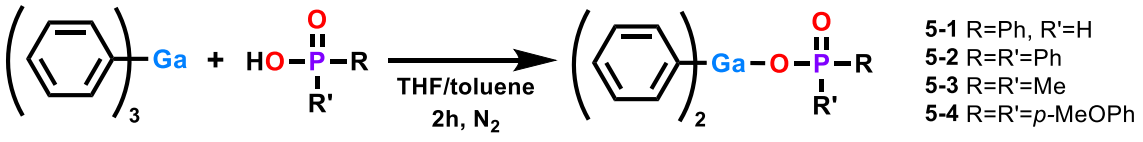

Scheme 5-3 Synthetic route to form diphenyl gallium *mono*-phosphinato complexes **5-1** – **5-4**.

Table 5-1 Synthetic summary of complexes **5-1** – **5-4** including synthesis solvent, percentage yield and complex colour.

Compound		Solvent	Yield (%)	Colour
$[GaPh_2O(O)P(H)Ph]_2$	**5-1**	Toluene	64	White
$[GaPh_2O(O)PPh_2]_2$	**5-2**	THF	79	White
$[GaPh_2O(O)PMe_2]_2$	**5-3**	Toluene	56	Pale yellow
$[GaPh_2O(O)P(p\text{-}MeOPh)_2]_2$	**5-4**	Toluene	55	Cream

5.2.2 Phenyl gallium *bis*-phosphinates

Initial attempts to synthesise the phenyl gallium *bis*-phosphinato complexes $[GaPh(O(O)P(H)Ph)_2]$ **5-5**, $[GaPh(O(O)PPh_2)_2]$ **5-6**, $[GaPh(O(O)PMe_2)_2]$ **5-7** and $[GaPh(O(O)P(p\text{-}MeOPh)_2)_2]$ **5-8** utilised two equivalents of the phosphinic acid reacted with $GaPh_3$ in toluene at reflux. The reaction was monitored over time, however only the *mono*-phosphinato products could be identified for all reactions, as similarly noted for reactions of $GaMe_3$ with phosphinic acids.[188]

An alternative solvent free (SF) synthetic approach to form the phenyl gallium *bis*-phosphinato complexes **5-5** – **5-8** was investigated using thermal gravimetric analysis (TGA) to follow the reaction. The viability of the SF method was assessed with either $GaPh_3$ or the *mono*-phosphinato complexes **5-1** – **5-4** reacted with the respective phosphinic acid. Figure 5-2 depicts the TGA trace for the reactions of diphenylphosphinic acid with either $GaPh_3$ or the *mono*-phosphinato complex **5-2**.

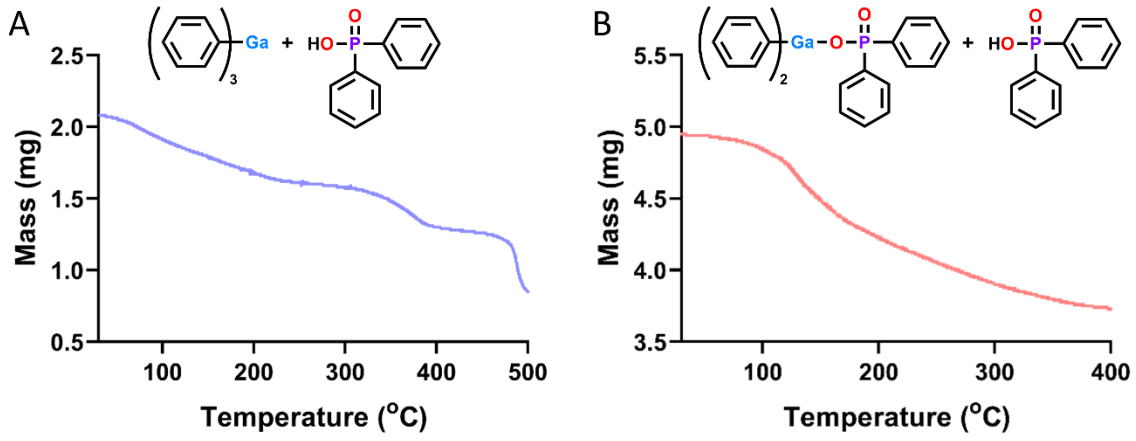

Figure 5-2 TGA profile to form phenyl gallium *bis*-diphenylphosphinato complex **5-6** through reaction of diphenylphosphinic acid with $GaPh_3$ (A) or complex **5-2** (B).

There is a stepwise loss of phenyl moieties in the $GaPh_3$ reaction, while only a single phenyl loss is observed for the reaction with **5-2**, suggesting that both SF routes are viable to form the phenyl

gallium *bis*-phosphinato complex **5-6**. The *mono*-phosphinato SF reaction is advantageous due to the moisture sensitivity of $GaPh_3$, requiring use of a dry box to prepare the reaction mixture.

From this, the phenyl gallium *bis*-phosphinato complexes **5-5** – **5-8** were synthesised through the reaction of the *mono*-phosphinato complexes **5-1** – **5-4** with their respective phosphinic acids. The SF reaction temperatures were determined by differential scanning calorimetry (DSC), where the observed exotherm coincided with a mass loss of a phenyl group by TGA. Table 5-2 details the reaction temperatures as determined by DSC and percentage mass loss observed by TGA. The solids were washed with ethanol and assessed by ^{1}H NMR to determine the product, however only one of the desired complexes **5-5** could be identified. The starting *mono*-phosphinato complexes **5-2** – **5-4**, were isolated from the remaining reactions. Reaction time lengths were varied up to 8 hours to promote the SF reaction, however complexes **5-6** – **5-8** could not be isolated and their synthesis was not pursued further. Characterisation beyond ^{1}H NMR was not conducted for complex **5-5** owing to the need for purification stemming from complex **5-1** and due to time limitations.

Table 5-2 Complexes **5-5** – **5-8** reaction temperatures, as determined from the exothermic peak of the DSC, corresponding percentage mass loss by TGA with the expected mass loss.

Compound		SF temperature (°C)	Mass loss (%)	Expected mass loss (%)
$[GaPh(O(O)P(H)Ph)_2]$	**5-5**	79	13.4	15.4
$[GaPh(O(O)PPh_2)_2]$	**5-6**	118	12.9	11.9
$[GaPh(O(O)PMe_2)_2]$	**5-7**	117	18.3	19.0
$[GaPh(O(O)P(p\text{-}MeOPh)_2)_2]$	**5-8**	119	10.4	10.0

5.2.3 Gallium *tris*-phosphinates

Gallium *tris*-dimethylphosphinato complex $[Ga(O(O)PMe_2)_3]_\infty$ **5-11** has previously been synthesised from $GaCl_3$, with the elimination of methyl chloride or triethylammonium chloride driving the reactions.[191,192] The gallium *tris*-phosphinato complexes $[Ga(O(O)P(H)Ph)_3]_\infty$ **5-9**, $[Ga(O(O)PPh_2)_3]_\infty$ **5-10**, $[Ga(O(O)PMe_2)_3]_\infty$ **5-11** and $[Ga(O(O)P(p\text{-}MeOPh)_2)_3]_\infty$ **5-12** were prepared herein through salt metathesis of $GaCl_3$ and sodium phosphinato salts, as shown in Scheme 5-4. The sodium phosphinato salts all display poor solubility in diethyl ether which prompted the 20 hour reaction time to allow the heterogeneous mixture to react. The white suspension was isolated by filtration and washed by sonication with ethanol and water to afford complexes in yields ranging from 19 to 87 %.

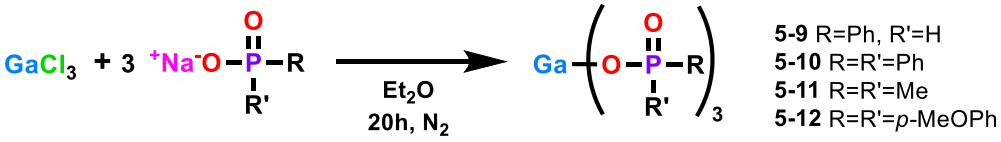

Scheme 5-4 Salt metathesis route to form the gallium *tris*-phosphinato complexes **5-9** – **5-12**.

Further investigations were conducted to form complex **5-11** via an alternative SF synthesis route, utilising the *mono*-phosphinato complex $[GaPh_2O(O)PMe_2]_2$ **5-3** and two equivalents of dimethylphosphinic acid. The DSC trace is shown in Figure 5-3, displaying two exotherms which suggests the formation of the *bis*-phosphinato complex $[GaPh(O(O)PMe_2)_2]$ **5-7** at 117 °C followed by formation of the *tris*-phosphinato complex **5-11** at 186 °C. The SF reaction was conducted over 30 minutes with stirring at 186 °C, which produced a white solid that was washed with hot ethanol to afford **5-11** in a 32 % yield.

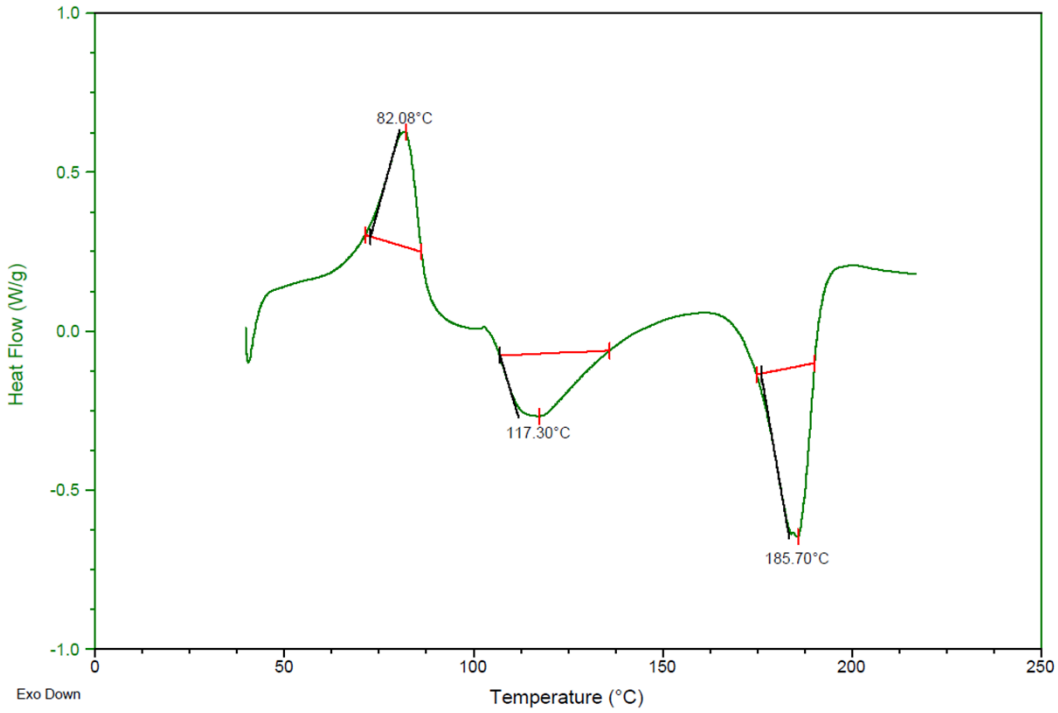

Figure 5-3 DSC trace of 1:2 mixture of **5-3** and dimethylphosphinic acid from 40 to 210 °C.

5.2.4 Gallium cluster

Heating complexes **5-1**, **5-2** and **5-4** in DMSO and leaving the solutions to crystallise resulted in the isolation of the phenyl gallium oxido-hydroxido cluster $[Ga_{12}Ph_{12}(\mu_3\text{-}O)_8(\mu\text{-}O)_2(\mu\text{-}OH)_4].4DMSO$ (denoted **5-13**). Further investigations found that adding $GaPh_3$ to wet DMSO initially formed $GaPh_2OH$, then hydrolysed further to give **5-13**, as shown in Scheme 5-5. The crystalline **5-13** was collected by filtration in a yield of 32 %. Analogous aryl and alkyl gallium clusters have been

reported containing *o*-methoxyphenyl and *iso*-propyl moieties, where their formation also resulted from the hydrolysis of Ga(*o*-MeOPh)$_3$ or Ga^{i}Pr$_3$ respectively in 30 to 40 % yields.[196]

Scheme 5-5 Hydrolysis of GaPh$_3$ forming gallium cluster [Ga$_{12}$Ph$_{12}$(μ_3-O)$_8$(μ-O)$_2$(μ-OH)$_4$].4DMSO **5-13**.

5.3 Characterisation

Complexes **5-1** – **5-4**, **5-11** and **5-13** show solubility in DMSO, allowing for solution-state ^{1}H and ^{31}P NMR spectroscopic analyses in d$_6$-DMSO. The *tris*-phosphinato gallium complexes **5-9**, **5-10** and **5-12** are poorly soluble in all solvents and were characterised by solid-state ^{13}C and ^{31}P NMR. Further solid-state characterisation techniques include IR spectroscopy, melting point and elemental analysis.

The ^{1}H NMR spectra of complexes **5-1** – **5-5** and **5-11** show an upfield shift of the phosphinato protons following complexation to gallium. This shift is due to the delocalisation of the PO$_2$ moiety compared with the phosphinic acids, as depicted in Figure 5-4. Both [GaPh$_2$O(O)P(H)Ph]$_2$ **5-1** and [GaPh(O(O)P(H)Ph)$_2$] **5-5** display the characteristic phenyl *ortho*-, *meta*- and *para*-proton signals. It is interesting to note that the gallium-phenyl protons do not shift between *mono*- and *bis*-phosphinato complexes, unlike the bismuth compounds which is likely due to the greater electronegativity of bismuth compared with gallium. The solution- and solid-state ^{31}P spectra of complexes **5-1** – **5-4**, **5-9**, **5-10** and **5-12** show a high field shift when compared to the phosphinic acids, as similarly observed in the bismuth phosphinato complexes. While complex **5-11** shows some solubility in d$_6$-DMSO, it proved difficult to obtain well-resolved NMR spectra, so only the ^{1}H NMR spectrum is reported.

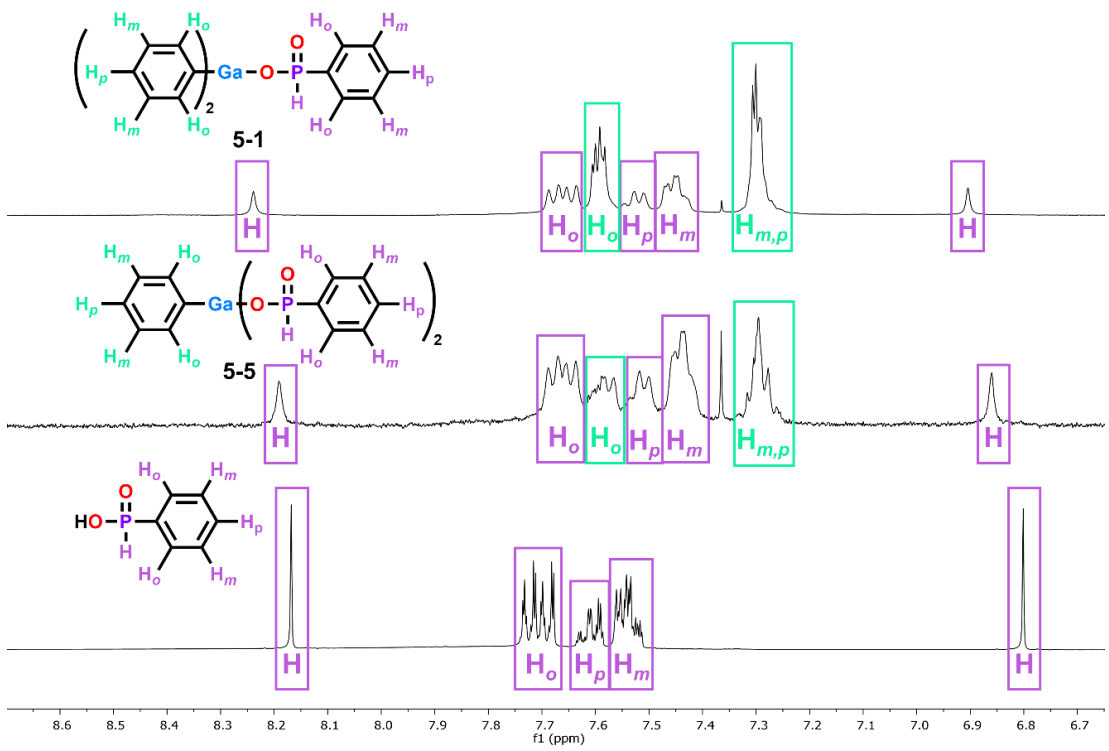

Figure 5-4 ^{1}H NMR in d_6-DMSO of complexes **5-1** (top), **5-5** (middle) and phenylphosphinic acid (bottom) showing an upfield shift of phenylphosphinato protons upon complex formation.

The hydrolysis of $GaPh_3$ can be observed by NMR spectroscopy, where the water in the d_6-DMSO reacts to produce $GaPh_2OH$, as seen in Figure 5-5. Crystals of **5-13** can be isolated from DMSO and dissolved in d_6-DMSO to give a distinct NMR spectrum (Figure 5-6). The aromatic region integrates to 60 protons corresponding to the 12 phenyl moieties, with 24 protons for the 4 DMSO solvent molecules at 2.54 ppm. The downfield shift of the hydroxyl protons from 6.88 ppm in $GaPh_2OH$ to the range of 9.1 to 9.6 ppm in **5-13** can be attributed to the exchange of the hydroxyl protons with water in solution, where typical aqua ligands show proton signals in the region of 6.3 to 10 ppm.[197] The resulting lack of symmetry in the cluster owing to water exchange will also cause multiple signals, explaining the five singlets observed for the expected four hydroxyl protons.

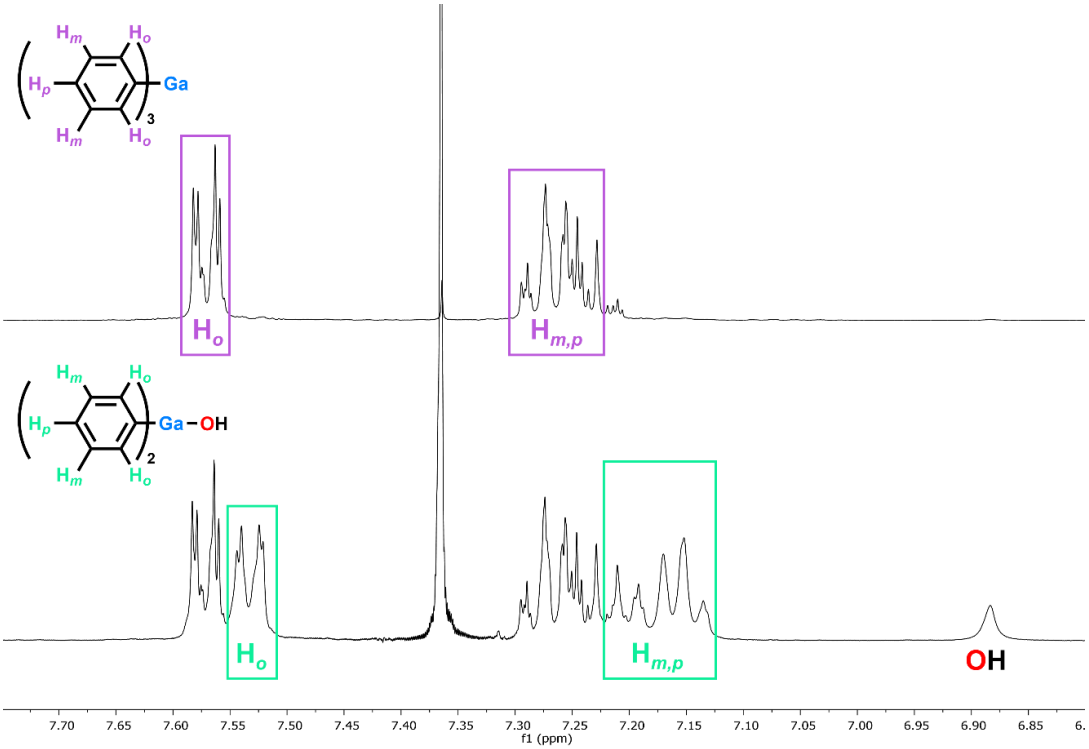

Figure 5-5 ^{1}H NMR of $GaPh_3$ (top) and 24 hours later showing hydrolysis to form $GaPh_2OH$ (bottom) in d_6-DMSO.

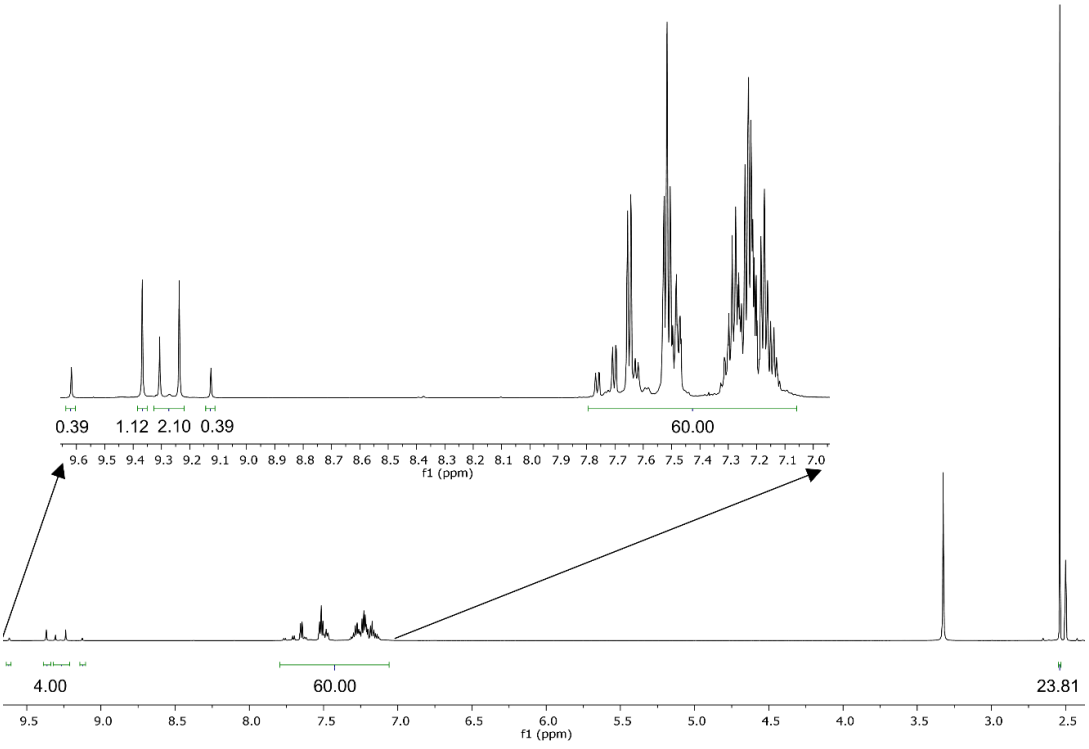

Figure 5-6 ^{1}H NMR of cluster $[Ga_{12}Ph_{12}(\mu_3\text{-}O)_8(\mu\text{-}O)_2(\mu\text{-}OH)_4].4DMSO$ **5-13** in d_6-DMSO with integrations.

The binding mode of the phosphinato moiety can be determined through IR spectroscopy, due to the strong asymmetric and symmetric PO_2 stretching bands. It can be noted that the gallium

phosphinato complexes **5-1** – **5-4** and **5-9** – **5-12** all display a small difference in asymmetric and symmetric PO_2 stretching bands ($\Delta\nu$) compared with their respective phosphinic acids and sodium phosphinato salts, as detailed in Table 5-3. This small $\Delta\nu$ is indicative of symmetric binding in a chelating or bridging fashion. The dimethyl gallium *mono*-phosphinato complexes $[GaMe_2O(O)PPh_2]_2$ and $[GaMe_2O(O)PMe_2]_2$ have reported $\Delta\nu$ values of 113 and 102 cm^{-1} respectively,[184] very similar to their diphenyl gallium analogues with $\Delta\nu$ values of 109 cm^{-1} for **5-2** and 102 and 95 cm^{-1} for **5-3**.

Table 5-3 The difference ($\Delta\nu$) between asymmetric and symmetric PO_2 stretching bands in the IR spectra of complexes **5-1** – **5-12**, their respective phosphinic acids and phosphinato sodium salts.

Compound		$\Delta\nu$ (cm^{-1})	Compound		$\Delta\nu$ (cm^{-1})
$[GaPh_2O(O)P(H)Ph]_2$	**5-1**	90, 125	$[GaPh_2O(O)PMe_2]_2$	**5-3**	102, 95
$[Ga(O(O)P(H)Ph)_3]_\infty$	**5-9**	90	$[Ga(O(O)PMe_2)_3]_\infty$	**5-11**	94
$Ph(H)P(O)OH$		164	$Me_2P(O)OH$		180
$Na^+O^-(O)P(H)Ph$		150	$Na^+O^-(O)PMe_2$		102
$[GaPh_2O(O)PPh_2]_2$	**5-2**	109, 109	$[GaPh_2O(O)P(p\text{-}MeOPh)_2]_2$	**5-4**	103, 106
$[Ga(O(O)PPh_2)_3]_\infty$	**5-10**	94, 108	$[Ga(O(O)P(p\text{-}MeOPh)_2)_3]_\infty$	**5-12**	92, 98
$Ph_2P(O)OH$		168	$(p\text{-}MeOPh)_2P(O)OH$		177
$Na^+O^-(O)PPh_2$		153	$Na^+O^-(O)P(p\text{-}MeOPh)_2$		140

The elemental analysis of compounds **5-2**, **5-3**, **5-10**, **5-12** and **5-13** matched with the expected values, as detailed in the Experimental (section 7.10). Complexes **5-9** and **5-11** showed lower carbon values due to the presence of salt which was difficult to remove owing to the hydrophobicity of the compounds. Complexes **5-1** and **5-4** also had lower than expected carbon values, which is likely due to the presence of hydrolysis products. The heating of **5-4** in toluene resulted in the formation of $[Ga_4Ph_4(O(O)P(p\text{-}MeOPh)_2)_4(\mu_3\text{-}O)_2]$, which is further described in the X-ray crystallography section (5.3.1). Interestingly, both the complex $[GaPh_2O(O)P(p\text{-}MeOPh)_2]_2$ **5-4** and gallium oxido hydrolysis product can be observed by high resolution mass spectrometry (MS) (Figure 5-7). Similarly, for complex **5-1**, both the complex $[GaPh_2O(O)P(H)Ph]_2$ and hydrolysis product $[Ga_2Ph_2(O(O)P(H)Ph)_2(O)]$ can be identified through MS. The lower carbon values in the elemental analysis can be attributed to the presence of the hydrolysis product in the solid-state for both complexes **5-1** and **5-4**. Both complexes **5-2** and **5-3** show much smaller amounts of the hydrolysis product through MS, however given the elemental analysis of these crystalline samples, it is likely the hydrolysis is only occurring in the solution-state. Purification via high pressure liquid chromatography was investigated to separate the complex (**5-1** or **5-4**) and its hydrolysis product.

While separation is possible using a THF and water gradient, there were concerns of further hydrolysis occurring so the compounds remained as mixtures in the interest of time.

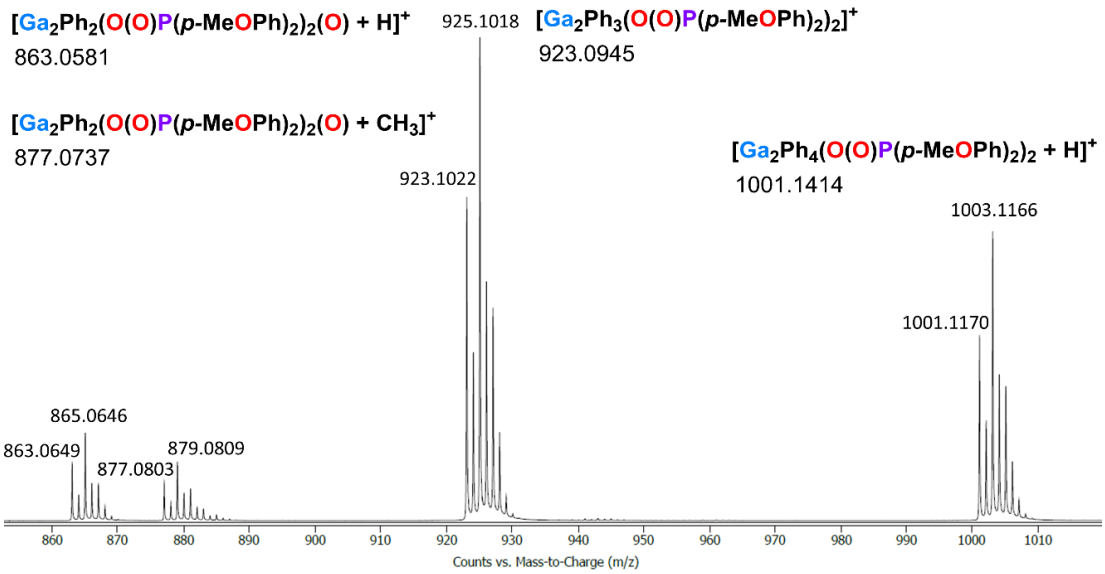

Figure 5-7 High resolution mass spectrum of complex **5-4** showing typical gallium isotopic patterns and evidence of the hydrolysis product.

5.3.1 X-ray crystallography

Crystals suitable for single-crystal X-ray diffraction were isolated following dissolution of complex $[GaPh_2O(O)PPh_2]_2$ **5-2** in a mixture of methanol and DMSO, and $[GaPh_2O(O)PMe_2]_2$ **5-3** in DMSO, then allowing to stand for several days, producing colourless crystals. The *mono*-phosphinato gallium complexes form dimers in the expected an eight-membered ring configuration, with gallium centres bridged by the phosphinato moiety. The binding mode is reminiscent of previously reported dialkyl gallium *mono*-phosphinato complexes $[GaMe_2O(O)PPh_2]_2$, $[GaEt_2O(O)PPh_2]_2$ and $[Ga^tBu_2O(O)PPh_2]_2$ shown in Figure 5-8.[188–190]

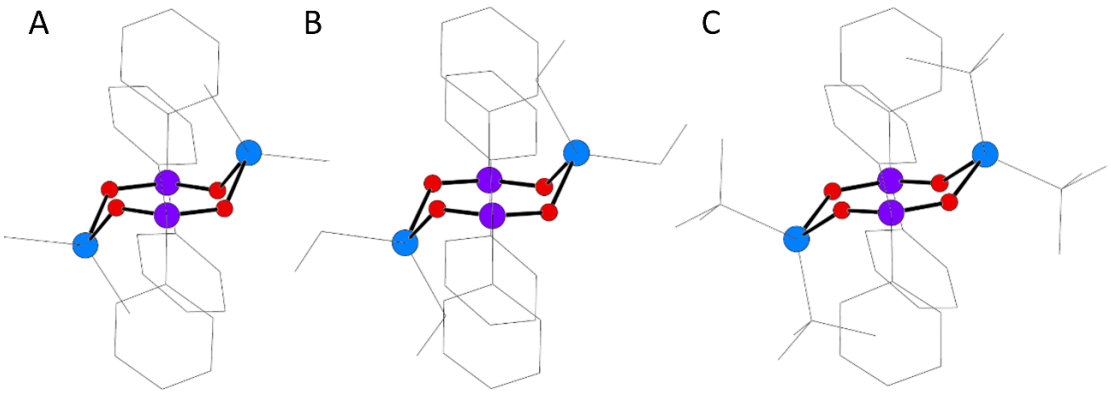

Figure 5-8 Dimeric structures of $[GaMe_2O(O)PPh_2]_2$ (A), $[GaEt_2O(O)PPh_2]_2$ (B) and $[Ga^tBu_2O(O)PPh_2]_2$ (C).[188–190] Hydrogen atoms are omitted for clarity.

Complex **5-2** forms a dimer with an eight-membered ring containing two gallium atoms bridged by two phosphinato moieties, as shown in Figure 5-9. The phosphinato moiety binds in a delocalised coordination mode, with P(1)-O(1), P(1)-O(2), P(2)-O(3) and P(2)-O(4) bond lengths of 1.5213(13), 1.5199(15), 1.5255(14) and 1.5215(14) Å respectively. It is interesting to note that the dimeric metal phosphinato ring is not the same as shown in Figure 5-8, which is due to two phenyl groups on both the gallium and phosphorus increasing the steric bulk.

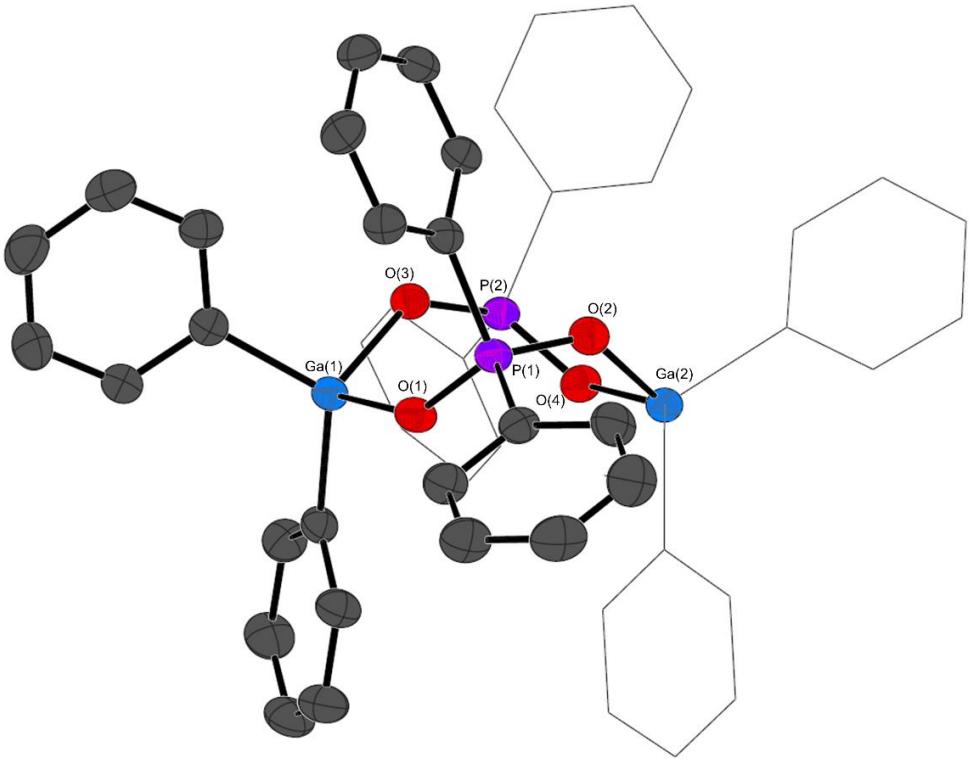

Figure 5-9 Dimeric structure of $[GaPh_2O(O)PPh_2]_2$ **5-2**. Thermal ellipsoids shown at 50 % probability. Ga(2) and P(2) phenyl groups shown as wire frame, and hydrogen atoms are omitted for clarity.

Interestingly, solvent plays a role in the obtained crystalline structure, as different crystals were isolated following dissolution of **5-2** in an acetonitrile and DMSO mixture. The obtained structure is shown in Figure 5-10, where the complex $[GaPh_2O(O)PPh_2]_\infty$ forms a 1D coordination polymer as similarly observed for the analogous bismuth complex $[BiPh_2O(O)PPh_2]_\infty$ **2-2** in Chapter 2. Gallium adopts a distorted tetrahedral geometry as evidenced by bond angles of 97.25(9), 122.06(14) and an average of 108.65 ° for O(1)-Ga-O(4)', C(1)-Ga(1)-C(7) and O-Ga(1)-C respectively. The bridging phosphinato groups bind in a delocalised coordination mode, with an average O-P-O bond length of 1.525 Å.

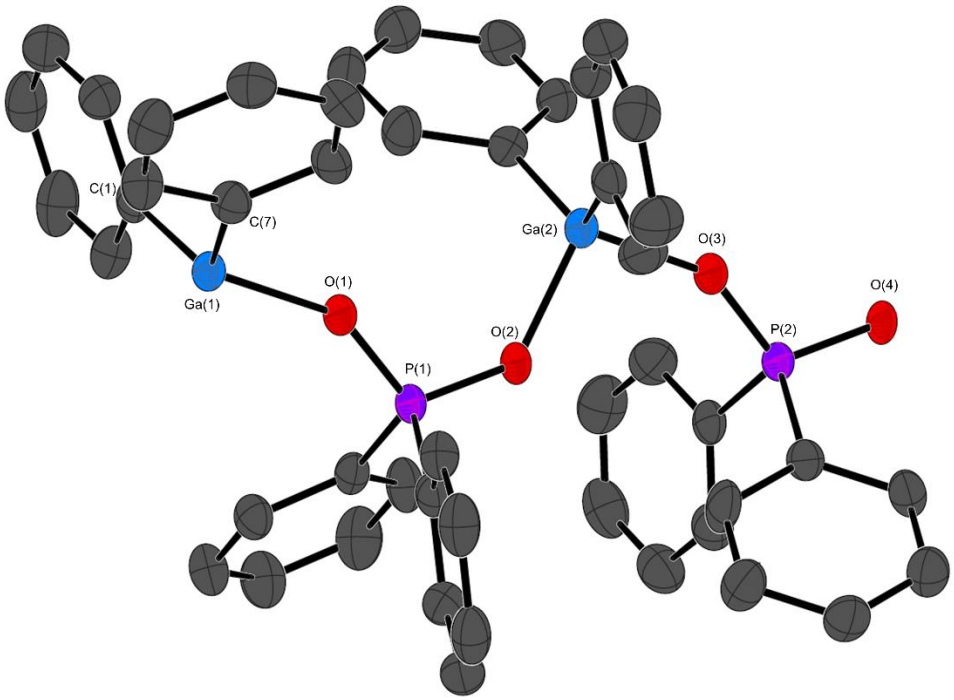

Figure 5-10 Polymeric structure of $[GaPh_2O(O)PPh_2]_\infty$ **5-2**. Thermal ellipsoids shown at 50 % probability. Hydrogen atoms are omitted for clarity.

The molecular and dimeric structure of **5-3** are depicted in Figure 5-11. Both gallium and phosphorus atoms have a tetrahedral geometry, with the similar P-O bond lengths of 1.521(3) and 1.522(3) Å as evidence of a delocalised coordination mode of the phosphinato group. The dimeric structure shows a puckered eight-membered ring with almost coplanar phosphorus and oxygen atoms, while both gallium atoms are displaced from the plane, as similarly reported in the dimethyl and diethyl gallium *mono*-diphenylphosphinato complexes.[188,189]

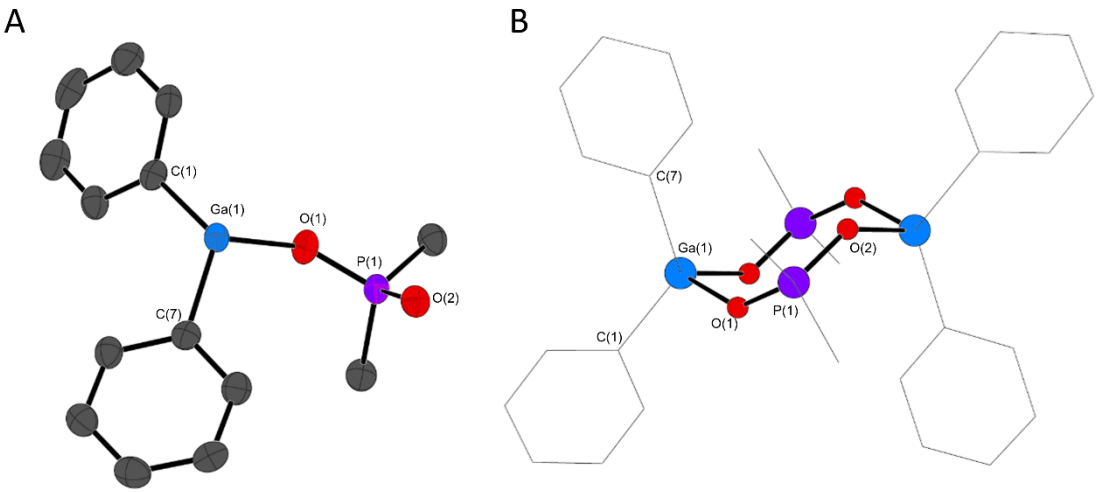

Figure 5-11 Molecular (A) and dimeric (B) structure of $[GaPh_2O(O)PMe_2]_2$ **5-3**. Thermal ellipsoids shown at 50 % probability in molecular structure. Hydrogen atoms are omitted for clarity.

The hydrolysis of $GaPh_3$ in DMSO results in crystals of $[Ga_{12}Ph_{12}(\mu_3\text{-}O)_8(\mu\text{-}O)_2(\mu\text{-}OH)_4].4DMSO$ **5-13**, as depicted in Figure 5-12. Attempts to crystallise complexes **5-1** and **5-4** from DMSO proved unsuccessful, where the isolated crystals proved to be a phenyl gallium oxido-hydroxido cluster. The cluster contains 12 gallium atoms, each coordinated to two triply bridging oxygen atoms (μ_3-O) and one doubly bridging oxygen (μ-O) as either an oxido or hydroxido group. Typical oxido ligand coordination environments in gallium clusters are μ_3-O, where μ-O is much less commonly observed.[198] The gallium centres adopt distorted tetrahedral geometries, with an average O–Ga–O and O–Ga–C bond angle of 102.71 and 115.51 °. The four DMSO molecules interact with the hydroxide protons through hydrogen-bonding at an average distance of 1.732 Å. A similar alkyl gallium cluster $[Ga_{12}{}^tBu_{12}(\mu_3\text{-}O)_8(\mu\text{-}O)_2(\mu\text{-}OH)_4].4Et_2O$ was obtained through the oxidation and subsequent hydrolysis of di-*tert*-butyl gallium *o*-mercaptopyridine.[199] Two further reports of methyl and *p*-tolyl gallium oxido-hydroxido clusters indicate that the diprotonated derivative maintains the same structure observed for the aryl and alkyl analogues.[196,200]

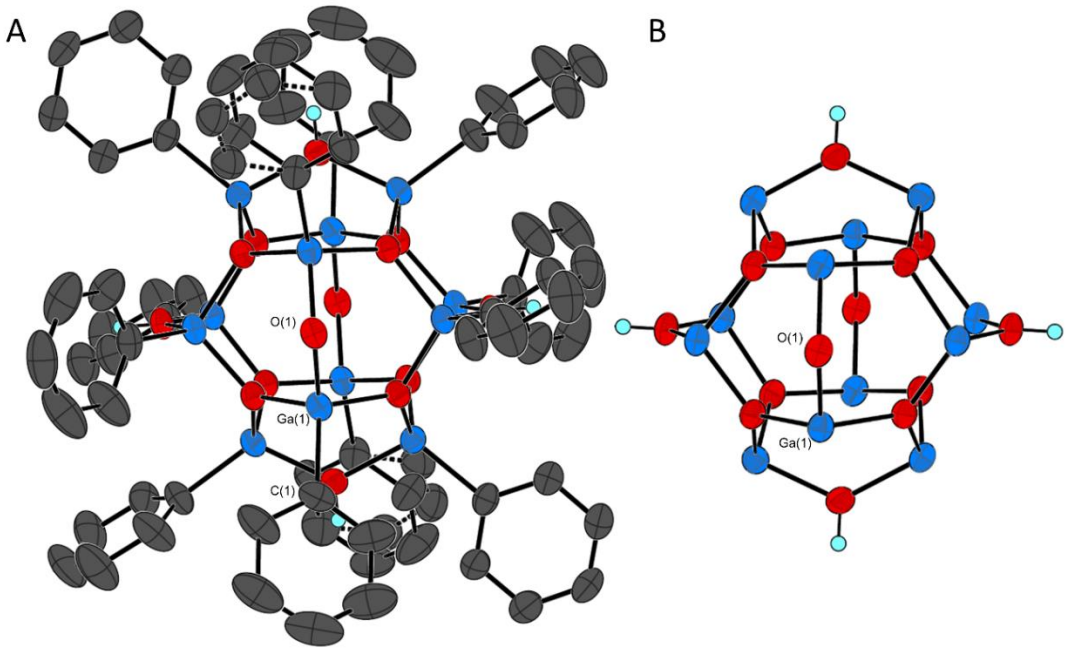

Figure 5-12 Structure of phenyl gallium oxido-hydroxido cluster $[Ga_{12}Ph_{12}(\mu_3\text{-}O)_8(\mu\text{-}O)_2(\mu\text{-}OH)_4].4DMSO$ **5-13** (A) and the gallium oxido-hydroxido core $[Ga_{12}O_{10}(OH)_4]$ (B). Thermal ellipsoids shown at 50 % probability. DMSO and hydrogen atoms on phenyl rings are omitted for clarity.

Further crystallisation attempts for complexes **5-1** and **5-4** were trialled in toluene due to its lower water content, with the aim to avoid hydrolysis. Solubilisation of complex **5-4** in hot toluene immediately yielded colourless crystals suitable for single crystal X-ray diffraction. The isolated crystals proved to be the *mono*-(*bis*-*p*-methoxyphenyl)phosphinato phenyl gallium oxido compound $[Ga_4Ph_4(O(O)P(p\text{-}MeOPh)_2)_4(\mu_3\text{-}O)_2]$ shown in Figure 5-13. This is the first known example of a tetra-gallium phosphinato oxido cluster based on literature and Cambridge

Crystallographic Data Centre searches (as of February 2021). Two gallium atoms have a distorted tetrahedral geometry, where gallium is bound to one phenyl, two phosphinato and one tripling bridging oxido group. The remaining two gallium atoms adopt a trigonal bipyramidal geometry, each coordinated with one phenyl group, two bridging phosphinato groups and two triply bridging oxido groups. The phosphinato moiety adopts a delocalised coordination mode with P(1)-O(2), P(1)-O(3), P(2)-O(4) and P(2)-O(5) bond lengths of 1.544(5), 1.511(6), 1.512(5) and 1.523(5) Å respectively. The gallium-phosphinato Ga(1)-O(2) and Ga(1)-O(5)' bond lengths of 1.891(5) and 1.895(5) Å respectively are representative of a covalent interaction, where typical five-coordinate equatorial Ga-O bond lengths are 1.935 Å.[201]

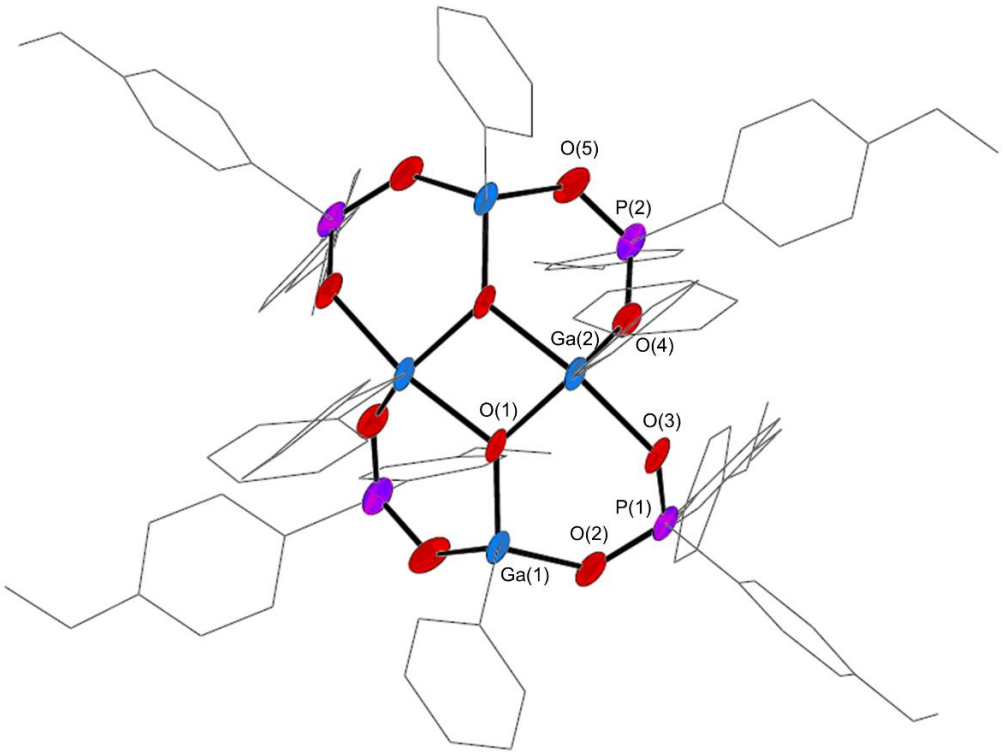

Figure 5-13 Structure of *mono*-(*bis*-*p*-methoxyphenyl)phosphinato phenyl gallium oxido complex $[Ga_4Ph_4(O(O)P(p\text{-}MeOPh)_2)_4(\mu_3\text{-}O)_2]$. Thermal ellipsoids shown at 50 % probability. Phenyl and *p*-methoxyphenyl moieties shown as wire frame and hydrogen atoms are omitted for clarity.

5.4 Stability

The solution-state stability of complexes $[GaPh_2O(O)P(H)Ph]_2$ **5-1**, $[GaPh_2O(O)PPh_2]_2$ **5-2**, $[GaPh_2O(O)PMe_2]_2$ **5-3** and $[GaPh_2O(O)P(p\text{-}MeOPh)_2]_2$ **5-4** were assessed by ^{1}H NMR spectroscopy in d_6-DMSO. After 24 hours in d_6-DMSO at room temperature, both complexes **5-1** and **5-4** show the appearance of benzene which is due to a small amount of hydrolysis occurring to form $[Ga_2Ph_2(O(O)P(H)Ph)_2(O)]$ and $[Ga_4Ph_4(O(O)P(p\text{-}MeOPh)_2)_4(\mu_3\text{-}O)_2]$ respectively, as determined by

MS and X-ray crystallography. The production of benzene can be increased by heating complex **5-4** at 100 °C in d_6-DMSO for 2 hours, further promoting hydrolysis as seen in Figure 5-14. The crystalline complexes **5-2** and **5-3** do not show the formation of benzene at room temperature after 24 hours.

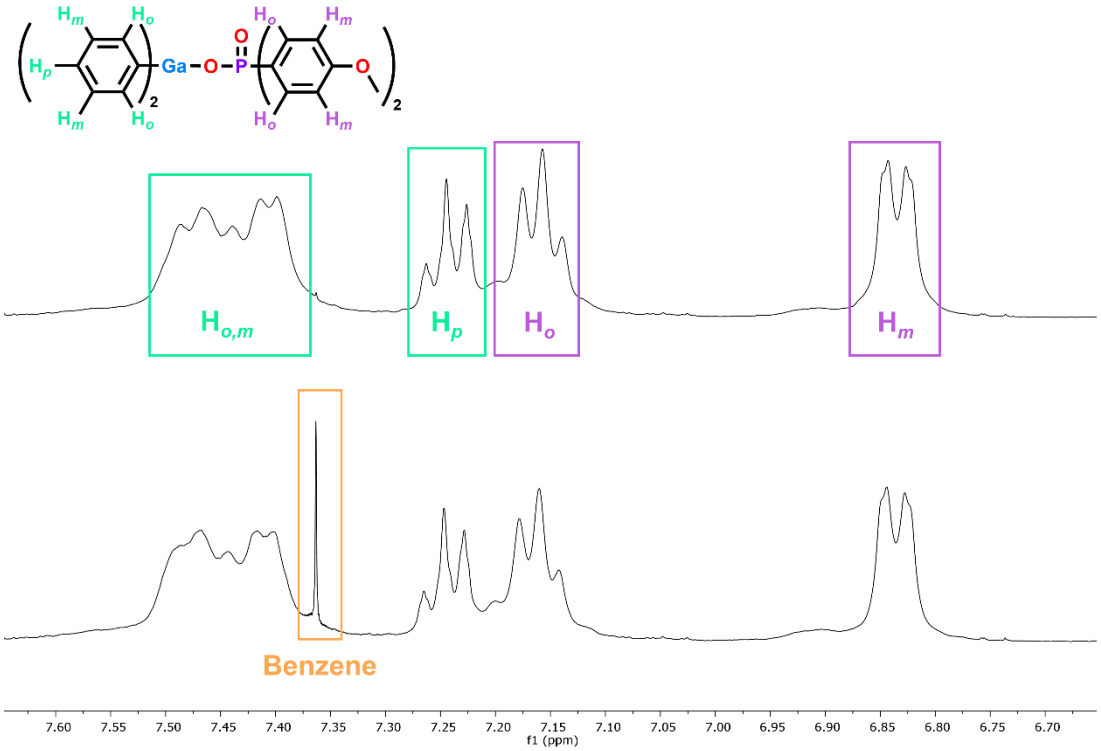

Figure 5-14 ^{1}H NMR in d_6-DMSO of complex **5-4** before (top) and after 2 hours heating at 100 °C (bottom) showing benzene formation.

While the crystalline complex **5-2** does not show hydrolysis, the crude powder sample can be heated in DMSO and the gallium cluster **5-13** can be isolated as a crystalline solid, as similarly noted for complexes **5-1** and **5-4**. It is apparent that the diphenyl gallium *mono*-phosphinato complexes containing bulkier phosphinato groups are poorly stable to hydrolysis, which is further exacerbated by the introduction of heat.

5.5 Biology

The gallium compounds $[GaPh_2O(O)P(H)Ph]_2$ **5-1**, $[GaPh_2O(O)PPh_2]_2$ **5-2**, $[GaPh_2O(O)PMe_2]_2$ **5-3**, $[GaPh_2O(O)P(p\text{-}MeOPh)_2]_2$ **5-4**, $[Ga(O(O)P(H)Ph)_3]_\infty$ **5-9**, $[Ga(O(O)PPh_2)_3]_\infty$ **5-10**, $[Ga(O(O)PMe_2)_3]_\infty$ **5-11**, $[Ga(O(O)P(p\text{-}MeOPh)_2)_3]_\infty$ **5-12** and cluster $[Ga_{12}Ph_{12}(\mu_3\text{-}O)_8(\mu\text{-}O)_2(\mu\text{-}OH)_4].4DMSO$ **5-13** were assessed for their antibacterial activity towards the Gram positive bacteria methicillin-resistant *S. aureus* (MRSA) and vancomycin-resistant *Enterococcus* (VRE), and the Gram negative bacteria *E. coli*, *P. aeruginosa* and *Acinetobacter baumannii* (*A. baumannii*). The addition of *A. baumannii* to

the test bacterial strains is due to gallium compounds typically displaying greater antibacterial activity towards Gram negative bacteria. The four phosphinic acids were assessed for their activity towards *A. baumannii* and showed no activity at 100 µM, as similarly observed for the other bacterial strains (Chapter 2, section 2.5.1). The poor solubility of complexes **5-9** – **5-12** allowed for only solid-state antibacterial analysis, while the minimum inhibitory concentration (MIC) could be determined through solution-based assays for complexes **5-1** – **5-4** and **5-13**. The soluble compounds were also assessed for their effect on the viability of Cos-7 cells.

5.5.1 Antibacterial activity

The zone of inhibition assay examines the area where bacteria does not grow around an antibacterial compound due to diffusion into the agar. This qualitative test was utilised to examine if the *tris*-phosphinato gallium complexes displayed any antibacterial activity. The solid complexes **5-9** – **5-12** are placed onto a pre-spread lawn of bacteria on agar and incubated overnight at 37 °C. The resulting zones of inhibition are measured and the listed in Table 5-4, with Figure-5-15 showing some examples of the zone of inhibition agar plates.

Table 5-4 Zone of inhibition measured as the diameter across the solid complexes **5-9** – **5-12** following 24 hour incubation at 37 °C. Assays were conducted in triplicate and the measurements are averages with the standard deviation.

Compound		Zone of inhibition (mm)				
		MRSA	VRE	*E. coli*	*P. aeruginosa*	*A. baumannii*
$[Ga(O(O)P(H)Ph)_3]_\infty$	**5-9**	0	0	0	7.7 ± 1.5	3.0 ± 1.7
$[Ga(O(O)PPh_2)_3]_\infty$	**5-10**	0	0	0	3.7 ± 3.2	0
$[Ga(O(O)PMe_2)_3]_\infty$	**5-11**	0	0	0	7.7 ± 0.6	2.7 ± 0.6
$[Ga(O(O)P(p\text{-}MeOPh)_2)_3]_\infty$	**5-12**	0	0	0	5.0 ± 0	0.7 ± 1.2

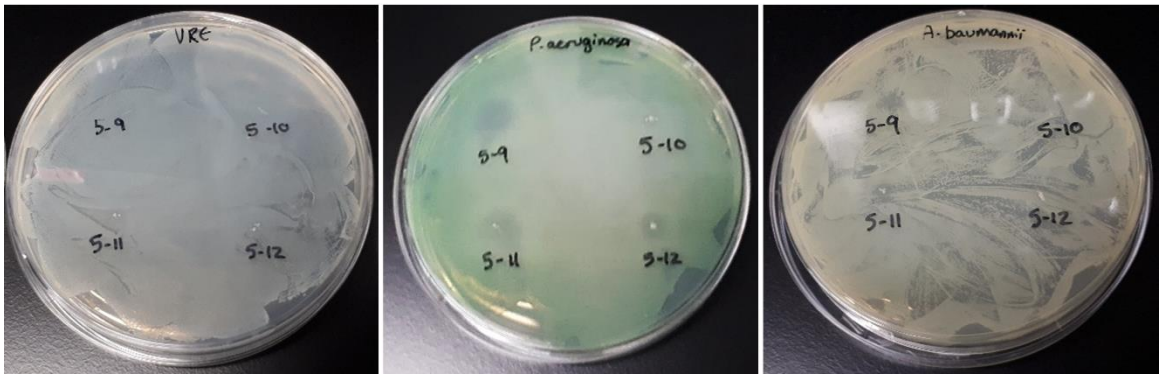

Figure 5-15 Zone of inhibition test against VRE, *P. aeruginosa* and *A. baumannii* using <1 mg of complexes **5-9** – **5-12** incubated for 24 hours at 37 °C.

It is apparent that the gallium *tris*-phosphinato complexes display antibacterial activity towards *P. aeruginosa* and *A. baumannii*, while they are not active towards *E. coli* or the Gram positive MRSA and VRE. Similar activity has been previously reported for gallium compounds such as $Ga(NO_3)_3$ and gallium citrate ($GaO(O)CC(OH)(O(O)CCH_2)_2$), where negligible activity was noted for Gram positive bacteria and greater activity was observed for the Gram negative bacteria *P. aeruginosa* and *A. baumannii*.[103,110] Gallium has been shown to cross the outer membrane of Gram negative bacteria by passive diffusion through porins, however transport mechanisms are necessary for the gallium to cross the cytoplasmic membrane, often by exploiting iron uptake mechanisms.[97] Interestingly, gallium citrate displayed poor antibacterial activity towards *E. coli* despite iron-citrate transport systems, likely due to the citrate-mediated gallium uptake not being sufficient for toxicity.[97] It is noteworthy that the phenylphosphinato and dimethylphosphinato complexes **5-9** and **5-11** display the largest zones of inhibition. This is likely due to better diffusion in the agar owing to greater solubility based on the clogP values of 0.233 for **5-9** and -3.874 for **5-11**, compared with complexes **5-10** and **5-12** with clogP values of 7 and 6.514 respectively.

The DMSO soluble compounds were assessed by solution-based assay. Bacterial growth was examined following exposure to complexes **5-1** – **5-4** and the cluster **5-13**. DMSO solutions were prepared at 10 mM (1 mM for **5-13**) and diluted to give concentrations of 25, 50 and 100 μM (2.5, 5.0 and 10 μM **5-13**) in bacterial broth within 96 well plates. Overnight bacterial cultures were added to the broth and incubated overnight at 37 °C. Bacterial growth was measured by absorbance at 600 nm, where the positive bacterial control with no added compound was treated as 100 % growth and broth only was the negative control. The growth curves for complexes **5-1** – **5-4** and cluster **5-13** are shown in Figure 5-16. The MIC is determined as the lowest concentration to inhibit ≥80 % growth, suggesting the MIC values are >100 μM for all bacteria with the exception of *P. aeruginosa*, where the MIC values are 50 μM for **5-1** and 100 μM for **5-2** and **5-4**.

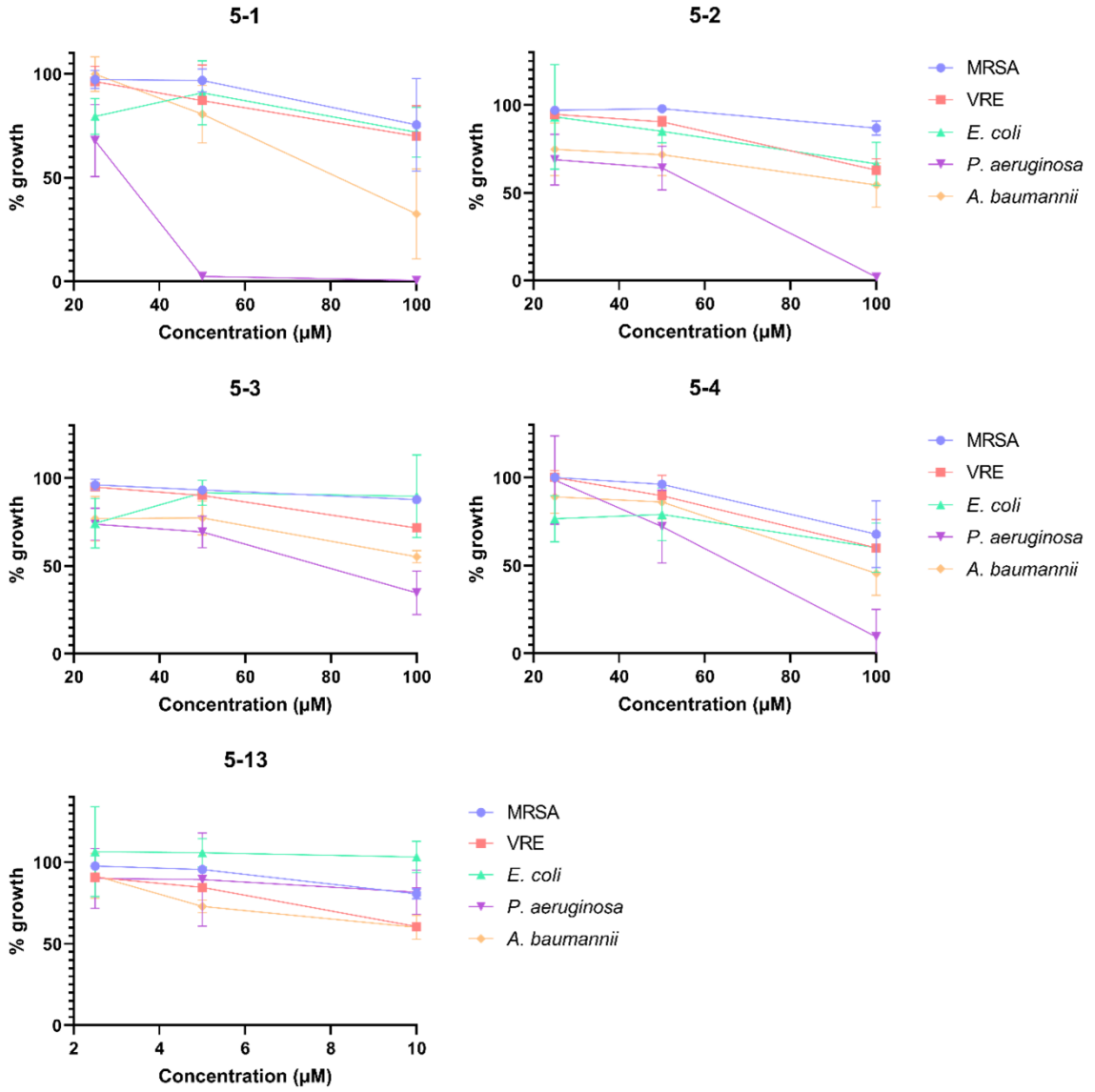

Figure 5-16 Bacterial growth as measured by absorbance at 600 nm following 20 hour incubation at 37 °C with complexes **5-1** – **5-4** and cluster **5-13**.

Compounds such as gallium citrate are known to be poorly active towards bacteria, with between 80 and 640 μM needed to inhibit 90 % of *P. aeruginosa* growth.[97] This suggests that some of the antibacterial activity observed for complexes **5-1** – **5-4** is likely due to the combined effect of gallium and the phosphinato ligand. It can be noted that as the gallium compound concentration increases, the bacterial growth decreases. This is likely due to the effect of gallium on iron uptake, resulting in reduced growth in bacteria.[97] Further studies could look into the effect that changing iron concentration within the broth has upon the determined MIC values, where it is expected that reduced iron would improve antibacterial activity and conversely, increasing the iron concentration would decrease the activity.[103] It is interesting that the gallium cluster at 10 μM contains more gallium than complexes **5-1** – **5-4** at 100 μM, however did not exert a greater effect

on bacterial growth. It is possible the gallium within the cluster is not as bioavailable as the dimeric complexes, as similarly observed for bismuth oxido-clusters where lower antibacterial activity was reported compared with their initial bismuth carboxylate complexes towards *Helicobacter pylori*.[78]

5.5.2 Mammalian cell toxicity

The CellTiter-Blue viability assay was used to assess the complexes **5-1** – **5-4** and the cluster **5-13** for their cytotoxicity towards Cos-7 cells. The cells were seeded and adhered to 96 well plates 24 hours prior to the addition of the gallium compounds, which were made up at 10 mM (1 mM **5-13**) in DMSO and diluted in media such that the maximum concentration tested was 100 µM for **5-1** – **5-4** and 10 µM **5-13** (DMSO 1 %). The CellTiter-Blue dye is added after 20 hours incubation at 37 °C and incubated for a further 4 hours before measuring the cell viability by fluorescence. Controls of cells without added compound were treated as 100 % viable and cells with 1 % DMSO were included where the average viability was 90 %. The results of the Cos-7 cell viability assay for compounds **5-1** – **5-4** and **5-13** are shown in Figure 5-17.

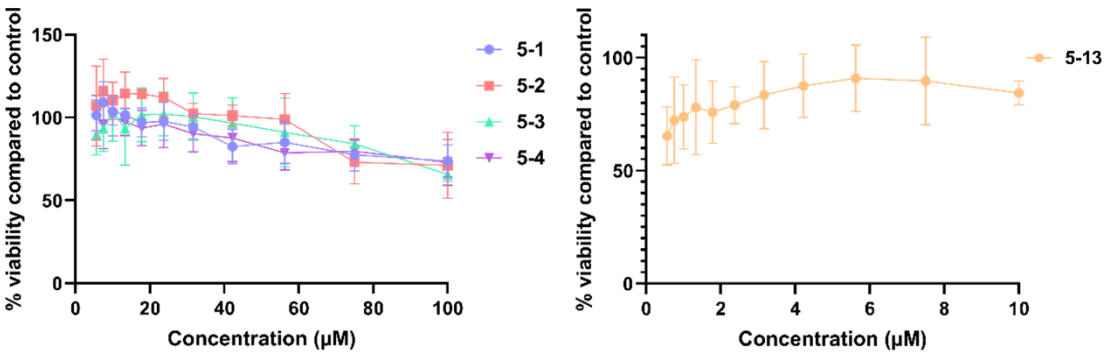

Figure 5-17 Cos-7 viability following 24 hour incubation at 37 °C with complexes **5-1** – **5-4** and **5-13**.

It is apparent that the gallium compounds do not greatly impact the viability of Cos-7 cells at the highest tested concentration of 100 µM for **5-1** – **5-4** and 10 µM **5-13**, with viabilities ranging from 65 to 84 %. Previous reports of organogallium compounds have shown to minimally effect the viability of mammalian cells, with dimethyl gallium quinolinolates showing IC_{50} values of >100 µM towards Cos-7 cells and dimethyl gallium heterocyclic thiolato with IC_{50} values of >100 µM towards human fibroblast cell lines.[100,112] It must be noted that typical gallium compound assays look at anti-cancer activity, and thus compare cancer and mammalian cell lines after longer incubation times with the compounds such as 96 hours.[112] Gallium is known to be taken up by iron-uptake pathways, so more metabolically-active cancerous cell lines and bacteria will take up gallium faster due to higher iron needs compared with other mammalian cell lines.[97,202] The time point of 24

hours was chosen to be consistent with bacterial assays, however future investigations could look into the effect of longer incubation times.

5.6 Conclusions

A series of novel heteroleptic diphenyl gallium *mono*-phosphinato complexes were synthesised through reaction of phosphinic acids with $GaPh_3$ to afford complexes **5-1** – **5-4** with the general formula $[GaPh_2O(O)PRR']_2$. The *tris*-phosphinato complexes were produced by salt metathesis of $GaCl_3$ with the sodium phosphinate salts to give complexes **5-9** – **5-12** with general formula $[Ga(O(O)PRR')_3]_\infty$. Further synthetic route investigations to form complex **5-11** involved the solvent free reaction of dimethylphosphinic acid with complex **5-3**. Hydrolysis of $GaPh_3$ in DMSO also yielded the phenyl gallium oxido-hydroxido cluster $[Ga_{12}Ph_{12}(\mu_3\text{-}O)_8(\mu\text{-}O)_2(\mu\text{-}OH)_4].4DMSO$ **5-13**. The solid gallium phosphinato complexes were characterised by IR spectroscopy, ^{31}P NMR spectroscopy, TGA and elemental analysis. Complexes **5-1** and **5-4** proved to be mixtures of the expected diphenyl *mono*-phosphinato gallium complexes $[GaPh_2O(O)PRR']_2$ and their hydrolysis product $[Ga_2Ph_2(O(O)PRR')_2O]$, as determined by MS. Compounds **5-2**, **5-3** and **5-13** were structurally authenticated by X-ray crystallography, as well as the *bis*-(*p*-methoxyphenyl)phosphinato hydrolysis product $[Ga_4Ph_4(O(O)P(p\text{-}MeOPh)_2)_4(\mu_3\text{-}O)_2]$.

The crystalline diphenyl gallium *mono*-phosphinato complexes proved to be stable in DMSO up to 24 hours, while complexes **5-1** and **5-4** saw the production of benzene which suggested hydrolysis was occurring. Further examination of complex **5-4** showed that heat promoted the hydrolysis reaction, with greater quantities of benzene produced, as observed by ^1H NMR spectroscopy.

The biological activity of the gallium phosphinato complexes were assessed towards Gram positive and Gram negative bacteria. Solid-state zone of inhibition assays for the poorly soluble homoleptic complexes **5-9** – **5-12** showed activity towards *P. aeruginosa* and complexes **5-9** and **5-11** showed activity towards *A. baumannii*. Solution-based bacterial assays were conducted for complexes **5-1** – **5-4** and the cluster **5-13**, where the determined MIC values towards *P. aeruginosa* are 50 µM for **5-1** and 100 µM for **5-2** and **5-4**, and >100 µM for all other bacteria. Complexes **5-1** – **5-4** and **5-13** were assessed for their cytotoxicity towards Cos-7 cells, where the determined IC_{50} values were greater than the highest examined concentration (100 µM for **5-1** – **5-4** and 10 µM for **5-13**). It can be noted that bacterial growth reduced as the gallium compound concentration increased, which was similarly noted for mammalian cell studies. The gallium phosphinato complexes display antibacterial activity, highlighting their potential as antibacterial agents to combat Gram negative bacteria.

Chapter 6 Summary

Chapter 2

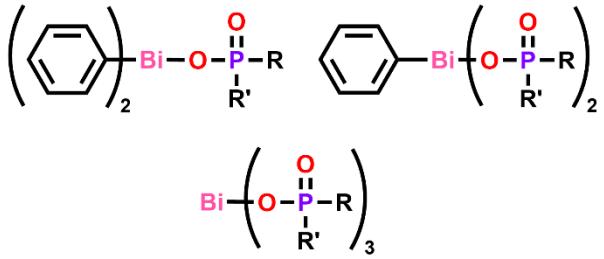

Chapter 3

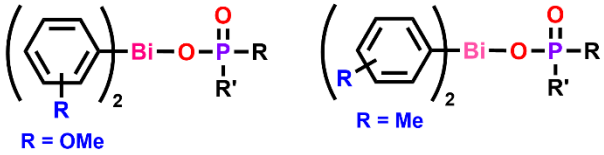

R = OMe

R = Me

Chapter 4

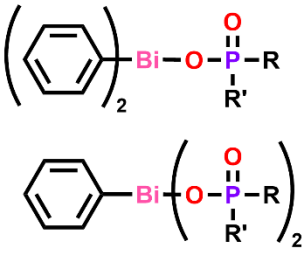

Bi-cellulose composite

Chapter 5

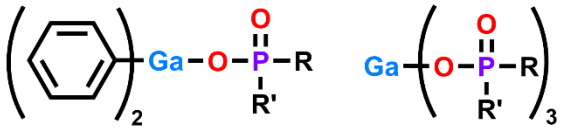

$[Ga_{12}Ph_{12}O_{10}(OH)_4].4DMSO$

6 Summary

Antibacterial resistance remains a global concern, with a need for novel antibacterial agents. In particular, metals and their compounds should be examined given resistance is less commonly observed when compared with natural and synthetic organic compounds. Phosphinato ligand systems were used to investigate the synthesis of hetero- and homoleptic bismuth complexes (Chapter 2), heteroleptic diaryl bismuth complexes (Chapter 3), and hetero- and homoleptic gallium complexes (Chapter 5). Bismuth-cellulose composites were also produced and their properties discussed in Chapter 4. The antibacterial properties of the produced complexes and composites were assessed towards Gram positive (*S. aureus*, MRSA or VRE) and Gram negative bacteria (*E. coli*, *P. aeruginosa* or *A. baumannii*), and their minimum inhibitory concentration (MIC) determined where solubility permitted. Further mammalian cell viability studies were conducted towards Cos-7 monkey kidney cells to determine the concentration to inhibit 50 % growth (IC_{50}), providing an idea of compound cytotoxicity.

In Chapter 2, 12 bismuth phosphinato complexes were synthesised and characterised; 8 novel phenyl bismuth complexes $[BiPh_2O(O)P(H)Ph]_\infty$ **2-1**, $[BiPh_2O(O)PPh_2]_\infty$ **2-2**, $[BiPh_2O(O)PMe_2]_\infty$ **2-3**, $[BiPh_2O(O)P(p\text{-}MeOPh)_2]_\infty$ **2-4**, $[BiPh(O(O)P(H)Ph)_2]_\infty$ **2-5**, $[BiPh(O(O)PPh_2)_2]_\infty$ **2-6**, $[BiPh(O(O)PMe_2)_2]_\infty$ **2-7** and $[BiPh(O(O)P(p\text{-}MeOPh)_2)_2]_\infty$ **2-8**, and 4 homoleptic complexes $[Bi(O(O)P(H)Ph)_3]_\infty$ **2-9**, $[Bi(O(O)PPh_2)_3]_\infty$ **2-10**, $[Bi(O(O)PMe_2)_3]_\infty$ **2-11** and $[Bi(O(O)P(p\text{-}MeOPh)_2)_3]_\infty$ **2-12**, where **2-10** and **2-11** had been previously characterised.[117] Solid-state structures were obtained for the *mono*-phosphinato complexes **2-1** – **2-4**, where it was found that they form 1D coordination polymers. It is also likely that the bismuth *bis*- and *tris*-phosphinato complexes **2-5** – **2-12** exist as polymers due to their generally poor solubility in all solvents. Solution-state solubility studies found that complexes **2-1** – **2-4** were stable up to 24 hours in DMSO. Solid-state zone of inhibition bacterial studies were conducted and showed that the homoleptic complexes **2-9** – **2-12** did not show any antibacterial activity, despite displaying greater water solubility in comparison to the antibacterial heteroleptic complexes. The DMSO soluble complexes **2-1** – **2-4** were further tested for their cytotoxicity towards Cos-7 and human fibroblasts, and their antibacterial activity towards Gram positive and Gram negative bacteria. All complexes exhibited excellent antibacterial activity towards VRE and *E. coli*, however were also cytotoxic towards human fibroblasts more so than Cos-7 cells. It is apparent that the diphenyl bismuth *mono*-phosphinato complexes are non-selectively toxic, which is likely due to their interaction with both mammalian and bacterial cell membranes.

Given the non-selective toxicity of the diphenyl bismuth *mono*-phosphinato complexes, it was of interest to expand on this research and explore different bismuth aryl groups in Chapter 3. Thus a series of 12 novel diaryl bismuth *mono*-phosphinato complexes were synthesised and characterised; 6 *bis*-methoxyphenyl complexes [Bi(*o*-MeOPh)$_2$O(O)P(H)Ph]$_\infty$ **3-1**, [Bi(*o*-MeOPh)$_2$O(O)PPh$_2$]$_\infty$ **3-2**, [Bi(*o*-MeOPh)$_2$O(O)P(*p*-MeOPh)$_2$]$_\infty$ **3-3**, [Bi(*m*-MeOPh)$_2$O(O)P(H)Ph]$_\infty$ **3-4**, [Bi(*m*-MeOPh)$_2$O(O)PPh$_2$]$_\infty$ **3-5**, [Bi(*m*-MeOPh)$_2$O(O)P(*p*-MeOPh)$_2$]$_\infty$ **3-6**, [Bi(*m*-tol)$_2$O(O)P(H)Ph]$_\infty$ and 6 *bis*-tolyl complexes **3-13**, [Bi(*m*-tol)$_2$O(O)PPh$_2$]$_\infty$ **3-14**, [Bi(*m*-tol)$_2$O(O)P(*p*-MeOPh)$_2$]$_\infty$ **3-15**, [Bi(*p*-tol)$_2$O(O)P(H)Ph]$_\infty$ **3-16**, [Bi(*p*-tol)$_2$O(O)PPh$_2$]$_\infty$ **3-17** and [Bi(*p*-tol)$_2$O(O)P(*p*-MeOPh)$_2$]$_\infty$ **3-18**. Attempts were made to synthesise complexes **3-7** – **3-9** ([Bi(*p*-MeOPh)$_2$O(O)PRR']$_\infty$) and **3-10** – **3-12** ([Bi(*o*-tol)$_2$O(O)PRR']$_\infty$) through solvent mediated, solvent free and salt metathesis reactions, however pure complexes could not be isolated in reasonable yields and were not further pursued. Complexes **3-4**, **3-13** and **3-17** were structurally authenticated by X-ray crystallography, proving the formation of 1D coordination polymers as suggested by IR spectroscopy for all of the diaryl bismuth *mono*-phosphinato complexes. The complexes were found to be stable for up to 24 hours in DMSO, thus allowing for their antibacterial and cytotoxicity assessment. It is apparent that the bismuth aryl group influences biological activity, with the *o*-methoxyphenyl complexes **3-1** – **3-3** showing poor antibacterial activity and minimal cytotoxicity towards Cos-7 cells. The *m*-methoxyphenyl series (**3-4** – **3-6**) exhibited the greatest antibacterial activity, showing good selectivity towards the Gram positive bacteria MRSA and VRE over Cos-7 cells. The *bis*-tolyl complexes **3-13** – **3-18** displayed cytotoxicity towards Cos-7 and good antibacterial activity towards MRSA and VRE, with the *p*-tolyl series (**3-16** – **3-18**) proving to be more selective despite greater cytotoxicity compared with the *m*-tolyl complexes. All complexes showed relatively poor antibacterial activity towards Gram negative bacteria.

Chapter 4 examined the potential use of the heteroleptic phenyl bismuth phosphinato complexes as antibacterial additives, where a series of novel Bi-cellulose composites were produced containing complexes [BiPh$_2$O(O)P(H)Ph]$_\infty$ **2-1**, [BiPh$_2$O(O)PPh$_2$]$_\infty$ **2-2**, [BiPh$_2$O(O)PMe$_2$]$_\infty$ **2-3**, [BiPh$_2$O(O)P(*p*-MeOPh)$_2$]$_\infty$ **2-4**, [BiPh(O(O)P(H)Ph)$_2$]$_\infty$ **2-5**, [BiPh(O(O)PPh$_2$)$_2$]$_\infty$ **2-6**, [BiPh(O(O)PMe$_2$)$_2$]$_\infty$ **2-7** and [BiPh(O(O)P(*p*-MeOPh)$_2$)$_2$]$_\infty$ **2-8**. Given the extensive use of silver in consumer products, composites containing silver sulfadiazine (**Ag**) were also produced for comparison. The metal content of the composites were determined by ICP-OES, and the morphology and dispersion of bismuth compounds on the surface examined by SEM. The leaching properties of composites with loadings between 1.12 and 5.32 wt% were investigated in water, where both phenylphosphinato-containing complexes **2-1** and **2-5** displayed the highest leaching

levels at 15 and 24 % respectively. The leachates were assessed for their antibacterial activity and cytotoxicity, where only the concentrated leachates exerted an effect. The aqueous leachates containing complexes **2-1** and **2-5** were bacteriostatic towards MRSA and VRE and bactericidal towards *E. coli* at 4.3 and 4.5 μM respectively. Cos-7 cells were not as effected by the leachates as human fibroblast cells, where Cos-7 had a viability of 70 % at 3.3 μM **2-5** compared with the 2 % viability of human fibroblast cells. The **Ag** leachate also exerted an effect on human fibroblasts at 1.7 μM, reducing cell viability to 80 %. While the heteroleptic bismuth compounds are non-selectively toxic, this study highlighted that simple changes in the phosphinato moiety greatly impacted the interaction of the complexes within a cellulosic matrix. Furthermore, this method of incorporation could allow for the biological assessment of other poorly soluble metal compounds as antibacterial materials.

Chapter 5 described the synthesis and characterisation of a series of gallium phosphinato complexes $[GaPh_2O(O)P(H)Ph]_2$ **5-1**, $[GaPh_2O(O)PPh_2]_2$ **5-2**, $[GaPh_2O(O)PMe_2]_2$ **5-3**, $[GaPh_2O(O)P(p\text{-}MeOPh)_2]_2$ **5-4**, $[Ga(O(O)P(H)Ph)_3]_\infty$ **5-9**, $[Ga(O(O)PPh_2)_3]_\infty$ **5-10**, $[Ga(O(O)PMe_2)_3]_\infty$ **5-11** and $[Ga(O(O)P(p\text{-}MeOPh)_2)_3]_\infty$ **5-12**. Complexes **5-1** and **5-4** were not pure, with their hydrolysis product $[Ga_2Ph_2(O(O)PRR')_2O]$ present in the mixture. Hydrolysis of $GaPh_3$ yielded a phenyl gallium oxido-hydroxido cluster $[Ga_{12}Ph_{12}(\mu_3\text{-}O)_8(\mu\text{-}O)_2(\mu\text{-}OH)_4]$.4DMSO **5-13** which was structurally authenticated by X-ray crystallography, as were the dimeric complexes **5-2** and **5-3**, and the hydrolysis product of **5-4**, $[Ga_4Ph_4(O(O)P(p\text{-}MeOPh)_2)_4(\mu_3\text{-}O)_2]$. Solid-state zone of inhibition assays were conducted on the poorly soluble *tris*-phosphinato complexes, where antibacterial activity was exhibited towards *P. aeruginosa* (complexes **5-9** – **5-12**) and *A. baumannii* (complexes **5-9** and **5-11**). Solution-based antibacterial assays were conducted on complexes **5-1** – **5-4** and cluster **5-13** and the MICs were determined as greater than 100 μM (10 μM **5-13**) for all bacteria except *P. aeruginosa* (MIC 50 μM **5-1** and 100 μM **5-2** and **5-4**). Organogallium compounds have not been extensively studied as antibacterial agents, so this highlights the potential of diphenyl gallium phosphinato complexes to combat Gram negative bacteria. The mammalian cell viability was also assessed towards Cos-7 and the determined IC_{50} values were greater than 100 μM for **5-1** – **5-4** and greater than 10 μM for **5-13**. Given the known role of gallium in the inhibition of iron uptake, it is important to investigate the influence of iron concentration on gallium compound activity towards bacteria and mammalian cells. It would also be of interest to study the effect that the presence of serum (such as FBS) has on both the stability and antibacterial activity of the diphenyl gallium phosphinato complexes.

Overall, this study shows that the antibacterial activity of bismuth phosphinato complexes can be tuned based on the ligands, where simple changes of the phosphinato moiety or the aryl bismuth group can have a significant effect. Typically, more lipophilic compounds have greater membrane permeability and thus exert greater toxicity. This statement holds true for the phosphinato moiety, with the more lipophilic diphenylphosphinato-containing complexes usually showing higher antibacterial activity and cytotoxicity. Interestingly, changing the bismuth-bound aryl groups demonstrated the largest effect on antibacterial activity. The diphenyl bismuth complexes showed the greatest activity towards *E. coli*, while the *m*-methoxyphenyl complexes were the most active towards the Gram positive bacteria and displayed lower cytotoxicity towards Cos-7 cells. This highlights the importance of further research into heteroleptic bismuth complexes as potential antibacterial agents. A greater understanding into the mechanism of action is also needed to further assist in fine tuning the structural chemistry of bismuth complexes.

Chapter 7 Experimental

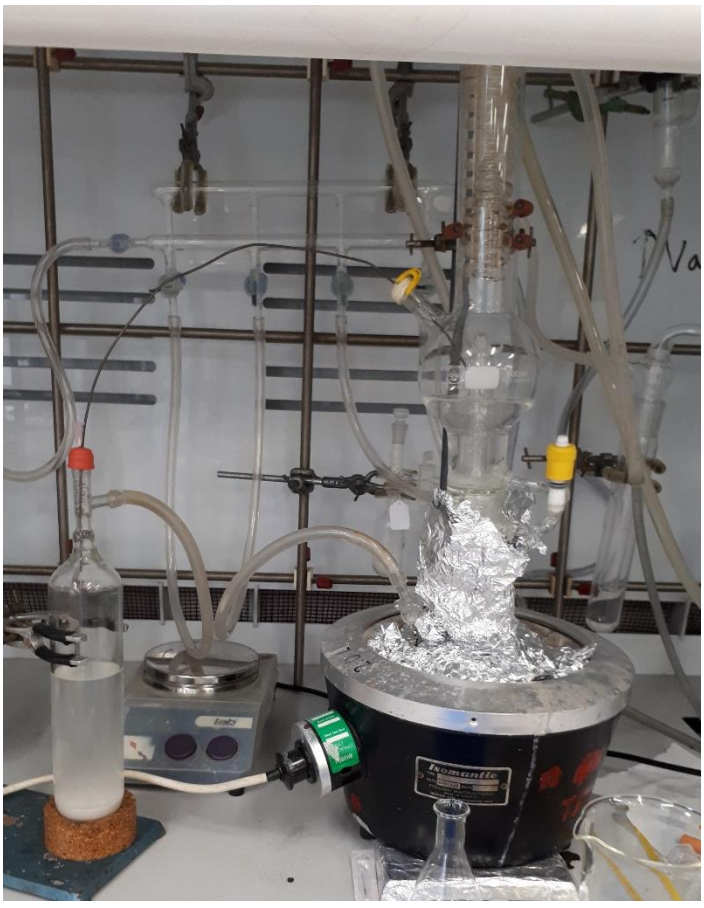

7 Experimental

7.1 General

All compounds have been named using the IUPAC convention for nomenclature of organic and metal compounds. The appropriate numbering system classified in the schemes of each substance was not used in agreement with IUPAC convention, for practical reasons.

7.2 Instrumentation

^{1}H NMR and ^{31}P NMR spectra were recorded on Bruker Avance DPX400 (400 MHz). All chemical shifts were recorded on the δ scale in parts per million (ppm) and referenced to the appropriate deuterated solvent (d_1-chloroform ($CDCl_3$) δ = 7.26 ppm, d_6-dimethyl sulfoxide (d_6-DMSO) δ = 2.50 ppm, deuterium oxide (D_2O) δ = 4.79 ppm and d_6-benzene (C_6D_6) δ = 7.16 ppm) for ^{1}H NMR or externally referenced to H_3PO_4 for ^{31}P NMR. Signals were reported using the following format: chemical shift (δ ppm) (integration, multiplicity and assignment). Multiplicities have been designated as singlet (s), doublet (d), doublet of doublets (dd), triplet (t) or multiplet (m).

Solid-state ^{13}C NMR and ^{31}P NMR was conducted on a BRUKER ADVANCE 300 and recorded using cross polarisation with magic angle spinning (CP-MAS) or high-power decoupling with magic angle spinning (HPDEC-MAS) respectively. Chemical shifts (δ) were recorded in the scale of parts per million (ppm) and referenced externally to glycine (^{13}C) or ammonium phosphate (^{31}P).

Infrared spectra were recorded using a range of 4000-600 cm^{-1} on an Agilent Technologies Cary 630 FTIR spectrometer. The frequencies are reported as wavenumbers (cm^{-1}) with qualitative intensities reported as strong = s, medium = m, weak = w, shoulder= sh and broad = b. High resolution electrospray ionisation mass spectrometry (ESI-MS) was obtained for complexes **5-1** and **5-4** using a Micromass Platform QMS spectrometer, with an electrospray source and a cone voltage of 35 eV. Ultraviolet-visible (UV-Vis) spectra were obtained on an Agilent Cary 60 UV-Vis spectrophotometer scanning in the range 200 to 750 nm.

Differential scanning calorimetry (DSC) was performed using a DSC Q100 Thermogravimetric Analyser. The materials were ground together and 5 mg to 10 mg of this mixture was placed in an aluminium pan. This was heated from 30 °C to 250 °C using a ramp of 10 °C/minute. Combined thermogravimetric analysis (TGA) and differential scanning calorimetry (DSC) were carried out using a Mettler Toledo TGA/DSC 1 Star System with heating up to 500 °C.

Elemental microanalyses were performed on a Perkin Elmer 2400 Series II CHNS/O Elemental Analyser within the Department of Chemistry, Monash University (Clayton, Australia), or through The Campbell Microanalytical Laboratory, Department of Chemistry, University of Otago (Dunedin, New Zealand).

Bismuth, silver and mercury analyses were conducted using either a PerkinElmer Avio 200 ICP-OES (measuring Bi at 223.06 nm and Ag at 328.068 nm) or a PerkinElmer NexION 350 ICP-MS (measuring Bi at 208.98 amu, Ag at 106.905 amu and Hg at 200.59 amu). ICP-OES samples were prepared through digestion in 70 % wt/wt nitric acid, followed by dilution with 3 % wt/wt nitric acid in ultrapure water. Cellulose composite analysis was conducted following ashing of the cellulose in a furnace at 600 °C for 3 hours, where the resulting residue was digested in 70 % wt/wt nitric acid and diluted using 3 % wt/wt nitric acid. ICP-MS samples were typically water-based samples (such as leachates) that were diluted to give a final nitric acid content of 5 % wt/wt. Raw count rates from the analyses were externally standardised by means of a calibration curve constructed using a commercially available Bi stock solution, the Instrument Calibration Standard 2 (containing Ag, part number N9301721) or Hg stock solution (part number N9300253). For ICP-MS an internal standard of 80 ppb Pb was used for Bi analysis, Ag analysis used an internal standard of 20 ppb Rh and Hg analysis used 20 ppb Tb as the internal standard. Precision is of the order of 3.2 % RSD from the single analyses. The final % Bi calculation was averaged from three replicates and total error calculated with the following equation: $\sqrt{(weighing\ error)^2 + (instrument\ error)^2 + (RSD)^2}$ which is shown as a plus or minus (±) value. The final wt% Bi or wt% Ag calculation was averaged from three samples and sample standard deviation was calculated.

Samples analysed by scanning electron microscopy (SEM) were mounted, using carbon adhesive discs, onto an SEM specimen stub and coated with iridium. Analyses were carried out on a JEOL JSM-7001F FEGSEM fitted with a retractable backscattered-electron detector. Samples were studied using 15 kV accelerating voltage.

Crystallographic data was collected on one of the following: Bruker X8 APEXII CCD diffractometer equipped with an OXFORD Cryosystems 700 Cryostream and cooled to 123(1) K. Data was collected with monochromatic (graphite) MoK_α radiation (λ = 0.71073 Å) and processed using the Bruker Apex2 v2014.7-1 software.[203] OXFORD Gemini Ultra equipped with an OXFORD Cryosystems 700 Cryostream and cooled to 123.00(13) K. Data was collected with monochromatic (graphite) CuK_α (λ = 1.54184 Å) and processed using the CrysAlisPro v 1.171.34.36 software.[204] OXFORD XtaLAB Synergy Dualflex, HyPix diffractometer equipped with an OXFORD 700

Cryostream and cooled to 123(1) K. Data was collected with monochromatic (graphite) CuK_α (λ = 0.71073) or MoK_α (λ = 0.71070) and processed using CrysAlisPro v 1.171.40.53 software. Lorentz, polarisation and absorption corrections (multi-scan – SADABS)[205] were applied. MX1 beamline at the Australian Synchrotron, Melbourne, Victoria, with synchrotron radiation (17.4 keV, λ = 0.71073 Å).[206] Data was collected at 100(1) K, maintained using an open flow of nitrogen. XDS was used for data collection and reduction of data.[207] Multi-scan absorption corrections (SADABS) were applied.[208] All compounds were solved and refined with SHELX-2016[209] and Olex2.[210] A summary of crystallographic data can be found under the experimental data of each complex.

7.3 Biological testing

7.3.1 Bacteria preparation

S. aureus (A134/ATCC6538), MRSA (M118797, methicillin-resistant *S. aureus*) and VRE (M846910, vancomycin-resistant *E. faecalis*) were grown in BHI (Brain Heart Infusion) media (Oxoid), *E. coli* (G102), *P. aeruginosa* (ATCC27853) and *A. baumannii* (C403/ATCC17978) were grown in LB (Luria-Bertani) broth. Bacteria from glycerol stocks were streaked onto agar (Nutrient agar or LB agar) overnight at 37 °C and subsequently a single colony was inoculated into 3 mL of broth (BHI or LB) and incubated overnight at 37 °C and 180 rpm to give turbid overnight cultures.

7.3.1.1 Zone of inhibition assay

Nutrient agar was spread with 80 µL overnight cultures for *S. aureus*, MRSA or VRE, while LB agar was used for *E. coli* or *P. aeruginosa*. A small amount of solid complex was added to the agar plate pre-spread with bacterial culture and incubated at 37 °C overnight. Similarly, for the Bi-cellulose composites, discs were taken from the papers and placed onto the agar plate before overnight incubation at 37 °C. Zones of inhibition were measured around the solid compound or discs with a ruler. These tests were carried out in triplicate for each bacterial line.

7.3.1.2 Minimum inhibitory concentration determination

7.3.1.2.1 Visual method

Complexes **2-1** – **2-4** and their respective phosphinic acids were solubilised in DMSO at 1 mM and 10 mM respectively. The stocks were first diluted in sterile water, then broth to give a maximum concentration of 10 µM for the complexes or 100 µM for the phosphinic acids. This was further diluted in broth (BHI or LB) to give a concentration range of 0.313 to 10 µM or 25 to 100 µM. Overnight bacterial cultures were diluted to approximately 10^6 CFU/mL in BHI or LB broth, before

addition to the complexes and incubated at 37 °C for 20 hours. MIC values were determined by visual examination and recorded as the minimum concentration to inhibit growth. Experiments were independently conducted at least three times including controls of untreated broth to show no growth.

7.3.1.2.2 Absorbance method

DMSO stocks were similarly prepared for complexes **3-1** – **3-6**, **3-13** – **3-18**, **5-1** – **5-4** and **5-13** and triaryl bismuth precursors in the range of 1 to 10 mM, depending on their DMSO solubility. All stocks were diluted in sterile water then either BHI or LB broth in 96 well plates, giving a maximum concentration range of 10 to 100 µM. This was serially diluted by a factor of two with a total of 100 µL/well. Overnight bacterial cultures were diluted to approximately 10^4 CFU/mL in broth before the addition of 5 µL to each well and incubation at 37 °C for 20 hours. Bacterial growth was determined by absorbance readings at 600 nm using a BMG-Labtech ClarioStar microplate reader. A positive control of no compound was treated as 100 % growth and the broth alone was the negative control. MIC values were determined as the concentration that inhibited ≥80 % growth (growth was ≤20 %) from a minimum of three independent experiments.

7.3.1.3 Leachate assay

Bacterial killing assays were conducted using leachates **2-1** – **2-8** and **Ag** after overnight soaking in water at 25 °C. Overnight bacterial cultures were diluted to approximately 10^6 CFU/mL in BHI or LB broth, before addition of the composite's leachate in a 3:1 ratio of broth to leachate and incubated at 37 °C for 20 hours. Bacterial survivors were determined by plating serial dilutions in PBS on to agar (Nutrient agar for Gram positive and LB agar for Gram negative). After 24 hours incubation of the agar plates at 37 °C, the number of viable colonies was used to determine the CFU/mL of survived bacteria. Experiments were independently conducted at least three times, including controls of water in media and media without additives.

7.3.2 Cell culture

Cos-7 and human dermal fibroblasts were cultured and maintained in DMEM supplemented with 10% FBS, 1% Pen-Strep and 1% Glutamax (purchased from Gibco™) at 37 °C in a 5 % CO_2 incubator.[135] Cos-7 cultured for the CytoTox-ONE ™ Homogeneous Membrane Integrity Assay were maintained in DMEM without pyruvate, supplemented with 5 % FBS, 1 % Pen-Strep and 1% Glutamax at 37 °C in a 5 % CO_2 incubator.

7.3.2.1 *In vitro* testing towards Cos-7 and human fibroblasts

CellTiter-Blue Cell Viability Assay was purchased from Promega ™, and used for the determination of the percentage viability of Cos-7 and human fibroblast cells. Compounds and their respective triaryl bismuth or phosphinic acid precursor were solubilised in DMSO to make up a working stock in the range of 1 to 10 mM and sequentially diluted out in the appropriate culture media. Leachate assays were tested at the maximum concentration with 25 µL leachate added to media to total 100 µL (100 µL added to total 400 µL when using 24 well plates). Assays were set up in duplicate in Falcon 96 well plates or 24 well plates for leachate assays. Volumes of 10^5 Cos-7/mL and 10^5 fibroblasts/mL were seeded and adhered to 96 well plates 24 hours prior to compound addition (2.5 x 10^5 cells/mL for 24 well plates). 20 hours after compound addition, 20 µL of CellTiter-Blue was added to each well in the 96 well plates, or 80 µL to the 24 well plates, then incubated for a further 4 hours to total 24 hour incubation with compound. All cell assays were measured spectroscopically using fluorescence excitation at 544 nm and emission at 590 nm. The compounds were compared to a positive control of no drug and the percent inhibition calculated.[80] Fluorescence measurements were conducted on a BMG-Labtech ClarioStar microplate reader. Experiments were conducted independently at least three times, with values averaged between the experiments. IC_{50} values were determined using GraphPad Prism 8.

7.3.2.2 Cytotoxicity assay

CytoTox-ONE ™ Homogeneous Membrane Integrity Assay was purchased from Promega ™, and used for the determination of % cytotoxicity of Cos-7 cells. Complex **2-1** was solubilised in DMSO to make up 1 mM working stock and diluted to 8, 4 and 2 µM. $BiPh_3$ and phenylphosphinic acid were solubilised in DMSO at 10 mM and diluted to give 100 µM, along with a DMSO control. Cos-7 cells were seeded at 10^4 cells/well and allowed to adhere overnight. Samples including the DMSO control were incubated for 24 hours, with negative control containing media with no cells and a positive control which was treated with Lysis Solution (0.18 % Triton) 4 hours prior to reading as the maximum LDH release control. CytoTox-ONE ™ reagent was added after 24 hours and incubated at room temperature for 10 minutes before addition of the Stop Solution. The cells were measured spectroscopically using fluorescence excitation at 544 nm and emission at 590 nm on a BMG-Labtech ClarioStar microplate reader. The compounds were compared to a positive control of lysed cells and the percent cytotoxicity calculated. The experiment was independently run at least three times in quadruplicate, with the cytotoxicity values averaged over all experiments.

7.4 Reagents and solvents

Diethyl ether (Et_2O), tetrahydrofuran (THF), toluene and dichloromethane (DCM) were dried using a MBRAUN SPS-800 solvent purification system and stored over 4 Å molecular sieves under nitrogen. Methanol was distilled over CaH_2 and stored under nitrogen over molecular sieves (3 Å). *N*-pentane was distilled over Na metal and stored over 4 Å molecular sieves under nitrogen. All other laboratory reagents and solvents were purchased from Merck, Sigma-Aldrich and Oakwood Chemical.

7.5 Schlenk protocol

Reactions requiring anhydrous conditions were conducted in oven dried glassware under an atmosphere of dry nitrogen using a vacuum/nitrogen line and Schlenk techniques. All glassware was dried at 105 °C for approximately 24 hours prior to use and allowed to cool under vacuum to reduce moisture content. Flasks were placed under high vacuum to purge moisture and air and backfilled with nitrogen in triplicate. Solvents and reagents were transferred through rubber seals using oven dried and nitrogen purged syringes or cannulas. Solid reagents were typically placed under vacuum for a minimum of one hour with stirring to remove moisture. Filtering of solutions was conducted through rubber seals using oven dried and nitrogen purged cannulas with glass microfiber filters (GF/A, circles ø 42.5 mm, Whatman®) fixed with Teflon tape.

7.6 Precursor synthesis

7.6.1 Synthesis of triaryl bismuth

The general synthetic route to form triaryl bismuth compounds is through Grignard metathesis reaction with $BiCl_3$ and the respective ArMgBr under inert conditions. $BiCl_3$ is collected into a three-neck flask equipped with magnetic stirrer bar, dropping funnel and Schlenk tap. The $BiCl_3$ is suspended in dry Et_2O prior to cooling to 0 °C in an ice bath, in preparation for the addition of the metathesis reagent (Grignard or aryl-lithium) via dropping funnel. Following the slow addition, the reaction is stirred overnight before quenching over ice and subsequent recrystallisation of the precipitate with hot ethanol or acetone.

Synthesis of the ArMgBr was necessary when the Grignard was not commercially available. The synthesis involved stirring magnesium metal (3.1 equivalents) in a three-neck flask equipped with magnetic stirrer bar, dropping funnel, condenser and Schlenk tap. The apparatus was placed under vacuum and backfilled with nitrogen in triplicate before addition of dry THF. The appropriate aryl

bromide (3 equivalents) was added dropwise via dropping funnel as a dilute solution in dry THF. Upon stirring, heat was generated and the solution was allowed to self-reflux for approximately 1 hour, where a dark coloured solution was produced. This solution was transferred to a dropping funnel via filter cannula to be added to $BiCl_3$ as above.

7.6.1.1 Triphenyl bismuth [$BiPh_3$]

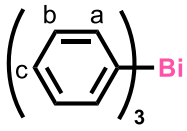

One equivalent of $BiCl_3$ (14.59 g, 44 mmol) and three equivalents of PhMgBr (132 mL, 1.0 M solution in THF) were reacted as per Section 7.6.1 and recrystallised from hot ethanol to afford 12.80 g, 66 % yield $BiPh_3$. m.p: 79 - 81 °C (Lit. 78 - 80 °C).[211] ^{1}H NMR (400 MHz, d6-DMSO) δ = 7.74 (6H, d, H^a), 7.40 (6H, t, H^b), 7.32 (3H, t, H^c). IR (cm^{-1}) 3057 m, 3035 m, 1566 s, 1425 s, 994 s, 720 s.

7.6.1.2 *Tris*-(*o*-methoxyphenyl) bismuth [Bi(*o*-MeOPh)$_3$]

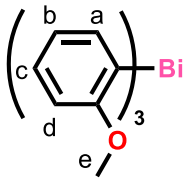

Three equivalents of anisole (5.2 mL, 48 mmol) and ^{n}BuLi (31 mL, 1.6 M solution in hexanes) were reacted at -78 °C in THF before their dropwise addition to $BiCl_3$ (5.00 g, 16 mmol) as per Section 7.6.1, then recrystallised from hot acetone to afford 5.861 g, 70 % yield Bi(*o*-MeOPh)$_3$. m.p: 163 - 164 °C (Lit. 167 °C).[212] ^{1}H NMR (400 MHz, d_6-DMSO) δ = 7.34 (3H, m, H^c), 7.25 (3H, dt, H^a), 7.12 (3H, dd, H^d), 6.85 (3H, m, H^b), 3.72 (9H, s, H^e). IR (cm^{-1}) 3051 w, 2956 w, 1567 s, 1456 s, 1426 s, 1267 s, 1221 s, 1112 s, 1048 s, 1016 s, 751 s.

7.6.1.3 *Tris*-(*m*-methoxyphenyl) bismuth [Bi(*m*-MeOPh)$_3$]

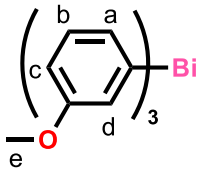

The Grignard *m*-MeOPhMgBr was prepared with magnesium metal (1.32 g, 54 mmol), 1,2-bromoethane (0.5 mL) and 3-bromoanisole (6.2 mL, 49 mmol), which was added to one equivalent of $BiCl_3$ (5.02 g, 16 mmol) and reacted as per Section 7.6.1 then recrystallised from hot acetone to afford 2.05 g, 24 % yield Bi(*m*-MeOPh)$_3$. m.p: 91 – 92 °C. ^{1}H NMR (400 MHz, d_6-DMSO) δ = 7.34 (6H, m, $H^{a,d}$), 7.27 (3H, dt, H^c), 6.86 (3H, m, H^b), 3.66 (9H, s, H^e). IR (cm^{-1}) 3048 w, 2968 m, 1574 s, 1466 s, 1222 s, 1026 s, 987 s, 792 s.

7.6.1.4 *Tris*-(*p*-methoxyphenyl) bismuth [Bi(*p*-MeOPh)$_3$]

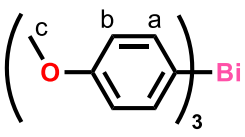

One equivalent of $BiCl_3$ (5.00 g, 16 mmol) and 3.1 equivalents of *p*-MeOPhMgBr (100 mL, 0.5 M solution in THF) were reacted as per Section 7.6.1 and recrystallised from hot acetone to afford 4.30 g, 51 % yield $BiPh_3$. m.p: 193 – 195 °C (Lit. 190 °C).[211] ^{1}H NMR (400 MHz, d6-DMSO) δ = 7.56 (6H, d, H^a), 6.94 (6H, d,

H^b), 3.72 (9H, s, H^c). IR (cm^{-1}) 3007 w, 2965 w, 1574 s, 1561 s, 1484 s, 1435 s, 1276 s, 1230 s, 1174 s, 1023 s, 999 m, 815 s, 783 s.

7.6.1.5 *Tris*-(*o*-tolyl) bismuth [Bi(*o*-tol)$_3$]

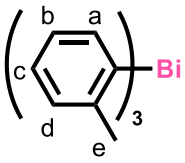

The Grignard *o*-tolMgBr was prepared with magnesium metal (1.63 g, 67 mmol) and 2-bromotoluene (8.0 mL, 67 mmol), which was added to one equivalent of $BiCl_3$ (7.00 g, 22 mmol) and reacted as per Section 7.6.1 then recrystallised from hot acetone to afford 6.00 g, 57 % yield Bi(*o*-tol)$_3$. m.p: 126 – 129 °C (Lit. 131 – 132 °C).[213] ^{1}H NMR (400 MHz, d_6-DMSO) δ = 7.43 (3H, dd, H^a), 7.37 (3H, d, H^d), 7.28 (3H, td, H^b), 7.08 (3H, t, H^c), 2.38 (9H, s, H^e). IR (cm^{-1}) 3051 w, 2965 w, 1578 m, 1445 s, 1266 m, 1201 m, 1114 m, 1016 m, 747 s, 736 s.

7.6.1.6 *Tris*-(*m*-tolyl) bismuth [Bi(*m*-tol)$_3$]

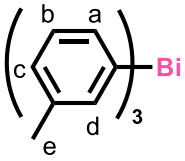

The Grignard *m*-tolMgBr was prepared with magnesium metal (1.01 g, 42 mmol) and 3-bromotoluene (4.2 mL, 35 mmol), which was added to one equivalent of $BiCl_3$ (3.38 g, 11 mmol) and reacted as per Section 7.6.1 then recrystallised from hot ethanol to afford 1.47 g, 28 % yield Bi(*m*-tol)$_3$. m.p. 74 – 75 °C (Lit. 65 °C).[214] ^{1}H NMR (400 MHz, d_6-DMSO) δ = 7.57 (3H, s, H^d), 7.48 (3H, d, H^a), 7.28 (3H, t, H^b), 7.11 (3H, d, H^c), 2.23 (9H, s, H^e). IR (cm^{-1}) 3037 w, 2981 m, 1581 s, 1560 s, 1465 m, 1376 m, 1097 s, 1000 s, 984 s, 771 s, 691 s.

7.6.1.7 *Tris*-(*p*-tolyl) bismuth [Bi(*p*-tol)$_3$]

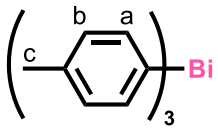

The Grignard *p*-tolMgBr was prepared with magnesium metal (3.5 g, 144 mmol) and 4-bromotoluene (15.4 mL, 125 mmol), which was added to one equivalent of $BiCl_3$ (13.14 g, 42 mmol) and reacted as per Section 7.6.1 then recrystallised from hot ethanol to afford 9.35 g, 47 % yield Bi(*p*-tol)$_3$. m.p: 118 – 120 °C (Lit. 119 – 120 °C).[211] ^{1}H NMR (400 MHz, d_6-DMSO) δ = 7.57 (6H, d, H^a), 7.18 (6H, d, H^b), 2.25 (9H, s, H^c). IR (cm^{-1}) 3035 w, 2916 w, 1486 s, 1385 s, 1051 m, 1010 s, 787 s.

7.6.2 Synthesis of diaryl bismuth chloride

The general synthetic route to form diaryl bismuth chloride utilises the redistribution reaction between 2.0 equivalents of triaryl bismuth and 1.0 equivalents of $BiCl_3$. The reaction is conducted under inert conditions in dry diethyl ether, where the resulting suspension is stirred for one hour, then washed with further diethyl ether and dried *in vacuo* to afford the diaryl bismuth chloride.

7.6.2.1 Diphenyl bismuth chloride [$BiPh_2Cl$]

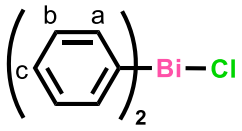

$BiPh_3$ (2.943 g, 6.68 mmol) and $BiCl_3$ (1.061 g, 3.36 mmol) were reacted as per Section 7.6.2 to afford 2.989 g (75 % yield) of $BiPh_2Cl$. m.p: 185 – 186 °C (Lit. 184 – 185 °C).[215] ^{1}H NMR (400 MHz, d_6-DMSO): δ = 8.33 (4H, d, H^a), 7.62 (4H, t, H^b), 7.34 (2H, t, H^c).

7.6.2.2 *Bis*-(*p*-methoxyphenyl) bismuth chloride [Bi(*p*-MeOPh)$_2$Cl]

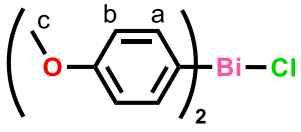

Bi(*p*-MeOPh)$_3$ (1.222 g, 2.30 mmol) and $BiCl_3$ (0.363 g, 1.15 mmol) were reacted as per Section 7.6.2 to afford 1.220 g (77 % yield) of Bi(*p*-MeOPh)$_2$Cl. m.p: 163 – 164 °C (Lit. 158 – 159 °C).[152] ^{1}H NMR (400 MHz, d_6-DMSO): δ = 8.16 (4H, d, H^a), 7.13 (4H, d, H^b), 3.74 (6H, s, H^c).

7.6.3 Synthesis of bismuth *tris*-(*tert*-butoxide) [Bi(O^{t}Bu)$_3$][216]

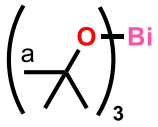

Sublimed $BiCl_3$ (10.26 g, 32.5 mmol) and three equivalents of KO^{t}Bu (10.96 g, 97.6 mmol) were combined at 0 °C in dry THF with the exclusion of light. The resulting suspension was stirred for 16 hours at room temperature before the solvent was removed *in vacuo*. The residue was extracted with *n*-pentane using a Soxhlet extractor, then concentrated *in vacuo* to afford a pale yellow solid in 56 % yield (7.80 g). ^{1}H NMR (400 MHz, d_6-DMSO): δ = 1.43 (27H, s, H^a).

7.6.4 Synthesis of triphenyl gallium [$GaPh_3$][195]

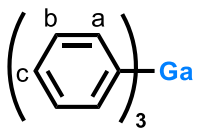

Ga metal (1.31 g, 18.8 mmol) and $HgPh_2$ (9.52 g, 26.8 mmol) were combined under inert conditions and heated at 170 °C for 5 hours with stirring. The resulting solid was washed with toluene and cannulated to a fresh Schlenk to remove Hg, then concentrated *in vacuo* to afford an off-white solid in 60 % yield (3.23 g). ^{1}H NMR (400 MHz, d_6-DMSO): δ = 7.58 (6H, m, H^a), 7.27 (9H, m, $H^{b,c}$).

7.6.5 Synthesis of phosphinato sodium salts

The general synthetic route to form phosphinato sodium salts is through reaction of sodium hydroxide with the respective phosphinic acid in methanol. The solution is stirred overnight before removing the solvent *in vacuo* and isolating the solid phosphinato sodium salts.

7.6.5.1 Phenylphosphinato sodium salt $Na^+O^-(O)P(H)Ph$

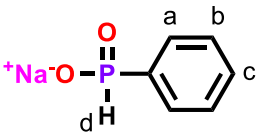

Phenylphosphinic acid (1.075 g, 7.6 mmol) and sodium hydroxide (0.303 g, 7.6 mmol) were reacted in accordance with Section 7.6.5 to afford a white solid in 99 % yield (1.228 g). ^{1}H NMR (400 MHz, d_6-DMSO): δ = 7.96 (2H, m, H^a), 7.37 (1H, d, $^1J_{P-H}$ = 472 Hz, H^d), 7.32 (3H, m, $H^{b,c}$). ^{31}P NMR (400 MHz, d_6-DMSO): δ = 6.68 ppm. IR (cm^{-1}): 3050 w (P-Ph), 2395 w (P-H), 1591 m, 1435 m (P-Ph), 1196 s $\nu_{asym}(PO_2)$, 1046 s $\nu_{sym}(PO_2)$, 983 s (P-H), 738 s (P-Ph).

7.6.5.2 Diphenylphosphinato sodium salt $Na^+O^-(O)PPh_2$

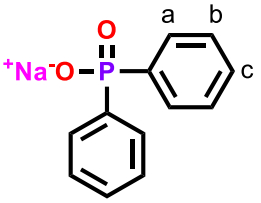

Diphenylphosphinic acid (0.654 g, 3.0 mmol) and sodium hydroxide (0.120 g, 3.0 mmol) were reacted in accordance with Section 7.6.5 to afford a white solid in 92 % yield (0.663 g). ^{1}H NMR (400 MHz, d_6-DMSO): δ = 7.62 (4H, m, H^a), 7.21 (6H, m, $H^{b,c}$). ^{31}P NMR (400 MHz, d_6-DMSO): δ = 10.20 ppm. IR (cm^{-1}): 3061 w (P-Ph), 1591 w (P-Ph), 1436 m, 1190 s $\nu_{asym}(PO_2)$, 1123 s, 1037 s $\nu_{sym}(PO_2)$, 998 m, 751 m (P-Ph).

7.6.5.3 Dimethylphosphinato sodium salt $Na^+O^-(O)PMe_2$

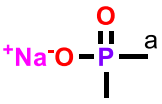

Dimethylphosphinic acid (0.560 g, 6.0 mmol) and sodium hydroxide (0.238 g, 6.0 mmol) were reacted in accordance with Section 7.6.5 to afford a white solid in 98 % yield (0.680 g). ^{1}H NMR (400 MHz, d_6-DMSO): δ = 0.84 (6H, d, H^a). ^{31}P NMR (400 MHz, d_6-DMSO): δ = 22.15 ppm. IR (cm^{-1}): 3182 w, 2981 w, 2916 w, 1428 m, 1294 s (P-Me), 1165 s $\nu_{asym}(PO_2)$, 1063 s $\nu_{sym}(PO_2)$, 849 s (P-Me), 724 s, 694 m.

7.6.5.4 *Bis*-(*p*-methoxyphenyl)phosphinato sodium salt $Na^+O^-(O)P(p\text{-}MeOPh)_2$

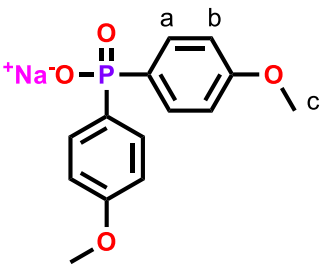

Bis-(*p*-methoxyphenyl)phosphinic acid (0.580 g, 2.1 mmol) and sodium hydroxide (0.083 g, 2.1 mmol) were reacted in accordance with Section 7.6.5 to afford a white solid in 82 % yield (0.511 g). ^{1}H NMR (400 MHz, d_6-DMSO): δ = 7.52 (4H, m, H^a), 6.76 (4H, m, H^b), 3.69 (6H, s, H^c). ^{31}P NMR (400 MHz, d_6-DMSO): δ = 10.37 ppm. IR (cm^{-1}): 3010 w (P-Ph), 2835 w, 1596 m, 1500 m (P-Ph), 1464 m, 1253 (O-Me), 1165 s $\nu_{asym}(PO_2)$, 1057 m (O-Me), 1026 s $\nu_{sym}(PO_2)$, 818 m, 798 s.

7.7 Phenyl bismuth phosphinato complexes

7.7.1 General procedure 1 (GP1)

All reactions were conducted using 1.0 equivalents of $BiPh_3$ and 1.1 or 2.1 equivalents of phosphinic acid to yield the diphenyl bismuth or phenyl bismuth phosphinate complexes respectively. Crystalline $BiPh_3$ and the phosphinic acid were placed in a round bottom flask equipped with magnetic stirrer bar. The solvent (ethanol or DMSO) was added and the flask heated (unless otherwise stated) overnight, yielding a precipitate. The precipitate was collected by gravimetric filtration and washed with hot ethanol and diethyl ether to remove any unreacted reagents prior to air drying.

7.7.1.1 Diphenyl *mono*-phenylphosphinato bismuth $[BiPh_2O(O)P(H)Ph]_\infty$, 2-1

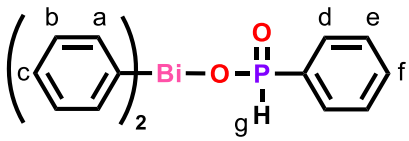

$BiPh_3$ (0.238 g, 0.54 mmol) and phenylphosphinic acid (0.083 g, 0.58 mmol) were reacted in accordance with GP1 using ethanol as the solvent and stirring overnight at room temperature to afford a white precipitate in 70 % yield (0.19 g). m.p. 158 °C. ^{1}H NMR (400 MHz, d_6-DMSO): δ = 8.25 (4H, d, H^a), 7.62 (4H, t, H^b), 7.47 (3H, m, $H^{d,f}$), 7.39 (1H, d, $^1J_{P\text{-}H}$ = 508 Hz, H^g), 7.35 (4H, m, $H^{c,e}$). ^{31}P NMR (400 MHz, d_6-DMSO): δ = 13.85 ppm. IR (cm^{-1}): 3043 w (P-Ph), 2328 m (P-H), 1590 w (P-Ph), 1473 w, 1438 m, 1427 m, 1163 sh $\nu_{asym}(PO_2)$, 1125 s $\nu_{asym}(PO_2)$, 1056 sh, 1033 s $\nu_{sym}(PO_2)$, 1018 s $\nu_{sym}(PO_2)$, 968 s (P-H), 750 m (P-Ph), 721 s. Elemental analysis cald (%): C 42.87, H 3.20, Bi 41.4. Found: C 42.82, H 3.16, Bi 40.8 (± 2.3).

Crystallographic data of **2-1**: $C_{18}H_{16}BiO_2P$, M_w = 504.26, monoclinic, space group C2/c, *a* = 18.5068(11), *b* = 8.9144(6), *c* = 21.9738(18) Å, α = 90, β = 112.186(4), λ = 90 °, V = 3356.8(4) Å^3, Z = 8, density = 1.996 g/cm^3, F_{000} = 1904, μ = 10.604 mm^{-1}, $2\theta_{max}$ = 55.0 °, 14755 reflections collected, 3858 unique (R_{int} = 0.0530). Final GooF = 1.003, R_1 = 0.0280, wR_2 = 0.0556. CCDC: 1943310.

7.7.1.2 Diphenyl *mono*-diphenylphosphinato bismuth $[BiPh_2O(O)PPh_2]_\infty$, 2-2

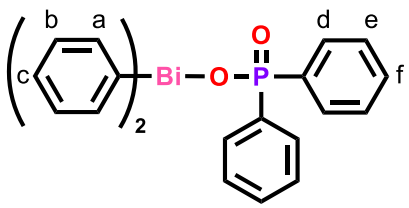

$BiPh_3$ (0.447 g, 1.0 mmol) and diphenylphosphinic acid (0.244 g, 1.1 mmol) were reacted in accordance with GP1 using ethanol as the solvent and stirring overnight at 50 °C to afford a white precipitate in 90 % yield (0.53 g). m.p. 207 °C. ^{1}H NMR

(400 MHz, d_6-DMSO): δ = 8.27 (4H, d, H^a), 7.57 (8H, m, $H^{b,d}$), 7.32 (8H, m, $H^{c,e,f}$). ^{31}P NMR (400 MHz, d_6-DMSO): δ = 20.40 ppm. IR (cm^{-1}): 3041 w (P-Ph), 1591 w (P-Ph), 1473 w, 1436 m, 1427 m, 1126 sh $\nu_{asym}(PO_2)$, 1104 s $\nu_{asym}(PO_2)$, 1034 sh, 1012 s $\nu_{sym}(PO_2)$, 994 s $\nu_{sym}(PO_2)$, 748 m (P-Ph), 724 s. Elemental analysis cald (%): C 49.67, H 3.47, Bi 36.0. Found: C 49.73, H 3.38, Bi 36.4 (± 2.1).

Crystallographic data of **2-2**: $C_{24}H_{20}BiO_2P$, M_w = 580.35, orthorombic, space group $P2_12_12_1$, *a* = 9.9875(5), *b* = 11.0201(4), *c* = 19.3941(7) Å, α = 90, β = 90, λ = 90 °, V = 2134.58(15) Å^3, Z = 4, density = 1.806 g/cm^3, F_{000} = 1112, μ = 17.045 mm^{-1}, $2\theta_{max}$ = 133.9 °, 7878 reflections collected, 3565 unique (R_{int} = 0.0357). Final GooF = 1.062, R_1 = 0.0291, wR_2 = 0.0719, Flack parameter = -0.043(11). CCDC: 1943307.

7.7.1.3 Diphenyl *mono*-dimethylphosphinato bismuth $[BiPh_2O(O)PMe_2]_\infty$, 2-3

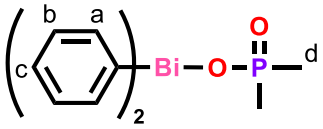

Dimethylphosphinato sodium salt (0.299 g, 2.6 mmol) was weighed into a Schlenk flask and dried *in vacuo* prior to the addition of dry methanol under nitrogen. $BiPh_2Cl$ (0.937 g, 2.4 mmol) was collected into a solid addition tube then combined with the sodium salt and allowed to stir for one hour. The resulting precipitate was collected by gravimetric filtration washed with hot ethanol and water to afford a white solid in 69 % yield (0.813 g). m.p. 190 °C. ^{1}H NMR (400 MHz, d_6-DMSO): δ = 8.23 (4H, d, H^a), 7.59 (4H, t, H^b), 7.30 (2H, t, H^c), 1.07 (6H, d, H^d). ^{31}P NMR (400 MHz, d_6-DMSO): δ = 38.95 ppm. IR (cm^{-1}): 3062 w, 1571 w, 1474 w, 1428 m (P-Me), 1291 m (P-Me), 1137 sh $\nu_{asym}(PO_2)$, 1098 s $\nu_{asym}(PO_2)$, 1059 sh, 1024 s $\nu_{sym}(PO_2)$, 995 s $\nu_{sym}(PO_2)$, 861 s (P-Me), 722 s. Elemental analysis cald (%): C 36.86, H 3.54, Bi 45.8. Found: C 36.64, H 3.71, Bi 48.3 (± 2.7).

Crystallographic data of **2-3**: $C_{14}H_{16}BiO_2P$, M_w = 456.22, orthorombic, space group $P2_12_12_1$, *a* = 9.0005(2), *b* = 16.2512(3), *c* = 10.0290(2) Å, α = 90, β = 90, λ = 90 °, V = 1466.93(5) Å^3, Z = 4, density = 2.066 g/cm^3, F_{000} = 856, μ = 24.557 mm^{-1}, $2\theta_{max}$ = 133.7 °, 15386 reflections collected, 2595 unique (R_{int} = 0.0374). Final GooF = 1.044, R_1 = 0.0192, wR_2 = 0.0454, Flack parameter = -0.034(8). CCDC: 1943309.

7.7.1.4 Diphenyl *mono*-(*bis*-*p*-methoxyphenyl)phosphinato bismuth $[BiPh_2O(O)P(p\text{-}MeOPh)_2]_\infty$, 2-4

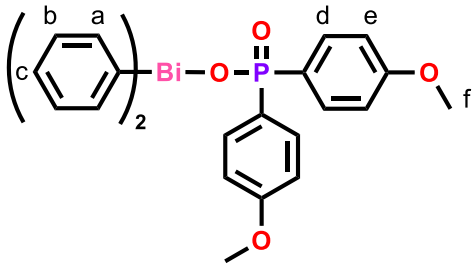

$BiPh_3$ (0.224 g, 0.51 mmol) and *bis*-(*p*-methoxyphenyl)phosphinic acid (0.156 g, 0.56 mmol) were reacted in accordance with GP1 using ethanol as the solvent and stirring overnight at 50 °C to afford a white precipitate in 86 % yield (0.28 g). m.p. 221 °C. ^{1}H NMR (400 MHz, d_6-DMSO): δ = 8.26 (4H, d, H^a), 7.58 (4H, t, H^b), 7.44 (4H, t, H^d), 7.30 (4H, t, H^c), 6.84 (4H, d, H^e), 3.72 (6H, s, H^f). ^{31}P NMR (400 MHz, d_6-DMSO): δ = 21.38 ppm. IR (cm^{-1}): 3055 w (P-Ph), 1594 w (P-Ph), 1568 sh, 1500 m, 1464 m, 1290 m, 1244 s (O-Me), 1121 s $\nu_{asym}(PO_2)$, 1085 s $\nu_{asym}(PO_2)$, 1016 s $\nu_{sym}(PO_2)$, 991 s $\nu_{sym}(PO_2)$, 829 s, 806 s, 726 s (P-Ph). Elemental analysis cald (%): C 48.76, H 3.78, Bi 32.6. Found: C 48.75, H 3.69, Bi 31.1 (± 1.7).

Crystallographic data of **2-4**: $C_{26}H_{24}BiO_4P$, M_w = 640.40, monoclinic, space group $P2_1/n$, a = 12.0180(3), b = 10.7673(3), c = 17.6146(4) Å, α = 90, β = 94.874(2), λ = 90 °, V = 1171.11(10) Å^3, Z = 4, density = 1.873 g/cm^3, F_{000} = 1240, μ = 16.159 mm^{-1}, $2\theta_{max}$ = 134.1 °, 15407 reflections collected, 4027 unique (R_{int} = 0.0389). Final GooF = 1.071, R_1 = 0.0371, wR_2 = 0.0774. CCDC: 1943308.

7.7.1.5 Phenyl *bis*-phenylphosphinato bismuth $[BiPh(O(O)P(H)Ph)_2]_\infty$, 2-5

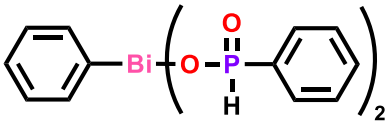

$BiPh_3$ (0.176 g, 0.4 mmol) and phenylphosphinic acid (0.135 g, 0.95 mmol) were reacted in accordance with GP1 using ethanol as the solvent and stirring overnight at reflux to afford a white precipitate in 78 % yield (0.179 g). m.p. 197 °C. ^{13}C CP-MAS: δ = 140.5, 132.0, 130.7, 127.2 ppm. ^{31}P HPDEC-MAS: δ = 20.05, 13.64 ppm. IR (cm^{-1}): 3058 w (P-Ph), 2366 w (P-H), 2338 w (P-H), 1591 w (P-Ph), 1438 m, 1137 s $\nu_{asym}(PO_2)$, 1090 s $\nu_{asym}(PO_2)$, 1034 sh $\nu_{sym}(PO_2)$, 1016 s $\nu_{sym}(PO_2)$, 970 m (P-H), 748 m (P-Ph), 725 m, 690 s. Elemental analysis cald (%): C 38.05, H 3.02, Bi 36.8. Found: C 38.01, H 2.97, Bi 37.0.

7.7.1.6 Phenyl *bis*-diphenylphosphinato bismuth $[BiPh(O(O)PPh_2)_2]_\infty$, 2-6

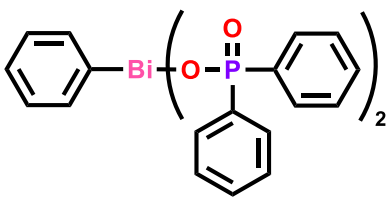

$BiPh_3$ (0.459 g, 1.0 mmol) and diphenylphosphinic acid (0.514 g, 2.4 mmol) were reacted in accordance with GP1 using ethanol as the solvent and stirring overnight at reflux to afford a white precipitate in 72 % yield (0.559 g). m.p. 330 °C. ^{13}C CP-MAS: δ = 138.9, 131.3, 129.2 ppm. ^{31}P HPDEC-MAS: δ = 20.47, ppm. IR (cm^{-1}): 3050 w (P-Ph), 1592

w (P-Ph), 1437 m, 1181 w, 1127 s $\nu_{asym}(PO_2)$, 1097 s $\nu_{asym}(PO_2)$, 1011 s $\nu_{sym}(PO_2)$, 992 s $\nu_{sym}(PO_2)$, 750 m (P-Ph), 725 m, 699 s. Elemental analysis cald (%): C 50.01, H 3.50, Bi 29.0. Found: C 49.72, H 3.45, Bi 30.4.

7.7.1.7 Phenyl *bis*-dimethylphosphinato bismuth $[BiPh(O(O)PMe_2)_2]_\infty$, 2-7

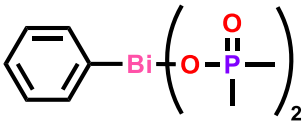

$BiPh_3$ (1.135 g, 2.6 mmol) and diphenylphosphinic acid (0.504 g, 5.4 mmol) were reacted in accordance with GP1 using DMSO as the solvent and stirring overnight at reflux to afford a white precipitate in 92 % yield (1.121 g). m.p. 300 °C. ^{13}C CP-MAS: δ = 176.3, 43.5 ppm. ^{31}P HPDEC-MAS: δ = 46.3, 42.4 ppm. IR (cm^{-1}): 3053 w, 1654 w, 1436 m, 1417 m (P-Me), 1137 sh $\nu_{asym}(PO_2)$, 1083 sh $\nu_{asym}(PO_2)$, 1007 s $\nu_{sym}(PO_2)$, 952 sh $\nu_{sym}(PO_2)$, 860 s (P-Me), 736 s, 694 s. Elemental analysis cald (%): C 25.44 H 3.36, Bi 44.3. Found: C 25.48, H 3.57, Bi 43.2.

7.7.1.8 Phenyl *bis*-(*bis*-*p*-methoxyphenyl)phosphinato bismuth $[BiPh(O(O)P(p\text{-}MeOPh)_2)_2]_\infty$, 2-8

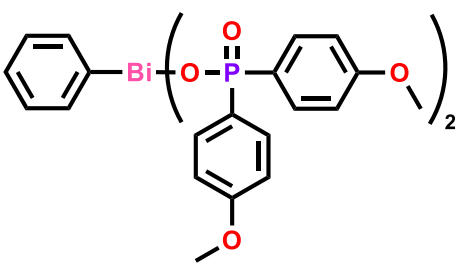

$BiPh_3$ (0.115 g, 0.26 mmol) and *bis*-(*p*-methoxyphenyl)phosphinic acid (0.145 g, 0.52 mmol) were grinded together and reacted in a solvent free reaction using a Kugelrohr oven at 130 °C for 4 hours. The white solid was washed with hot ethanol and dried by air to afford 72 % yield (0.16 g). m.p. 250 °C. ^{13}C CP-MAS: δ = 161.3, 136.8, 131.7, 129.1, 127.2, 123.9, 118.1, 112.1, 110.3, 55.5, 54.3 ppm. ^{31}P HPDEC-MAS: δ = 24.60 ppm. IR (cm^{-1}): 3058 w (P-Ph), 1596 s (P-Ph), 1463 m, 1246 s (O-Me), 1121 s $\nu_{asym}(PO_2)$, 1081 s $\nu_{asym}(PO_2)$, 1016 s $\nu_{sym}(PO_2)$, 990 s $\nu_{sym}(PO_2)$, 803 s, 733 m (P-Ph), 697 m. Elemental analysis cald (%): C 48.58, H 3.96, Bi 24.9. Found: C 48.82, H 3.82, Bi 23.8.

7.7.2 General procedure 2 (GP2)

All reactions were conducted using 1.0 equivalents of $Bi(O^tBu)_3$ and 3.1 equivalents of phosphinic acid to yield *tris*-phosphinato bismuth complexes. Phosphinic acids were dried under vacuum in a Schlenk flask equipped with magnetic stirrer bar prior to addition of dry DCM and cooled to -78 °C in an *iso*-propanol-liquid nitrogen bath. A solution of $Bi(O^tBu)_3$ in DCM was slowly added and the mixture allowed to room temperature overnight. The resulting precipitate was collected by gravimetric filtration and washed with hot ethanol and diethyl ether prior to air drying.

7.7.2.1 *Tris*-phenylphosphinato bismuth $[Bi(O(O)P(H)Ph)_3]_\infty$, 2-9

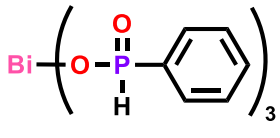

$Bi(O^tBu)_3$ (0.407 g, 0.95 mmol) and phenylphosphinic acid (0.411 g, 2.9 mmol) were reacted in accordance with GP2 to afford a white precipitate in 76 % yield (0.466 g). m.p. 130 °C. ^{13}C CP-MAS: δ = 136.9, 133.1, 130.9, 128.9, 127.8, 126.3 ppm. ^{31}P HPDEC-MAS: δ = 17.28 ppm. IR (cm^{-1}): 3049 w (P-Ph), 2377 w (P-H), 1591 w (P-Ph), 1436 m, 1098 s $\nu_{asym}(PO_2)$, 1031 s $\nu_{sym}(PO_2)$, 1016 s $\nu_{sym}(PO_2)$, 974 s (P-H), 740 m (P-Ph), 688 s. Elemental analysis cald (%): C 34.20, H 2.87, Bi 33.05. Found: C 34.39, H 2.93, Bi 34.1.

7.7.2.2 *Tris*-diphenylphosphinato bismuth $[Bi(O(O)PPh_2)_3]_\infty$, 2-10

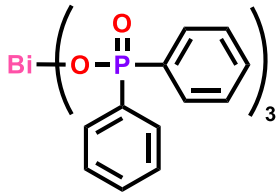

$Bi(O^tBu)_3$ (0.299 g, 0.70 mmol) and diphenylphosphinic acid (0.472 g, 2.2 mmol) were reacted in accordance with GP2 to afford a white precipitate in 96 % yield (0.593 g). m.p. 340 °C. ^{13}C CP-MAS: δ = 142.2, 135.0, 133.3, 127.3 ppm. ^{31}P HPDEC-MAS: δ = 24.22 ppm. IR (cm^{-1}): 3062 w (P-Ph), 1591 w (P-Ph), 1436 m, 1125 sh $\nu_{asym}(PO_2)$, 1091 s $\nu_{asym}(PO_2)$, 1032 s $\nu_{sym}(PO_2)$, 1010 s $\nu_{sym}(PO_2)$, 746 m (P-Ph), 728 s, 692 s. Elemental analysis cald (%): C 50.25, H 3.51, Bi 24.3. Found: C 50.26, H 3.56, Bi 23.5.

7.7.2.3 *Tris*-dimethylphosphinato bismuth $[Bi(O(O)PMe_2)_3]_\infty$, 2-11

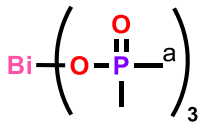

$Bi(O^tBu)_3$ (0.529 g, 1.2 mmol) and dimethylphosphinic acid (0.349 g, 3.7 mmol) were reacted in accordance with GP2 to afford a white precipitate in 53 % yield (0.321 g). m.p. 420 °C. ^1H NMR (400 MHz, $CDCl_3$): δ = 1.49 (18H, d, H^a). ^{31}P NMR (400 MHz, $CDCl_3$): δ = 47.65 ppm. IR (cm^{-1}): 2990 w, 2120 w, 1425 m (P-Me), 1291 m, 1080 s $\nu_{asym}(PO_2)$, 1013 s $\nu_{sym}(PO_2)$, 868 s (P-Me), 741 m, 706 m. Elemental analysis cald (%): C 14.24, H 3.98, Bi 41.3. Found: C 14.24, H 3.58, Bi 39.6.

7.7.2.4 *Tris*-(*bis*-*p*-methoxyphenyl)phosphinato bismuth $[Bi(O(O)P(p\text{-}MeOPh)_2)_3]_\infty$, 2-12

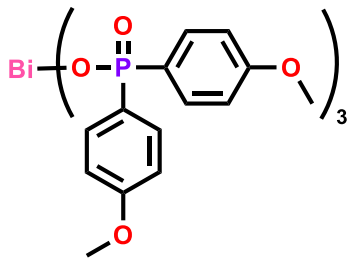

$Bi(O^tBu)_3$ (0.248 g, 0.58 mmol) and *bis*-(*p*-methoxyphenyl)phosphinic acid (0.494 g, 1.8 mmol) were reacted in accordance with GP2 to afford a white precipitate in 78 % yield (0.479 g). m.p. 230 °C. ^{13}C CP-MAS: δ = 137.4, 135.9, 133.3, 131.3, 126.6, 124.7 ppm. ^{31}P HPDEC-MAS: δ = 23.82 ppm. IR (cm^{-1}): 3055 w (P-Ph), 1596 m (P-Ph), 1458 w, 1252 m (O-Me), 1122 m

$\nu_{asym}(PO_2)$, 1083 s $\nu_{asym}(PO_2)$, 1018 s $\nu_{sym}(PO_2)$, 828 m, 723 w (P-Ph), 670 m. Elemental analysis cald (%): C 48.47, H 4.07, Bi 20.1. Found: C 48.53, H 4.09, Bi 19.6.

7.8 Aryl bismuth phosphinato complexes

7.8.1 General procedure 3 (GP3)

All reactions were conducted using 1.0 equivalents of $BiAr_3$ and 1.1 equivalents of phosphinic acid to yield the diaryl bismuth *mono*-phosphinato bismuth complexes Crystalline $BiAr_3$ and the phosphinic acid were placed in a round bottom flask equipped with magnetic stirrer bar. The solvent (ethanol) was added and the flask heated (unless otherwise stated) overnight, yielding a precipitate. The precipitate was collected by gravimetric filtration and washed with hot ethanol, acetone and diethyl ether to remove any unreacted reagents prior to air drying.

7.8.1.1 *Bis-o*-methoxyphenyl *mono*-phenylphosphinato bismuth [Bi(*o*-MeOPh)$_2$O(O)P(H)Ph]$_\infty$, 3-1

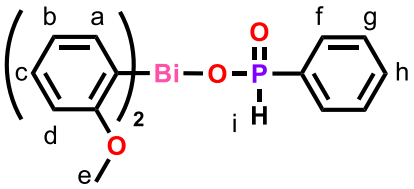

Bi(*o*-MeOPh)$_3$ (0.100 g, 0.19 mmol) and phenylphosphinic acid (0.047 g, 0.33 mmol) were reacted in accordance with GP3 using ethanol as the solvent and stirring overnight at room temperature to afford a white precipitate in 27 % yield (0.029 g). m.p. 149 °C. ^{1}H NMR (400 MHz, d_6-DMSO): δ = 7.69 (1H, d, $^1J_{P\text{-}H}$ = 536 Hz, H^i), 7.65 (2H, dd, H^f), 7.51 (1H, t, H^h), 7.41 (2H, t, H^g), 7.34 (2H, t, H^c), 7.25 (2H, d, H^a), 7.12 (2H, d, H^d), 6.86 (2H, t, H^b), 3.72 (6H, s, H^e). IR (cm^{-1}): 3052 w (P-Ph), 2831 w (C-H), 2338 w (P-H), 1568 w (P-Ph), 1457 m, 1426 m, 1267 w, 1222 m (O-Me), 1136 sh $\nu_{asym}(PO_2)$, 1109 s $\nu_{asym}(PO_2)$, 1083 s, 1031 s $\nu_{sym}(PO_2)$, 1015 s $\nu_{sym}(PO_2)$, 996 s (P-H), 743 s (P-Ph), 691 s. Elemental analysis cald (%): C 42.57, H 3.57, Bi 37.03. Found: C 42.67, H 3.59, Bi 39.20 (± 2.44).

7.8.1.2 *Bis-o*-methoxyphenyl *mono*-diphenylphosphinato bismuth [Bi(*o*-MeOPh)$_2$O(O)PPh$_2$]$_\infty$, 3-2

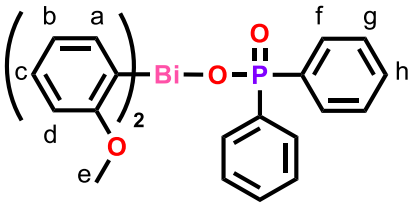

Bi(*o*-MeOPh)$_3$ (0.100 g, 0.19 mmol) and diphenylphosphinic acid (0.052 g, 0.24 mmol) were reacted in accordance with GP3 using ethanol as the solvent and stirring overnight at 50 °C to afford a white precipitate in 76 % yield (0.095 g). m.p. 177 °C. ^{1}H NMR (600 MHz, d_6-DMSO): δ = 7.67 (4H, m, H^f), 7.38 (8H, m, H^{c,g,h}), 7.27 (2H, d, H^a), 7.13 (2H, d, H^d), 6.86 (2H, t, H^b), 3.73 (6H, s, H^e). IR (cm^{-1}): 3051 w (P-Ph), 2951 w, 2826 w (C-H), 1568

w (P-Ph), 1466 w, 1437 m, 1267 w, 1248 m (O-Me), 1144 sh $\nu_{asym}(PO_2)$, 1123 s $\nu_{asym}(PO_2)$, 1034 s $\nu_{sym}(PO_2)$, 1012 s $\nu_{sym}(PO_2)$, 751 m (P-Ph), 719 s, 693 s. Elemental analysis cald (%): C 48.76 H 3.78, Bi 32.63. Found: C 48.98, H 3.73, Bi 32.79 (± 2.12).

7.8.1.3 *Bis-o*-methoxyphenyl *mono*-(*bis-p*-methoxyphenyl)phosphinato bismuth $[Bi(o\text{-}MeOPh)_2O(O)P(p\text{-}MeOPh)_2]_\infty$, 3-3

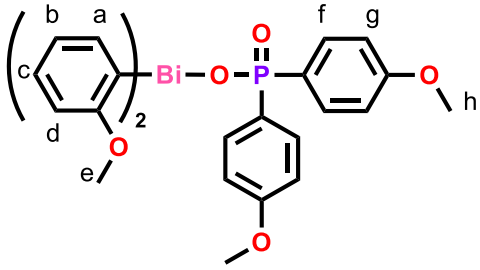

$Bi(o\text{-}MeOPh)_3$ (0.101 g, 0.19 mmol) and *bis*-(*p*-methoxyphenyl)phosphinic acid (0.053 g, 0.19 mmol) were reacted in accordance with GP3 using ethanol as the solvent and stirring overnight at 50 °C to afford a white precipitate in 63 % yield (0.084 g). m.p. 186 °C. ^{1}H NMR (400 MHz, d_6-DMSO): δ = 7.58 (4H, m, H^f), 7.35 (2H, t, H^c), 7.26 (2H, d, H^a), 7.13 (2H, d, H^d), 6.86 (6H, m, $H^{b,g}$), 3.73 (12H, s, $H^{e,h}$). IR (cm^{-1}): 3025 w (P-Ph), 2832 w (C-H), 1597 m (P-Ph), 1457 m, 1426 m, 1254 m (O-Me), 1155 sh $\nu_{asym}(PO_2)$, 1131 m $\nu_{asym}(PO_2)$, 1082 s, 1048 sh $\nu_{sym}(PO_2)$, 1019 s $\nu_{sym}(PO_2)$, 830 m, 751 m (P-Ph), 672 m. Elemental analysis cald (%): C 48.01, H 4.03, Bi 29.83. Found: C 48.04, H 4.09, Bi 30.92 (± 2.00).

7.8.1.4 *Bis-m*-methoxyphenyl *mono*-phenylphosphinato bismuth $[Bi(m\text{-}MeOPh)_2O(O)P(H)Ph]_\infty$, 3-4

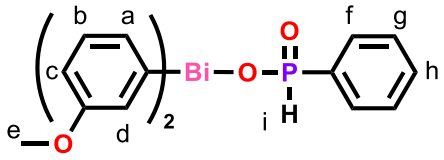

$Bi(m\text{-}MeOPh)_3$ (0.099 g, 0.19 mmol) and phenylphosphinic acid (0.033 g, 0.23 mmol) were reacted in accordance with GP3 using ethanol as the solvent and stirring overnight at room temperature to afford a white precipitate in 33 % yield (0.039 g). m.p. 127 °C. ^{1}H NMR (400 MHz, d_6-DMSO): δ = 7.96 (2H, s, H^d), 7.80 (2H, d, H^a), 7.61 (2H, t, H^b), 7.52 (2H, dd, H^f), 7.42 (1H, d, $^1J_{P\text{-}H}$ = 508 Hz, H^i), 7.41 (3H, m, $H^{g,h}$), 6.85 (2H, d, H^c), 3.68 (6H, s, H^e). IR (cm^{-1}): 3043 w (P-Ph), 2830 w (C-H), 2336 w (P-H), 1577 m (P-Ph), 1470 m, 1411 m, 1284 m, 1226 s (O-Me), 1130 sh $\nu_{asym}(PO_2)$, 1110 s $\nu_{asym}(PO_2)$, 1058 sh, 1032 s $\nu_{sym}(PO_2)$, 1012 s $\nu_{sym}(PO_2)$, 976 s (P-H), 873 w,752 m (P-Ph), 691 s. Elemental analysis cald (%): C 42.57, H 3.57, Bi 37.03. Found: C 42.21, H 3.22, Bi 37.16 (± 2.04).

Crystallographic data of **3-4**: $C_{20}H_{20}BiO_4P$, M_w = 564.31, orthorombic, space group $P2_12_12_1$, *a* = 9.4175(4), *b* = 9.4368(3), *c* = 21.9641(6) Å, α = 90, β = 90, λ = 90 °, V = 1951.97(12) $Å^3$, Z = 4, density = 1.920 g/cm^3, F_{000} = 1080, μ = 9.136 mm^{-1}, $2\theta_{max}$ = 134.1 °, 18660 reflections collected, 4810 unique (R_{int} = 0.0462). Final GooF = 1.044, R_1 = 0.0264, wR_2 = 0.0463, Flack parameter = -0.038(6).

7.8.1.5 *Bis-m*-methoxyphenyl *mono*-diphenylphosphinato bismuth [Bi(*m*-MeOPh)$_2$O(O)PPh$_2$]$_\infty$, 3-5

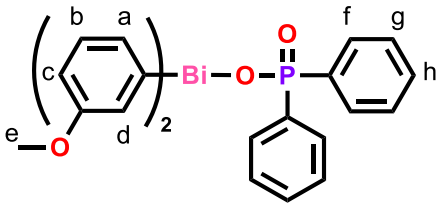

Bi(*m*-MeOPh)$_3$ (0.097 g, 0.18 mmol) and diphenylphosphinic acid (0.042 g, 0.19 mmol) were reacted in accordance with GP3 using ethanol as the solvent and stirring overnight at 50 °C to afford a white precipitate in 43 % yield (0.044 g). m.p. 161 °C. ^{1}H NMR (400 MHz, d$_6$-DMSO): δ = 8. (2H, s, H^d), 7.81 (2H, d, H^a), 7.58 (6H, dd, H^{f,h}), 7.31 (4H, d, H^g), 6.82 (2H, m, H^b), 3.64 (6H, s, H^e). IR (cm^{-1}): 3053 w (P-Ph), 2955 w, 2832 w (C-H), 1577 m (P-Ph), 1466 m, 1437 m, 1223 m (O-Me), 1164 sh $\nu_{asym}(PO_2)$, 1114 s $\nu_{asym}(PO_2)$, 1034 s $\nu_{sym}(PO_2)$, 1013 s $\nu_{sym}(PO_2)$, 753 m (P-Ph), 720 m, 691 s. Elemental analysis cald (%): C 48.76 H 3.78, Bi 32.63. Found: C 48.53, H 3.55, Bi 34.74 (± 2.62).

7.8.1.6 *Bis-m*-methoxyphenyl *mono*-(*bis-p*-methoxyphenyl)phosphinato bismuth [Bi(*m*-MeOPh)$_2$O(O)P(*p*-MeOPh)$_2$]$_\infty$, 3-6

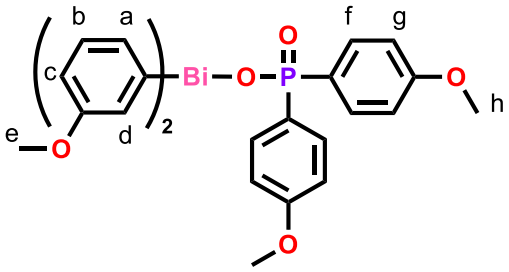

Bi(*m*-MeOPh)$_3$ (0.102 g, 0.19 mmol) and *bis*-(*p*-methoxyphenyl)phosphinic acid (0.053 g, 0.19 mmol) were reacted in accordance with GP3 using ethanol as the solvent and stirring overnight at 50 °C to afford a white precipitate in 33 % yield (0.045 g). m.p. 151 °C. ^{1}H NMR (400 MHz, d$_6$-DMSO): δ = 7.98 (2H, s, H^d), 7.81 (2H, d, H^a), 7.58 (2H, m, H^c), 7.48 (4H, dd, H^f), 6.85 (6H, m, H^{b,g}), 3.72 (6H, s, H^h), 3.65 (6H, s, H^e). IR (cm^{-1}): 3063 w (P-Ph), 2832 w (C-H), 1565 m (P-Ph), 1470 m, 1437 w, 1219 s (O-Me), 1177 m $\nu_{asym}(PO_2)$, 1127 s $\nu_{asym}(PO_2)$, 1085 s $\nu_{sym}(PO_2)$, 1017 s $\nu_{sym}(PO_2)$, 828 m, 780 s (P-Ph), 673 s. Elemental analysis cald (%): C 48.01, H 4.03, Bi 29.83. Found: C 47.76, H 3.83, Bi 30.16 (± 2.21).

7.8.1.7 *Bis-m*-tolyl *mono*-phenylphosphinato bismuth [Bi(*m*-tol)$_2$O(O)P(H)Ph]$_\infty$, 3-13

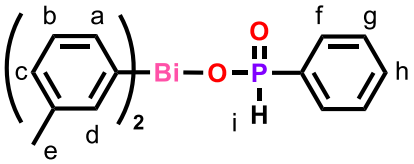

Bi(*m*-tol)$_3$ (0.108 g, 0.22 mmol) and phenylphosphinic acid (0.044 g, 0.31 mmol) were reacted in accordance with GP3 using ethanol as the solvent and stirring overnight at room temperature to afford a white precipitate in 42 % yield (0.050 g). m.p. 139 °C. ^{1}H NMR (400 MHz, d$_6$-DMSO): δ = 8.03 (4H, m, H^{a,d}), 7.50 (4H, m, H^{b,f}), 7.40 (3H, m, H^{g,h}), 7.39 (1H, d, $^1J_{P\text{-}H}$ = 516 Hz, H^i), 7.13 (2H, d, H^c), 2.26 (6H, s, H^e). IR (cm^{-1}): 3040 w (P-

Ph), 2924 w (C-H), 2328 w (P-H), 1581 m (P-Ph), 1475 w, 1438 m, 1391 w, 1133 m $\nu_{asym}(PO_2)$, 1106 s $\nu_{asym}(PO_2)$, 1069 sh, 1033 s $\nu_{sym}(PO_2)$, 1016 s $\nu_{sym}(PO_2)$, 968 s (P-H), 774 s, 750 m (P-Ph), 693 s. Elemental analysis cald (%): C 45.13, H 3.79, Bi 39.26. Found: C 44.82, H 3.64, Bi 41.51 (± 3.13).

Crystallographic data of **3-13**: $C_{20}H_{20}BiO_2P$, M_w = 532.31, monoclinic, space group $P2_1$, *a* = 8.7590(18), *b* = 9.4710(19), *c* = 11.418(2) Å, α = 90, β = 99.95(3), λ = 90 °, V = 932.9(3) Å^3, Z = 2, density = 1.895 g/cm^3, F_{000} = 508, μ = 9.543 mm^{-1}, $2\theta_{max}$ = 57.1 °, 11399 reflections collected, 3694 unique (R_{int} = 0.0198). Final GooF = 1.211, R_1 = 0.0187, wR_2 = 0.0492, Flack parameter = -0.017(3).

7.8.1.8 *Bis-m*-tolyl *mono*-diphenylphosphinato bismuth [Bi(*m*-tol)$_2$O(O)PPh$_2$]$_\infty$, 3-14

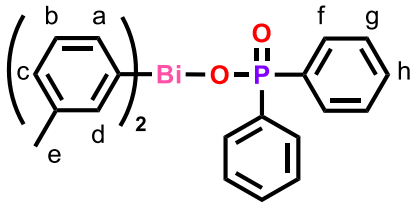

Bi(*m*-tol)$_3$ (0.153 g, 0.32 mmol) and diphenylphosphinic acid (0.075 g, 0.34 mmol) were reacted in accordance with GP3 using ethanol as the solvent and stirring overnight at 55 °C to afford a white precipitate in 51 % yield (0.098 g). m.p. 152 °C. ^{1}H NMR (400 MHz, d_6-DMSO): δ = 8.05 (4H, m, H^{a,d}), 7.56 (4H, m, H^f), 7.51 (2H, t, H^b), 7.33 (6H, m, H^{g,h}), 7.10 (2H, m, H^c), 2.22 (6H, s, H^e). IR (cm^{-1}): 3052 w (P-Ph), 1591 w (P-Ph), 1438 m, 1113 s $\nu_{asym}(PO_2)$, 1070 s $\nu_{asym}(PO_2)$, 1015 s $\nu_{sym}(PO_2)$, 995 s $\nu_{sym}(PO_2)$, 750 m (P-Ph), 722 m, 692 s. Elemental analysis cald (%): C 51.33, H 3.98, Bi 34.35. Found: C 50.99, H 3.61, Bi 34.20 (± 2.22).

7.8.1.9 *Bis-m*-tolyl *mono*-(*bis-p*-methoxyphenyl)phosphinato bismuth [Bi(*m*-tol)$_2$O(O)P(*p*-MeOPh)$_2$]$_\infty$, 3-15

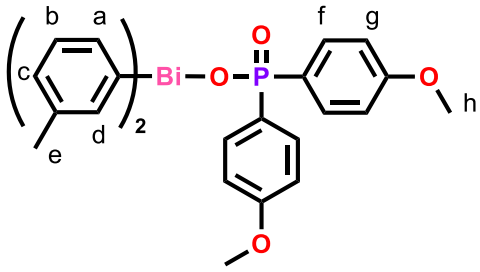

Bi(*m*-tol)$_3$ (0.153 g, 0.32 mmol) and *bis*-(*p*-methoxyphenyl)phosphinic acid (0.098 g, 0.35 mmol) were reacted in accordance with GP3 using ethanol as the solvent and stirring overnight at 55 °C to afford a white precipitate in 57 % yield (0.120 g). m.p. 239 °C. ^{1}H NMR (400 MHz, d_6-DMSO): δ = 8.03 (4H, m, H^{a,d}), 7.48 (6H, m, H^{b,f}), 7.10 (2H, m, H^c), 6.85 (4H, d, H^g), 3.73 (6H, s, H^h), 2.23 (6H, s, H^e). IR (cm^{-1}): 3055 w (P-Ph), 2836 w (C-H), 1598 m (P-Ph), 1570 sh, 1503 m, 1464 w, 1439 sh, 1291 m, 1252 s (O-Me), 1122 s $\nu_{asym}(PO_2)$, 1098 s $\nu_{asym}(PO_2)$, 1023 s $\nu_{sym}(PO_2)$, 1000 s $\nu_{sym}(PO_2)$, 828 m, 803 m, 720 w (P-Ph), 667 m. Elemental analysis cald (%): C 50.31, H 4.22, Bi 31.26. Found: C 50.18, H 4.03, Bi 30.51 (± 2.82).

7.8.1.10 *Bis-p*-tolyl *mono*-phenylphosphinato bismuth [Bi(*p*-tol)$_2$O(O)P(H)Ph]$_\infty$, 3-16

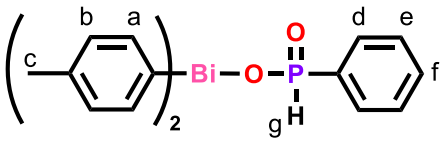

Bi(*p*-tol)$_3$ (0.153 g, 0.32 mmol) and phenylphosphinic acid (0.051 g, 0.36 mmol) were reacted in accordance with GP3 using ethanol as the solvent and stirring overnight at room temperature to afford a white precipitate in 54 % yield (0.090 g). m.p. 156 °C. ^{1}H NMR (400 MHz, d_6-DMSO): δ = 8.11 (4H, d, H^a), 7.43 (9H, m, H^{b,d,e,f}), 7.34 (1H, d, $^1J_{P-H}$ = 508 Hz, H^g), 2.27 (6H, s, H^c). IR (cm^{-1}): 3045 w (P-Ph), 2889 w (C-H), 2316 m (P-H), 1589 w (P-Ph), 1486 w, 1436 m, 1386 m, 1166 sh $\nu_{asym}(PO_2)$, 1128 s $\nu_{asym}(PO_2)$, 1056 sh, 1033 s $\nu_{sym}(PO_2)$, 1020 s $\nu_{sym}(PO_2)$, 995 s, 968 s (P-H), 791 s, 748 m (P-Ph), 694 m. Elemental analysis cald (%): C 45.13, H 3.79, Bi 39.26. Found: C 45.18, H 3.46, Bi 41.28 (± 2.16).

7.8.1.11 *Bis-p*-tolyl *mono*-diphenylphosphinato bismuth [Bi(*p*-tol)$_2$O(O)PPh$_2$]$_\infty$, 3-17

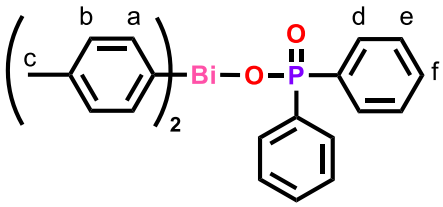

Bi(*p*-tol)$_3$ (0.153 g, 0.32 mmol) and diphenylphosphinic acid (0.079 g, 0.36 mmol) were reacted in accordance with GP3 using ethanol as the solvent and stirring overnight at 50 °C to afford a white precipitate in 93 % yield (0.179 g). m.p. 219 °C. ^{1}H NMR (400 MHz, d_6-DMSO): δ = 8.12 (4H, d, H^a), 7.54 (4H, dd, H^d), 7.40 (4H, d, H^b), 7.31 (6H, m, H^{e,f}), 2.26 (6H, s, H^c). IR (cm^{-1}): 3055 w (P-Ph), 2863 w (C-H), 1592 w (P-Ph), 1484 w, 1437 m, 1387 w, 1156 sh, 1123 sh $\nu_{asym}(PO_2)$, 1108 s $\nu_{asym}(PO_2)$, 1069 m, 1036 s $\nu_{sym}(PO_2)$, 1015 s $\nu_{sym}(PO_2)$, 994 s, 793 s, 755 s (P-Ph), 723 s, 698 s. Elemental analysis cald (%): C 51.33, H 3.98, Bi 34.35. Found: C 51.22, H 3.83, Bi 33.30 (± 1.88).

Crystallographic data of **3-17**: $C_{26}H_{24}BiO_2P$, M_w = 608.40, monoclinic, space group $P2_1$, *a* = 11.7325(2), *b* = 9.3795(2), *c* = 20.9611(5) Å, α = 90, β = 96.470(2), λ = 90 °, V = 2291.97(8) Å^3, Z = 4, density = 1.763 g/cm^3, F_{000} = 1176, μ = 7.782 mm^{-1}, $2\theta_{max}$ = 52.7 °, 25295 reflections collected, 9013 unique (R_{int} = 0.0373). Final GooF = 1.013, R_1 = 0.0310, wR_2 = 0.0768, Flack parameter = -0.021(5).

7.8.1.12 *Bis-p*-tolyl *mono*-(*bis-p*-methoxyphenyl)phosphinato bismuth $[Bi(p\text{-tol})_2O(O)P(p\text{-MeOPh})_2]_\infty$, 3-18

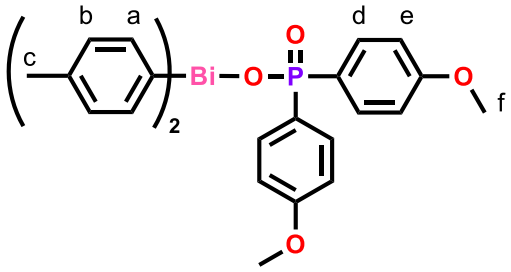

Bi(*p*-tol)$_3$ (0.153 g, 0.32 mmol) and *bis*-(*p*-methoxyphenyl)phosphinic acid (0.095 g, 0.34 mmol) were reacted in accordance with GP3 using ethanol as the solvent and stirring overnight at 50 °C to afford a white precipitate in 77 % yield (0.163 g). m.p. 188 °C. ^{1}H NMR (400 MHz, d_6-DMSO): δ = 8.11 (4H, d, H^a), 7.42 (8H, m, H^{b,d}), 6.84 (4H, d, H^e), 3.72 (6H, s, H^f), 2.26 (6H, s, H^c). IR (cm^{-1}): 3003 w (P-Ph), 2838 w (C-H), 1596 m (P-Ph), 1502 m, 1461 w, 1439 m, 1386 m, 1292 m, 1244 m (O-Me), 1165 m, 1121 s $\nu_{asym}(PO_2)$, 1105 s $\nu_{asym}(PO_2)$, 1020 s $\nu_{sym}(PO_2)$, 997 s $\nu_{sym}(PO_2)$, 792 s, 719 m (P-Ph), 664 s. Elemental analysis cald (%): C 50.31, H 4.22, Bi 31.26. Found: C 50.24, H 4.00, Bi 31.54 (± 1.67).

7.9 Bismuth-cellulose composites

The MFC sample was Celish grade KY-100G from Daicel Corporation, Japan. The measured average diameter was 73 nm and the aspect ratio estimated by sedimentation was within the range 125–142.[217,218] The never-dried material, received at 25% solids content, was dispersed in deionised water at 0.2 wt% by agitating using a 3 L disintegrator. Suspensions of complexes **2-1** – **2-8** and **Ag** were prepared by dispersion within 20% isopropanol/water and stirred for 16 hours at room temperature. Cationic dimethylaminoethyl methacrylate poly-acrylamide (CPAM) polymer with high molecular weight (13 MDa) and charge density of 40 wt% (F1, SnowFlake Cationics) was used for retaining inorganic particles in a cellulose nanofibre matrix.[179] The polymer solution was prepared by dissolving the CPAM in deionized water at 0.01 wt% for 8 hours at room temperature.

Preparation of the cellulose-bismuth suspension was done using a two-step process. Bismuth complex and CPAM suspensions were carefully mixed first and then the CPAM-bismuth suspension and MFC suspension were mixed. The final suspension was then poured through the British hand sheet maker and the suspension was allowed to filter under gravity over Whatman hardened ashless filter paper of grade 541, diameter 185 mm. Once a thin film was formed on the filter paper, the film was removed using blotting papers and then dried using a drier at 105 °C. For all samples, the MFC content was kept constant at 1.2 dry grams (60 gm^{-2} of film), while the amount of the compound suspension was adjusted to achieve the desired loading of the bismuth complex or silver sulfadiazine. The CPAM loading was 10 mg per total dry grams of material.

7.10 Gallium phosphinato complexes

7.10.1 General procedure 4 (GP4)

All reactions were conducted using 1.0 equivalents of $GaPh_3$ and 1.1 equivalents of phosphinic acid to yield the diphenyl gallium *mono*-phosphinato complexes. Phosphinic acids were dried under vacuum in a Schlenk flask equipped with magnetic stirrer bar prior to addition of dry toluene or THF, forming a heterogeneous solution. A solution of $GaPh_3$ in toluene or THF was slowly added and the mixture and allowed to stir for two hours (unless otherwise stated). The solvent was removed by rotary evaporation and the resulting solid was collected by gravimetric filtration and washed with hot ethanol and diethyl ether prior to air drying.

7.10.1.1 Diphenyl *mono*-phenylphosphinato gallium $[GaPh_2O(O)P(H)Ph]_2$, 5-1

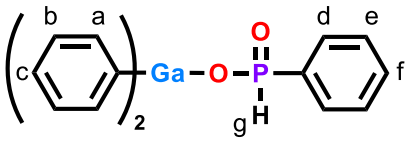

$GaPh_3$ (0.163 g, 0.54 mmol) and phenylphosphinic acid (0.080 g, 0.56 mmol) were reacted in accordance with GP4 using toluene as the solvent. Upon toluene removal, a sticky solid is obtained which is sonicated in an ethanol-water mixture producing a white suspension. The solvents are removed *in vacuo* to afford a white solid in 64 % yield (0.126 g). m.p. 98 °C. ^{1}H NMR (400 MHz, d_6-DMSO): δ = 7.62 (6H, m, $H^{a,d}$), 7.54 (1H, d, $^1J_{P-H}$ = 536 Hz, H^g), 7.51 (2H, m, H^e), 7.43 (3H, m, $H^{c,f}$), 7.28 (4H, m, H^b). ^{31}P NMR (400 MHz, d_6-DMSO): δ = 13.45 ppm. IR (cm^{-1}): 3045 w (P-Ph), 2372 w (P-H), 1592 w (P-Ph), 1438 m, 1426 m, 1157 sh $\nu_{asym}(PO_2)$, 1135 s $\nu_{asym}(PO_2)$, 1092 sh, 1047 s $\nu_{sym}(PO_2)$, 1010 s $\nu_{sym}(PO_2)$, 971 s (P-H), 749 m (P-Ph), 700 s. Elemental analysis cald (%): C 59.23, H 4.42. Found: C 55.54, H 4.72. ESI-MS$^+$ (solvent: DMSO) *m/z*: 729.0086 ($[Ga_2Ph_4(O(O)P(H)Ph)_2 + H]^+$), 650.9910 ($[Ga_2Ph_3(O(O)P(H)Ph)_2]^+$), 590.9567 ($[Ga_2Ph_2(O(O)P(H)Ph)_2(O) + H]^+$).

7.10.1.2 Diphenyl *mono*-diphenylphosphinato gallium $[GaPh_2O(O)PPh_2]_2$, 5-2

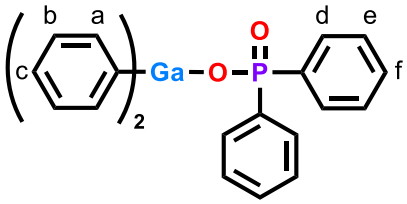

$GaPh_3$ (0.151 g, 0.5 mmol) and diphenylphosphinic acid (0.110 g, 0.51 mmol) were reacted in accordance with GP4 overnight using THF as the solvent to afford a white solid in 79 % yield (0.231 g). m.p. 131 °C. ^{1}H NMR (400 MHz, d_6-DMSO): δ = 7.63 (4H, m, H^a), 7.46 (6H, m, $H^{b,c}$), 7.33 (4H, td, H^d), 7.24 (2H, m, H^f), 7.19 (4H, dd, H^e). ^{31}P NMR (400 MHz, d_6-DMSO): δ = 22.87 ppm. IR (cm^{-1}): 3041 w (P-Ph), 1593 w (P-Ph), 1438 m,

1426 m, 1146 sh $\nu_{asym}(PO_2)$, 1127 s $\nu_{asym}(PO_2)$, 1092 m, 1037 s $\nu_{sym}(PO_2)$, 1018 s $\nu_{sym}(PO_2)$, 752 m (P-Ph), 727 s, 688 s. Elemental analysis cald (%): C 65.35, H 4.57. Found: C 64.86, H 4.85.

Crystallographic data of **5-2** dimer: $C_{48}H_{40}Ga_2O_4P_2$, M_w = 882.18, monoclinic, space group $P2_1/n$, *a* = 16.5121(3), *b* = 13.6115(2), *c* = 20.1121(3) Å, α = 90, β = 109.947(2), λ = 90 °, V = 4249.10(13) Å^3, Z = 4, density = 1.379 g/cm^3, F_{000} = 1808, μ = 2.607 mm^{-1}, $2\theta_{max}$ = 52.7 °, 45897 reflections collected, 8848 unique (R_{int} = 0.0468). Final GooF = 1.078, R_1 = 0.0335, wR_2 = 0.0865.

Crystallographic data of **5-2** polymer: $C_{24}H_{20}GaO_2P$, M_w = 441.09, monoclinic, space group I2/*a*, *a* = 19.6145(2), *b* = 10.18120(10), *c* = 41.6028(5) Å, α = 90, β = 95.0340(10), λ = 90 °, V = 8276.00(15) Å^3, Z = 16, density = 1.416 g/cm^3, F_{000} = 3616, μ = 2.677 mm^{-1}, $2\theta_{max}$ = 154.0 °, 43565 reflections collected, 8581 unique (R_{int} = 0.0237). Final GooF = 1.111, R_1 = 0.0527, wR_2 = 0.1606.

7.10.1.3 Diphenyl *mono*-dimethylphosphinato gallium $[GaPh_2O(O)PMe_2]_2$, 5-3

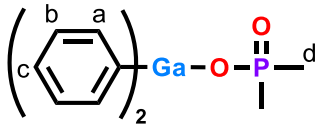

$GaPh_3$ (0.151 g, 0.5 mmol) and dimethylphosphinic acid (0.052 g, 0.55 mmol) were reacted in accordance with GP4 using toluene as the solvent to afford a pale yellow solid in 56 % yield (0.128 g). m.p. 171 °C. ^{1}H NMR (400 MHz, d_6-DMSO): δ = 7.58 (4H, m, H^a), 7.30 (6H, m, H^{b,c}), 1.38 (6H, d, H^d). ^{31}P NMR (400 MHz, d_6-DMSO): δ = 53.63 ppm. IR (cm^{-1}): 3061 w, 1599 m, 1505 m, 1427 m (P-Me), 1298 m, 1127 s $\nu_{asym}(PO_2)$, 1093 sh $\nu_{asym}(PO_2)$, 1025 s $\nu_{sym}(PO_2)$, 998 s $\nu_{sym}(PO_2)$, 874 s (P-Me), 733 s, 703 s. Elemental analysis cald (%): C 53.05, H 5.09. Found: C 53.07, H 5.36.

Crystallographic data of **5-3**: $C_{28}H_{32}Ga_2O_4P_2$, M_w = 633.91, monoclinic, space group $P2_1/c$, *a* = 7.9968(5), *b* = 9.8111(5), *c* = 18.1105(12) Å, α = 90, β = 99.242(7), λ = 90 °, V = 1405.46(15) Å^3, Z = 2, density = 1.501 g/cm^3, F_{000} = 648, μ = 2.067 mm^{-1}, $2\theta_{max}$ = 64.2 °, 19173 reflections collected, 4144 unique (R_{int} = 0.1181). Final GooF = 0.934, R_1 = 0.0567, wR_2 = 0.1392.

7.10.1.4 Diphenyl *mono*-(*bis*-*p*-methoxyphenyl)phosphinato gallium $[GaPh_2O(O)P(p\text{-}MeOPh)_2]_2$, 5-4

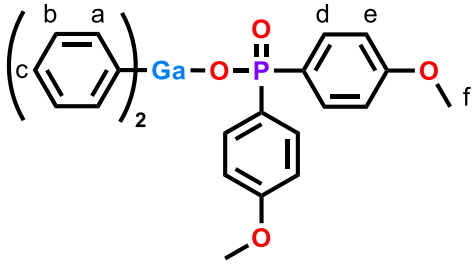

$GaPh_3$ (0.151 g, 0.5 mmol) and *bis*-(*p*-methoxyphenyl)phosphinic acid (0.142 g, 0.51 mmol) were reacted in accordance with GP4 using toluene as the solvent to afford a cream coloured solid in 55 % yield (0.176 g). m.p. 130 °C. ^{1}H NMR (400 MHz, d_6-DMSO): δ = 7.49 (8H, m, H^{a,b}), 7.23 (6H, m, H^{c,d}), 6.85

(4H, d, H^e), 3.74 (6H, s, H^f). ^{31}P NMR (400 MHz, d_6-DMSO): δ = 28.30 ppm. IR (cm^{-1}): 3062 w (P-Ph), 1598 m (P-Ph), 1504 m, 1462 w, 1252 s (O-Me), 1127 s $\nu_{asym}(PO_2)$, 1110 sh $\nu_{asym}(PO_2)$, 1024 s $\nu_{sym}(PO_2)$, 1004 s $\nu_{sym}(PO_2)$, 804 s, 733 m (P-Ph), 672 s. Elemental analysis cald (%): C 62.31, H 4.83. Found: C 61.58, H 4.99. ESI-MS$^+$ (solvent: DMSO) *m/z*: 1001.1170 ($[Ga_2Ph_4(O(O)P(p\text{-}MeOPh)_2)_2 + H]^+$), 923.1022 ($[Ga_2Ph_3(O(O)P(p\text{-}MeOPh)_2)_2]^+$), 877.0803 ($[Ga_2Ph_2(O(O)P(p\text{-}MeOPh)_2)_2(O) + CH_3]^+$), 863.0649 ($[Ga_2Ph_2(O(O)P(p\text{-}MeOPh)_2)_2(O) + H]^+$).

7.10.1.4.1 Di-μ$_3$-oxido tetra-phenyl tetra-(*bis*-*p*-methoxyphenyl)phosphinato tetra-gallium [$Ga_4Ph_4(O(O)P(p\text{-}MeOPh)_2)_4(\mu_3\text{-}O)_2$]

Hydrolysis of **5-4** in hot toluene produced colourless crystals. Crystallographic data of $[Ga_4Ph_4(O(O)P(p\text{-}MeOPh)_2)_4(\mu_3\text{-}O)_2]$: $C_{80}H_{76}Ga_4O_{18}P_4$, M_w = 1728.16, monoclinic, space group C2/c, *a* = 25.973(2), *b* = 15.1756(9), *c* = 24.128(2) Å, α = 90, β = 127.719(14), λ = 90 °, V = 7522.9(15) Å^3, Z = 4, density = 1.526 g/cm^3, F_{000} = 3536, μ = 3.030 mm^{-1}, $2\theta_{max}$ = 144.2 °, 37593 reflections collected, 7417 unique (R_{int} = 0.0990). Final GooF = 1.042, R_1 = 0.0904, wR_2 = 0.2034.

7.10.2 General Procedure 5 (GP5)

All reactions were conducted using 1.0 equivalents of $GaCl_3$ and 3.1 equivalents of phosphinato sodium salts to yield the gallium *tris*-phosphinato complexes. Phosphinato sodium salts were weighed into a Schlenk flask and dried *in vacuo* prior to the addition of dry diethyl ether or THF under nitrogen, forming a heterogeneous solution. $GaCl_3$ was collected into a Schlenk flask with dry THF or diethyl ether, then combined with the sodium salt and allowed to stir overnight. The resulting precipitate was sonicated in hot water and ethanol, then collected by gravimetric filtration prior to air drying.

7.10.2.1 *Tris*-phenylphosphinato gallium [$Ga(O(O)P(H)Ph)_3]_\infty$, 5-9

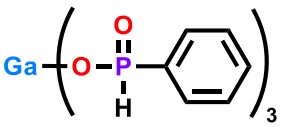

$GaCl_3$ (0.175 g, 1.0 mmol) and phenylphosphinato sodium salt (0.505 g, 3.1 mmol) were reacted in accordance with GP5 using diethyl ether as the solvent to afford a white precipitate in 74 % yield (0.365 g). m.p. 370 °C. ^{13}C CP-MAS: δ = 149.4, 146.0, 144.0. ^{31}P HPDEC-MAS: δ = 15.35 ppm. IR (cm^{-1}): 3056 w (P-Ph), 2398 w (P-H), 1593 w (P-Ph), 1439 m, 1247 m, 1134 s $\nu_{asym}(PO_2)$, 1044 sh $\nu_{sym}(PO_2)$, 1020 m $\nu_{sym}(PO_2)$, 973 s (P-H), 753 s (P-Ph), 695 s. Elemental analysis cald (%): C 43.86, H 3.68. Found: C 41.66, H 3.56.

7.10.2.2 *Tris*-diphenylphosphinato gallium $[Ga(O(O)PPh_2)_3]_\infty$, 5-10

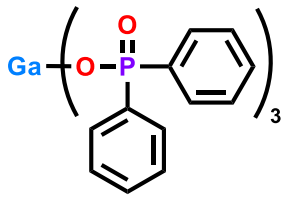

$GaCl_3$ (0.120 g, 0.68 mmol) and diphenylphosphinato sodium salt (0.505 g, 2.1 mmol) were reacted in accordance with GP5 using THF as the solvent to afford a white precipitate in 59 % yield (0.292 g). m.p. 496 °C. ^{13}C CP-MAS: δ =153.7, 149.2, 145.0, 142.3. ^{31}P HPDEC-MAS: δ = 12.38 ppm. IR (cm^{-1}): 3051 w (P-Ph), 1592 w (P-Ph), 1436 m, 1168 m $\nu_{asym}(PO_2)$, 1132 s $\nu_{asym}(PO_2)$, 1074 s $\nu_{sym}(PO_2)$, 1024 m $\nu_{sym}(PO_2)$, 750 m (P-Ph), 724 s, 693 s. Elemental analysis cald (%): C 59.95, H 4.19. Found: C 59.93, H 4.07.

7.10.2.3 *Tris*-dimethylphosphinato gallium $[Ga(O(O)PMe_2)_3]_\infty$, 5-11

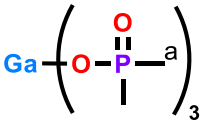

$GaCl_3$ (0.175 g, 1.0 mmol) and dimethylphosphinato sodium salt (0.346 g, 3.0 mmol) were reacted in accordance with GP5 using diethyl ether as the solvent to afford a white precipitate in 19 % yield (0.066 g). Alternatively, **5-3** (0.042 g, 0.13 mmol) and dimethylphosphinic acid (0.025 g, 0.27 mmol) were reacted SF with stirring at 186 °C for 30 minutes, then washed with hot ethanol to afford a white solid in 32 % yield (0.015 g). m.p. >500 °C. ^1H NMR (400 MHz, d_6-DMSO): δ = 1.24 (18H, d, H^a). IR (cm^{-1}): 2987 w, 2084 w, 1423 w (P-Me), 1294 m, 1139 s $\nu_{asym}(PO_2)$, 1107 m, 1045 s $\nu_{sym}(PO_2)$, 868 s (P-Me), 752 m, 706 w. Elemental analysis cald (%): C 20.66, H 5.20. Found: C 17.55, H 4.77.

7.10.2.4 *Tris*-(*bis*-*p*-methoxyphenyl)phosphinato gallium $[Ga(O(O)P(p\text{-}MeOPh)_2)_3]_\infty$, 5-12

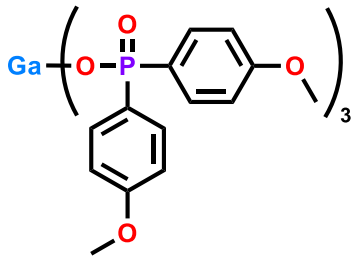

$GaCl_3$ (0.103 g, 0.58 mmol) and *bis*-(*p*-methoxyphenyl)phosphinato sodium salt (0.446 g, 1.5 mmol) were reacted in accordance with GP5 using diethyl ether as the solvent to afford a white precipitate in 87 % yield (0.389 g). m.p. 461 °C. ^{13}C CP-MAS: δ = 176.3, 151.5, 146.1, 130.5, 125.4, 69.8. ^{31}P HPDEC-MAS: δ = 12.62 ppm. IR (cm^{-1}): 3067 w (P-Ph), 2834 w, 1596 m (P-Ph), 1501 m, 1461 w, 1251 s (O-Me), 1167 s $\nu_{asym}(PO_2)$, 1126 s $\nu_{asym}(PO_2)$, 1075 s $\nu_{sym}(PO_2)$, 1028 s $\nu_{sym}(PO_2)$, 828 m, 801 s, 721 w (P-Ph), 665 s. Elemental analysis cald (%): C 55.96, H 4.70. Found: C 55.65, H 4.53.

7.10.2.5 Octa-μ$_3$-oxido di-μ-oxido tetra-μ-hydroxido dodeca-phenyl dodeca-gallium DMSO tetrasolvate [$Ga_{12}Ph_{12}(\mu_3\text{-}O)_8(\mu\text{-}O)_2(\mu\text{-}OH)_4$].4DMSO , 5-13

$GaPh_3$ (0.261 g, 0.867 mmol) was placed in 20 mL of DMSO and allowed to stand open to air for one week. The resulting crystalline solid was filtered and dried to afford 32 % yield (0.054 g). ^{1}H NMR (400 MHz, d_6-DMSO): δ = 9.35 (4H, m, OH), 7.40 (60H, m, Ph-H), 2.54 (24H, s, DMSO-H). IR (cm^{-1}): 3041 w, 2964 w, 2897 w, 2345 w, 1584 w, 1484 m, 1427 s, 1261 s, 1090 s, 1003 s, 1004 s, 949 m, 778 s, 730 s, 694 s (Ga-O), 670 s. Elemental analysis cald (%): C 41.73, H 3.85. Found: C 41.60, H 3.72.

Crystallographic data of **5-13**: $C_{72}H_{64}Ga_{12}O_{14}.4(C_2H_6OS)$, M_w = 2302.38, orthorombic, space group Pbca, *a* = 21.1503(3), *b* = 19.5642(2), *c* = 21.7240(4) Å, α = 90, β = 90, λ = 90 °, V = 8989.1(2) Å^3, Z = 4, density = 1.701 g/cm^3, F_{000} = 4592, μ = 5.290 mm^{-1}, $2\theta_{max}$ = 155.0 °, 48760 reflections collected, 9366 unique (R_{int} = 0.0518). Final GooF = 1.033, R_1 = 0.0569, wR_2 = 0.1547.

8 References

(1) *Antimicrobial Resistance: Global Report on Surveillance*; World Health Organisation, **2014**.

(2) Alves, M. J.; Ferreira, I. C. F. R.; Lourenço, I.; Castro, A.; Pereira, L.; Martins, A.; Pintado, M. *J. Appl. Microbiol.* **2014**, *116* (1), 32–38.

(3) Dantas, G.; Sommer, M. O. A. *Am. Sci.* **2014**, *102* (1), 42–51.

(4) Munita, J. M.; Arias, C. A. *Microbiol. Spectr.* **2016**, *4* (2), 1–24.

(5) Pagès, J.-M.; James, C. E.; Winterhalter, M. *Nat. Rev. Microbiol.* **2008**, *6* (12), 893–903.

(6) Fernandes, M. M.; Ivanova, K.; Hoyo, J.; Pérez-Rafael, S.; Francesko, A.; Tzanov, T. *ACS Appl. Mater. Interfaces* **2017**, *9* (17), 15022–15030.

(7) Mendes, R. E.; Deshpande, L. M.; Jones, R. N. *Drug Resist. Updat.* **2014**, *17* (1–2), 1–12.

(8) Fung, H. B.; Kirschenbaum, H. L.; Ojofeitimi, B. O. *Clin. Ther.* **2001**, *23* (3), 356–391.

(9) Bush, K. *Ann. N. Y. Acad. Sci.* **2013**, *1277* (1), 84–90.

(10) Wilkins, J.; Fareau, G. E.; Patzakis, M. J. *Clin. Orthop. Relat. Res.* **1984**, *190*, 23–30.

(11) Poole, K. *J. Antimicrob. Chemother.* **2005**, *56*, 20–51.

(12) McMurry, L.; Petrucci, R. E.; Levy, S. B.; Levy, S. B. *Proc. Natl. Acad. Sci. U. S. A.* **1980**, *77* (7), 3974–3977.

(13) Neu, H. C. *Science.* **1992**, *257*, 1064–1073.

(14) von Wintersdorff, C. J. H.; Penders, J.; van Niekerk, J. M.; Mills, N. D.; Majumder, S.; van Alphen, L. B.; Savelkoul, P. H. M.; Wolffs, P. F. G. *Front. Microbiol.* **2016**, *7*, 173.

(15) Costerton, J. W.; Stewart, P. S.; Greenberg, E. P. *Science* **1999**, *284* (5418), 1318–1322.

(16) Donlan, R. M.; Costerton, J. W. *Clin. Microbiol. Rev.* **2002**, *15* (2), 167–193.

(17) Coad, B. R.; Kidd, S. E.; Ellis, D. H.; Griesser, H. J. *Biotechnol. Adv.* **2014**, *32* (2), 296–307.

(18) Paladini, F.; Pollini, M.; Sannino, A.; Ambrosio, L. *Biomacromolecules* **2015**, *16* (7), 1873–1885.

(19) *List of Antibiotic Resistant Priority Pathogens*; World Health Organisation, **2017**.

(20) Rice, L. B. *Infect. Control Hosp. Epidemiol.* **2010**, *31* (S1), S7–S10.

(21) Pendleton, J. N.; Gorman, S. P.; Gilmore, B. F. *Expert Rev. Anti. Infect. Ther.* **2013**, *11* (3), 297–308.

(22) Chambers, H. F.; DeLeo, F. R. *Nat. Rev. Microbiol.* **2009**, *7* (9), 629–641.

(23) Miller, L. G.; Diep, B. A. *Clin. Infect. Dis.* **2008**, *46* (5), 752–760.

(24) Australian Group on Antimicrobial Resistance. *Australian Staphylococcal Sepsis Outcome Program (ASSOP)*; **2020**.

(25) European Centre for Disease Prevention and Control. *Antimicrobial resistance in the EU/EEA - Annual Epidemiological Report 2019*; Stockholm, **2020**.

(26) Kim, C.; Mwangi, M.; Chung, M.; Milheirço, C.; de Lencastre, H.; Tomasz, A. *PLoS One* **2013**, *8* (12), e82814.

(27) Mahajan, S. N.; Shah, J. N.; Hachem, R.; Tverdek, F.; Adachi, J. A.; Mulanovich, V.; Rolston, K. V; Raad, I. I.; Chemaly, R. F. *Oncologist* **2012**, *17* (10), 1329–1336.

(28) Sghir, A.; Gramet, G.; Suau, A.; Rochet, V.; Pochart, P.; Dore, J. *Appl. Environ. Microbiol.* **2000**, *66* (5), 2263–2266.

(29) Murray, B. E. *Clin. Microbiol. Rev.* **1990**, *3* (1), 46–65.

(30) Australian Group on Antimicrobial Resistance. *Australian Enterococcal Sepsis Outcome Programme (AESOP)*; **2020**.

(31) Fernández-Hidalgo, N.; Almirante, B.; Gavaldà, J.; Gurgui, M.; Peña, C.; de Alarcón, A.; Ruiz, J.; Vilacosta, I.; Montejo, M.; Vallejo, N.; López-Medrano, F.; Plata, A.; López, J.; Hidalgo-Tenorio, C.; Gálvez, J.; Sáez, C.; Lomas, J. M.; Falcone, M.; de la Torre, J.; Martínez-Lacasa, X.; Pahissa, A. *Clin. Infect. Dis.* **2013**, *56* (9), 1261–1268.

(32) Whang, D. W.; Miller, L. G.; Partain, N. M.; McKinnell, J. A. *Antimicrob. Agents Chemother.* **2013**, *57* (10), 5013–5018.

(33) Hancock, R. E. *Lancet Infect. Dis.* **2005**, *5* (4), 209–218.

(34) Katzung, B. G.; Trevor, A. J. *Basic & Clinical Pharmacology*, 13th ed.; Katzung, B., Ed.;

McGraw-Hill Education, **2015**.

(35) Marco, J. A.; Naranjo, O. R.; Castro, F. R. de; Buendía, B.; Sanz, J. S. In *Antimicrobial Resistance and Implications for the Twenty-First Century*; Springer US: Boston, MA, **2008**; 1–46.

(36) Tran, T. T.; Munita, J. M.; Arias, C. A. *Ann. N. Y. Acad. Sci.* **2015**, *1354* (1), 32–53.

(37) Australian Group on Antimicrobial Resistance. *Gram-negative Sepsis Outcome Program 2019 report*; **2020**.

(38) Wang, S. S.; Ratliff, P. D.; Judd, W. R. *Int. J. Clin. Pharm.* **2018**, *40* (3), 143–149.

(39) Nikaido, H. *Microbiol. Mol. Biol. Rev.* **2003**, *67* (4), 593–656.

(40) Hobman, J. L.; Crossman, L. C. *J. Med. Microbiol.* **2015**, *64* (5), 471–497.

(41) Sierra, M. A.; Casarrubios, L.; de la Torre, M. C. *Chem. Eur. J.* **2019**, *25* (30), 7232–7242.

(42) Lemire, J. A.; Harrison, J. J.; Turner, R. J. *Nat. Rev. Microbiol.* **2013**, *11* (6), 371–384.

(43) Frei, A.; Zuegg, J.; Elliott, A. G.; Baker, M.; Braese, S.; Brown, C.; Chen, F.; G. Dowson, C.; Dujardin, G.; Jung, N.; King, A. P.; Mansour, A. M.; Massi, M.; Moat, J.; Mohamed, H. A.; Renfrew, A. K.; Rutledge, P. J.; Sadler, P. J.; Todd, M. H.; Willans, C. E.; Wilson, J. J.; Cooper, M. A.; Blaskovich, M. A. T. *Chem. Sci.* **2020**, *11* (10), 2627–2639.

(44) Kaczmarek, M. T.; Zabiszak, M.; Nowak, M.; Jastrzab, R. *Coord. Chem. Rev.* **2018**, *370*, 42–54.

(45) Macomber, L.; Imlay, J. A. *Proc. Natl. Acad. Sci. U. S. A.* **2009**, *106* (20), 8344–8349.

(46) Xu, F. F.; Imlay, J. A. *Appl. Environ. Microbiol.* **2012**, *78* (10), 3614–3621.

(47) Imlay, J. A. *Annu. Rev. Microbiol* **2003**, *57*, 395–418.

(48) Stohs, S. J.; Bagchi, D. *Free Radic. Biol. Med.* **1995**, *18* (2), 321–336.

(49) Valko, M.; Morris, H.; Cronin, M. *Curr. Med. Chem.* **2005**, *12* (10), 1161–1208.

(50) Cun, S.; Sun, H. *Proc. Natl. Acad. Sci. U. S. A.* **2010**, *107* (11), 4943–4948.

(51) Erskine, P. T.; Senior, N.; Awan, S.; Lambert, R.; Lewis, G.; Tickle, I. J.; Sarwar, M.; Spencer, P.; Thomas, P.; Warren, M. J.; Shoolingin-Jordan, P. M.; Wood, S. P.; Cooper, J. B. *Nat. Struct.*

Biol. **1997**, *4* (12), 1025–1031.

(52) Macomber, L.; Elsey, S. P.; Hausinger, R. P. *Mol. Microbiol.* **2011**, *82* (5), 1291–1300.

(53) Ciriolo, M. R.; Civitareale, P.; Teresa, M.; De Martino, A.; Galiazzo, F.; Rotilios, G. *J. Biol. Chem.* **1994**, *269* (41), 25783–25787.

(54) Hong, R.; Kang, T. Y.; Michels, C. A.; Gadura, N. *Appl. Environ. Microbiol.* **2012**, *78* (6), 1776–1784.

(55) Jung, W. K.; Koo, H. C.; Kim, K. W.; Shin, S.; Kim, S. H.; Park, Y. H. *Appl. Environ. Microbiol.* **2008**, *74* (7), 2171–2178.

(56) Silver, S.; Phung, L. T.; Silver, G. *J. Ind. Microbiol. Biotechnol.* **2006**, *33* (7), 627–634.

(57) Rizzello, L.; Pompa, P. P. *Chem. Soc. Rev.* **2014**, *43* (5), 1501–1518.

(58) Rodriguez-Arguello, J.; Lienhard, K.; Patel, P.; Geransar, R.; Somayaji, R.; Parsons, L.; Conly, J.; Ho, C. *Ostomy Wound Manag.* **2018**, *64* (3), 14–16.

(59) Wood, C. M.; Playle, R. C.; Hogstrand, C. *Environ. Toxicol. Chem.* **1999**, *18* (1), 71–83.

(60) Siemianowicz, K.; Likus, W. In *Silver Nanoparticles for Antibacterial Devices: Biocompatibility and Toxicity*; Cao, H., Ed.; Taylor & Francis, **2017**; 193–210.

(61) Crosera, M.; Bovenzi, M.; Maina, G.; Adami, G.; Zanette, C.; Florio, C.; Filon Larese, F. *Int. Arch. Occup. Environ. Health* **2009**, *82*, 1043–1055.

(62) Korani, M.; Rezayat, S. M.; Arbabi Bidgoli, S. *Iran. J. Pharm. Res.* **2013**, *12* (3), 511–519.

(63) Martinez-Gutierrez, F.; Olive, P. L.; Banuelos, A.; Orrantia, E.; Nino, N.; Sanchez, E. M.; Ruiz, F.; Bach, H.; Av-Gay, Y. *Nanomedicine Nanotechnology, Biol. Med.* **2010**, *6* (5), 681–688.

(64) Martínez-Gutierrez, F.; Thi, E. P.; Silverman, J. M.; de Oliveira, C. C.; Svensson, S. L.; Hoek, A. Vanden; Sánchez, E. M.; Reiner, N. E.; Gaynor, E. C.; Pryzdial, E. L. G.; Conway, E. M.; Orrantia, E.; Ruiz, F.; Av-Gay, Y.; Bach, H. *Nanomedicine Nanotechnology, Biol. Med.* **2012**, *8* (3), 328–336.

(65) Shrivastava, S.; Bera, T.; Singh, S. K.; Singh, G.; Ramachandrarao, P.; Dash, D. *ACS Nano* **2009**, *3* (6), 1357–1364.

(66) Silver, S. *FEMS Microbiol. Rev.* **2003**, *27* (2–3), 341–353.

(67) Gunawan, C.; Marquis, C. P.; Amal, R.; Sotiriou, G. A.; Rice, S. A.; Harry, E. J. *ACS Nano* **2017**, *11* (4), 3438–3445.

(68) Turner, R. J. *Microb. Biotechnol.* **2017**, *10* (5), 1062–1065.

(69) Gupta, A.; Matsui, K.; Lo, J.-F.; Silver, S. *Nat. Med.* **1999**, *5* (2), 183–188.

(70) Feng, Q. L.; Wu, J.; Chen, G. Q.; Cui, F. Z.; Kim, T. N.; Kim, J. O. *J. Biomed. Mater. Res.* **2000**, *52* (4), 662–668.

(71) Dakal, T. C.; Kumar, A.; Majumdar, R. S.; Yadav, V. *Front. Microbiol.* **2016**, *7*, 1831.

(72) Sun, H.; Zhang, L.; Szeto, K. T. *Met. Ions Biol. Sys.* **2004**, *41*, 333–378.

(73) Salvador, J. A.; Figueiredo, S. A.; Pinto, R. M.; Silvestre, S. M. *Future Med. Chem.* **2012**, *4* (11), 1495–1523.

(74) Mendis, A.; Marshall, B. In *Biological Chemistry of Arsenic, Antimony and Bismuth*; Sun, H., Ed.; **2010**.

(75) Andrews, P. C.; Busse, M.; Deacon, G. B.; Ferrero, R. L.; Junk, P. C.; Huynh, K. K.; Kumar, I.; MacLellan, J. G. *Dalton Trans.* **2010**, *39* (40), 9633–9641.

(76) Andrews, P. C.; Ferrero, R. L.; Forsyth, C. M.; Junk, P. C.; MacLellan, J. G.; Peiris, R. M. *Organometallics* **2011**, *30* (22), 6283–6291.

(77) Busse, M.; Trinh, I.; Junk, P. C.; Ferrero, R. L.; Andrews, P. C. *Chem. Eur. J.* **2013**, *19* (17), 5264–5275.

(78) Busse, M.; Border, E.; Junk, P. C.; Ferrero, R. L.; Andrews, P. C. *Dalton Trans.* **2014**, *43* (48), 17980–17990.

(79) Pathak, A.; Blair, V. L.; Ferrero, R. L.; Junk, P. C.; Tabor, R. F.; Andrews, P. C. *Dalton Trans.* **2015**, *44*, 16903.

(80) Pathak, A.; Blair, V. L.; Ferrero, R. L.; Kedzierski, L.; Andrews, P. C. *J. Inorg. Biochem.* **2017**, *177*, 266–275.

(81) Suerbaum, S.; Michetti, P. *N. Engl. J. Med.* **2002**, *347* (15), 1175–1186.

(82) Domenico, P.; Reich, J.; Madonia, W.; Cunha, B. A. *J. Antimicrob. Chemother.* **1996**, *38* (6), 1031–1040.

(83) Zhang, L.; Szeto, K. Y.; Wong, W. B.; Loh, T. T.; Sadler, P. J.; Sun, H. *Biochemistry* **2001**, *40* (44), 13281–13287.

(84) Seng, H.-L.; Tiekink, E. In *Comprehensive Inorganic Chemistry II*; Reedijk, J., Poeppelmeier, K., Eds.; Elsevier: Oxford, **2013**; 951–974.

(85) Mahony, D. E.; Bryden, L.; Faulkner, G.; Agocs, L.; Briand, G. G.; Burford, N.; Maguire, H.; Hoffman, P. S. *Antimicrob. Agents Chemother.* **1999**, *43* (3), 582–588.

(86) Luqman, A.; Blair, V. L.; Brammananth, R.; Crellin, P. K.; Coppel, R. L.; Andrews, P. C. *Chem. Eur. J.* **2014**, *20* (44), 14362–14377.

(87) Raheel, A.; Imtiaz-ud-Din; Andleeb, S.; Ramadan, S.; Tahir, M. N. *Appl. Organomet. Chem.* **2017**, *31*, e3632.

(88) Stephens, L. J.; Munuganti, S.; Duffin, R. N.; Werrett, M. V; Andrews, P. C. *Inorg. Chem* **2020**, *59*, 3494–3508.

(89) Burke, K. J.; Stephens, L. J.; Werrett, M. V; Andrews, P. C. *Chem. Eur. J.* **2020**, *26* (34), 7657–7671.

(90) Senevirathna, D. C.; Duffin, R. N.; Stephens, L. J.; Herdman, M. E.; Werrett, M. V; Andrews, P. C. *Aust. J. Chem.* **2020**, *73* (12), 1226–1236.

(91) Kotani, T.; Nagai, D.; Asahi, K.; Suzuki, H.; Yamao, F.; Kataoka, N.; Yagura, T. *Antimicrob. Agents Chemother.* **2005**, *49* (7), 2729–2734.

(92) Badireddy, A. R.; Korpol, B. R.; Chellam, S.; Gassman, P. L.; Engelhard, M. H.; Lea, A. S.; Rosso, K. M. *Biomacromolecules* **2008**, *9* (11), 3079–3089.

(93) Folsom, J. P.; Baker, B.; Stewart, P. S. *J. Appl. Microbiol.* **2011**, *111* (4), 989–996.

(94) Domenico, P.; Baldassarri, L.; Schoch, P. E.; Kaehler, K.; Sasatsu, M.; Cunha, B. A. *Antimicrob. Agents Chemother.* **2001**, *45* (5), 1417–1421.

(95) Microbion https://microbioncorp.com/ (accessed Mar 1, 2021).

(96) Chitambar, C. R. *Future Med. Chem.* **2012**, *4* (10), 1257–1272.

(97) Minandri, F.; Bonchi, C.; Frangipani, E.; Imperi, F.; Visca, P. *Future Microbiol.* **2014**, *9* (3), 379–397.

(98) Chitambar, C. R. In *Metallo-Drugs: Development and Action of Anticancer Agents*; Sigel, A., Sigel, H., Freisinger, E., Sigel, R. K. O., Eds.; De Gruyter, **2018**; 281–302.

(99) Claudel, M.; Schwarte, J. V.; Fromm, K. M. *Chemistry (Easton).* **2020**, *2* (4), 849–899.

(100) Duffin, R. N.; Blair, V. L.; Kedzierski, L.; Andrews, P. C. *Eur. J. Med. Chem.* **2020**, *186*.

(101) Bernstein, L. R. *Pharmacol. Rev.* **1998**, *50* (4), 665–682.

(102) Chitambar, C. R. *Pharmacol. Res.* **2017**, *115*, 56–64.

(103) Kaneko, Y.; Thoendel, M.; Olakanmi, O.; Britigan, B. E.; Singh, P. K. *J. Clin. Invest.* **2007**, *117* (4), 877–888.

(104) Clevette, D. J.; Orvig, C. *Polyhedron* **1990**, *9* (2–3), 151–161.

(105) Chitambar, C. R. *Int. J. Environ. Res. Public Health* **2010**, *7* (5), 2337–2361.

(106) Hijazi, S.; Visaggio, D.; Pirolo, M.; Frangipani, E.; Bernstein, L.; Visca, P. *Front. Cell. Infect. Microbiol.* **2018**, *8*, 316.

(107) Bernstein, L. R. In *Metallotherapeutic Drugs and Metal-Based Diagnostic Agents: The Use of Metals in Medicine*; Gielen, M., Tiekink, E. R. T., Eds.; John Wiley & Sons, **2005**; 259–278.

(108) Chitambar, C. R.; Purpi, D. P.; Woodliff, J.; Yang, M.; Wereley, J. P. *J. Pharmacol. Exp. Ther.* **2007**, *322* (3), 1228–1236.

(109) Edwards, C. L.; Hayes, R. L. *J. Nucl. Med.* **1969**, *10* (2), 103–105.

(110) Rzhepishevska, O.; Ekstrand-Hammarström, B.; Popp, M.; Björn, E.; Bucht, A.; Sjöstedt, A.; Antti, H.; Ramstedt, M. *Antimicrob. Agents Chemother.* **2011**, *55* (12), 5568–5580.

(111) Enyedy, É. A.; Dömötör, O.; Krisztina Bali, ·; Hetényi, A.; Tuccinardi, T.; Keppler, B. K. *J Biol Inorg Chem* **2015**, *20*, 77–88.

(112) Gallego, B.; Kaluderovic, M. R.; Kommera, H.; Paschke, R.; Hey-Hawkins, E.; Remmerbach, T. W.; Kaluderovic, G. N.; Gómez-Ruiz, S. *Invest. New Drugs* **2011**, *29* (5), 932–944.

(113) Collinsova, M.; Jiracek, J. *Curr. Med. Chem.* **2000**, *7*, 629–647.

(114) Parsons, W. H.; Patchett, A. A.; Bull, H. G.; Schoen, W. R.; Tuab, D.; Davidson, J.; Combs, P. L.; Springer, J. P.; Gadebusch, H. *J. Med. Chem.* **1988**, *31* (9), 1772–1778.

(115) Al-Bar, O. A. M.; O ’connor, D.; Giles, I. G.; Akhtar, M. *Biochem. J. J. Med. Chem. Biochem.* **1992**, *282* (27), 747–752.

(116) Thaslim Basha, S.; Sudhamani, H.; Rasheed, S.; Venkateswarlu, N.; Vijaya, T.; Naga Raju, C. *Phosphorus. Sulfur. Silicon Relat. Elem.* **2016**, *191* (10), 1339–1343.

(117) Joensson, M.; Silvestru, A.; Silvestru, C. *Stud. UBB Chem.* **2006**, 83–90.

(118) Shimada, S.; Maruyama, J.; Choe, Y. K.; Yamashita, T. *Chem. Commun.* **2009**, No. 41, 6168–6170.

(119) Solyntjes, S.; Neumann, B.; Stammler, H.-G.; Ignat’ev, N.; Hoge, B. *Chem. Eur. J.* **2017**, *23* (7), 1568–1575.

(120) Metre, R. K.; Kundu, S.; Narayanan, R. S.; Chandrasekhar, V. *Phosphorus, Sulfur Silicon Relat. Elem.* **2015**, *190* (12), 2134–2141.

(121) Ali, J.; Navaneetha, T.; Baskar, V. *Inorg. Chem.* **2020**, *59* (1), 741–747.

(122) Breunig, H. J.; Haddad, N.; Lork, E.; Mehring, M.; Mügge, C.; Nolde, C.; Raţ, C. I.; Schürmann, M. *Organometallics* **2009**, *28* (4), 1202–1211.

(123) Xu, L.; Jiao, H.; Liu, B.; Zhang, Z.-H. *J. Struct. Chem.* **2016**, *57* (4), 744–753.

(124) Svoboda, T.; Jambor, R.; Ružička, A.; Padělkova, Z.; Erben, M.; Dostál, L. *Eur. J. Inorg. Chem.* **2010**, No. 33, 5222–5230.

(125) Edmundson, R. S. (Ronald S. *Dictionary of organophosphorus compounds*; Chapman and Hall, **1988**.

(126) Andrews, P. C.; Deacon, G. B.; Junk, P. C.; Spiccia, N. F. *Green Chem.* **2007**, *9* (12), 1319–1327.

(127) Gillman, H. D. *Inorg. Chem.* **1974**, *13* (8), 1921–1924.

(128) Begley, M. J.; Sowerby, D. B.; Wesolek, D. M.; Silvestru, C.; Haiduc, I. *J. Organomet. Chem.* **1986**, *316* (3), 281–289.

(129) Saraceno, A. J.; Block, B. P. *Inorg. Coord. Polym.* **1964**, *3* (12), 1699–1703.

(130) Cicha, W. V; Haynes, J. S.; Oliver, K. W.; Rettig, S. J.; Thompson, R. C.; Trotter, J. *Can. J. Chem* **1985**, *63*, 1055–1062.

(131) Oliver, K. W.; Rettig, S. J.; Thompson, R. C.; Trotter, J.; Xia, S. *Inorg. Chem.* **1997**, *36*, 2465–2468.

(132) Auer, A.; Mansfeld, D.; Nolde, C.; Schneider, W.; Schurmann, M.; Mehring, M. *Organometallics* **2009**, *28*, 5405–5411.

(133) Pike, S. D.; White, E. R.; Shaffer, M. S. P.; Williams, C. K. *Nat. Commun.* **2016**, *7*, 13008.

(134) Janiak, C. *J. Chem. Soc. Dalton Trans.* **2000**, No. 21, 3885–3896.

(135) Ong, Y. C.; Blair, V. L.; Kedzierski, L.; Andrews, P. C. *Dalton Trans.* **2014**, *43*, 12904.

(136) Ong, Y. C.; Blair, V. L.; Kedzierski, L.; Tuck, K. L.; Andrews, P. C. *Dalton Trans.* **2015**, *44* (41), 18215–18226.

(137) Anthony, E. J.; Bolitho, E. M.; Bridgewater, H. E.; Carter, O. W. L.; Donnelly, J. M.; Imberti, C.; Lant, E. C.; Lermyte, F.; Needham, R. J.; Palau, M.; Sadler, P. J.; Shi, H.; Wang, F. X.; Zhang, W. Y.; Zhang, Z. *Chem. Sci.* **2020**, *11* (48), 12888–12917.

(138) Yang, N.; Tanner, J. A.; Zheng, B. J.; Watt, R. M.; He, M. L.; Lu, L. Y.; Jiang, J. Q.; Shum, K. T.; Lin, Y. P.; Wong, K. L.; Lin, M. C. M.; Kung, H. F.; Sun, H.; Huang, J. D. *Angew. Chemie - Int. Ed.* **2007**, *46* (34), 6464–6468.

(139) Yuan, S.; Wang, R.; Chan, J. F. W.; Zhang, A. J.; Cheng, T.; Chik, K. K. H.; Ye, Z. W.; Wang, S.; Lee, A. C. Y.; Jin, L.; Li, H.; Jin, D. Y.; Yuen, K. Y.; Sun, H. *Nat. Microbiol.* **2020**, *5* (11), 1439–1448.

(140) Jozefczak, M.; Remans, T.; Vangronsveld, J.; Cuypers, A. *Int. J. Mol. Sci.* **2012**, *13* (3), 3145–3175.

(141) Czekanska, E. M. *Methods Mol. Biol.* **2011**, *740*, 27–32.

(142) Thomas, F.; Bialek, B.; Hensel, R. *J. Clin. Toxicol.* **2011**, *s3* (01), 1–5.

(143) Andrews, P. C.; Frank, R.; Junk, P. C.; Kedzierski, L.; Kumar, I.; MacLellan, J. G. *J. Inorg. Biochem.* **2011**, *105* (3), 454–461.

(144) Riss, T.; Moravec, R. *Cell Notes* **2002**, No. 4, 6–9.

(145) Abughazaleh, R. D.; Tracy, T. S. In *Wiley StatsRef: Statistics Reference Online*; John Wiley & Sons, Ltd: Chichester, UK, **2014**; 95–103.

(146) López-Cardoso, M.; Tlahuext, H.; Pérez-Salgado, M.; Vargas-Pineda, D. G.; Román-Bravo, P. P.; Cotero-Villegas, A. M.; Acevedo-Quiroz, M.; Razo-Hernández, R. S.; Alvarez-Fitz, P.; Mendoza-Catalán, M. A.; Jancik, V.; Cea-Olivares, R. *J. Mol. Struct.* **2020**, *1217*, 128456.

(147) Ghasemi, F.; Mehridehnavi, A.; Pérez-Garrido, A.; Pérez-Sánchez, H. *Drug Discov. Today* **2018**, *23* (10), 1784–1790.

(148) Murafuji, T.; Tomura, M.; Ishiguro, K.; Miyakawa, I. *Molecules* **2014**, *19* (8), 11077–11095.

(149) Ong, Y. C. Preparation, Characterisation and Development of Novel Bi (V) Complexes as Anti-Leishmanial Drug Candidates, Monash University, **2017**.

(150) Duffin, R. N.; Blair, V. L.; Kedzierski, L.; Andrews, P. C. *Dalton Trans.* **2018**, *47* (3), 971–980.

(151) Duffin, R. N.; Blair, V. L.; Kedzierski, L.; Andrews, P. C. *J. Inorg. Biochem.* **2020**, *203* (110932).

(152) Hartmann, H.; Habenicht, G.; Reiss, W. *ZAAC - J. Inorg. Gen. Chem.* **1962**, *317* (1–2), 54–62.

(153) Luqman, A.; Blair, V. L.; Brammananth, R.; Crellin, P. K.; Coppel, R. L.; Andrews, P. C. *Eur. J. Inorg. Chem.* **2016**, *2016* (17), 2738–2749.

(154) Luqman, A.; Blair, V. L.; Brammananth, R.; Crellin, P. K.; Coppel, R. L.; Andrews, P. C. *Eur. J. Inorg. Chem.* **2015**, *2015* (29), 4935–4945.

(155) Hughes, J. D.; Blagg, J.; Price, D. A.; Bailey, S.; DeCrescenzo, G. A.; Devraj, R. V.; Ellsworth, E.; Fobian, Y. M.; Gibbs, M. E.; Gilles, R. W.; Greene, N.; Huang, E.; Krieger-Burke, T.; Loesel, J.; Wager, T.; Whiteley, L.; Zhang, Y. *Bioorganic Med. Chem. Lett.* **2008**, *18* (17), 4872–4875.

(156) White, W. C.; Bellfield, R.; Ellis, J.; Vandendaele, I. P. In *Medical and Healthcare Textiles*; Woodhead Publishing, **2010**; 55–75.

(157) Salwiczek, M.; Qu, Y.; Gardiner, J.; Strugnell, R. A.; Lithgow, T.; McLean, K. M.; Thissen, H. *Trends Biotechnol.* **2014**, *32* (2), 82–90.

(158) Grass, G.; Rensing, C.; Solioz, M. *Appl. Environ. Microbiol.* **2011**, *77* (5), 1541–1547.

(159) Han, S.; Yang, Y. *Dye. Pigment.* **2005**, *64* (2), 157–161.

(160) Reddy, N.; Han, S.; Zhao, Y.; Yang, Y. *J. Appl. Polym. Sci.* **2013**, *127* (4), 2698–2702.

(161) Abel, T.; Cohen, J. L. I.; Engel, R.; Filshtinskaya, M.; Melkonian, A.; Melkonian, K. *Carbohydrate Research*. Carbohydrate Research **2002**, 2495–2499.

(162) Isquith, A. J.; Abbott, E. A.; Walters, P. A. *Appl. Microbiol.* **1972**, *24* (6), 859–863.

(163) Abel, T.; Cohen, J. L. I.; Escalera, J.; Engel, R.; Filshtinskaya, M.; Fincher, R.; Melkonian, A.; Melkonian, K. *J. Text. Apparel, Technol. Manag.* **2003**, *3* (2), 1–8.

(164) Thomas, M.; Montenegro, D.; Castaño, A.; Friedman, L.; Leb, J.; Huang, M. L.; Rothman, L.; Lee, H.; Capodiferro, C.; Ambinder, D.; Cere, E.; Galante, J.; Rizzo, J.; Melkonian, K.; Engel, R. *Carbohydr. Res.* **2009**, *344* (13), 1620–1627.

(165) Dizaj, S. M.; Lotfipour, F.; Barzegar-Jalali, M.; Zarrintan, M. H.; Adibkia, K. *Mater. Sci. Eng. C* **2014**, *44*, 278–284.

(166) Sharma, S.; Sanpui, P.; Chattopadhyay, A.; Ghosh, S. S.; Wang, H.-L.; Wu, J. C. G.; Lin, J.-G.; Yang, X.; Park, Y. H.; Hwang, C.-Y.; Kim, Y.-K.; Lee, Y.-S.; Jeong, D. H.; Cho, M.-H. *RSC Adv.* **2012**, *2* (13), 5837.

(167) De Jong, W. H.; Borm, P. J. A. *Int. J. Nanomedicine* **2008**, *3* (2), 133–149.

(168) Knetsch, M. L. W.; Koole, L. H. *Polymers (Basel).* **2011**, *3* (4), 340–366.

(169) Paladini, F.; Di Franco, C.; Panico, A.; Scamarcio, G.; Sannino, A.; Pollini, M. *Materials (Basel).* **2016**, *9* (6), 411.

(170) Cortese-Krott, M. M.; Münchow, M.; Pirev, E.; Heβner, F.; Bozkurt, A.; Uciechowski, P.; Pallua, N.; Kröncke, K.-D.; Suschek, C. V. *Free Radic. Biol. Med.* **2009**, *47*, 1570–1577.

(171) Moon, R. J.; Martini, A.; Nairn, J.; Simonsen, J.; Youngblood, J. *Chem. Soc. Rev* **2011**, *40*, 3941–3994.

(172) Kontturi, E.; Laaksonen, P.; Linder, M. B.; Nonappa; Gröschel, A. H.; Rojas, O. J.; Ikkala, O. *Adv. Mater.* **2018**, *30* (24), 1703779.

(173) Zhang, Q.; Zhang, L.; Wu, W.; Xiao, H. *Carbohydr. Polym.* **2020**, *229* (115454), 1–19.

(174) Lavoine, N.; Desloges, I.; Manship, B.; Bras, J. *J. Food Sci. Technol.* **2015**, *52* (9), 5590–5600.

(175) Liyaskina, E.; Revin, V.; Paramonova, E.; Nazarkina, M.; Pestov, N.; Revina, N.; Kolesnikova, S. In *J. Phys.: Conf. Ser*; **2017**; Vol. 784.

(176) Luan, J.; Wu, J.; Zheng, Y.; Song, W.; Wang, G.; Guo, J.; Ding, X. *Biomed. Mater* **2012**, *7*, 65006–65011.

(177) Wu, J.; Zheng, Y.; Song, W.; Luan, J.; Wen, X.; Wu, Z.; Chen, X.; Wang, Q.; Guo, S. *Carbohydr. Polym.* **2014**, *102* (1), 762–771.

(178) Maliha, M.; Herdman, M.; Brammananth, R.; McDonald, M.; Coppel, R.; Werrett, M.; Andrews, P.; Batchelor, W. *J. Clean. Prod.* **2020**, *246*, 119016.

(179) Garusinghe, U. M.; Varanasi, S.; Garnier, G.; Batchelor, W. *Cellulose* **2017**, *24* (6), 2511–2521.

(180) Garusinghe, U. M.; Raghuwanshi, V. S.; Garvey, C. J.; Varanasi, S.; Hutchinson, C. R.; Batchelor, W.; Garnier, G. *Colloids Surfaces A Physicochem. Eng. Asp.* **2017**, *513*, 373–379.

(181) Liedberg, H.; Lundeberg, T. *Urol. Res.* **1989**, *17* (6), 359–360.

(182) Boonkaew, B.; Kempf, M.; Kimble, R.; Cuttle, L. *Burns* **2014**, *40* (8), 1562–1569.

(183) McCauley, R. L.; Linares, H. A.; Pelligrini, V.; Herndon, D. N.; Robson, M. C.; Heggers, J. P. *J. Surg. Res.* **1989**, *46* (3), 267–274.

(184) Coates, G. E.; Mukherjee, R. N. *J. Chem. Soc.* **1964**, 1292–1295.

(185) Weidlein, J.; Schaible, B. *ZAAC - J. Inorg. Gen. Chem.* **1971**, *386* (2), 176–184.

(186) Olapinski, H.; Schaible, B.; Weidlein, J. *J. Organomet. Chem.* **1972**, *43* (1), 95–106.

(187) Schaible, S.; Weidlein, J. *J. Organomet. Chem.* **1972**, *35* (1), C7–C10.

(188) Hahn, F. E.; Schneider, B.; Reier, F. W. *Zeitschrift fur Naturforsch. - Sect. B J. Chem. Sci.* **1990**, *45* (2), 134–140.

(189) Browning, D. J.; Corker, J. M.; Webster, M. *Acta Crystallogr. Sect. C Cryst. Struct. Commun.* **1996**, *52* (4), 882–884.

(190) Landry, C. C.; Hynes, A.; Barron, A. R.; Haiduc, I.; Silvestru, C. *Polyhedron* **1996**, *15* (3), 391–402.

(191) Mikulski, C. M.; Unruh, J.; Rabin, R.; Iaconnianni, F. J.; Pytlewski, L. L.; Karayannis, N. M. *Transit. Met. Chem.* **1981**, *6* (2), 79–82.

(192) Ioannou, P. V. *Monatshefte fur Chemie* **2013**, *144* (6), 793–802.

(193) Andrews, P. C.; Junk, P. C.; Nuzhnaya, I.; Spiccia, L.; Vanderhoek, N. *J. Organomet. Chem.* **2006**, *691* (16), 3426–3433.

(194) Gilman, H.; Jones, R. G. *J. Am. Chem. Soc.* **1940**, *62* (4), 980–982.

(195) Luo, B.; Gladfelter, W. L. *Inorg. Chem.* **2002**, *41* (3), 590–597.

(196) McKinlay, R. M.; Dalgarno, S. J.; Nichols, P. J.; Papadopoulos, S.; Atwood, J. L.; Raston, C. L. *Chem. Commun.* **2007**, No. 23, 2393–2395.

(197) Oliveri, A. F.; Wills, L. A.; Hazlett, C. R.; Carnes, M. E.; Chang, I. Y.; Ha-Yeon Cheong, P.; Johnson, D. W. *Chem. Sci.* **2015**, *6* (7), 4071–4085.

(198) Mehring, M. In *Clusters - Contemporary Insight in Structure and Bonding*; Dehnen, S., Ed.; Springer Verlag, **2017**; 201–268.

(199) Landry, C. C.; Harlan, C. J.; Bott, S. G.; Barron, A. R. *Angew. Chemie Int. Ed. English* **1995**, *34* (11), 1201–1202.

(200) Swenson, D. C.; Dagorne, S.; Jordan, R. F. *Acta Crystallogr. Sect. C Cryst. Struct. Commun.* **2000**, *56* (10), 1213–1215.

(201) Onyiriuka, E. C.; Rettig, S. J.; Storr, A.; Trotter, J. *Can. J. Chem.* **1987**, *65* (4), 782–788.

(202) Jung, M.; Mertens, C.; Tomat, E.; Brüne, B. *Int. J. Mol. Sci.* **2019**, *20* (2).

(203) *Bruker APEX2 v2014.7-1*; Bruker AXS: Madison, WI, US, **2014**.

(204) *CrysAlisPro v1.171.34.36*; Oxford Diffraction Ltd (Agilent Technologies): Oxfordshire, UK, **2010**.

(205) Sheldrick, G. M. *Bruker AXS Inc, Madison, US* **2002**.

(206) Cowieson, N. P.; Aragao, D.; Clift, M.; Ericsson, D. J.; Gee, C.; Harrop, S. J.; Mudie, N.; Panjikar, S.; Price, J. R.; Riboldi-Tunnicliffe, A.; Williamson, R.; Caradoc-Davies, T. *J. Synchrotron Radiat.* **2015**, *22* (1), 187–190.

(207) Kabsch, W. *J. Appl. Crystallogr.* **1993**, *26* (pt 6), 795–800.

(208) Sheldrick, G. M. *Univ. Göttingen, Ger.* **2003**.

(209) Sheldrick, G. M. *Acta Crystallogr. Sect. C Struct. Chem.* **2015**, *71* (1), 3–8.

(210) Dolomanov, O. V.; Bourhis, L. J.; Gildea, R. J.; Howard, J. A. K.; Puschmann, H. *J. Appl. Crystallogr.* **2009**, *42* (2), 339–341.

(211) Barton, D. H. R.; Bhantnagar, N. Y.; Finet, J.-P.; Motherwell, W. B. *Tetrahedron* **1986**, *42* (12), 3111–3122.

(212) Levason, W.; Sheikh, B.; Mccullough, F. P.; *J. Coord. Chem.* **1982**, *12* (1), 53–57.

(213) Rao, M. L. N.; Dhanorkar, R. J. *RSC Adv.* **2016**, *6* (2), 1012–1017.

(214) Challenger, F.; Allpress, C. F. *J. Chem. Soc. Trans.* **1921**, *119*, 913–926.

(215) Challenger, F. *J. Chem. Soc. Trans.* **1914**, *105*, 2210–2218.

(216) Mansfield, D. Synthese und Charakterisierung neuartiger Bismutsilanolate, Bismut-oxo-cluster und Bismutkoordinationspolmere, Technische Universitaet Chemnitz, **2009**.

(217) Zhang, L.; Batchelor, W.; Varanasi, S.; Tsuzuki, T.; Wang, X. *Cellulose* **2012**, *19* (2), 561–574.

(218) Varanasi, S.; He, R.; Batchelor, W. *Cellulose* **2013**, *20* (4), 1885–1896.